

Diffusion, Advection and Pattern Formation

Jichen Yang

Dissertation
zur Erlangung des Grades
Dr. rer. nat.

Vorgelegt im
Fachbereich Mathematik und Informatik
der Universität Bremen
im Februar 2020



Datum des Promotionskolloquiums: 23.03.2020

Gutachter:

Prof. Dr. Jens Rademacher (Universität Bremen)

Prof. Dr. Christian Kühn (Technische Universität München)

To Chen Gai

Acknowledgements

First and foremost, I would like to express my sincere gratitude to Jens Rademacher, without whom this thesis would not have been written. His knowledge, patient advise, time and friendship have been invaluable.

I would like to thank Christian Kuehn for taking the time to serve on both my defence committee and my topics review committee. Thanks to Eric Siero for the helpful discussions and collaboration included in this thesis.

I would like to thank the members of my research group over my years at Bremen: Antoine, Artur, Dennis, Hendrik, Lars, Miriam, Sara, and former members Daniel and Ivan, for the interesting group meetings, their feedback, fruitful discussions in mathematics as well as everything.

I would like to thank all other members of Dynamical Systems group, for their help in life and friendly conversations. Thanks to Katie for her linguistic help in this thesis.

Finally, I want to express special thank to my wife Chen for her love and support. I would also like to thank my mother Suwen, my mother-in-law Mian, and all of my family and friends for their support. Thanks to my landlady Ursula and landlord Jürgen for their kindly help and support over my years in Lilienthal.

This work has been supported by China Scholarship Council, Degree Completion Grants from University of Bremen. I am grateful for the hospitality and support from Faculty of Mathematics, and the travel support through an Impulse Grants for Research Projects by University of Bremen as well as from Jens.

Abstract

Patterns are ubiquitous in nature and can arise in reaction-diffusion systems with differential diffusions. The existence and stability of (in)homogeneous steady state are the classical topics in the dynamics of reaction-diffusion systems. In this thesis we study the influences of anomalous diffusion and advection upon the patterns.

In the first part of this thesis we consider the impact of subdiffusive process on the instability of homogeneous states in three types of reaction-subdiffusion systems. The modelling of linear and nonlinear reaction-subdiffusion processes is more subtle than normal diffusion and causes different phenomena. The resulting equations feature a spatial Laplacian with a temporal memory term through a time-fractional derivative. It is known that the precise form depends on the interaction of dispersal and reaction, and leads to qualitative differences. We refine these results by defining generalised spectra through dispersion relations, which allows us to examine the onset of instability and in particular inspect Turing-type instabilities. These results are numerically illustrated. Moreover, we prove expansions that imply for one class of reaction-subdiffusion equations algebraic decay for stable spectrum, whereas for another class this is exponential. We also study the linearisation of a nonlinear reaction subdiffusion equation in a nonzero homogeneous state. Here the spectrum cannot be analysed directly by Fourier-Laplace transform, so we provide an energy estimate, existence, uniqueness and dynamics of Fourier modes of such a linearisation.

It is well known that for reaction-diffusion systems with differential isotropic diffusions, a Turing instability yields striped solutions. In the second part of this thesis we study the impact of weak anisotropy by directional advection on the stability of such solutions, and the role of quadratic nonlinearities. We focus on the generic form of planar reaction-diffusion systems with two components near such a bifurcation. Using Lyapunov-Schmidt reduction, Floquet-Bloch decomposition and centre manifold reduction we derive rigorous parameter expansions for existence, stability against large-wavelength and lattice modes, respectively. This provides detailed formulae for the loci of bifurcations and stability boundaries under the influences of the advection and quadratic terms. In particular, while destabilisation of the background state is through modes perpendicular to the advection (Squire-theorem), we show that stripes can bifurcate zigzag unstably. The well known destabilising effect of quadratic terms can be counterbalanced by advection, which leads to intriguing arrangements of stability boundaries.

We illustrate these results numerically by an example. Finally, we show numerical computations of these stability boundaries in the extended Klausmeier model for vegetation patterns and show stripes bifurcate stably in the presence of advection.

Zusammenfassung

Muster sind in der Natur allgegenwärtig und können in Reaktionsdiffusionssystemen mit Differentialdiffusionen auftreten. Die Existenz und Stabilität eines (in) homogenen stationären Zustands sind die klassischen Themen in der Dynamik von Reaktionsdiffusionssystemen. In dieser Arbeit untersuchen wir die Einflüsse von anomaler Diffusion und Advektion auf die Muster.

Im ersten Teil dieser Arbeit untersuchen wir den Einfluss von Subdiffusionsprozessen auf die Instabilität homogener Zustände in drei Arten von Reaktions-Subdiffusionssystemen. Die Modellierung linearer und nichtlinearer Reaktions-Subdiffusionsprozesse ist subtiler als die normale Diffusion und verursacht unterschiedliche Phänomene. Die resultierenden Gleichungen enthalten einen räumlichen Laplace-Operator mit einem zeitlichen Gedächtnisterm durch eine zeitfraktionale Ableitung. Es ist bekannt, dass die genaue Form vom Zusammenspiel von Diffusion und Reaktion abhängt und zu qualitativen Unterschieden führt. Wir verfeinern diese Ergebnisse, indem wir verallgemeinerte Spektren durch Dispersionsbeziehungen definieren, die es uns ermöglichen, den Beginn der Instabilität zu untersuchen und insbesondere Instabilitäten vom Turing-Typ zu untersuchen. Diese Ergebnisse sind numerisch dargestellt. Daraufhin beweisen wir Erweiterungen, die für eine Klasse von Reaktions-Subdiffusions-Gleichungen einen algebraischen Abfall für ein stabiles Spektrum implizieren, während dies für eine andere Klasse exponentiell ist. Wir untersuchen auch die Linearisierung einer nichtlinearen Reaktions-Subdiffusionsgleichung im homogenen Zustand ungleich Null. Hier kann das Spektrum nicht direkt durch Fourier-Laplace-Transformation analysiert werden, daher geben wir eine Energieeinschätzung, Existenz, Eindeutigkeit und Dynamik von Fourier-Moden einer solchen Linearisierung an.

Es ist bekannt, dass bei Reaktionsdiffusionssystemen mit differentiellen isotropen Diffusionen eine Turing-Instabilität zu gestreiften Lösungen führt. Im zweiten Teil dieser Arbeit untersuchen wir den Einfluss schwacher Anisotropie durch gerichtete Advektion auf die Stabilität solcher Lösungen und die Rolle quadratischer Nichtlinearitäten. Wir konzentrieren uns auf die generische Form von planaren Reaktionsdiffusionssystemen mit zwei Komponenten in der Nähe einer solchen Verzweigung. Durch Lyapunov-Schmidt-Reduktion, Floquet-Bloch-Zerlegung und Zentrumsmannigfaltigkeitsreduktion leiten wir rigorose Parameterentwicklung für Existenz, Stabilität gegen grosse Wellenlängen- bzw. Gittermoden ab. Dies liefert detaillierte Formeln für die Orte der Bifurkationen und Stabilitätsgrenzen unter dem Einfluss der

Advektion und der quadratischen Terme. Während die Destabilisierung des Hintergrundzustands durch Moden erfolgt, die senkrecht zur Advektion verlaufen (Squire-Theorem), zeigen wir insbesondere, dass Streifen instabil bezüglich Zick-Zack-Moden verzweigen können. Der bekannte destabilisierende Effekt quadratischer Terme kann durch Advektion ausgeglichen werden, was zu vielfältigen Anordnungen von Stabilitätsgrenzen führt. Wir veranschaulichen diese Ergebnisse numerisch an einem Beispiel. Schliesslich zeigen wir numerische Berechnungen dieser Stabilitätsgrenzen im erweiterten Klausmeier-Modell für Vegetationsmuster und zeigen Streifen, die in Gegenwart von Advektion stabil entstehen.

Contents

Acknowledgements	i
Abstract	iii
Zusammenfassung	v
List of Figures	xi
1 Introduction	1
1.1 Pattern formation and reaction-diffusion systems	1
1.2 Anomalous diffusion	3
1.3 Reactions with subdiffusion	5
1.4 Reaction-diffusion with advection	8
1.5 Outline	12
2 Reaction-subdiffusion systems	13
2.1 Introduction	13
2.2 Subdiffusion and reactions	14
2.3 Preliminaries	18
2.3.1 Fractional calculus	18
2.3.2 Subdiffusion equation	19
2.3.3 Turing instability	20
2.4 Subdiffusion with source and sink	21
2.4.1 Scalar case	23
2.4.2 Convergence to regular spectrum	26
2.4.3 Real spectrum and (pseudo-)spectrum for large wavenumber	27
2.4.4 Spectral instability for large wavenumbers	29
2.4.5 Numerical computations of (pseudo-)spectra	32
2.5 Subdiffusion with linear creation and annihilation	34
2.5.1 Scalar case	34
2.5.2 Spectral analysis	36

2.5.3	Convergence to regular spectrum	39
2.5.4	Numerical computations of spectra	43
2.6	Subdiffusion with nonlinear creation and annihilation	43
2.6.1	Energy estimate	45
2.6.2	Existence and uniqueness	46
2.6.3	Dynamics of Fourier modes	50
2.6.4	Linear analysis	51
2.6.5	Numerical solution	54
3	Reaction-diffusion-advection systems	57
3.1	Introduction	57
3.2	Turing instability	60
3.3	Bifurcation of stripes	64
3.4	Large wavelength stability	68
3.5	Stability of stripes on lattices	72
3.5.1	Centre manifold reduction	72
3.5.2	Stability in one space-dimension	73
3.5.3	Stability against (quasi-)square perturbations	75
3.5.4	Stability against hexagonal perturbations	76
3.5.5	Stability against quasi-hexagonal perturbations	83
3.6	Examples	88
3.6.1	Exact example: zigzag-unstable stripes	88
3.6.2	Numerical example: extended Klausmeier model	92
3.6.3	Further analysis of extended Klausmeier model	93
4	Outlook	95
4.1	Further analysis of reaction-subdiffusion equations	95
4.2	Turing-type systems coupled to ODE	96
4.3	Bifurcation and stability of oblique stripes	96
4.4	Subcritically bifurcating stripes	97
A	Prerequisites	99
A.1	Fourier transform	99
A.2	Laplace transform	100
A.3	Wright function	100
B	Inverse Laplace transform	103
B.1	Inverse Laplace transform with zero branch point	103
B.2	Inverse Laplace transform with nonzero branch points	108

C Some proofs	113
C.1 Proof of Lemma 2.4.18	113
C.2 Proof of Proposition 2.4.22	115
D Existence of stripes	119
E Stability of stripes	123
E.1 Spectrum for zigzag instability	123
E.2 Spectrum for Eckhaus instability	124
E.3 Stability of 2D and 4D centre manifolds	126
E.4 Stability of 6D centre manifold	129
Bibliography	131
Abbreviations and symbols	137

List of Figures

1.1	Sketch of continuous-time random walks in one-dimensional space	4
2.1	Comparison of numerically computed regular spectra and pseudo-spectra ¹	24
2.2	Numerically computations of (pseudo-)spectra of scalar model ¹	25
2.3	Illustrations of the case when the regular spectrum at fixed wavenumber either differs from or contains the origin	27
2.4	Existence and stability of large wavenumber (pseudo-)spectrum ¹	31
2.5	Comparison of numerically computed (pseudo-)spectra beyond the regular Turing instability ¹	33
2.6	Comparison of real parts of (pseudo-)spectra beyond the regular Turing instability ¹	33
2.7	Comparison of (pseudo-)spectra in the principal branch ¹	34
2.8	Illustrations of real parts of (pseudo-)spectra, and (pseudo-)spectra in single value holomorphic branches ¹	35
2.9	Comparison of real parts of (pseudo-)spectra versus wavenumber ¹	36
2.10	Illustrations of regular spectra in complex plane for a fixed wavenumber	39
2.11	Illustrations of (in)stability regions of spectra near the origin ¹	43
2.12	Numerical computations of (psudo-)spectra ¹	44
2.13	Numerical computations of real parts of (pseudo-)spectra versus wavenumbers ¹	44
2.14	Comparison of the logarithm of solutions of ordinary and fractional differential equations ²	55
3.1	Sketches of the leading order existence and stability boundaries near the Turing bifurcation point	58
3.2	Sketches of the quasi-hexagonal stability regions and the width of the stable connection	60
3.3	Sketches of the quasi-hexagonal stability regions near Turing bifurcation point and the width of the stable connection	61
3.4	Illustration of locations of the critical spectrum of homogeneous steady state ¹	63
3.5	Sketches of the different leading order zigzag instability boundaries	70
3.6	Sketches of the quasi-square stability regions of stripes	77
3.7	Sketches of the hexagonal stability regions of stripes	80

3.8	Sketches of the hexagonal stability regions near the Turing point	81
3.9	Sketch of the hexagonally unstable region	83
3.10	Sketches of the quasi-hexagonal stability regions near the Turing point	86
3.11	Sketches of the quasi-hexagonal and Eckhaus stability boundaries near the Turing point	89
3.12	The leading order of the rescaled striped solution ¹	90
3.13	Numerical computations of the leading order Eckhaus and zigzag (in)stability regions of the stripes for a designed example ¹	90
3.14	Numerical computations of leading order of instability regions and boundaries of stripes against lattice modes for a designed example ¹	91
3.15	Numerical computations of the leading order of hex- and quasi-hex-instability regions for a designed example ¹	92
3.16	Eckhaus and zigzag (in)stability regions of the stripes for extended Klausmeier model ³	93
3.17	Numerical computations of the leading order of Eckhaus and zigzag (in)stability regions of the stripes for extended Klausmeier model ¹	94
B.1	Notation and geometry of the integration contours where the branch cut is the origin	104
B.2	Notation and geometry of the integration contours where the branch points are complex with negative real parts	109

¹Computed using Mathematica

²Computed using SageMath

³Computed using pde2path - a Matlab package [63]

Chapter 1

Introduction

1.1 Pattern formation and reaction-diffusion systems

A pattern is a kind of spatially non-uniform structure with some spatial or temporal regularities, and these are ubiquitous in nature. In the early works, patterns were observed in the convectional motion. In 1900, Henri Bénard found that, under the influences of the temperature gradient and gravity, heating a fluid between two horizontal plates causes the fluid to rise and fall which can form spatial patterns [4]. These patterns are most commonly stripes or convection rolls; more complicated patterns such as squares or hexagons could also emerge, depending on the specific physical systems and the fluid properties [26]. In 1916, Lord Rayleigh published a paper [51] analysing the aforementioned experiment, and thus this kind of pattern-forming process is known as Rayleigh-Bénard convection. Patterns can be observed in the vibration of liquids as well, e.g. Faraday waves, named after Michael Faraday. Faraday waves are nonlinear standing waves that emerge on the surface of a fluid by vibrating the container. This observation was described in the appendix of the article [13]. Subsequent experiments show that a wide variety of patterns can appear, such as squares, hexagons, or even exotic patterns such as the one with twelvefold rotational symmetry [11], depending on the strength of the vibration and the type of fluids.

Patterns can also be observed in systems of reacting and diffusing chemicals, so-called *reaction-diffusion (RD) systems*. A famous example is the Belousov-Zhabotinsky reaction [3, 73]. During the reaction, the colour of the mixed substances (solution) is periodically changed by continuous stirring. Without the stirring, one can see the waves propagating and forming concentric rings or rotating spirals. Patterns are ubiquitous in animal skin markings as well, such as the stripes on zebras, irregular hexagons on giraffes, etc., and the process of the emergence is so-called morphogenesis. In 1952, Alan Turing published a famous paper [62] in which he suggested an explanation of the mechanism of morphogenesis. He predicted that two different chemical substances, an activator and an inhibitor with differentially diffusive rates, can produce the patterns, which are so-called *Turing patterns*. The activator causes growth in the concentration of substances, whereas the inhibitor causes depletion. The patterns can emerge if the inhibitor

diffuses much faster than the activator. Turing patterns can appear not only on the skins of animals, but also happen, for instance, in the formation of vegetation. In semi-/arid terrain, since the vegetation competes for the limited ground water, the former cannot uniformly cover the ground and thus patterns appear [28, 37, 59]. In flat terrain, a variety of patterns can emerge, such as spots, gaps, stripes or labyrinths. In contrast, in sloped terrain, striped patterns are more likely to happen than other types due to the water flow [2, 28, 59].

Reaction-diffusion systems arise naturally in chemical reactions which consist of many interacting components, and are widely used to describe the pattern-forming processes. A simple type of RD systems has the following form

$$\partial_t u = D\Delta u + F(u), \quad u(\mathbf{x}, t) \in \mathbb{R}^N, \quad \mathbf{x} \in \mathbb{R}^n, \quad t > 0, \quad (1.1)$$

where $u(\mathbf{x}, t)$ is a vector of the densities or the concentrations of the interacting species or chemicals with the spatial vector $\mathbf{x} = (x_1, \dots, x_n)$ and temporal variable t , $D \in \mathbb{R}^{N \times N}$ is a diagonal matrix of diffusion coefficients with positive diagonal entries which measures the rate of the dispersal of each component, $\Delta := \partial_{x_1}^2 + \dots + \partial_{x_n}^2$ is the spatial Laplacian, $F : \mathbb{R}^N \rightarrow \mathbb{R}^N$ is a nonlinear vector which represents the local reaction kinetics. More specifically, the source term F in an ecological context, for instance, may represent the birth and death process. Notably, the maximum principle is valid only for the scalar equation, i.e., $N = 1$.

As mentioned, the diffusion process plays a key role in Turing pattern formations. Diffusion is a mechanism by which the substances move from an area of higher concentration to an area of lower concentration. Diffusion is driven by the gradient in concentration and the substances gradually become homogeneous in the whole area. The (normal) diffusion process follows the Fick's law which suggests that the diffusive flux which goes from areas of higher concentration to areas of lower concentration is proportional to the concentration gradient. The corresponding proportion is the so-called *diffusion coefficient* which measures the rate of the dispersal. However, it has been found that many diffusion processes do not follow Fick's law, for instance, charge carrier transport in amorphous semiconductors [55], transport on fractal geometries [21], collective slip diffusion on solid surfaces [31], transport in turbulent plasma [1], etc. Such a non-Fickian diffusion process is called *anomalous diffusion*. Anomalous diffusion can be classified into two cases, *subdiffusion* and *superdiffusion*. Subdiffusion is, roughly speaking, a kind of diffusion process that is ‘slower’ than normal diffusion, whereas superdiffusion is ‘faster’ than normal diffusion.

Pattern formation in RD systems, in particular the Turing patterns, has been widely considered in the past seven decades. However, the study of the dynamics of the anomalous diffusion-reaction systems were just started in the past few decades [16, 18, 22, 25, 29, 42, 43, 45, 46, 66, 68]. In particular, there are only few works that concern the Turing patterns in reaction-subdiffusion systems.

An important aspect of nonlinear dynamics and pattern formation in RD systems is pattern selection. It is well known that, for instance, in flat terrain there is no pattern selection, so that

spots (vegetation surrounded by bare soil), gaps (bare soil surrounded by vegetation) and stripes (banded vegetation) coexist. In sloped terrain, however, the isotropy is broken and thus stripes are formed predominantly. The direction of the vegetation stripes extends parallel to the contour of the hill. Moreover, some evidence shows that the vegetation stripes slowly ‘climb up’ the hill, e.g. [9]. The explanation of this phenomena is as follows [28]: The water does not infiltrate in the bare soil between the vegetation stripes, then flows downhill to the next stripe where it can be absorbed by the plants and help these grow. Due to the absorption of water, the downhill side of the stripe lacks water, which causes the next bare area. The stripe slowly moves uphill since the uphill side of the stripe has moister soil which can grow the plants, whereas the plants on the downhill side of the stripe die as a result of insufficient water.

In this thesis, we study two aspects of the dynamics of RD systems (equations). On the one hand, we study the influence of anomalous diffusion, in particular the subdiffusion processes on the reactions of the substances. On the other hand, we study the impact of the slope (advection) on pattern-forming processes in RD systems.

1.2 Anomalous diffusion

In the normal diffusion process, the individual particles follow the Brownian motion which is a Markovian process such that the future states depend only upon the present state and not on the past states. This memoryless process follows the linear scaling law $\langle x^2(t) \rangle \sim t$, where the mean squared displacement (MSD), denoted by $\langle x^2(t) \rangle$, measures the average deviation of an individual particle with respect to the initial point during a given time. The diffusion process can be described by the diffusion equation

$$\partial_t u = d\Delta u, \quad u(\mathbf{x}, t) \in \mathbb{R}, \mathbf{x} \in \mathbb{R}^n, t > 0, \quad (1.2)$$

where $u(\mathbf{x}, t)$ is the density or the concentration of the substances with the spatial vector \mathbf{x} and the temporal variable t ; the diffusion coefficient d measures the rate of the dispersal. It is well known that Green’s function of (1.2) is given by $u(\mathbf{x}, t) = (4\pi dt)^{-n/2} \exp(-|\mathbf{x}|^2/(4dt))$. The MSD is then given by $\langle x^2(t) \rangle = \int_{\mathbb{R}^n} |\mathbf{x}|^2 u d\mathbf{x} = 2ndt$ which is linear in time.

Anomalous diffusion, however, arises from a transport process with a nonlinear temporal MSD of particles. Specifically, we say that a transport process exhibits anomalous diffusion if the MSD scales as a nonlinear power-law in time $\langle x^2(t) \rangle \sim t^\gamma$, with anomalous exponent $\gamma \neq 1$. Such an anomalous diffusion process is called *subdiffusion* if $0 < \gamma < 1$, and *superdiffusion* if $\gamma > 1$, cf. [35, 38]. In addition to power-law scaling, there are a variety of other scalings such as a logarithmic time dependence which we do not touch upon here.

The (anomalous) diffusion can be described by continuous-time random walks (CTRW), cf. [35, 38]. The CTRW is a generalisation of the random walk, in which the waiting times until the next displacements are random variables and the jump lengths can also be regarded as random

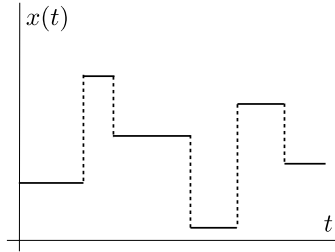


Figure 1.1: Sketch of continuous-time random walks in one-dimensional space. The solid lines represent the waiting times and the dashed lines represent the jump lengths.

variables. Fig. 1.1 shows a one-dimensional CTRW, i.e., $\mathbf{x} = x \in \mathbb{R}$: an individual particle stays at a position for some time, then it immediately jumps to the next position, and repeats such procedure. The probability for a jump length in the interval $(x, x + dx)$ is given by $\phi(x)dx$ where $\phi(x)$ denotes the probability density function (PDF) of the jump length. Analogously, the probability for a waiting time in the interval $(t, t + dt)$ is given by $w(t)dt$ where $w(t)$ denotes the PDF of the waiting time. The types of diffusion processes can be classified by the variance of the jump length, i.e., $\Sigma^2 := \int_{\mathbb{R}} x^2 \phi(x)dx$, and the expectation of the waiting time, i.e., $T := \int_0^\infty tw(t)dt$, as follows.

- $\Sigma^2 < \infty, T < \infty$: normal diffusion
- $\Sigma^2 = \infty, T < \infty$: superdiffusion
- $\Sigma^2 < \infty, T = \infty$: subdiffusion

In this thesis, we only consider the subdiffusion process and compare it to normal diffusion. We refer to [18, 35, 38, 39, 45, 66] for more details of superdiffusion.

Comparing subdiffusion with normal diffusion, the variances of the jump lengths are both finite, but the expectations of the waiting times are qualitatively different. The finite variance and expectation can be achieved by choosing the exponentially decaying functions $\phi(x)$ and $w(t)$ in space and time, respectively, e.g. the Gaussian distribution $\phi(x) = (4\pi\sigma^2)^{-1/2} \exp(-x^2/(4\sigma^2))$ with variance $\Sigma^2 = 2\sigma^2$ and Poissonian distribution $w(t) = \tau^{-1} \exp(-t/\tau)$ with the expectation $T = \tau$. Concerning the infinite expectation in subdiffusion, one may expect the non-exponential waiting time PDF, which gives a non-Markovian process with memory. Specifically, such PDF has the asymptotic behaviour for large time $w(t) \sim \gamma\tau^\gamma/(\Gamma(1 - \gamma)t^{1+\gamma})$, $0 < \gamma < 1$, $t \gg 1$ with the Gamma function Γ . Hence, the particles have a relatively high probability of remaining at certain positions for a very long time so that subdiffusion is, roughly speaking, slower than normal diffusion. The role of the diffusion equation in this context is taken by the *subdiffusion equation*, which has the form

$$\partial_t u = \mathcal{D}_{0,t}^{1-\gamma} d\partial_x^2 u, \quad u(x, t) \in \mathbb{R}, x \in \mathbb{R}, t > 0, \quad (1.3)$$

with *time-fractional Riemann-Liouville derivative* $\mathcal{D}_{0,t}^{1-\gamma}$, cf. Definition 2.3.2, a non-local convolution operator in time that entails the memory.

1.3 Reactions with subdiffusion

The modelling of reactions in the presence of subdiffusion is a complex task and leads to different models, which essentially come in two types. In the so-called diffusion-limited reactions the non-local operator acts on the diffusion terms as well as the reaction terms, or in other words the diffusion and reaction terms occur in an additive way but the time evolution is described by the fractional derivatives [23, 44, 57, 58, 65, 72], e.g.,

$$\partial_t u = \mathcal{D}_{0,t}^{1-\gamma} [d\partial_x^2 u + f(u)] \quad \text{or} \quad \mathcal{D}_{0,t}^\gamma (u - u_0) = \partial_x^2 u + f(u). \quad (1.4)$$

Here the reaction is “slow” even without subdiffusive transport, i.e., $d = 0$. This type of model is derived from the CTRW for the recombination kinetics [58] or instantaneous creation and annihilation processes in subdiffusive media [23].

In the so-called activation-limited reactions the non-local operator acts on the diffusion terms only, i.e., the reactive process does not depend on the subdiffusive medium [14, 23, 24, 42, 44, 60]. In this thesis, we focus on this type and study the following three different types of models in one-dimensional space, i.e. $\mathbf{x} = x \in \mathbb{R}$.

Subdiffusion with extra source and sink This model is derived by adding extra source or sink terms to the subdiffusive process [24, 25]. The model is described by the following time-fractional partial differential system

$$\partial_t u = D\mathcal{D}_{0,t}^{1-\gamma} \partial_x^2 u + F(u), \quad u(x, t) \in \mathbb{R}^N, \quad x \in \mathbb{R}, \quad t > 0. \quad (1.5)$$

Comparing to (1.1), the Riemann-Liouville derivative acts on the spatial Laplacian and thus causes memory in time. For the anomalous exponent $\gamma = 1$, (1.5) becomes the classical RD system (1.1). However, it has been shown in [23] that (1.5) with $N = 1$ and negative linear reaction dynamics, e.g., $F(u) = -u$, possesses a Green’s function with negative parts. Heuristically, the reason for the negative parts is that the sink removes substances which have not yet jumped from other positions due to the long waiting time PDF. If u represents an absolute density we therefore obtain a physically unrealistic model, see also [47]. However, in this thesis we are concerned with u modelling a vector of *density perturbations* from a saturated strictly positive state, and such perturbations can be negative. Specifically, the linearisation of (1.5) in a non-zero homogeneous steady state is a linear system in which $F(u)$ is replaced by a linear vector.

Subdiffusion with linear creation and annihilation In the subdiffusive process, the addition or removal of particles arises from the reaction during the waiting time with constant rates [23, 30, 47]. The model for multiple species is given by

$$\partial_t u = D e^{At} \mathcal{D}_{0,t}^{1-\gamma} (e^{-At} \partial_x^2 u) + Au, \quad u(x, t) \in \mathbb{R}^N, \quad x \in \mathbb{R}, \quad t > 0, \quad (1.6)$$

where $A \in \mathbb{R}^{N \times N}$ is a constant reaction rate matrix and $e^{\pm At}$ are the matrix exponentials. This model also coincides with the classical one at $\gamma = 1$, and it preserves positivity of solutions since the amount of removed substances is less than the amount of existing substances.

Subdiffusion with nonlinear creation and annihilation The addition or removal of particles arises from the reaction with nonlinear rate $r(u)$ and gives the scalar equation [14, 47]

$$\partial_t u = d\partial_x^2 \left(e^{\int_0^t r(u(x, \tau)) d\tau} \mathcal{D}_{0,t}^{1-\gamma} \left(u e^{-\int_0^t r(u(x, \tau)) d\tau} \right) \right) + r(u)u, \quad u(x, t) \in \mathbb{R}, \quad x \in \mathbb{R}, \quad t > 0, \quad (1.7)$$

where $r : \mathbb{R} \rightarrow \mathbb{R}$. One example of such specific reaction term is a Fisher-KPP type reaction kinetics which is in the form of $r(u)u := \alpha(1 - u)u$, $\alpha > 0$. This equation seems like the generalisation of (1.6) with $N = 1$. Indeed, the linearisation of (1.7) in a zero solution yields the form of (1.6). However, the linearisation in a non-zero homogeneous state yields

$$\partial_t u = d\partial_x^2 \left(\mathcal{D}_{0,t}^{1-\gamma} u - \sigma \mathcal{D}_{0,t}^{-\gamma} u + \sigma \mathcal{D}_{0,t}^{1-\gamma} 1 \cdot \mathcal{D}_{0,t}^{-1} u \right) + \sigma u, \quad (1.8)$$

where $\mathcal{D}_{0,t}^{-\gamma}$ is the fractional integral operator, cf. Definition 2.3.1. This equation is different from the aforementioned two types of reaction-subdiffusion models, and even more complicated due to the product term $\mathcal{D}_{0,t}^{1-\gamma} 1 \cdot \mathcal{D}_{0,t}^{-1} u$. This equation coincides with the classical RD equation for $\gamma = 1$ and reduces to the subdiffusion equation (1.3) for $\sigma = 0$.

Due to the non-local term in time, equations with subdiffusion are not dynamical systems on the phase space of the natural initial condition $u(x, 0)$. In particular, solutions do not form a cocycle since any restart at some $t > 0$ requires prescribing an initial condition on the preceding temporal interval $u(x, s)$, $0 \leq s \leq t$. One may interpret this as a variable delay, which is initially zero and extends indefinitely. Indeed, solutions can cross the initial state, and need not remain positive or satisfy a maximum principle, e.g. [23]. The fractional derivative operator also depends explicitly on time, so the stability of an equilibrium from a linearisation is not readily determined by the spectrum of a time-independent linear operator.

Concerning the models (1.5) and (1.6) in both scalar and two-component cases, inspired by the work of Henry and co-authors [22, 25], we study the linear equations through Fourier-Laplace transform which leads to dispersion relations of the form $D(s, q^2) = 0$ that relate the temporal mode through $s \in \mathbb{C}$ with the spatial mode through $q \in \mathbb{R}$. By analogy to evolution equations with normal diffusion, one might expect that the set of solutions determines the spectral stability, but the situation for reaction-subdiffusion systems (of the first two types) is more subtle. Since fractional powers occur in the dispersion relation, one has to choose branch cuts, and the canonical choice of the negative real line has been used in [22, 25, 42, 44]. As expected, for some cases it has been shown that positive real parts imply exponential instability. Negative real parts, however, do not necessarily imply exponential decay. Indeed, it has been found in [25] for $\gamma = 1/2$ that solutions decay as a power law.

In this thesis, we refine and extend the results of the the models (1.5) and (1.6), as informally summarised next.

Pseudo-spectrum and convergence We consider non-canonical branch cuts and show that the choice strongly influences the existence of solutions to the dispersion relation that lie to the left of the (rightmost) branch point, which we therefore refer to as *pseudo-spectrum*.

The reason for choosing non-canonical branch cuts is that it allows us to locate and track otherwise invisible solutions to the dispersion relation. In particular we identify those solutions that relate to the spectrum of classical RD equations (1.1) for $\gamma = 1$, and we prove the convergence of the spectrum as $\gamma \rightarrow 1$ using Rouché's theorem (Theorems 2.4.15, 2.5.8).

Decay and growth We show that, at least for rational $\gamma \in (0, 1)$ and $N \leq 2$, a strictly stable (pseudo-)spectrum in (1.5) implies that Fourier modes of solutions decay with an algebraic power law (Theorem 2.4.5). In contrast, the strictly stable (pseudo-)spectrum in (1.6) with $N \leq 2$ implies an exponential decay whose rate, however, may differ from that of RD systems (1.1) (Theorem 2.5.4); the Fourier modes of both (1.5) and (1.6) grow exponentially for unstable (pseudo-)spectrum. In fact, we provide a leading order expansion and provide formulae of the leading order coefficients. We also include a discussion of the scalar subdiffusion equation (1.3), in particular algebraic decay and positivity, which we found somewhat scattered in the literature, cf. §2.3.2.

We remark that different algebraic decay for a strictly stable spectrum has been obtained in [65, Theorem 5.1] for (1.4)(2) with homogeneous Dirichlet boundary condition.

Turing-type instability Concerning the onset of instability, models (1.5) and (1.6) differ significantly from each other and from the case of a classical RD system (1.1). We focus on the case of two-component systems, $N = 2$, and when parameters are such that $\gamma = 1$ admits a so-called Turing instability for a critical diffusion ratio. As already noticed in [22, 25, 42, 44], in case (1.5), if the spectrum for $\gamma = 1$ is Turing unstable, then the spectrum for all $\gamma \in (0, 1)$ is unstable. This means that, in terms of the diffusion ratio, the reaction-subdiffusion in (1.5) is always *less stable* than normal diffusion. In particular, the threshold of Turing instability in (1.5) is smaller than that for normal diffusion. As noticed in [42, 44], considering large wavenumbers shows that the spectrum becomes unstable via *infinite* wavenumber with oscillatory modes. In particular, there is no finite wavenumber selection at the onset of instability, which is a key feature of the normal Turing instability. Beyond the results in [42, 44], we in particular include an analysis of (pseudo-)spectrum, which reveals the transition to instability. Specifically, we show that for any diffusion ratio less than the Turing threshold for normal diffusion, the (pseudo-)spectrum is strictly stable for all wavenumbers if γ is close to 1 (Theorem 2.4.20).

Stable (pseudo-)spectrum of (1.6) and its transition to instability differs in character from that of (1.5). Specifically, the (pseudo-)spectrum of (1.6) is not close to the origin for large wavenumbers, which is similar to the spectrum of (1.1) and leads to the aforementioned exponential decay. We prove that stable (pseudo-)spectrum becomes unstable via finite wavenumber for γ close to 1, and we obtain the Turing instability threshold as a function of the anomalous exponent, and find a critical minimum anomalous exponent γ_A depending on A (Theorem 2.5.10). In particular, and in contrast to (1.5), the subdiffusive transport in (1.6) is always *more stable* than normal diffusion, and the Turing instability does not happen for $\gamma < \gamma_A$.

Concerning the nonlinear model (1.7), in this thesis we focus on the linearisation in the non-zero homogeneous steady state (1.8). In contrast to the linear equations of (1.5) and (1.6), the spectrum of (1.8) is still an open problem. The Laplace transform of the product $\mathcal{D}_{0,t}^{1-\gamma} \mathbf{1} \cdot \mathcal{D}_{0,t}^{-1} u$ yields a complex integral which is dependent on the temporal mode implicitly, and thus the spectrum is still unknown. We aim to prove the linear stability of the solutions to (1.8), in particular the stable solutions for $\sigma < 0$. Until now, we obtain some indirect results as follows. We provide an energy estimate which shows that a type of energy of the solution is decaying locally in time (Theorem 2.6.1). We consider the Fourier modes of (1.8) and prove the existence and uniqueness of the mild solution (Theorem 2.6.6). We also study the dynamics of the Fourier modes and prove that the solution is exponentially decaying for short time (Theorem 2.6.7), which is a typical property of the subdiffusion equation (1.3), but the decaying rates may be different. Moreover, one possible method to study the linear stability is the comparison principle. We find two auxiliary systems whose solutions are both algebraically decaying in time with differential rates, then try to prove that the solutions to (1.8) are bounded by the aforementioned solutions from auxiliary systems.

These insights may form the basis for further linear analysis, in particular estimates in x -space, but also nonlinear analysis in terms of estimates and possibly bifurcations. These are rather non-trivial due to the strongly different character of the linear dynamics and spectral properties compared to normal diffusion.

1.4 Reaction-diffusion with advection

It is well known that from the ubiquitous spatially isotropic Turing instabilities various patterned solutions bifurcate. In one dimension the basic spatially periodic ones are wavetrains, which trivially extend to stripe solutions in two-dimensional space, where they are in competition with hexagonal and square shaped states, e.g., [26]. The question arises, which pattern is selected at onset of the instability. It is well known that in the isotropic situation, stripes are unstable with respect to modes on the hexagonal lattice near onset in the presence of a generic quadratic term in the nonlinearity. This has been discussed in [19] in the context of vegetation patterns. In contrast, it has been found in [59] that in a sloped terrain, the banded vegetation patterns, i.e. the stripes, are stable at onset. Here the slope is modelled by an advective term in the water component, which breaks the spatial isotropy. Indeed, from a symmetry perspective for weakly anisotropic perturbations and on the hexagonal lattice this has already been predicted in [6]. The destabilising effects of advection terms on homogeneous states have been broadly studied in the context of differential flows, e.g., [8, 36, 52] and also appear in ecology, e.g., [5, 7, 67], where we believe our results can also be useful.

In this thesis, we consider a generic form of the planar reaction-diffusion-advection systems

with two components, up to cubic nonlinearity

$$\partial_t u = D\Delta u + Lu + \alpha Mu + \beta B\partial_x u + Q[u, u] + K[u, u, u], \quad (1.9)$$

with $u(\mathbf{x}, t) \in \mathbb{R}^2$, $\mathbf{x} = (x, y) \in \mathbb{R}^2$, $t > 0$, $\Delta := \partial_x^2 + \partial_y^2$, constant matrices L, M , multilinear functions Q, K and diagonal diffusion matrix $D > 0$; higher order nonlinear terms can be added without change to our results near bifurcation, i.e., in a small neighbourhood of $u = 0$. We assume that for $\alpha = \beta = 0$ the zero equilibrium is at a Turing instability with wavenumber \mathbf{k}_c , cf. Definition 3.2.1 below, and that α moves the spectrum through the origin. The isotropy is broken for $\beta \neq 0$, and we assume differential advection

$$B = B(c) = \begin{pmatrix} 1+c & 0 \\ 0 & c \end{pmatrix}, \quad c \in \mathbb{R},$$

which can be realised under the natural assumption of unidirectional anisotropy. Note that $\beta c \partial_x$ appears in both equations as a comoving frame in the x -direction, and positive (negative) β implies the advection of the first component in negative (positive) x -direction.

We study the stability of stripes in (1.1) for weak anisotropy. On the one hand, we consider the stability against large-wavelength perturbations. We are particularly interested in refining the results of [59] which indicate a stabilising effect of advection for stripes aligned with this. In particular, it was proven that the onset of instability of the homogeneous state, i.e., the nature of the Turing-Hopf instability, is due to one-dimensional modes (a ‘Squire’-theorem). However we shall explain in §3.4 that this does not necessarily imply stability of bifurcating stripes.

On the other hand, we study the stability of stripes with respect to lattice modes or equivalently stability on certain rectangular domains with periodic boundary conditions. We show that advection can have a stabilising effect on the stripes, counteracting in particular the destabilising effect of quadratic terms. The consideration of periodic domains adapted to suitable wavevectors is a classical theme in amplitude equations, and is a standard tool in the context of Turing instabilities, see [26, 48, 59] and the references therein. However, the analysis of weak anisotropy seems scarce.

We take a direct approach and first study the existence of stripes with detailed expansions by Lyapunov-Schmidt reduction. We then analyse the large-wavelength stability via Floquet-Bloch decomposition in the spirit of [10, 40, 50]. Large wavelength modes, also called sideband modes, are well understood in one space dimension through the Ginzburg-Landau formalism, e.g., [10, 26, 56], most directly from the fourth order Swift-Hohenberg (SH) equation. Here only sideband modes are relevant and the so-called Eckhaus region describes the stability boundary, which is crossed when stretching or compressing the wavetrains too much. In two-dimensional space, instabilities along the stripe that is formed by trivially extending the one-dimensional wavetrain, become additionally relevant. The large-wavelength modes of this type give rise to the so-called zigzag stability boundary. It is well known that for the SH equation this is

crossed when wavetrains are stretched by any amount in the isotropic case, but detailed rigorous studies for RD systems (even without advection) seem scarce; in [48] a reduction to hexagonal lattices is applied. Indeed, zigzag stability can also be studied with the aid of a modulation equation, the so-called Newell-Whitehead-Segel equation, again most directly linked with the SH equation [26].

We study the stability of stripes on lattices by employing centre manifold reductions on domains that are nearly square and nearly ‘hexagonal’, i.e., with the hexagonal lattice for wavevectors. We expand the critical eigenvalues of the stripes in anisotropic spatial scaling as well as the system parameters. The advantages of this approach are that it is fully rigorous and that we gain direct access to all relevant characteristic quantities in terms of the advection, the quadratic terms, stretching and compressing. A particular motivation is to bridge the discussion of stripe stability in [59] for a variant of the Klausmeier model, where zigzag modes were not considered in any detail, with rather large advection to the results from [19] for zero advection.

The approach applies to an arbitrary number of components, but the parameter spaces and determination of signs of relevant characteristics become analytically less accessible for more than two components. Hence we restrict our attention to two-component systems.

Our main results may be summarised as follows.

Existence of stripes We prove the existence of striped solutions to (1.1) with small amplitude near the onset of Turing instability (Theorem 3.3.1). Specifically, the stripes are in one-to-one correspondence with the solutions to an algebraic equation, which characterises a family of supercritical pitchfork bifurcations. Solving the leading order of such an algebraic equation gives the bifurcation loci which form a family of hyperbolic paraboloids. We provide an expansion of striped solutions in the parameters and the velocity parameter c . In the context of activator-inhibitor systems, in case the first component is an inhibitor the direction of the stripe motion is with β , and it is opposite β if the first component is an activator. This verifies the uphill movement of the banded vegetation patterns.

Having established the existence of stripes, we obtain the following results concerning the stabilities of stripes against large-wavelength and lattice modes. In particular, the in/stability of stripes against the large-wavelength modes parallel and perpendicular to the stripes, is referred to as *zigzag* and *Eckhaus* in/stability, respectively. Our results on these types of instability at the onset of Turing bifurcation may be summarised as follows.

Zigzag instability We determine the leading order curvature of the spectrum for modes parallel to the stripes (Theorem 3.4.1). The leading order zigzag boundary is independent of α if $M = \text{Id}$ and $Q = 0$, as in the isotropic case of SH equation [26]. While in the presence of the generic M, Q , we highlight their impacts on the shape of the zigzag boundary. Moreover, the advection β has either a stabilising or destabilising effect. As a result, the different combinations of the

advection β , constant matrix M and quadratic nonlinearity Q allow for moving and tilting the zigzag boundary, which leads to various arrangements of stability boundaries. In particular, it is possible that stripes are zigzag unstable at the onset of Turing instability, which shows a limitation of the ‘Squire theorem’ of [59], i.e., the fact that a *homogeneous* steady state is always destabilised by modes that are constant in the direction perpendicular to the advection. Specifically, the destabilisation of homogeneous state via transverse modes is naturally inherited by the stripes and thus they are zigzag-unstable, whereas the stabilisation of homogeneous state are not necessarily inherited by the stripes, i.e., the zigzag-unstable stripes may still bifurcate (Remark 3.2.7).

Eckhaus instability We determine the leading order curvature of the spectrum for modes perpendicular to the stripes (Theorem 3.4.4). As with the well-known Eckhaus boundary in the isotropic case [26], the stripes are always Eckhaus-unstable near the onset of Turing instability in the anisotropic case as well, except for the stripes with critical Turing wavenumber, i.e. $\tilde{\kappa} = 0$. In the anisotropic case, the larger advection strength produces a larger Eckhaus-stable region for fixed unfolding parameter $\check{\alpha}$, i.e., the stripes are more resilient to stretching/compressing compared to the isotropic case. Nevertheless, in contrast to the zigzag instability, relative to the bifurcation loci there is no leading order impact of the advection on this Eckhaus instability.

We aim to determine the full in/stability of stripes against L^2 -perturbations. In terms of the zigzag and Eckhaus instability, for sufficiently small and non-zero advection, the stripes are always stable against L^2 -perturbations if they are both zigzag and Eckhaus stable (Corollary 3.2.6).

Stability against lattice modes Here we are concerned with finite wavenumber in/stability. In fact, it is shown in Corollary 3.2.6 that in the anisotropic case stripes are spectrally stable near the onset of Turing instability, which is reflected in the results of lattice modes as well. It is natural to consider domains whose Fourier wavevectors form periodic lattices and where the symmetric lattices are square (rotation by $\pi/2$) and hexagonal (rotation by $\pi/3$). We refer to the lattice modes considered on the (nearly) square and (nearly) ‘hexagonal’ domains as the *(quasi-)square* and *(quasi-)hexagonal modes*, respectively. It turns out that certain quasi-hexagonal modes are more unstable than others, and therefore the dominant stability boundaries are determined by such quasi-hexagonal modes.

We highlight that the advection competes with the quadratic nonlinearity, i.e., the advection has a stabilising effect on the stripes whereas the quadratic nonlinearity has a destabilising effect. Specifically, in the isotropic case and for the generic quadratic form, the stripes are always unstable against quasi-hexagonal modes near the onset, whereas in the anisotropic case the stripes are stable near the Turing bifurcation point. In particular, the Eckhaus instability mechanism is always dominant near the Turing bifurcation point in anisotropic case, which is consistent with Corollary 3.2.6.

1.5 Outline

This thesis is organised as follows.

In Chapter 2, we consider three types of reaction-subdiffusion models mentioned in §1.3 and study the stabilities of their homogeneous steady states. Specifically, concerning the first two types, we study the Turing instabilities by approximating the (pseudo-)spectrum, prove the convergence using Rouché’s theorem and prove the decays/growths using the inverse Laplace transform (ILT). Concerning the third type, we provide the energy estimate, dynamics of Fourier modes and prove the existence and uniqueness of Fourier modes. We illustrate these results by a number of numerical computations.

In Chapter 3, we consider the reaction-diffusion-advection system (1.1). We prove the existence of the striped solutions using the Lyapunov-Schmidt reduction. We study the stabilities of stripes against large-wavelength modes using the Floquet-Bloch decomposition and expanding the eigenvalue problem. We also analyse the stability of stripes against lattice modes and employ centre manifold reduction to derive a rigorous parameter expansion for the critical eigenvalues. We illustrate these results numerically using a concrete example and show numerical computations of the stabilities in the extended Klausmeier model for vegetation patterns.

In the Appendices, we provide the background on Fourier and Laplace transforms as well as the Wright function which is commonly used in subdiffusion equations. Then we provide some proofs of the main results in this thesis.

The results presented in Chapter 2 except §2.6 are contained in the preprint [69]. Chapter 3 is a combination of the preprints [70] and the manuscript [71] which are the collaborations with the co-author Eric Siero (Carl von Ossietzky University of Oldenburg).

The author of this thesis, Jichen Yang, contributed the main analyses and the numerical computations under the supervision of Jens Rademacher, except the numerical implementation and creation of figures in §3.6.2 contributed by the co-author Eric Siero.

Chapter 2

Reaction-subdiffusion systems

2.1 Introduction

We study the in/stability properties for three classes of reaction-subdiffusion equations (systems) mentioned in §1.3. We recall these models with two components and the scalar cases as follows.

Subdiffusion with extra source and sink We consider the scalar case

$$\partial_t u = d\mathcal{D}_{0,t}^{1-\gamma} \partial_x^2 u + f(u), \quad u \in \mathbb{R}, \quad (2.1)$$

where $d > 0$ is the diffusion coefficient and $f(u)$ is the nonlinear reaction term. We refer to [24] for the derivation of this equations, also cf. (2.17). The corresponding model for two components is given by [25]

$$\partial_t u = D\mathcal{D}_{0,t}^{1-\gamma} \partial_x^2 u + F(u), \quad u \in \mathbb{R}^2, \quad (2.2)$$

where $u \in \mathbb{R}^2$ is a vector of the perturbation densities, $D = \text{diag}(1, d)$ is a diagonal matrix of diffusion coefficients with positive diagonal entries, and $F(u)$ is a nonlinear vector where $F : \mathbb{R}^2 \rightarrow \mathbb{R}^2$.

Subdiffusion with linear creation and annihilation The scalar equation is given by [23]

$$\partial_t u = d e^{at} \mathcal{D}_{0,t}^{1-\gamma} \left(e^{-at} \partial_x^2 u \right) + au, \quad u \in \mathbb{R}, \quad (2.3)$$

where $a \in \mathbb{R}$ is the reaction rate. See also (2.18) for the derivation. The corresponding model for two components is given by [30, 47], with a constant matrix $A \in \mathbb{R}^{2 \times 2}$ as

$$\partial_t u = D e^{At} \mathcal{D}_{0,t}^{1-\gamma} \left(e^{-At} \partial_x^2 u \right) + Au, \quad u \in \mathbb{R}^2. \quad (2.4)$$

Subdiffusion with nonlinear creation and annihilation We recall the nonlinear model (1.7) as follow

$$\partial_t u = d \partial_x^2 \left(e^{\int_0^t r(u(x, \tau)) d\tau} \mathcal{D}_{0,t}^{1-\gamma} \left(u e^{-\int_0^t r(u(x, \tau)) d\tau} \right) \right) + r(u)u, \quad u \in \mathbb{R},$$

where $r : \mathbb{R} \rightarrow \mathbb{R}$. We refer to [14] for the details of the derivation. We focus on the linearisation in non-zero homogeneous steady state (1.8) reads

$$\partial_t u = d\partial_x^2 \left(\mathcal{D}_{0,t}^{1-\gamma} u - \sigma \mathcal{D}_{0,t}^{-\gamma} u + \sigma \mathcal{D}_{0,t}^{1-\gamma} \mathbf{1} \cdot \mathcal{D}_{0,t}^{-1} u \right) + \sigma u.$$

In particular, the stability of the solution for $\sigma < 0$.

This chapter is organised as follows: In §2.2, we briefly illustrate the derivations of the subdiffusion and three different reaction-subdiffusion equations. We introduce the background on fractional calculus, subdiffusion and Turing instability in §2.3. In §2.4, we consider (2.2) and perform a detailed spectral analysis. We prove the local convergence theorem, obtain large wavenumber asymptotics and show the Turing instability results. In §2.5, we consider (2.4) and give the analogous convergence theorem of spectra and the Turing instability analysis. In §2.6 we consider (1.7) and particularly the linearisation (1.8). We prove a local energy estimate, the existence and uniqueness of the Fourier solutions as well as their dynamics. We illustrate the results with a number of numerical computations.

2.2 Subdiffusion and reactions

We introduce the derivations of the diffusion, subdiffusion and reaction-subdiffusion equations from CTRW. Let $u(x, t) \in \mathbb{R}$ be the density or the concentration of the substances at position $x \in \mathbb{R}$ and time $t \geq 0$. We start with the following balance equation

$$u(x, t) = u(x, 0)\Psi(t) + \int_{\mathbb{R}} \int_0^t u(y, s)\phi(x - y)w(t - s)dsdy, \quad (2.5)$$

where $\phi(x)$ and $w(t)$ are the PDFs of displacement and waiting time, respectively. The so-called cumulative function $\Psi(t) = \int_t^\infty w(s)ds$ represents the probability that particles have no jump during the time interval $(0, t)$. The physical interpretation of the summands on the right-hand side as follows: The first summand represents the particles that stay at the position x from the initial time up to the time t ; the second summand represents the particles which moved from some position y and some past time $s < t$ to the position x and stay until time t . This is an integral equation which is nonlocal in both space and time, and the solutions provide the complete information of the diffusion processes. Using Fourier and Laplace transforms in space and time, respectively (cf. Appendices A.1 & A.2), the balance equation (2.5) leads to the following algebraic equation

$$\hat{u}(q, s) = \frac{1 - \tilde{w}(s)}{s} \frac{\hat{u}_0(q)}{1 - \hat{\phi}(q)\tilde{w}(s)} \quad (2.6)$$

where the ‘hat’ and the ‘tilde’ represent the Fourier and Laplace transforms, respectively; q is the spatial frequency (also called wavenumber), and s is the temporal frequency; $\hat{u}_0(q)$ is the Fourier transform of the initial condition $u(x, 0) = u_0(x)$.

Normal diffusion Let us consider a PDF of jump length given by the Gaussian distribution

$$\phi(x) = \frac{1}{\sqrt{4\pi\sigma^2}} \exp\left(-\frac{x^2}{4\sigma^2}\right) \quad (2.7)$$

which leads to the finite variance $\Sigma^2 = 2\sigma^2 < \infty$, together with a PDF of waiting time given by an exponentially decaying function

$$w(t) = \frac{1}{\tau} \exp\left(-\frac{t}{\tau}\right) \quad (2.8)$$

which leads to the finite expectation $T = \tau < \infty$. Then the corresponding Fourier and Laplace transforms of the PDFs can be expanded by

$$\hat{\phi}(q) = 1 - \sigma^2 q^2 + O(q^4), \quad (2.9)$$

$$\tilde{w}(s) = 1 - \tau s + O(s^2), \quad (2.10)$$

for sufficiently small $|q|, |s| \ll 1$. Small q and s in Fourier and Laplace spaces are corresponding to the large-scale and long-time limits in the physical space, respectively. Substituting (2.9) and (2.10) into (2.6) and the leading order reads

$$\hat{u}(q, s) = \frac{\hat{u}_0(q)}{s + dq^2}, \quad d = \sigma^2/\tau. \quad (2.11)$$

Then by using inverse Fourier-Laplace transform, the solution in physical space is given by

$$u(x, t) = \frac{1}{\sqrt{4\pi dt}} \int_{\mathbb{R}} e^{-\frac{|x-y|^2}{4dt}} u_0(y) dy. \quad (2.12)$$

On the other hand, rearranging the equation (2.11) yields

$$s\hat{u}(q, s) - \hat{u}_0(q) = -dq^2\hat{u}(q, s)$$

and using inverse Fourier-Laplace transform, yields

$$u_t = du_{xx}. \quad (2.13)$$

Notably, it is well known that the function (2.12) is the solution of (2.13) with initial condition $u(x, 0) = u_0(x)$. Since the PDFs of jump length and waiting time are both exponentially decaying, the (nonlocal) integral equation (2.5) finally reduces to the (local) diffusion equation (2.13) at the leading order.

Subdiffusion Let us consider the waiting time PDF given by an algebraically decaying function, cf. [35, Eq. 4.48], which has asymptotic behaviour

$$w(t) \sim \frac{\gamma}{\Gamma(1-\gamma)} \frac{\tau^\gamma}{t^{1+\gamma}} \quad \text{for } t \gg 1, \quad (2.14)$$

together with the jump length PDF given by Gaussian distribution (2.7). One can obtain the Laplace transform $\tilde{w}(s)$ using the Tauberian theorem which relates the behaviour of $\tilde{w}(s)$ near

the origin to the asymptotic behaviour of $w(t)$ as $t \rightarrow \infty$ [15]. As a result, the Laplace transform of $w(t)$ is given by

$$\tilde{w}(s) \sim 1 - (\tau s)^\gamma \quad \text{as } s \rightarrow 0$$

cf. [35]. Analogous to the derivation of the diffusion equation, substituting the above $\tilde{w}(s)$ together with (2.9) into (2.6) gives the leading order

$$\hat{u}(q, s) = \frac{\hat{u}_0(q)}{s + s^{1-\gamma} d_\gamma q^2}, \quad d_\gamma = \sigma^2 / \tau^\gamma. \quad (2.15)$$

Using inverse Fourier-Laplace transform, yields

$$u(x, t) = (\Phi(\cdot, t) * u_0)(x)$$

where $\Phi(x, t)$ is the fundamental solution (Green's function) of the subdiffusion equation and can be expressed by the series expansion (2.31) below. On the other hand, reformulating (2.15) yields,

$$s\hat{u}(q, s) - \hat{u}_0(q) = -s^{1-\gamma} d_\gamma q^2 \hat{u}(q, s),$$

and using the inverse Fourier-Laplace transform, yields

$$u_t = \mathcal{D}_{0,t}^{1-\gamma} d_\gamma u_{xx}, \quad (2.16)$$

with time-fractional Riemann-Liouville derivative $\mathcal{D}_{0,t}^{1-\gamma}$, cf. Definition 2.3.2, which is a nonlocal operator and thus causes memory in time. Unlike the normal diffusion, due to the slower decaying property of the waiting time PDF, the integral equation (2.5) cannot be localised by simply choosing the leading order term. In §2.3.2 below, we introduce some fundamental knowledge about the subdiffusion equation. We refer to [32, 33, 38] for more details about (1.3)

Subdiffusion with extra source and sink In [24], a balance equation for the density of substances $u(x, t) \in \mathbb{R}$ at position $x \in \mathbb{R}$ and time $t \geq 0$ is derived from the CTRW as

$$u(x, t) = u(x, 0)\Psi(t) + \int_{\mathbb{R}} \int_0^t u(y, s)\phi(x - y)w(t - s)dsdy + \int_0^t h(x, s)\Psi(t - s)ds, \quad (2.17)$$

with $\phi(x)$ the Gaussian distribution (2.7), and $w(t)$ a power law distribution (2.14). The function $h(x, s)$ represents the added or removed particles at position x and time $s < t$, and thus the source or sink.

A physical interpretation of the summands on the right-hand side of (2.17) as follows: The first and second summands have the same meaning as those on the right-hand side of (2.5), respectively; the last summand represents the particles which were added at (removed from) position x and time s , and remain at (do not return to) position x until time t .

The Fourier-Laplace transform of (2.17) gives an algebraic equation in terms of the Fourier transform of $\phi(x)$ and Laplace transform of $w(t)$. Considering the leading order large-scale, long-time limit and using the inverse Fourier-Laplace transform yield the reaction-subdiffusion equation (2.1), where $f(u(x, t))$ replaces $h(x, t)$ as the (nonlinear) reaction term, see [24] for details. The corresponding model for two components (2.2) is obtained by extending to two-components system.

Subdiffusion with linear creation and annihilation The idea of the model derived in [23] is that reactions occur at a constant per capita rate during the waiting time, i.e. $\partial_t u = au$ which gives $u(x, t) = u(x, t_0)e^{a(t-t_0)}$. The resulting analogue to the balance equation (2.5) is

$$u(x, t) = u(x, 0)e^{at}\Psi(t) + \int_{\mathbb{R}} \int_0^t u(y, s)e^{a(t-s)}\phi(x-y)w(t-s)dsdy. \quad (2.18)$$

Since all terms are positive for positive initial $u(x, 0)$, the density u is always positive; the amount of removed particles is always less than the existing ones. Compared to (2.17), the extra source or sink does not appear in the process in (2.18). Instead, the particles are created or annihilated intrinsically with exponential rate during the waiting time, cf. (2.5). The associated fractional differential equation reads (2.3). In the case of two species, (2.4) can also be derived from the CTRW, cf. [30].

Yet another model for which Turing-type instability has been discussed was proposed in [43] and reads

$$v(\mathbf{x}, t) = v(\mathbf{x}, 0)\delta(t) + \int_{\mathbb{R}^n} \int_0^t \phi(\mathbf{x} - \mathbf{y})w(t-s)e^{A(t-s)}v(\mathbf{y}, s)dsd\mathbf{y}, \quad (2.19)$$

where the components of $v(x, t) \in \mathbb{R}^N$ represent the number of particles which arrive at the position $\mathbf{x} \in \mathbb{R}^n$ exactly at time $t \geq 0$, and $v(\mathbf{x}, 0)\delta(t)$ represents the input of particles at initial time; here $\delta(t)$ is the Dirac delta distribution. The relation between (2.4) and (2.19) with $N = 2, n = 1$ is given by

$$u(x, t) = \int_0^t \Psi(t-s)e^{A(t-s)}v(x, s)ds, \quad (2.20)$$

cf. [30], which can lead to different behaviour of the individual solutions for two models.

Subdiffusion with nonlinear creation and annihilation Concerning nonlinear reactions, [14] incorporates the reaction term with nonlinear rate $r(u)$ into subdiffusive transport. The equation is then derived from CTRW and characterised by balance equations

$$u(x, t) = u(x, 0)e^{\int_0^t r(u(x,s))ds}\Psi(t) + \int_0^t v(x, s)e^{\int_s^t r(u(x,s))ds}\Psi(t-\tau)d\tau, \quad (2.21)$$

$$\begin{aligned} v(x, t) &= \int_{\mathbb{R}} u(x-y, 0)e^{\int_0^t r(u(x,s))ds}\phi(y)w(t)dy \\ &\quad + \int_0^t \int_{\mathbb{R}} v(x-y, \tau)e^{\int_\tau^t r(u(x-y,s))ds}\phi(y)w(t-\tau)dyd\tau, \end{aligned} \quad (2.22)$$

where $v(x, t) \in \mathbb{R}$ represents the numbers of particles arrive at position $x \in \mathbb{R}$ exactly at time $t \geq 0$. Combining (2.21) with (2.22) together and using Fourier-Laplace transform give the nonlinear reaction-subdiffusion equation (1.7). We refer to [14] for the physical interpretation and the details of the derivation.

2.3 Preliminaries

2.3.1 Fractional calculus

We define the Riemann-Liouville fractional integral and derivative for the subdiffusion range $\gamma \in (0, 1)$.

Definition 2.3.1. Let $f(t) \in L^1(0, T)$ for any $T > 0$. The integral

$$(\mathcal{D}_{0,t}^{-\gamma} f)(t) := \int_0^t \frac{(t-s)^{\gamma-1}}{\Gamma(\gamma)} f(s) ds, \quad \gamma \in (0, 1), \quad (2.23)$$

is called fractional integral of the order γ , where $\Gamma(\gamma)$ is Gamma function.

This fractional integral is the (Laplace) convolution with kernel $k_\gamma(t) := t^{\gamma-1}/\Gamma(\gamma)$ via

$$(k_\gamma * f)(t) := \int_0^t k_\gamma(t-s) f(s) ds, \quad (2.24)$$

i.e., $(\mathcal{D}_{0,t}^{-\gamma} f)(t) = (k_\gamma * f)(t)$. Notably, for $\gamma = 1$ we get $(\mathcal{D}_{0,t}^{-1} f)(t) = \int_0^t f(s) ds$.

Definition 2.3.2. For $f : [0, T] \rightarrow \mathbb{R}$ the Riemann-Liouville fractional derivative of order $1 - \gamma$ is (formally) defined as

$$(\mathcal{D}_{0,t}^{1-\gamma} f)(t) := \frac{d}{dt} (k_\gamma * f)(t) = \frac{d}{dt} \int_0^t \frac{(t-s)^{\gamma-1}}{\Gamma(\gamma)} f(s) ds, \quad \gamma \in (0, 1). \quad (2.25)$$

Notably, this fractional derivative is non-zero on constants,

$$(\mathcal{D}_{0,t}^{1-\gamma} 1)(t) = k_\gamma(t),$$

which tends to zero as $t^{\gamma-1}$ for $t \rightarrow \infty$ and is unbounded for $t \rightarrow 0$. At $\gamma = 1$, $\mathcal{D}_{0,t}^{1-\gamma}$ is the identity operator, i.e., $(\mathcal{D}_{0,t}^{1-\gamma} f)(t) = f(t)$, while for $\gamma = 0$, $(\mathcal{D}_{0,t}^{1-\gamma} f)(t)$ formally yields $(d/dt)(\delta * f)(t) = f'(t)$ with Dirac delta distribution $\delta(t)$ and $' := d/dt$.

A simple sufficient condition for the existence of the Riemann-Liouville fractional derivative is as follows.

Lemma 2.3.3 ([53], Lemma 2.2). Let $f(t) \in AC([0, T])$, then $(\mathcal{D}_{0,t}^{1-\gamma} f)(t)$ exists almost everywhere for $\gamma \in (0, 1)$. Moreover $(\mathcal{D}_{0,t}^{1-\gamma} f)(t) \in L^p(0, T)$, $1 \leq p < 1/(1 - \gamma)$, and

$$(\mathcal{D}_{0,t}^{1-\gamma} f)(t) = (k_\gamma * f')(t) + k_\gamma(t)f(0).$$

Here $AC([0, T])$ is the space of functions f which are absolutely continuous on $[0, T]$, i.e., $f(t) = c + \int_0^t g(s) ds$ for some $g \in L^1(0, T)$ and constant c .

The Laplace transform, denoted by \mathcal{L} , cf. Appendix A.2, will be used below and has the following property, see also [49, §2.8], [27, §2.2].

Lemma 2.3.4. Let $f : [0, \infty) \rightarrow \mathbb{R}$ be exponentially bounded, i.e., $|f(t)| \leq Ae^{ct}$ for some $A > 0$ and $c \in \mathbb{R}$. For $\operatorname{Re}(s) > \max\{0, c\}$ and $\gamma \in (0, 1)$ the following hold.

(1) If $f(t) \in L^1(0, T)$ for any $T > 0$, then $(\mathcal{L}\mathcal{D}_{0,t}^{-\gamma}f)(s) = s^{-\gamma}(\mathcal{L}f)(s)$.

(2) If $f(t) \in AC([0, T])$ for any $T > 0$, then $(\mathcal{D}_{0,t}^{-\gamma}f)(0) = 0$ and

$$(\mathcal{L}\mathcal{D}_{0,t}^{1-\gamma}f)(s) = s^{1-\gamma}(\mathcal{L}f)(s). \quad (2.26)$$

Proof. This directly follows from [27, Lemma 2.14 and Remark 2.8], where $\operatorname{Re}(s) > \max\{0, c\}$ stems from the calculation of $(\mathcal{L}\mathcal{D}_{0,t}^{-\gamma}f)(s)$ and guarantees convergence of the Laplace transform integral. In (2) we also used that $f(t) \in AC([0, T])$ is bounded so that $(\mathcal{D}_{0,t}^{-\gamma}f)(0) = 0$. \square

2.3.2 Subdiffusion equation

As mentioned, the analogue of the heat equation is the basic time-fractional diffusion equation is

$$\partial_t u = d\mathcal{D}_{0,t}^{1-\gamma} \partial_x^2 u, \quad u \in \mathbb{R}, x \in \mathbb{R}, \quad (2.27)$$

with diffusion coefficient $d > 0$, which we refer to as the subdiffusion equation. Compared to the heat equation, it is more subtle to see that solutions (2.27) remain positive and to determine the decay properties. We found this scattered in the literature and next give a brief account of these results.

For the Fourier-Laplace transform, the right-hand side of (2.27) defines the linear operator $\mathcal{L}_{\text{sub}} := \mathcal{D}_{0,t}^{1-\gamma} \partial_x^2$ with $\mathcal{L}_{\text{sub}} : AC([0, T]; H^2(\mathbb{R})) \rightarrow L^1(0, T; L^2(\mathbb{R}))$.

The Green's function of (2.27) has the Fourier transform [38, Eq. 49]

$$\widehat{\Phi}(q, t) = E_\gamma(-dq^2 t^\gamma), \quad (2.28)$$

where $E_\gamma(z) = \sum_{n=0}^{\infty} z^n / \Gamma(1 + n\gamma)$ is the Mittag-Leffler function and q is the wavenumber. The function (2.28) possesses the asymptotic behaviour [39, Eq. 20]

$$E_\gamma(-dq^2 t^\gamma) \sim \begin{cases} \exp(-\frac{dq^2 t^\gamma}{\Gamma(1+\gamma)}), & t \ll (dq^2)^{1/\gamma} \\ (dq^2 t^\gamma \Gamma(1 - \gamma))^{-1}, & t \gg (dq^2)^{1/\gamma} \end{cases} \quad (2.29)$$

which shows the effect of memory for non-zero wavenumber: short time exponential decay and long time algebraic decay, here with power $-\gamma$. Note the above separation of decay depends on the wavenumber. In Fourier-Laplace space, the Green's function of (2.27) is given by

$$(\mathcal{L}\widehat{\Phi})(q, s) = (s + dq^2 s^{1-\gamma})^{-1}, \quad \operatorname{Re}(s) > 0, \quad (2.30)$$

and for the inverse Laplace transform the poles of (2.30) with non-zero s contribute to the exponential growth/decay, while the trivial pole creates the algebraic decay, cf. Theorem 2.5.4 below.

We observe that the solutions to (2.27) have a self-similar scaling property, i.e. if $u(x, t)$ solves (2.27) then so does $u(\varepsilon x, \varepsilon^{2/\gamma} t)$ for $\varepsilon \in \mathbb{R}$. The similarity variable $x/t^{\gamma/2}$ leads to a series expansion of the Green's function [38, Eq. 46] [32, Eq. 4.23] given by

$$\Phi(x, t) = \frac{1}{\sqrt{4dt^\gamma}} \sum_{n=0}^{\infty} \frac{(-1)^n}{n! \Gamma(1 - \frac{\gamma}{2} - \frac{\gamma}{2}n)} \left(\frac{|x|}{\sqrt{dt^\gamma}} \right)^n, \quad t > 0, \quad (2.31)$$

In [32] this is related to the Wright function, which turns out to be positive and algebraically decaying locally uniformly in x for $t \gg 1$ with power $-\gamma/2$, and with power $-\gamma/(4 - 2\gamma) \in (-\gamma/2, 0)$ for $|x| \gg \sqrt{dt^\gamma}$. We give a few details in Appendix A.3.

As an aside we remark that the initial-boundary value problem (2.27) with homogeneous Dirichlet boundary condition has been studied in [34]. Here solutions decay pointwise algebraically with power $-\gamma$ for $t \gg 1$, i.e., faster than on the unbounded domain.

2.3.3 Turing instability

Consider a classical reaction-diffusion system (1.1) with two components, i.e., $N = 2$, namely

$$\partial_t u = D\partial_x^2 u + F(u), \quad u \in \mathbb{R}^2, \quad x \in \mathbb{R}, \quad (2.32)$$

where u is the vector of density of the species, $F(u)$ represents the reaction kinetics where $F : \mathbb{R}^2 \rightarrow \mathbb{R}^2$ and $D = \text{diag}(1, d)$ is the diagonal matrix of positive constant diffusion coefficients. Suppose that (2.32) possesses a homogeneous steady state $u_* = (u_{1*}, u_{2*})^T$, i.e., $F(u_*) = 0$. The linearisation of (2.32) about u_* is given by

$$\partial_t u = D\partial_x^2 u + Au, \quad A = (\partial_u F(u))_{u=u_*} =: \begin{pmatrix} a_1 & a_2 \\ a_3 & a_4 \end{pmatrix}. \quad (2.33)$$

In an activator-inhibitor system $a_1 > 0$ and $a_4 < 0$. A Turing or diffusion-driven instability occurs if the homogeneous steady state of (2.32) is strictly linearly stable in the absence of diffusion, but is linearly unstable in the presence of diffusion. Being a 2-by-2 matrix, strictly linear stability without diffusion means $\text{tr}(A) = a_1 + a_4 < 0$ and $\det(A) = a_1 a_4 - a_2 a_3 > 0$.

The right-hand side of (2.33) defines the linear operator $\mathcal{L} := D\partial_x^2 + A$, whose eigenvalue problem reads

$$\mathcal{L}u = D\partial_x^2 u + Au = su,$$

where s is the temporal eigenvalue. In Fourier space, the eigenvalue problem becomes

$$\mathcal{L}\hat{u} = -q^2 D\hat{u} + A\hat{u} = s\hat{u},$$

where q is the wavenumber, and yields the dispersion relation

$$D_{\text{reg}}(s, q^2) := \det(s\text{Id} + q^2 D - A) = (s + q^2 - a_1)(s + dq^2 - a_4) - a_2 a_3 = 0. \quad (2.34)$$

The solutions set $\Lambda_{\text{reg}} := \{s \in \mathbb{C} : D_{\text{reg}}(s, q^2) = 0 \text{ for a } q \in \mathbb{R}\}$ is the L^2 -*spectrum* of \mathcal{L} with domain $(H^2(\mathbb{R}))^2$, e.g., [54]. In order to distinguish this from spectra in the subdiffusion cases, we refer to it as the *regular spectrum*.

Concerning (2.32), the homogeneous steady state u_* is called strictly spectrally stable (unstable) if $\max(\text{Re}(\Lambda_{\text{reg}})) < 0 (> 0)$. It is then also linearly and nonlinearly stable (unstable) for (2.33) and (2.32), respectively [54]. Furthermore, it is well known [41, Eq. 2.27] that there exists a critical diffusion coefficient (also called Turing bifurcation point or Turing threshold) d_c for which (i) $\text{sgn}(\max(\text{Re}(\Lambda_{\text{reg}}))) = \text{sgn}(d - d_c)$ and (ii) in case $d = d_c$ we have $D_{\text{reg}}(s_c(q), q^2) = 0$ for $q^2 \approx q_c^2$ with real $s_c \approx -s_0(q - q_c)^2$, $s_0 > 0$.

2.4 Subdiffusion with source and sink

As the first reaction-subdiffusion model, we consider (2.2). We will study linear stability properties of a homogeneous steady state u_* where $F(u_*) = 0$.

The (formal) linearisation of (2.2) in u_* reads

$$\partial_t u = D\mathcal{D}_{0,t}^{1-\gamma} \partial_x^2 u + Au, \quad u \in \mathbb{R}^2, \quad A \in \mathbb{R}^{2 \times 2}, \quad (2.35)$$

its Fourier-transform with respect to $x \in \mathbb{R}$ is

$$\partial_t \hat{u} = -q^2 D\mathcal{D}_{0,t}^{1-\gamma} \hat{u} + A\hat{u}, \quad u \in \mathbb{R}^2, \quad (2.36)$$

and the Fourier-Laplace transform reads

$$(s\text{Id} + s^{1-\gamma} q^2 D - A) \mathcal{L} \hat{u} = \hat{u}_0, \quad \text{Re}(s) > 0, \quad q \in \mathbb{R},$$

Analogous to (2.34) we obtain the dispersion relation

$$\begin{aligned} D_{ss}(s, q^2) &:= \det(s\text{Id} + s^{1-\gamma} q^2 D - A) \\ &= (s + s^{1-\gamma} q^2 - a_1)(s + s^{1-\gamma} dq^2 - a_4) - a_2 a_3 = 0, \quad s \in \Omega_0^+, \end{aligned}$$

where $\Omega_0^+ := \{s \in \mathbb{C} : \arg(s) \in (-\pi/2, \pi/2)\}$.

Branch and branch cut Since $s^{1-\gamma}$ is a multivalued function in \mathbb{C} , we need to choose a branch which preserves positive reals. For given $q \in \mathbb{R}$ we choose $\theta_1(q) \in (0, \pi/2)$ such that on the branch cut

$$\mathfrak{B}_0^{\theta_1(q)} := \{s \in \mathbb{C} : \text{Im}(s)/\text{Re}(s) = \tan(\theta_1(q)), \text{Re}(s) < 0\}$$

there is no solution of the dispersion relation, i.e., $D_{ss}(s, q^2) \neq 0$ for $s \in \mathfrak{B}_0^{\theta_1(q)}$.

Since Theorems 2.4.5 for (2.36) and Theorem 2.5.4 for (2.4) give decay and growth behaviour essentially independent of θ_1 , for simplicity we suppress the dependence of θ_1 on q . The corresponding principal branch is defined by

$$\Omega_0 := \{s \in \mathbb{C} \setminus \{0\} : \arg(s) \in (-\pi + \theta_1, \pi + \theta_1), \theta_1 \in (0, \pi/2)\}.$$

Setting $s^\delta = z$, where $\delta := 1 - \gamma$, we obtain $z \in \Sigma_0 := \{z \in \mathbb{C} \setminus \{0\} : \arg(z) \in ((-\pi + \theta_1)\delta, (\pi + \theta_1)\delta)\}$ if and only if $s \in \Omega_0$. Since $\operatorname{Re}(s) > 0$, we restrict our dispersion relation to $s \in \Omega_0^+$ and $z \in \Sigma_0^+ := \{z \in \Sigma_0 : \arg(z) \in (-\pi\delta/2, \pi\delta/2)\}$.

Remark 2.4.1. *In the computation of the ILT, we consider the integral along a vertical line in Ω_0^+ . It is natural to take the Bromwich contour (Fig. B.1) and combine it with the residue theorem in order to calculate the ILT. However, this does not only depend on the roots of the dispersion relation in Ω_0^+ , but also in $\Omega_0^{0-} := \Omega_0 \setminus \Omega_0^+$. Hence, in order to study the temporal behaviour of \hat{u} , we extend the domain of D_{ss} and consider*

$$D_{ss}(s, q^2) = (s + s^{1-\gamma}q^2 - a_1)(s + s^{1-\gamma}dq^2 - a_4) - a_2a_3 = 0, \quad s \in \Omega_0. \quad (2.37)$$

Definition 2.4.2. We call the set of roots $\Lambda_{ss}^+ := \{s \in \Omega_0^+ : D_{ss}(s, q^2) = 0 \text{ for a } q \in \mathbb{R}\}$ (subdiffusion) spectrum of the linear operator $\mathcal{L}_{ss} := D\mathcal{D}_{0,t}^{1-\gamma}\partial_x^2 + A$, and the set of roots $\Lambda_{ss}^{0-} := \{s \in \Omega_0^{0-} : D_{ss}(s, q^2) = 0 \text{ for a } q \in \mathbb{R}\}$ (subdiffusion) pseudo-spectrum of \mathcal{L}_{ss} .

We denote $\Lambda_{ss} := \Lambda_{ss}^{0-} \cup \Lambda_{ss}^+$, $\Omega_0^- := \Omega_0^{0-} \setminus i\mathbb{R}$. As usual for spectral stability, we say the (pseudo-)spectrum of \mathcal{L}_{ss} is (strictly) *stable (unstable)* if $\sup(\operatorname{Re}(\Lambda_{ss})) < 0 (> 0)$.

For our result on algebraic decay, the expansion yields the following technical hypotheses for non-zero coefficients.

Hypothesis 2.4.3. Given $q \in \mathbb{R}$ and reduced fraction $\gamma = 1 - \ell/m$, $\ell, m \in \mathbb{Z}_+$, let k_j be the multiplicity of the roots z_j of the polynomial in z of degree $2m$ defined by $D_{ss}(z^m, q^2)$, so $\sum_j k_j = 2m$. Let

$$\alpha_{jk} := \frac{1}{(k_j - k)!} \lim_{z \rightarrow z_j} \left(\frac{d}{dz} \right)^{k_j - k} \frac{(z - z_j)^{k_j} P(z^m)}{D_{ss}(z^m, q^2)}$$

and, for at least one of $P(s) = 1$ or $P(s) = s + s^{\ell/m}dq^2 - a_4$ or $P(s) = s + s^{\ell/m}q^2 - a_1$, assume

$$\sum_j \sum_{k=1}^{k_j} \alpha_{jk} k(-z_j)^{-k-1} \neq 0.$$

Remark 2.4.4. For simple roots, $k_j = 1$ for all j , we show in Appendix B.1 that Hypothesis 2.4.3 simplifies to $\sum_{j=1}^{2m} P(z_j^m) / (\partial_s D_{ss}(z_j^m, q^2) m z_j^{m+1}) \neq 0$. Hypothesis 2.4.3 can be checked numerically, e.g., for the model in [25, Section 4.4], we found the coefficient C_{alg} is non-zero for generic parameters, wavenumbers and anomalous exponents γ .

Theorem 2.4.5. Let $\gamma \in (0, 1) \cap \mathbb{Q}$ be a reduced fraction with denominator m and $\lambda := \sup(\operatorname{Re}(\Lambda_{ss}))$.

- (1) If $\lambda > 0$ then $S^+ := \{(s, q) \in \Omega_0^+ \times \mathbb{R} : D_{ss}(s, q^2) = 0 \text{ and } \operatorname{Re}(s) \text{ maximal}\} \neq \emptyset$ and for any $(s, q) \in S^+$ the solution to (2.36) for almost all initial data satisfies $\hat{u}(q, t) = C_{\text{exp}} t^{k-1} e^{st} + o(t^{k-1} e^{\operatorname{Re}(s)t})$ for a non-zero $C_{\text{exp}} \in \mathbb{C}^2$, where k is the multiplicity of root $z = s^{1/m}$ of the polynomial $D_{ss}(z^m, q^2)$.

- (2) If $\lambda = 0$, then $Q^- := \{q \in \mathbb{R} \setminus \{0\} : s \in \Omega_0^- \text{ and } (s, q) \text{ solves } D_{ss}(s, q^2) = 0\} \neq \emptyset$ and for any $q \in Q^-$ there exists $C_{\text{alg}} \in \mathbb{C}^2$ such that $\hat{u}(q, t) = C_{\text{alg}} t^{-1-1/m} + o(t^{-1-1/m})$, and $C_{\text{alg}} \neq 0$ under Hypothesis 2.4.3 for almost all initial data.
- (3) If $\lambda < 0$ or $\Lambda_{ss} = \emptyset$, then for any $q \in \mathbb{R} \setminus \{0\}$ there exists $C_{\text{alg}} \in \mathbb{C}^2$ such that $\hat{u}(q, t) = C_{\text{alg}} t^{-1-1/m} + o(t^{-1-1/m})$, and $C_{\text{alg}} \neq 0$ under Hypothesis 2.4.3 for almost all initial data.

We defer the technical proof to Appendix B.1.

Regarding the case $q = 0$, note that (2.36) then reduces to $\partial_t \hat{u} = A \hat{u}$ whose solutions decay exponentially due to the assumption on the Turing instability.

Remark 2.4.6. A more detailed decomposition into exponential terms and algebraically decaying terms, including formulae for C_{exp} , C_{alg} is given in (B.4) ((B.6) in case of multiple roots).

In particular, Theorem 2.4.5 reveals the roots of (2.37) determine the temporal behaviour of \hat{u} as exponentially growing for unstable spectrum, and algebraically decaying for strictly stable pseudo-spectrum. Therefore, the main work of the present section is to analyse the (pseudo-)spectrum.

Remark 2.4.7. Somewhat surprisingly, the algebraic decay rate in Theorem 2.4.5 depends only on the denominator of the rational γ . However, our approach does not apply to irrational γ for which the decay remains an open problem to our knowledge.

Here we do not transfer the decay to physical x -space and related function spaces, since the dependence of the constants in the estimate on the wavenumber are convoluted.

Notably, the algebraic decay with $t^{-3/2}$ [25, Eq. 4.27] where $\gamma = 1/2$ and $\theta_1 = 0$ is a special case of Theorem 2.4.5.

Remark 2.4.8. The ansatz $u(x, t) = v(t)e^{iqx}$ is a specific case of the Fourier transform and substitution into (2.35) also gives the fractional ODE (2.36). Hence, the initial condition in Theorem 2.4.5 can be seen as $\hat{u}(q, 0) = \hat{v}_0 e^{iqx}$, where $\hat{v}_0 \in \mathbb{R}^2$. Such an ansatz can find spatially period solutions, and can be applied equally to the model (2.4). We do not discuss this further here.

2.4.1 Scalar case

In order to illustrate further the fundamental difference between $\gamma = 1$ (normal diffusion) and $\gamma \neq 1$ (subdiffusion), we consider the scalar case of (2.35),

$$\partial_t u = d\mathcal{D}_{0,t}^{1-\gamma} \partial_x^2 u + au, \quad u \in \mathbb{R}, a \in \mathbb{R}. \quad (2.38)$$

The dispersion relation is given by

$$d_{ss}(s, q^2) = s + dq^2 s^\delta - a = 0, \quad s \in \Omega_0, q \in \mathbb{R}, \quad (2.39)$$

where $\delta = 1 - \gamma$. Clearly, $s = a$ is the unique solution of (2.39) for $q = 0$.

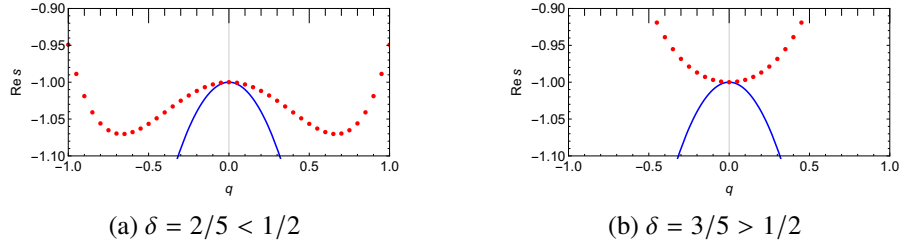


Figure 2.1: Comparison of numerically computed regular spectra (blue solid, $\delta = 0$) and pseudo-spectra (red dotted) of (2.35) for $a < 0$, $\theta_1 = \pi/2$.

Remark 2.4.9. *The branch point $s = 0$ is a solution to $d_{ss} = 0$ if and only if $a = 0$, i.e., the case of the subdiffusion equation, cf. §2.3.2. Theorem 2.4.5 does not apply and the long term decay is $t^{-\gamma}$, which is as predicted by the more general Theorem 2.5.4 below.*

In the following, we give some characteristics of the (pseudo-)spectrum of (2.38).

Lemma 2.4.10. *For any $\delta \in (0, 1)$ a unique smooth curve of solutions $s = s(q)$ to (2.39) crosses $s = a$ at $q = 0$. For $0 < |q| \ll 1$ we have $s(q) < a$ if either $a > 0$ or $a < 0$ as well as $\delta \in (0, 1/2)$, while $s(q) > a$ if $a < 0$ and $\delta \in (1/2, 1)$.*

Proof. Implicit differentiation of the left-hand side with respect to q^2 and s at $s = a$, $q = 0$ gives da^δ and 1, respectively. The statement follows from the implicit function theorem and $a^\delta > 0$ for $a > 0$, and $\text{sgn}(\text{Re}(a^\delta)) = \text{sgn}(1/2 - \delta)$ for $a < 0$ with $\delta \in (0, 1)$. \square

Lemma 2.4.10 shows the concavity of (pseudo-)spectrum for $|q| \ll 1$, and Fig. 2.1 illustrate it numerically. However, the concavity changes for larger $|q|$, cf. Fig. 2.1a. In the following, we give the analysis and numerical computation of (pseudo-)spectrum.

Lemma 2.4.11. *If $a > 0$, then for each $q \in \mathbb{R}$ the solution $s = s(q)$ to (2.39) in Ω_0^+ is unique, positive and satisfies $\lim_{|q| \rightarrow \infty} s(q) = 0$.*

Proof. First, we show that the solution of (2.39) must be positive in Ω_0^+ . Set $s = re^{i\theta}$, $r > 0$ and $\theta \in (-\pi/2, \pi/2)$, then we can rewrite (2.39) as $re^{i\theta} + dq^2 r^\delta e^{i\delta\theta} = a$. Since $a \in \mathbb{R}$, the imaginary part of the left-hand side must be zero, i.e., $r \sin(\theta) + dq^2 r^\delta \sin(\delta\theta) = 0$, which is equivalent to $\theta = 0$ since $\delta \in (0, 1)$. Hence we have $s > 0$.

Clearly, $s = a$ is the unique solution for $q = 0$. Implicit differentiation of the left-hand side of (2.39) with respect to s gives $1 + dq^2 \delta s^{\delta-1}$ which is continuous and non-zero for any $q \in \mathbb{R}$ and $s > 0$. Therefore, the uniqueness for $|q| \ll 1$ can be extended to all $q \in \mathbb{R}$.

Since $s > 0$ we can rescale $q^2 = \kappa^2/s^\delta$ with $\kappa \in \mathbb{R}$, cf. [42, Section 4.1], which gives

$$s + d\kappa^2 - a = 0, \quad s > 0, \quad \kappa \in \mathbb{R}. \quad (2.40)$$

As $a > 0$, the solution of (2.40) is a parabola in the (κ, s) -plane and $s \rightarrow 0$ for $\kappa^2 \rightarrow a/d$. Hence, according to the scaling $q^2 \rightarrow \infty$ as $\kappa^2 \rightarrow a/d$. In contrast, $s \rightarrow 0$ for $q^2 \rightarrow \infty$ in (q, s) -plane. See the right column in Fig. 2.2. \square

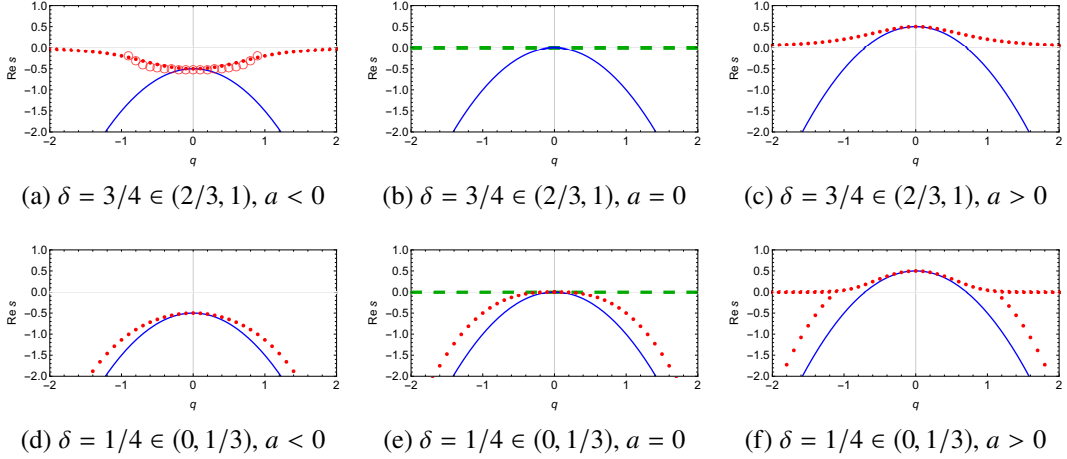


Figure 2.2: Model (2.38). Blue solid lines: regular spectra; red dotted lines: subdiffusion (pseudo-)spectrum; green dashed lines: $s(q) = 0 \notin \Omega_0$. Here $\theta_1 = \pi/2$. In (b) the (pseudo-)spectrum is empty. In case $\delta \in [1/3, 2/3]$: the (pseudo-)spectrum for $a = 0$ and $a > 0$ are qualitatively same as (b) and (c), respectively, whereas the pseudo-spectrum for $a < 0$ (hollow circle) is empty for large $|q|$.

Solving (2.39) explicitly for general $a \in \mathbb{R}$, $s \in \Omega_0$, seems not possible, but we can approximate solutions for $|q| \gg 1$ as follows.

Lemma 2.4.12. *For any $\delta \in (0, 1)$, there exists a $Q > 0$, such that for $q > Q$, the solutions to (2.39) are approximated by $s_0(q)$ and $s_\infty(q)$, where*

- (1) $s_0(q) \in \Omega_0^+$ and $\lim_{|q| \rightarrow \infty} s_0(q) = 0$ for any $a > 0$,
- (2) $s_0(q) \in \Omega_0^-$ and $\lim_{|q| \rightarrow \infty} s_0(q) = 0$ for any $a < 0$ and $\delta \in (\pi/(\pi + \theta_1), 1)$,
- (3) $s_\infty(q) \in \Omega_0^-$ and $\lim_{|q| \rightarrow \infty} s_\infty(q) = -\infty$ for any $\delta \in (0, \theta_1/(\pi + \theta_1))$.

Proof. A straightforward computation gives the solutions to (2.39) for $|q| \gg 1$ as

$$s_0(q) = \left(\frac{a}{dq^2} \right)^{1/\delta} + o\left(q^{-2/\delta}\right), \quad (2.41)$$

$$s_\infty(q) = \left(-dq^2\right)^{\frac{1}{1-\delta}} + \frac{a}{1-\delta} + o(1), \quad (2.42)$$

where $\lim_{|q| \rightarrow \infty} o(1) = 0$. See also the proof of Lemma 2.4.18 for $s_0(q)$ and $s_\infty(q)$.

Concerning $s_0(q)$: For $a > 0$ the leading order term is positive real and $\lim_{|q| \rightarrow \infty} s_0(q) = 0$, which coincides with Lemma 2.4.11. For $a < 0$ the argument of the leading order term is π/δ so $\arg(s_0) \in \Omega_0$ if $\pi/\delta \in (-\pi + \theta_1, \pi + \theta_1)$ which leads to $\delta > \pi/(\pi + \theta_1)$ (cf. Fig. 2.2a). Since $\delta \in (0, 1)$, we have $\pi/\delta > \pi$, which leads to $\operatorname{Re}(s_0) < 0$.

Concerning $s_\infty(q)$: We note that the leading order term is independent of a and its argument is $\pi/(1 - \delta)$. Then we have $\arg(s_\infty) \in \Omega_0$ if $\pi/(1 - \delta) \in (-\pi + \theta_1, \pi + \theta_1)$ which implies $\delta < \theta_1/(\pi + \theta_1)$ (cf. bottom row in Fig. 2.2). Since $\delta \in (0, 1)$, we have $\pi/(1 - \delta) > \pi$, which leads to $\operatorname{Re}(s_\infty) < 0$. \square

Remark 2.4.13. *The choice of branch cut is relevant here: if $\theta_1 \rightarrow 0$, then $\pi/(\pi + \theta_1) \rightarrow 1$ and $\theta_1/(\pi + \theta_1) \rightarrow 0$, which leads to the disappearance of red dotted (pseudo)-spectrum in Fig. 2.2. Nevertheless, it is instructive to choose $\theta_1 = \pi/2$ as this reveals all phenomena in the pseudo-spectrum, in particular regarding the relation to the regular spectrum.*

We note that the plotting of $s = 0$ (green dashed) in the middle column of Fig. 2.2 only shows the transition of $s_0(q)$ from negative to positive but is not in the (pseudo-)spectrum. Moreover, for instance in Fig. 2.2b, the (pseudo-)spectrum is empty. Yet, by Theorem 2.4.5 there is still algebraic decay, at least for rational δ .

For constant initial $u(0, x) = u_0 \in \mathbb{R}$ (2.38) is the ODE $\dot{u} = au$ so $a < 0$ indeed yields exponential decay. Fourier-transforming (2.38) in x gives

$$\partial_t \hat{u} = -dq^2 \mathcal{D}_{0,t}^{1-\gamma} \hat{u} + a\hat{u}, \quad (2.43)$$

and, for rational $\gamma = n/m$ (reduced fraction), Theorem 2.4.5 implies each Fourier mode decays algebraically as $t^{-1-1/m}$ for $a < 0$.

2.4.2 Convergence to regular spectrum

We return to the system (2.35) and study the convergence of subdiffusion (pseudo-)spectrum for $\gamma \rightarrow 1$, i.e., as the anomalous exponent approaches normal diffusion $\gamma = 1$. With $\delta = 1 - \gamma$ the dispersion relation (2.37) can be written as

$$D_{ss}(s, q^2) = (s + s^\delta q^2 - a_1)(s + s^\delta dq^2 - a_4) - a_2 a_3 = 0, \quad s \in \Omega_0, \quad (2.44)$$

and we consider $\delta \rightarrow 0$. In preparation, we note that the difference between subdiffusion and regular dispersion relation is

$$\begin{aligned} E(s, q^2) &= D_{ss}(s, q^2) - D_{reg}(s, q^2) \\ &= (s^\delta - 1) \left((q^2 + dq^2)s + dq^4 s^\delta + dq^4 - a_4 q^2 - a_1 dq^2 \right). \end{aligned}$$

Lemma 2.4.14. *The subdiffusion (pseudo-)spectrum converges to the regular spectrum locally uniformly in $q \in \mathbb{R}$ as $\gamma \rightarrow 1$.*

Proof. Denote $f(s) := D_{reg}(s, q^2)$ and $g(s) := E(s, q^2)$, then $f(s) + g(s) = D_{ss}(s, q^2)$. First, we claim that for fixed parameters and wavenumber q , $g(s) \rightarrow 0$ locally uniformly in $s \in \Omega_0$ as $\delta \rightarrow 0$. This follows from $s^\delta - 1 = e^{\delta \ln s} - 1$ being holomorphic in Ω_0 with $e^{\delta \ln s} - 1 \rightarrow 0$ pointwise in Ω_0 as $\delta \rightarrow 0$.

Second, we discuss $f(s)$. For fixed parameters and wavenumber q , there are two regular eigenvalues $s_1, s_2 \in \mathbb{C}$ and $f(s) \neq 0$ for $s \neq s_1, s_2$, cf. Fig. 2.3a. We choose two disjoint open balls $B_{r_1}(s_1)$ and $B_{r_2}(s_2)$, where $B_{r_*}(s_*) := \{s \in \Omega_0 : |s - s_*| < r_*\}$. Then we have $f(s) \neq 0$ for $s \in \partial B_{r_j}(s_j)$, $j = 1, 2$. From the first step, we know that $g(s) \rightarrow 0$ as $\delta \rightarrow 0$, hence $|f(s)| > |g(s)|$ for $s \in \partial B_{r_j}(s_j)$, $j = 1, 2$ as $\delta \rightarrow 0$. Since $f(s)$ and $g(s)$ are holomorphic in Ω_0 ,

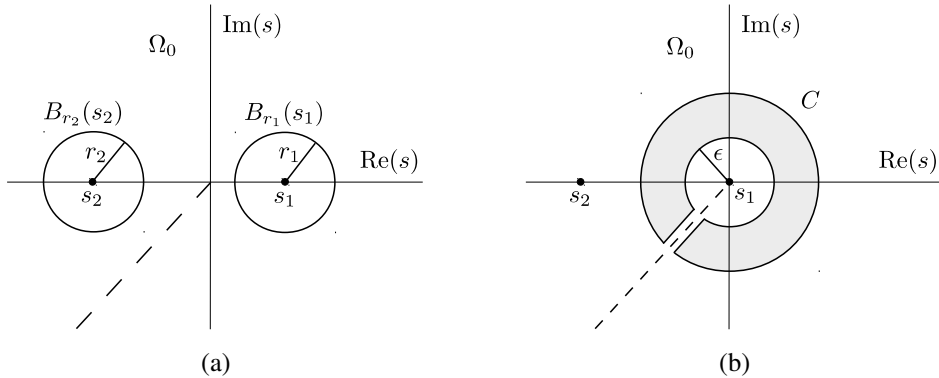


Figure 2.3: Dashed straight lines: branch cut $\mathcal{B}_0^{\theta_1}$. Illustrations of the case when the regular spectrum at fixed q is (a) different from 0 (b) contains the origin; here the grey region is the interior of the contour C .

Rouché's theorem implies $f + g$ also has two zeros $s_1(\delta)$ and $s_2(\delta)$ inside $B_{r_1}(s_1)$ and $B_{r_2}(s_2)$, respectively. Since we can choose r_j arbitrarily small as $\delta \rightarrow 0$ we have $s_j(\delta) \rightarrow s_j$ locally uniformly in q , $j = 1, 2$.

However, the regular spectrum can contain 0, whereas $g(s)$ is not holomorphic on $\mathfrak{B}_0^{\theta_1}$. In such a case, we take a neighbourhood $B_\epsilon(0)$ of the origin and choose a contour C such that its interior covers a region near 0, but excludes $B_\epsilon(0)$ and $\mathfrak{B}_0^{\theta_1}$, cf. Fig. 2.3b. Since there is no zero of f inside C , Rouché's theorem implies that there is no zero of $f + g$ inside C as $\delta \rightarrow 0$ either. Hence the zeros of $f + g$ have to be in $B_\epsilon(0)$ and also such zeros of $f + g$ will converge to 0 as $\delta \rightarrow 0$. \square

Theorem 2.4.15. *For any compact set $K \subset\subset \Omega_0$, $\lim_{\gamma \rightarrow 1} (K \cap \Lambda_{ss}) = (K \cap \Lambda_{reg})$.*

Proof. Lemma 2.4.14 shows that the subdiffusion (pseudo-)spectrum converges to the regular spectrum in any compact set of wavenumber. Lemma 2.4.18 below tells us the subdiffusion (pseudo-)spectrum either tends to 0 (denote by $s_0(q)$) or the real part tends to $-\infty$ for $|q| \gg 1$, i.e., outside the compact set of wavenumber. If the regular spectrum contains 0, then the (pseudo-)spectrum naturally converges to the regular one in a compact set of Ω_0 . If the regular spectrum is negative for maximum, then Corollary 2.4.23 below shows that $s_0(q)$ does not exist in Ω_0 for $|q| \gg 1$ as $\delta \rightarrow 0$. Therefore, the claim is proved. \square

We illustrate the convergence theorem numerically in Fig. 2.5.

2.4.3 Real spectrum and (pseudo-)spectrum for large wavenumber

As in the scalar case, we cannot solve the dispersion relation (2.44) explicitly in general. However, as in Lemma 2.4.11 we can determine real unstable spectrum as follows. This was observed in [42, Eq. 4.7] and we include the proof for completeness.

Lemma 2.4.16. $D_{\text{reg}}(s_r, \kappa^2) = 0$ with $\kappa \in \mathbb{R}$ and $s_r > 0$ if and only if $D_{\text{ss}}(s_r, q^2) = 0$ with $q = \kappa s_r^{-\delta/2} \in \mathbb{R}$.

Proof. Rescaling the wavenumber of the regular and subdiffusion dispersion relation (2.34) and (2.44), we find the relation

$$\begin{aligned} D_{\text{reg}}(s_r(\kappa), \kappa^2) &= \left(s_r(\kappa) + \kappa^2 - a_1 \right) \left(s_r(\kappa) + d\kappa^2 - a_4 \right) - a_2 a_3 \\ &= \left(s_r(\kappa) + s_r^\delta(\kappa) \frac{\kappa^2}{s_r^\delta(\kappa)} - a_1 \right) \left(s_r(\kappa) + s_r^\delta(\kappa) \frac{d\kappa^2}{s_r^\delta(\kappa)} - a_4 \right) - a_2 a_3 \\ &= D_{\text{ss}} \left(s_r(\kappa), \frac{\kappa^2}{s_r^\delta(\kappa)} \right) \\ &= D_{\text{ss}}(s_r(\kappa), q^2(\kappa)), \end{aligned}$$

where

$$q(\kappa) = \kappa s_r^{-\delta/2}(\kappa), \quad q(\kappa) \in \mathbb{R}, \quad (2.45)$$

and $s_r(\kappa)$ denotes the regular spectrum with wavenumber κ . \square

The following consequence of the lemma was noticed in [42, Section 4.1]. Again for completeness and in preparation of the following, we include the simple proof.

Proposition 2.4.17. *For any $\delta \in (0, 1)$, if the diffusion coefficient $d > d_c$, then there exists a curve of real and strictly positive subdiffusion spectrum $s_0(q)$ with $q \in [\pm q_{\min}, \pm \infty)$. Furthermore, $\lim_{d \rightarrow d_c} q_{\min} = \infty$ and $\lim_{|q| \rightarrow \infty} s_0(q) = 0$. Specifically, $s_0(q) = s_r(\kappa)$ and $q = \kappa s_r^{-\delta/2} \in \mathbb{R}$.*

Proof. For $d > d_c$ there is a curve of real unstable regular spectrum $s_r(\kappa) > 0$ and $s_0(q)$ is given by Lemma 2.4.16, i.e., $s_0(q(\kappa)) = s_r(\kappa)$. Specifically, there is an interval (κ_-^2, κ_+^2) such that $s_r(\kappa) > 0$ for $\kappa^2 \in (\kappa_-^2, \kappa_+^2)$. If $\kappa^2 \rightarrow \kappa_-^2, \kappa_+^2$, then $s_r(\kappa) \rightarrow 0$, which leads to $s_0(q) \rightarrow 0$ and $q(\kappa) \rightarrow \infty$. Furthermore, from (2.45) $q_{\min}^2 := \min_{\kappa^2 \in (\kappa_-^2, \kappa_+^2)} q^2(\kappa) = \min_{\kappa^2 \in (\kappa_-^2, \kappa_+^2)} \kappa^2 / s_r^\delta(\kappa)$, and $q_{\min}^2 \rightarrow \infty$ as $d \rightarrow d_c$. \square

We illustrate Proposition 2.4.17 numerically in Fig. 2.6. Note that the curve from Proposition 2.4.17 is only one part of the subdiffusion spectrum when $d > d_c$. Similar to the scalar case, next we discuss the (pseudo-)spectrum for $|q| \gg 1$.

Lemma 2.4.18. *For any $\delta \in (0, 1)$ the solutions to (2.44) for $|q| \gg 1$ are approximated by $s_{\infty 1}(q)$, $s_{\infty 2}(q)$ and $s_{0\pm}(q)$ that satisfy $\lim_{|q| \rightarrow \infty} s_{0\pm}(q) = 0$ and $\lim_{|q| \rightarrow \infty} \operatorname{Re}(s_{\infty j}(q)) = -\infty$, $j = 1, 2$. Moreover, there exists a $Q > 0$ such that for $q > Q$ and $\delta \in (0, \theta_1/(\pi + \theta_1))$ we have*

$$\begin{aligned} \operatorname{Re}(s_{\infty 1}(q)) &< \operatorname{Re} \left(\left(-Q^2 \right)^{\frac{1}{1-\delta}} + \frac{a_1}{1-\delta} + 1 \right) < 0, \\ \operatorname{Re}(s_{\infty 2}(q)) &< \operatorname{Re} \left(\left(-dQ^2 \right)^{\frac{1}{1-\delta}} + \frac{a_4}{1-\delta} + 1 \right) < 0. \end{aligned}$$

Proof. We seek the asymptotic approximation of solutions to (2.44) for $|q| \gg 1$ by rescaling $q = \kappa/\varepsilon$, so $q \rightarrow \infty$ for $\varepsilon \rightarrow 0$. We show in Appendix C.1 that the approximate solutions are given by

$$s_{\infty 1}(q) = \left(-q^2\right)^{\frac{1}{1-\delta}} + \frac{a_1}{1-\delta} + O(q^{\alpha-\beta}), \quad (2.46)$$

$$s_{\infty 2}(q) = \left(-dq^2\right)^{\frac{1}{1-\delta}} + \frac{a_4}{1-\delta} + O(q^{\alpha-\beta}), \quad (2.47)$$

$$s_{0\pm}(q) = \varepsilon^{2/\delta} y_{1\pm}^{1/\delta} + o(\varepsilon^{2/\delta}), \quad (2.48)$$

where $\beta > \alpha = \frac{2}{1-\delta} > 0$, and $y_{1\pm}$ are the solutions to the following quadratic equation

$$dk^4 y_1^2 - (a_1 d + a_4) \kappa^2 y_1 + a_1 a_4 - a_2 a_3 = 0. \quad (2.49)$$

These lead to the claimed results. We refer to Appendix C.1 for a detailed proof. \square

Remark 2.4.19. We emphasise that $s_{0\pm}(q)$ do not converge to the regular spectrum pointwise in q as $\delta \rightarrow 0$ as they move out of the principal branch for any fixed d as $\delta \rightarrow 0$ (cf. Corollary 2.4.23 and Fig. 2.4 below). It is the combination of parts $s_{\infty 1}$ and $s_{\infty 2}$, which converges to the regular spectrum locally uniformly in q , relating to Theorem 2.4.15.

2.4.4 Spectral instability for large wavenumbers

Here we discuss the stability and instability of (pseudo-)spectrum of (2.35) for $|q| \gg 1$ in Ω_0 . Our aim is to give a complete picture of (pseudo-)spectrum and to understand how (pseudo-)spectrum moves in Ω_0 to instability. The onset of Turing instability, in particular the critical diffusion coefficients d for the subdiffusion model, has been studied in [42]. We reformulate the instability results scattered in [42] and combine these with the convergence theorem in §2.4.2 as well as additional results of this section. This yields Theorem 2.4.20; recall d_c denotes the critical diffusion coefficient for the onset of the Turing instability with normal diffusion.

Theorem 2.4.20. For any $\delta \in (0, 1)$, there exists a unique $d_\delta^\infty \in (-a_4/a_1, d_c)$ and $Q > 0$ such that for $d > d_\delta^\infty$ and any $|q| > Q$ there is spectrum $s(q) \in \Omega_0^+$. In particular, $\sup(\operatorname{Re}(\Lambda_{ss})) > \sup(\operatorname{Re}(\Lambda_{\text{reg}}))$ for $d \in (d_\delta^\infty, d_c)$. Moreover, for any fixed $d_* \in (0, d_c)$, there exists a $\delta_* \in (0, 1)$ such that $\sup(\operatorname{Re}(\Lambda_{ss})) < 0$ for any $\delta \in (0, \delta_*)$.

Since $d_\delta^\infty < d_c$ the subdiffusive transport of model (2.1) destabilises the homogeneous steady state before normal diffusion does. This was already found in [25] and may seem counterintuitive as subdiffusion heuristically slows down dynamics [38]. As mentioned, we add here a more detailed analysis and include the transition to instability. Recall that for the subdiffusion model, positive real parts imply exponential growth, so Theorem 2.4.20 means exponential growth of Fourier modes with arbitrarily large wavenumbers. Moreover, the critical diffusion coefficient d_δ^∞ has Turing-Hopf character, since the solutions to linearisation become unstable through oscillatory modes.

The remainder of this section combined proves in particular Theorem 2.4.20.

From (2.48), we observe that $s_0 \in \Omega_0^+$ ($\in \Omega_0^-$) if $y_1^{1/\delta} \in \Omega_0^+$ ($\in \Omega_0^-$) so we only discuss $y_1^{1/\delta}$. In case $y_1^{1/\delta} \in i\mathbb{R}$ the sign of $\text{Re}(s_0)$ is determined by higher order terms, which we do not consider.

We start from (2.49) and take $\kappa = \pm 1$, so $q = \pm 1/\varepsilon$ and $|q| \rightarrow \infty$ as $\varepsilon \rightarrow 0$. Then (2.49) becomes

$$P(y_1) := dy_1^2 - (a_1d + a_4)y_1 + a_1a_4 - a_2a_3 = 0, \quad (2.50)$$

which is quadratic in y_1 and, since $d > 0$, the minimum of P is given by

$$P_{\min} = \frac{1}{4d} \left(4d(a_1a_4 - a_2a_3) - (a_1d + a_4)^2 \right).$$

Case 1: $P_{\min} \leq 0$. There are two real solutions to (2.50).

Case 1a: $a_1d + a_4 > 0$, i.e., $d > -a_4/a_1$. Equation (2.50) has one or two positive solutions, which leads to positive $y_{1\pm}^{1/\delta}$. It holds that

$$P_{\min} \leq 0 \Rightarrow F(d) := a_1^2 d^2 + (4a_2a_3 - 2a_1a_4)d + a_4^2 \geq 0, \quad (2.51)$$

whose roots d_{fr-} and d_{fr+} are both positive, but we exclude $d \leq d_{fr-}$ because $d_{fr-} < -a_4/a_1$ does not satisfy our assumption. Notably, $d_{fr+} = d_c$ is the Turing bifurcation point of system (2.32) and for $d > d_c$ there exists a curve of real and strictly positive $s_0(q)$ as $q \in [\pm q_{\min}, \pm\infty)$, cf. Proposition 2.4.17. For $d = d_c$, (2.50) has a positive double root y_1 which corresponds to positive $y_1^{1/\delta}$, thus there exists a $Q > 0$ such that $\text{Re}(s_0(q)) > 0$ for all $|q| > Q$. However, we do not know whether $\text{Im}(s_0(q))$ is zero or not due to the higher order term.

Case 1b: $a_1d + a_4 < 0$, i.e., $d < -a_4/a_1$. Equation (2.50) has one or two negative solutions and in the present case we exclude $d \geq d_{fr+}$. Since $\arg(y_{1\pm}) = \pi$, we have $\arg(y_{1\pm}^{1/\delta}) = \pi/\delta$ so that $y_{1\pm}^{1/\delta} \in \Omega_0$ if $\delta \in (\pi/(\pi + \theta_1), 1)$ and thus in fact $y_{1\pm}^{1/\delta} \in \Omega_0^-$. In conclusion, if $\delta \in (\pi/(\pi + \theta_1), 1)$ and $d \leq d_{fr-}$, then $y_1^{1/\delta} \in \Omega_0^-$. See also Remark C.2.4.

Case 1c: $a_1d + a_4 = 0$, i.e., $d = -a_4/a_1$. Since $(a_1a_4 - a_2a_3) > 0$, the minimum P_{\min} is always positive, which is the next case.

Case 2: $P_{\min} > 0$. In this case, the solutions to (2.50) are complex conjugate. Denote $b := a_1d + a_4$, $\zeta := 4d(a_1a_4 - a_2a_3) - (a_1d + a_4)^2$; note $P_{\min} > 0$ implies $\zeta > 0$.

The following lemma provides the explicit formula of critical diffusion coefficient d_δ^∞ , cf. the implicit result [42, Eq. 4.25].

Lemma 2.4.21. *For any $\delta \in (0, 1)$, there exists $d_\delta^\infty \in (-a_4/a_1, d_c)$ with $\lim_{\delta \rightarrow 0} d_\delta^\infty = d_c$, and $Q > 0$ such that $s_{0\pm}(q) \in \Omega_0^+$ if $d > d_\delta^\infty$ and $|q| > Q$. Here d_δ^∞ is the larger root of*

$$H(d) := a_1^2 d^2 + \left(4(a_2a_3 - a_1a_4) \cos^2(\pi\delta/2) + 2a_1a_4 \right) d + a_4^2 = 0. \quad (2.52)$$

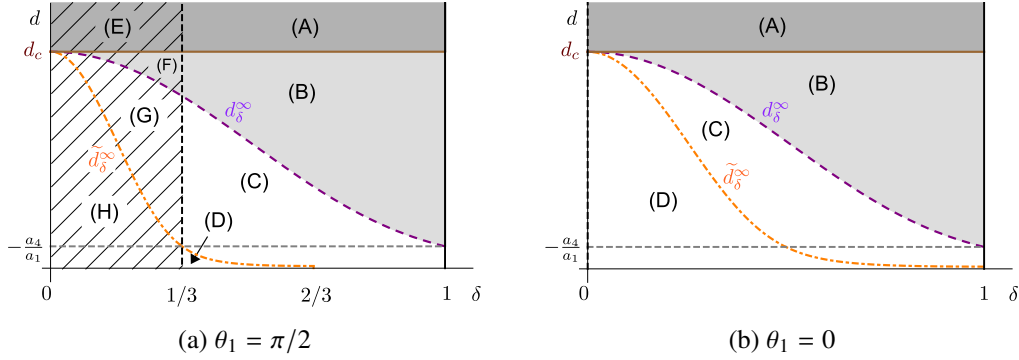


Figure 2.4: Existence and stability of large wavenumber (pseudo-)spectrum. Brown solid horizontal lines: Turing instability threshold for normal diffusion in (2.32); purple dashed curves $d = d_\delta^\infty$: Turing-Hopf threshold for (2.2), i.e., $s_{0\pm} > 0$ in regions (A), (E), whereas $s_{0\pm} \in \Omega_0^+$ with non-zero imaginary parts in regions (B), (F). Orange dashed dotted curves $d = \tilde{d}_\delta^\infty$: existence of $s_{0+} \in \Omega_0^-$ in regions (C), (G) and $s_{0\pm} \notin \Omega_0$ in regions (D), (H). Vertical dashed line $\delta = \theta_1/(\pi + \theta_1)$ where $\delta = 1/3$ in (a) and $\delta = 0$ in (b): existence of $s_{\infty 1}, s_{\infty 2} \in \Omega_0^-$ in regions (E)–(H) and $s_{\infty 1}, s_{\infty 2} \notin \Omega_0$ in regions (A)–(D).

Proof. First, consider $b > 0$, i.e., $d > -a_4/a_1$. The solutions to (2.50) are $y_{1\pm} = (b \pm i\sqrt{\zeta})/(2d) =: \rho e^{\pm i\theta}$, where $\pm\theta := \arg(y_{1\pm})$ and $\rho > 0$. Clearly, $y_{1\pm}^{1/\delta} \in \Omega_0^+$ if $\arg(y_{1\pm}^{1/\delta}) = \pm\theta/\delta \in (-\pi/2, \pi/2)$. Since $b > 0$, we have $\theta = \arg(y_{1+}) = \arctan(\sqrt{\zeta}/b)$. Thus $\theta/\delta \in (-\pi/2, \pi/2) \Rightarrow \arctan(\sqrt{\zeta}/b) \in (-\pi\delta/2, \pi\delta/2)$. Since $\arctan(\sqrt{\zeta}/b) > 0$, we obtain $\arctan(\sqrt{\zeta}/b) \in (0, \pi\delta/2)$ which leads to

$$4d(a_1a_4 - a_2a_3) - (a_1d + a_4)^2 < (a_1d + a_4)^2 \tan^2(\pi\delta/2),$$

or equivalently $H(d) > 0$. The roots d_- and d_δ^∞ are both real valued, but we exclude $d < d_- < d_\delta^\infty$ because $d_- < -a_4/a_1$ contradicts the assumption.

For $b \leq 0$, i.e., $d \leq -a_4/a_1$ we have $\arg(y_{1+}) \geq \pi/2$ and thus $\arg(y_{1+}^{1/\delta}) \geq \pi/(2\delta) \notin (-\pi/2, \pi/2)$ as well as $\arg(y_{1-}^{1/\delta}) \leq -\pi/(2\delta) \notin (-\pi/2, \pi/2)$.

The fact that $d_\delta^\infty < d_c$ for $\delta \in (0, 1)$ follows by straightforward comparison of the solutions to (2.51) and (2.52). \square

The following makes the dependence of the pseudo-spectrum on the choice of branch cut explicit. From Fig. 2.4 we can see that the range of existence is decreasing when $\theta_1 \rightarrow 0$, i.e., $\mathfrak{B}_0^{\theta_1}$ moves to the negative real line. In particular, for the canonical choice $\theta_1 = 0$ the pseudo-spectrum $s_{\infty 1}, s_{\infty 2}$ is invisible. This explains the absence in [22, 25, 42, 44].

Proposition 2.4.22. *For any $\delta \in (0, 1)$, there exist $Q > 0$ and $\tilde{d}_\delta^\infty \in [0, d_\delta^\infty)$ with $\lim_{\delta \rightarrow 0} \tilde{d}_\delta^\infty = d_c$ such that for any $|q| > Q$ we have $s_{0+}(q) \in \Omega_0^-$ if $d \in (\tilde{d}_\delta^\infty, d_\delta^\infty)$, and for any $\delta \in (0, \frac{\pi}{\pi+\theta_1})$, $s_{0\pm}(q) \notin \Omega_0$ if $d < \tilde{d}_\delta^\infty$. More specifically, \tilde{d}_δ^∞ is given by*

$$\tilde{d}_\delta^\infty = \begin{cases} \tilde{d}_{\delta+}^\infty, & \delta \in (0, \frac{\pi}{2(\pi+\theta_1)}) \\ -\frac{a_4}{a_1}, & \delta = \frac{\pi}{2(\pi+\theta_1)} \\ \tilde{d}_{\delta-}^\infty, & \delta \in (\frac{\pi}{2(\pi+\theta_1)}, \frac{\pi}{\pi+\theta_1}) \end{cases}$$

where $\tilde{d}_{\delta+}^{\infty}$ and $\tilde{d}_{\delta-}^{\infty}$ are the larger and smaller roots of

$$\tilde{H}(d) := a_1^2 d^2 + \left(4(a_2 a_3 - a_1 a_4) \cos^2((\pi + \theta_1)\delta) + 2a_1 a_4\right) d + a_4^2 = 0. \quad (2.53)$$

Proof. The somewhat technical proof is given in Appendix C.2. \square

Corollary 2.4.23. *For any fixed $d \in (0, d_c)$, there exist $\delta_{\text{exist}} \in (0, 1]$ and $Q > 0$ such that $s_{0\pm}(q) \notin \Omega_0$ for any $\delta \in (0, \delta_{\text{exist}})$ and any $|q| > Q$.*

Concerning the approximations $s_{\infty 1}$ and $s_{\infty 2}$, we have the following lemma.

Lemma 2.4.24. *For any $\delta \in (0, 1)$ there exists a $Q > 0$ such that for any $|q| > Q$ we have $s_{\infty 1}(q), s_{\infty 2}(q) \in \Omega_0^-$ if $\delta \in (0, \frac{\theta_1}{\pi + \theta_1})$ whereas $s_{\infty 1}(q), s_{\infty 2}(q) \notin \Omega_0$ if $\delta \in [\frac{\theta_1}{\pi + \theta_1}, 1)$.*

Proof. Recall the approximations (2.46), (2.47) for $|q| \gg 1$ in the proof of Lemma 2.4.18. When $|q| \rightarrow \infty$, the arguments of $s_{\infty 1}$ and $s_{\infty 2}$ are determined by $(-q^2)^{\frac{1}{1-\delta}}$ and $(-dq^2)^{\frac{1}{1-\delta}}$, respectively, and are given by $\arg(s_{\infty 1}) = \arg(s_{\infty 2}) = \frac{\pi}{1-\delta}$. If $\frac{\pi}{1-\delta} \in (-\pi + \theta_1, \pi + \theta_1) \Rightarrow \delta < \frac{\theta_1}{\pi + \theta_1}$, then $s_{\infty 1}, s_{\infty 2} \in \Omega_0$. Moreover, $\frac{\pi}{1-\delta} > \pi/2$, so $s_{\infty 1}, s_{\infty 2} \in \Omega_0^-$. \square

Theorem 2.4.20 now follows from combining Theorem 2.4.15, Proposition 2.4.17, Lemma 2.4.21, Proposition 2.4.22 and Lemma 2.4.24.

2.4.5 Numerical computations of (pseudo-)spectra

Here we present some numerical computations of (pseudo-)spectrum for finite wavenumber. We choose $\theta_1 = \pi/2$ to give a most complete picture of the pseudo-spectrum. With $s = z^m$ and $\delta = \ell/m \in (0, 1)$, $\ell, m \in \mathbb{Z}_+$ we get the dispersion relation

$$D_{ss}(z^m, q^2) = \left(z^m + z^\ell q^2 - a_1\right) \left(z^m + z^\ell dq^2 - a_4\right) - a_2 a_3 = 0. \quad (2.54)$$

in the z -plane. The principal branch $\Omega_0 = \left\{s \in \mathbb{C} \setminus \{0\} : \arg(s) \in \left(-\frac{\pi}{2}, \frac{3\pi}{2}\right)\right\}$ of s corresponds to the branch in z -plane given by $\Sigma_0^m := \left\{z \in \mathbb{C} \setminus \{0\} : \arg(z) \in \left(-\frac{\pi}{2m}, \frac{3\pi}{2m}\right)\right\}$. We set $a_1 = 1/2$, $a_2 = -3/16$, $a_3 = 8$, $a_4 = -1$ so the regular Turing threshold is $d_c \approx 19.798$.

Fig. 2.5 illustrates Theorem 2.4.15: the subdiffusion (pseudo-)spectra and regular spectra in the complex plane are plotted. We observe that when δ decreases, the subdiffusion (pseudo-)spectrum approaches the regular spectrum in Ω_0 .

Fig. 2.6 illustrates Lemma 2.4.17: when the regular spectrum has positive part, unstable subdiffusion spectrum along the scaled curve appears from large wavenumbers and moves towards smaller wavenumbers as d increases. Note that maximum real parts of regular spectrum and scaled curve are the same. For decreasing real parts the wavenumber of the scaled curve tends to infinity.

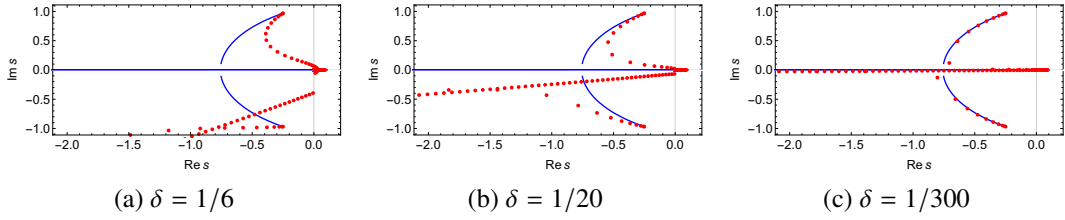


Figure 2.5: Comparison of numerically computed spectra of (2.35) beyond the regular Turing instability for diffusion coefficient $d = 30$ and wavenumbers $q = 0.02n$, $n = 0, 1, \dots, 150$. Blue solid lines: regular spectra; red dotted lines: subdiffusion (pseudo-)spectra.

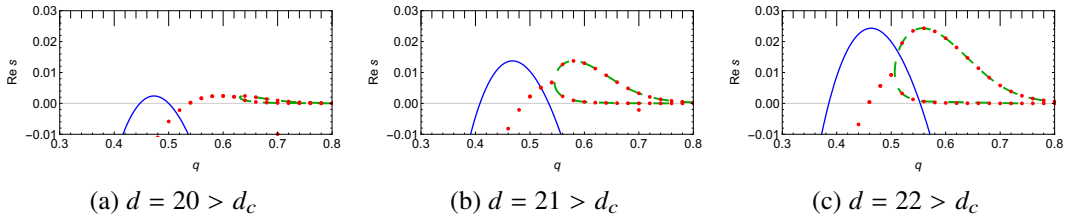


Figure 2.6: Comparison of real parts of spectra of versus wavenumber beyond the regular Turing instability in (2.35) for anomalous exponent $\delta = 1/10$ and $q = 0.02n$, $n = 0, 1, \dots, 150$. Blue solid lines: regular spectra; red dotted lines: subdiffusion (pseudo-)spectra; green dashed lines: real and positive curves scaled from the positive part of regular spectra.

In Fig. 2.7 we exhibit the behaviour of (pseudo-)spectrum as d changes. In Fig. 2.7a, $d < \tilde{d}_\delta^\infty \approx 16.5$ so the real part of the regular spectrum and the more ‘unstable’ subdiffusion pseudo-spectrum are both negative. As d increases, the pseudo-spectrum moves towards imaginary axis and $\sup(\operatorname{Re}(\Lambda_{ss})) = 0$ for $\tilde{d}_\delta^\infty < d < d_\delta^\infty \approx 19.4$, cf. Fig. 2.7b. For $d > d_\delta^\infty$, the Turing-Hopf threshold, the subdiffusion spectrum is unstable, whereas the regular spectrum is stable as $d < d_c$, the regular Turing threshold, cf. Fig. 2.7c. Finally, when d is larger than d_c , both spectra are unstable and additional purely real subdiffusion spectrum emerges as the scaled curve of regular spectrum, cf. Fig. 2.7d. These variations coincide with moving through regions (H), (G), (F), (E) in Fig. 2.4, respectively.

Finally, in Fig. 2.8 we compare the subdiffusion (pseudo-)spectrum in Ω_0 and in Σ_0^m in order to illustrate how pseudo-spectrum moves across the branch cut. For fixed δ and increasing d , the pseudo-spectrum in the z -plane moves into Σ_0^m , giving rise to the part of pseudo-spectrum which tends to zero. For $d > d_c$, the spectra in the z -plane move along the real line, which leads to the parts of the spectrum that tends to zero in Ω_0 . For fixed d and decreasing δ , the region Σ_0^m becomes narrower, which removes certain pseudo-spectrum.

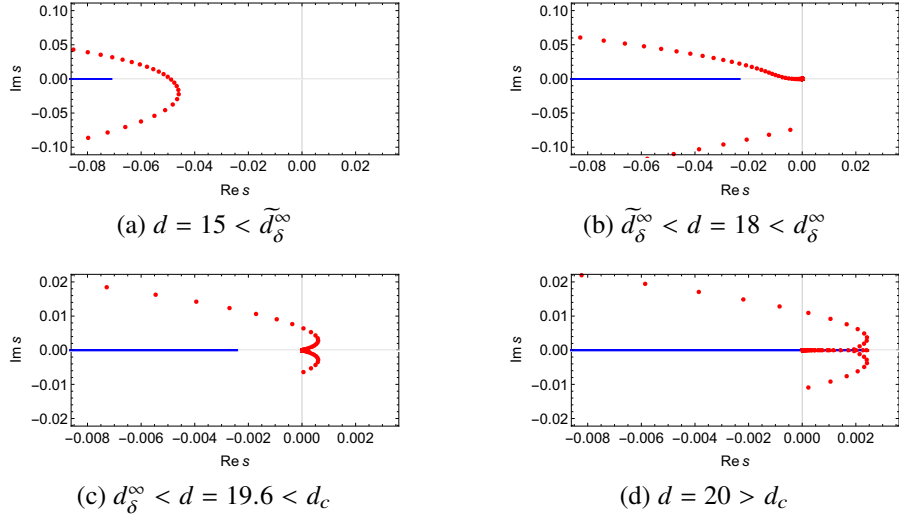


Figure 2.7: Comparison of spectra of (2.35) in the principal branch Ω_0 for anomalous exponent $\delta = 1/10$ and wavenumber $q = 0.01n$, $n = 0, 1, \dots, 300$. Blue solid lines: regular spectra; red dotted lines: subdiffusion (pseudo-)spectra.

2.5 Subdiffusion with linear creation and annihilation

In this section we discuss the model (2.4) which was derived from a process that only removes particles that have jumped to a location during the dynamics. Indeed, it was numerically shown in [30] that the Green's function is non-negative. Similar to the previous section we refine and augment some of the analysis done in the literature, in particular regarding the transition to Turing instability.

2.5.1 Scalar case

We recall the scalar case (2.3) and apply the Fourier-Laplace transform to obtain the dispersion relation

$$d_{\text{ca}}(s, q^2) := (s - a)^{1-\gamma} \left((s - a)^\gamma + dq^2 \right) = 0, \quad s \in \Omega_a, \quad (2.55)$$

where $\Omega_a := \{s \in \mathbb{C} \setminus \{a\} : \arg(s - a) \in (-\pi + \theta_1, \pi + \theta_1), \theta_1 \in (0, \pi/2)\}$ is the extended domain from $\text{Re}(s) > a$ of the Laplace transform, cf. Remark 2.4.1. We denote $\Omega_a^+ := \{s \in \mathbb{C} \setminus \{a\} : \arg(s - a) \in (-\pi/2, \pi/2)\}$ and $\Omega_a^{0-} := \Omega_a \setminus \Omega_a^+$.

Notably, $s = a$ is a constant solution to $d_{\text{ca}}(s, q^2) = 0$, but not in Ω_a .

Definition 2.5.1. We call the set of roots $\lambda_{\text{ca}}^+ := \{s \in \Omega_a^+ : d_{\text{ca}}(s, q^2) = 0 \text{ for a } q \in \mathbb{R}\}$ (subdiffusion) spectrum of the linear operator $\mathcal{L}_{\text{ca}}^{\text{scal}} := d e^{at} \mathcal{D}_{0,t}^{1-\gamma} (e^{-at} \partial_x^2 \cdot) + a$, and the set of roots $\lambda_{\text{ca}}^{0-} := \{s \in \Omega_a^{0-} : d_{\text{ca}}(s, q^2) = 0 \text{ for a } q \in \mathbb{R}\}$ (subdiffusion) pseudo-spectrum of $\mathcal{L}_{\text{ca}}^{\text{scal}}$.

We formulate the simple explicit solutions of (2.55) as a lemma for reference and illustrate it numerically in Fig. 2.9.

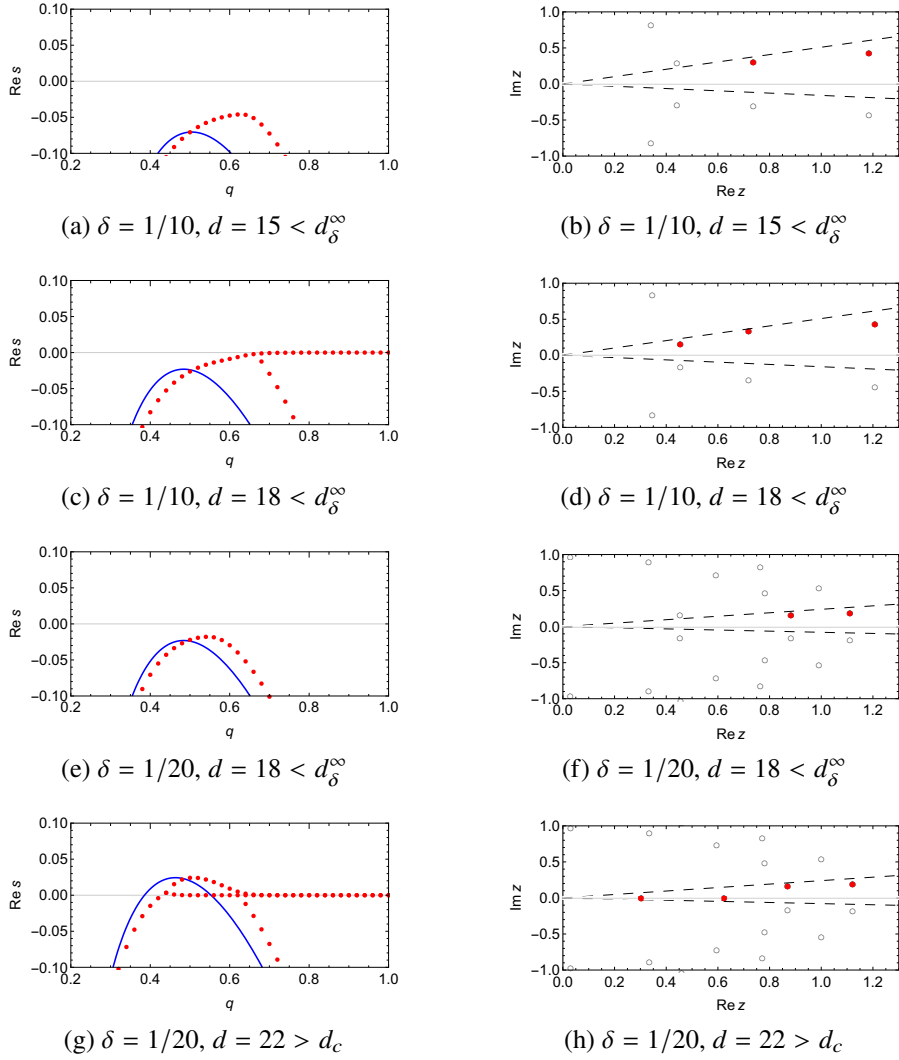


Figure 2.8: Model (2.35). Left column: the real part of spectra versus wavenumber; blue solid lines: regular spectrum; red dotted lines: subdiffusion (pseudo-)spectrum. Right column: (pseudo-)spectrum for $q = 0.7$ in z -plane; hollow circles: roots of (2.54); red dots: roots of (2.54) in Σ_0^m with $\theta_1 = \pi/2$; dashed lines: borders of Σ_0^m .

Lemma 2.5.2. *For any $\gamma \in (\frac{\pi}{\pi+\theta_1}, 1)$ and $|q| > 0$, the solution to (2.55) is $s = s_*(q) = (dq^2)^{1/\gamma} e^{i\pi/\gamma} + a \in \Omega_a$. In particular, $\lim_{|q| \rightarrow 0} \operatorname{Re}(s_*(q)) = a$ and $\lim_{|q| \rightarrow \infty} \operatorname{Re}(s_*(q)) = -\infty$; if $\gamma \in (0, \frac{\pi}{\pi+\theta_1}]$, then $s_*(q) \notin \Omega_a$ for each q ; moreover, $s_*(0) \notin \Omega_a$.*

Proof. The solution is $s(q) = (-dq^2)^{1/\gamma} + a = (dq^2)^{1/\gamma} e^{i\pi/\gamma} + a$. Since $\arg(s - a) = \pi/\gamma$ we have $s \in \Omega_a$ if $\pi/\gamma \in (-\pi + \theta_1, \pi + \theta_1) \Rightarrow \gamma \in (\frac{\pi}{\pi+\theta_1}, 1)$. Since $\pi/\gamma > \pi$, we obtain that $\operatorname{Re}(s - a) < 0$ for $|q| > 0$, and $\lim_{|q| \rightarrow \infty} \operatorname{Re}(s - a) = -\infty$. Moreover, $s(q) \notin \Omega_a$ if $\gamma \notin (\frac{\pi}{\pi+\theta_1}, 1)$, and $s(0) = a \notin \Omega_a$. \square

Notably, unlike the (pseudo-)spectrum of (2.38), the (pseudo-)spectrum of (2.3) is strictly

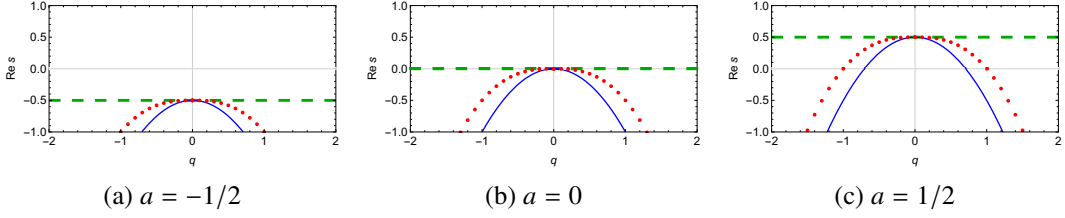


Figure 2.9: Model (2.3): comparison of real parts of spectra versus wavenumber with the branch cut angle $\theta_1 = \pi/2$ and $\gamma = 3/4 > 2/3$. Blue solid lines: regular spectra; red dotted lines: subdiffusion (pseudo-)spectra; green dashed lines: $s(q) = a \notin \Omega_a$. Taking $\gamma = 1/4 < 2/3$ the results are the same except the pseudo-spectrum is empty.

stable for $|q| \gg 1$ and $\gamma \in (\frac{\pi}{\pi+\theta_1}, 1)$.

The solution to (2.3) with initial condition $u(x, 0) = \delta(x)$ has been discussed in [23, Section V.B] by establishing the relation with (2.27), which is given by

$$u(x, t) = \Phi(x, t)e^{at}, \quad t > 0.$$

Recall that $\Phi(x, t)$ is the Green's function to (2.27) given by (2.31). Notably, it follows that the non-trivial solutions to (2.3) is exponentially growing (decaying) for $a > 0$ ($a < 0$) and $t \gg 1$.

The solution to the system (2.4) with $D = d\text{Id}$ has been discussed as well [30, Section III], which is given by

$$u(x, t) = \Phi(x, t)e^{At}u_0,$$

with initial condition $u(x, 0) = \delta(x)u_0$. The eigenvalues of A determine the decay as they are both negative, so the Turing instability cannot happen. For general diffusion matrix this approach fails and other instabilities occur as discussed next.

2.5.2 Spectral analysis

We turn to the system (2.4) with general diagonal diffusion matrix $D = \text{diag}(1, d)$, cf. [47, Eq. 3.5], where the (pseudo-)spectrum determines the temporal features of solutions analogous to Theorem 2.4.5. Moreover, we discuss the convergence of subdiffusion (pseudo-)spectrum when the subdiffusive exponent $\gamma \rightarrow 1$ as well as approximate (pseudo-)spectra to detect instabilities.

In order to simplify the problem, as in [30] we assume that A is a diagonalisable matrix, so that

$$P = \begin{pmatrix} a_2 & a_2 \\ \mu_1 - a_1 & \mu_2 - a_1 \end{pmatrix}, \quad P^{-1} = \begin{pmatrix} \frac{a_1 - \mu_2}{a_2(\mu_1 - \mu_2)} & \frac{1}{\mu_1 - \mu_2} \\ -\frac{a_1 - \mu_1}{a_2(\mu_1 - \mu_2)} & -\frac{1}{\mu_1 - \mu_2} \end{pmatrix}$$

gives $\bar{A} := P^{-1}AP = \text{diag}(\mu_1, \mu_2)$ (cf. [43, Eq. 27]), where μ_1 and μ_2 are the eigenvalues of A . The conditions for Turing instability become $\text{tr}(A) = \mu_1 + \mu_2 < 0$ and $\det(A) = \mu_1\mu_2 > 0$. Without loss of generality we assume throughout that $\text{Re}(\mu_1) \geq \text{Re}(\mu_2)$.

Changing coordinates $u = Pw$ turns (2.4) into

$$\partial_t w = \bar{D} e^{\bar{A}t} \mathcal{D}_{0,t}^{1-\gamma} \left(e^{-\bar{A}t} \partial_x^2 w \right) + \bar{A} w, \quad (2.56)$$

where $\bar{D} := P^{-1} D P = \begin{pmatrix} d_1 & d_2 \\ d_3 & d_4 \end{pmatrix}$. Transforming (2.56) into Fourier space yields

$$\partial_t \hat{w} = -q^2 \bar{D} e^{\bar{A}t} \mathcal{D}_{0,t}^{1-\gamma} \left(e^{-\bar{A}t} \hat{w} \right) + \bar{A} \hat{w}. \quad (2.57)$$

Laplace transform then gives for $\operatorname{Re}(s - \mu_1), \operatorname{Re}(s - \mu_2) > 0$ the dispersion relation

$$\begin{aligned} D_{\text{ca}}(s, q^2) &:= \det \left(s \operatorname{Id} - \bar{A} + (s \operatorname{Id} - \bar{A})^{1-\gamma} \bar{D} q^2 \right) \\ &= \det \left((s \operatorname{Id} - \bar{A})^{1-\gamma} \right) \det \left((s \operatorname{Id} - \bar{A})^\gamma + \bar{D} q^2 \right) \\ &= (s - \mu_1)^{1-\gamma} (s - \mu_2)^{1-\gamma} \left(((s - \mu_1)^\gamma + d_1 q^2) ((s - \mu_2)^\gamma + d_4 q^2) - d_2 d_3 q^4 \right) = 0. \end{aligned} \quad (2.58)$$

As in §2.4, we extend the domain to $\Omega_{\text{ca}} \subset \mathbb{C}$ as follows. Clearly, the finite branch points of (2.58) are μ_1, μ_2 . Taking s along a contour around μ_1 and μ_2 , the change in argument of s is $\gamma(2\pi + 2\pi) = 4\pi\gamma$ and for $\gamma \neq 1/2$ we have $e^{4i\pi\gamma} \neq 1$ so $s = \infty$ is a branch point of $(s - \mu_1)^\gamma (s - \mu_2)^\gamma$. As we are most interested in the vicinity of $\gamma = 1$, we take $\gamma \in (1/2, 1)$.

The conditions $\operatorname{Re}(\mu_1), \operatorname{Re}(\mu_2) < 0$ for a Turing instability yield two cases:

cc: μ_1, μ_2 are complex conjugate with negative real parts;

nr: μ_1, μ_2 are negative real.

In order to keep non-integer powers of positive reals on the positive real axis, we choose the principal branch as follows:

cc: $\Omega_{\text{ca}}^{\text{cc}} := \{s \in \mathbb{C} \setminus \{\mu_1, \mu_2\} : \arg(s - \mu_1) \in (-\pi - \theta_1, \pi - \theta_1), \arg(s - \mu_2) \in (-\pi + \theta_2, \pi + \theta_2), \theta_1, \theta_2 \in (0, \pi/2), \operatorname{Im}(\mu_1) > 0 > \operatorname{Im}(\mu_2)\}$ (cf. Fig. 2.10a), i.e., branch cuts $\mathfrak{B}_{\mu_1}^{-\theta_1}$ and $\mathfrak{B}_{\mu_2}^{\theta_2}$.

nr: $\Omega_{\text{ca}}^{\text{nr}} := \{s \in \mathbb{C} \setminus \{\mu_1, \mu_2\} : \arg(s - \mu_1) \in (-\pi + \theta_1, \pi + \theta_1), \arg(s - \mu_2) \in (-\pi + \theta_2, \pi + \theta_2), \theta_1, \theta_2 \in (0, \pi/2), \mu_2 < \mu_1 < 0\}$ (cf. Fig. 2.10b), i.e., branch cuts $\mathfrak{B}_{\mu_1}^{\theta_1}$ and $\mathfrak{B}_{\mu_2}^{\theta_2}$.

We write Ω_{ca} for $\Omega_{\text{ca}}^{\text{cc}}$ or $\Omega_{\text{ca}}^{\text{nr}}$ whenever the case is not relevant, and denote:

$$\Omega_{\text{ca}}^+ := \{s \in \Omega_{\text{ca}} : \operatorname{Re}(s) > \operatorname{Re}(\mu_1)\}, \quad \Omega_{\text{ca}}^- := \{s \in \Omega_{\text{ca}} : \operatorname{Re}(s) < \operatorname{Re}(\mu_1)\}, \quad \Omega_{\text{ca}}^{0-} := \Omega_{\text{ca}} \setminus \Omega_{\text{ca}}^+.$$

Definition 2.5.3. We call the set of roots $\Lambda_{\text{ca}}^+ := \{s \in \Omega_{\text{ca}}^+ : D_{\text{ca}}(s, q^2) = 0 \text{ for a } q \in \mathbb{R}\}$ (subdiffusion) spectrum of the linear operator $\mathcal{L}_{\text{ca}} := D e^{\bar{A}t} \mathcal{D}_{0,t}^{1-\gamma} (e^{-\bar{A}t} \partial_x^2 \cdot) + A$, and the set of roots $\Lambda_{\text{ca}}^{0-} := \{s \in \Omega_{\text{ca}}^{0-} : D_{\text{ca}}(s, q^2) = 0 \text{ for a } q \in \mathbb{R}\}$ (subdiffusion) pseudo-spectrum of \mathcal{L}_{ca} .

We denote the union as $\Lambda_{\text{ca}} := \Lambda_{\text{ca}}^+ \cup \Lambda_{\text{ca}}^{0-}$.

In preparation, we note that if $1 - \gamma = n/m \in \mathbb{Q}$ then $D_{\text{ca}}(\cdot, q^2)$ can be cast as a polynomial with respect to the two variables $z_j = (s - \mu_j)^{1/m}$, $j = 1, 2$, of degree m in each variable, given by

$$D_{\text{ca}}(z_1, z_2, q^2) = \left(z_1^m + z_1^n d_1 q^2\right) \left(z_2^m + z_2^n d_4 q^2\right) - z_1^n z_2^n d_2 d_3 q^4.$$

Now we can state the analogue of Theorem 2.4.5 for the present model.

Theorem 2.5.4. *Let $\gamma \in (0, 1) \cap \mathbb{Q}$, $\lambda := \sup(\text{Re}(\Lambda_{\text{ca}}))$ and $\lambda_0 := \text{Re}(\mu_1) \geq \text{Re}(\mu_2)$.*

- (1) *If $\lambda > \lambda_0$, then $S^+ := \{(s, q) \in \Omega_{\text{ca}}^+ \times \mathbb{R} : D_{\text{ca}}(s, q^2) = 0, \text{ and } \text{Re}(s) \text{ maximal}\} \neq \emptyset$ and for any $(s, q) \in S^+$ the solution to (2.57) for almost all initial data satisfies $\hat{w}(q, t) = C_{\text{exp}} t^{k-1} e^{st} + o(t^{k-1} e^{\text{Re}(s)t})$ for a non-zero $C_{\text{exp}} \in \mathbb{C}^2$, where $k = \max\{k_j, j = 1, 2\}$ and k_j is the multiplicity of $z_j = (s - \mu_j)^{1/m}$ as the root of $D_{\text{ca}}(z_1, z_2, q^2) = 0$.*
- (2) *If $\lambda = \lambda_0$, then $Q^- := \{q \in \mathbb{R} \setminus \{0\} : s \in \Omega_{\text{ca}}^- \text{ and } (s, q) \text{ solves } D_{\text{ca}}(s, q^2) = 0\} \neq \emptyset$ and for any $q \in Q^-$ there exists a non-zero $C_{\text{bp}} \in \mathbb{C}^2$ such that $\hat{w}(q, t) = C_{\text{bp}} t^{-\gamma} e^{\mu_1 t} + o(t^{-\gamma} e^{\lambda_0 t})$ for almost all initial data.*
- (3) *If $\lambda < \lambda_0$ or $\Lambda_{\text{ca}} = \emptyset$, then for any $q \in \mathbb{R} \setminus \{0\}$ there exists a non-zero $C_{\text{bp}} \in \mathbb{C}^2$ such that $\hat{w}(q, t) = C_{\text{bp}} t^{-\gamma} e^{\mu_1 t} + o(t^{-\gamma} e^{\lambda_0 t})$ for almost all initial data.*

We defer the technical proof to Appendix B.2. Regarding the case $q = 0$, note that (2.57) reduces to $\partial \hat{w} = \bar{A} \hat{w}$, whose solutions decay exponentially.

Remark 2.5.5. *The statement also holds for $\lambda_0 = 0$ and scalar equations, and thus includes (2.3) as well as the subdiffusion equation (2.27). Notably, for the latter Theorem 2.5.4 gives the decay as $t^{-\gamma}$ (for rational γ), which coincides with that derived in §2.3.2 via (2.29).*

Remark 2.5.6. *As for Theorem 2.4.5 the method of proof only allows for rational γ and it would be interesting to investigate the general case. Likewise, the dependence of the constants on q and thus decay in, e.g., L^2 is beyond the scope of this thesis.*

Similar to Theorem 2.4.5, Theorem 2.5.4 reveals that the roots of (2.58) determine the temporal behaviour of \hat{w} . However, in contrast to Theorem 2.4.5, the Turing instability condition $\lambda_0 < 0$ implies exponential decay for stable (pseudo-)spectrum. The key point is that on the one hand μ_1, μ_2 are the branch points of (2.57), while for the branch point of (2.36) is the origin. On the other hand, $s = \mu_1, \mu_2$ also solves the dispersion relation. This is the reason for the algebraic decay $t^{-\gamma}$ compared with $t^{-1-1/m}$ in Theorem 2.4.5.

Remark 2.5.7. *As mentioned in §2.2, model (2.4) is different from (2.19) discussed in [43] due to (2.20), as well as the dispersion relations, cf. (2.58) and [43, Eq. 24]. This can be illustrated for the scalar case. The dispersion relation of (2.19) reads $(s - a)^\gamma + dq^2 = 0$ which has no roots on the branch point $s = a$ for $q \neq 0$, whereas (2.55) does. Then according to Theorem*

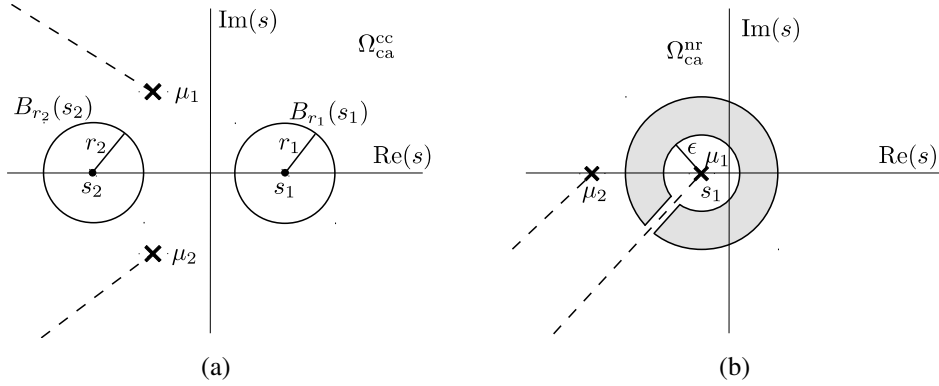


Figure 2.10: Branch cuts (dashed) and points (crosses) for (2.58), and regular spectrum (dots) s_1, s_2 . (a) Case **cc**; (b) case **nr**.

2.4.5, each Fourier mode of (2.19) with $q \neq 0$ decays algebraically as $t^{-1-1/m}$, whereas the one of (2.3) decays exponentially by Theorem 2.5.4.

In the multispecies case, the eigenvalues of A are roots of (2.58) as well as the branch points, whereas they are not roots of [43, Eq. 24] in general. This implies the Fourier modes of (2.4) and (2.19) have different decays. Another difference in the system case in [43, Eq. 28] is the perhaps unrecognised implicit assumption that $P^{-1}(s\text{Id} - A)^\gamma P$ is equal to $(s\text{Id} - P^{-1}AP)^\gamma$.

2.5.3 Convergence to regular spectrum

As in Theorem 2.4.15 the subdiffusion (pseudo-)spectrum converges to the regular spectrum as $\gamma \rightarrow 1$. The regular dispersion relation of (2.33) in the coordinates $u = Pw$ reads

$$D_{\text{reg}}(s, q^2) = (s - \mu_1 + d_1 q^2)(s - \mu_2 + d_4 q^2) - d_2 d_3 q^4 = 0, \quad s \in \mathbb{C} \quad (2.59)$$

which allows for direct comparison with the non-trivial factor of (2.58) given by

$$D_{\text{ca2}}(s, q^2) := ((s - \mu_1)^\gamma + d_1 q^2)((s - \mu_2)^\gamma + d_4 q^2) - d_2 d_3 q^4 = 0, \quad s \in \Omega_{\text{ca}}. \quad (2.60)$$

Notably, $s = \mu_1, \mu_2$ solve (2.58) for any q but are not in Ω_{ca} , while these are roots for (2.59) at $q = 0$, and generically not otherwise.

Theorem 2.5.8. For any compact set $K \subset \subset \Omega_{\text{ca}}$, $\lim_{\gamma \rightarrow 1} (K \cap \Lambda_{\text{ca}}) = (K \cap \Lambda_{\text{reg}})$.

Proof. The basis of the proof is the analogue of Lemma 2.4.14. In both cases, the application of Rouché theorem near and away from the branch points are completely analogous to that in Lemma 2.4.14, cf. Fig. 2.10. \square

Spectrum near zero and Turing instability

Since the onset of Turing instability concerns spectrum near the origin, we can analyse this by Taylor expanding the dispersion relation at $s = 0$.

We will show that the Taylor expansion of $D_{\text{ca}2} = 0$ to quadratic order is

$$\tilde{D}_{\text{ca}2}(s, q^2) := s^2 + \gamma^{-1} \left(\beta_1 q^2 - \text{tr}(A) \right) s + \gamma^{-2} h(q^2) = 0, \quad (2.61)$$

where $\beta_1(\gamma, d) := c_1 + c_4 d$, $\beta_2(\gamma) := a_1 c_4 - a_2 c_3$, $\beta_3(\gamma) := a_4 c_1 - a_3 c_2$, and

$$C := P (-\bar{A})^{1-\gamma} P^{-1} = \begin{pmatrix} c_1 & c_2 \\ c_3 & c_4 \end{pmatrix}, \quad h(q^2) := \det(C) \cdot d q^4 - (\beta_2 d + \beta_3) q^2 + \det(A).$$

Now the computation of the Turing instability parameters for (2.61) follows, with some caveats, the approach for two component systems with regular diffusion. Since this gives the onset of instability through the origin, the same follows for the subdiffusion spectrum. As detailed in the following Theorem statement, the Turing instability parameters are

$$\begin{aligned} \gamma_{\text{cc}} &:= \frac{1}{\theta} \arccot \left(\frac{a_1}{|\mu| \sin(\theta)} + \cot(\theta) \right) \in (0, 1), \\ \gamma_{\text{nr}} &:= \left(\ln \left(\frac{a_1 - \mu_1}{a_1 - \mu_2} \right) \right) \left(\ln \left(\frac{\mu_1}{\mu_2} \right) \right)^{-1} \in (0, 1), \\ d_\gamma &:= -\frac{\beta_3}{\beta_2} + \frac{2}{\beta_2^2} \left(\det(AC) + \sqrt{(\det(AC))^2 - \beta_2 \beta_3 \det(AC)} \right), \quad q_\gamma^2 := \frac{\beta_2 d_\gamma + \beta_3}{2 d_\gamma \det(C)}. \end{aligned}$$

We write $\Lambda_{\text{ca}}^\epsilon := \Lambda_{\text{ca}} \cap B_\epsilon(0)$ for the spectrum within a small ball $B_\epsilon(0)$ near the origin and set $\lambda_\epsilon := \sup(\text{Re}(\Lambda_{\text{ca}}^\epsilon))$.

Remark 2.5.9. *The following Theorem holds verbatim for (2.61) instead of (2.60) and any ϵ , i.e., replacing $\Lambda_{\text{ca}}^\epsilon$ by the roots of $\tilde{D}_{\text{ca}2}$.*

Theorem 2.5.10. *For any sufficiently small $\epsilon > 0$ there exists a unique minimal anomalous exponent $\gamma_A \in (0, 1)$ given by γ_{cc} in case **cc** and γ_{nr} in case **nr**, such that for any $\gamma \in (0, \gamma_A)$, either $\lambda_\epsilon < 0$, or $\Lambda_{\text{ca}}^\epsilon = \emptyset$, and for any $\gamma \in (\gamma_A, 1)$ the following hold.*

- (1) d_γ is the unique critical diffusion coefficient such that $\text{sgn}(\lambda_\epsilon) = \text{sgn}(d - d_\gamma)$.
- (2) For $d = d_\gamma$, there exists a unique critical wavenumber given by q_γ such that $\lambda_\epsilon = 0$, $\Lambda_{\text{ca}}^\epsilon \cap i\mathbb{R} = \{0\}$, and $\tilde{D}_{\text{ca}2}(0, q^2) = 0$ precisely for $q = q_\gamma$.
- (3) $\lim_{\gamma \rightarrow \gamma_A} d_\gamma = +\infty$ and $\lim_{\gamma \rightarrow 1} d_\gamma = d_c$.

Proof. Case cc: Taylor expanding, with $\mu_j \neq 0$, $j = 1, 2$,

$$(s - \mu_j)^\gamma = (-\mu_j)^\gamma + \gamma(-\mu_j)^{\gamma-j} s + O(|s|^2),$$

gives the approximate dispersion relation (2.60) in $B_\epsilon(0)$ quadratic in s as

$$\left((- \mu_1)^\gamma + \gamma(-\mu_1)^{\gamma-1}s + d_1 q^2\right) \left((- \mu_2)^\gamma + \gamma(-\mu_2)^{\gamma-1}s + d_4 q^2\right) - d_2 d_3 q^4 = 0. \quad (2.62)$$

In order to see the dependence on the diffusion ratio d , we perform the following transform. First, multiply (2.62) with $\gamma^{-1}(-\mu_1)^{1-\gamma}\gamma^{-1}(-\mu_2)^{1-\gamma}$ and rewrite the resulting equation as

$$\det\left(s\text{Id} + \gamma^{-1}q^2\bar{D}(-\bar{A})^{1-\gamma} - \gamma^{-1}\bar{A}\right) = 0.$$

Second, change coordinates through left-multiplying by P and right-multiplying by P^{-1} to

$$\det\left(s\text{Id} + \gamma^{-1}q^2DP(-\bar{A})^{1-\gamma}P^{-1} - \gamma^{-1}A\right) = 0.$$

Here the matrix $C = P(-\bar{A})^{1-\gamma}P^{-1}$ can be expressed as

$$C = \begin{pmatrix} c_1 & c_2 \\ c_3 & c_4 \end{pmatrix} = \begin{pmatrix} \frac{(-\mu_1)^{1-\gamma}(a_1-\mu_2)-(-\mu_2)^{1-\gamma}(a_1-\mu_1)}{\mu_1-\mu_2} & \frac{a_2((- \mu_1)^{1-\gamma}-(- \mu_2)^{1-\gamma})}{\mu_1-\mu_2} \\ \frac{(a_1-\mu_1)(a_1-\mu_2)((-\mu_2)^{1-\gamma}-(-\mu_1)^{1-\gamma})}{a_2(\mu_1-\mu_2)} & \frac{(-\mu_2)^{1-\gamma}(a_1-\mu_2)-(-\mu_1)^{1-\gamma}(a_1-\mu_1)}{\mu_1-\mu_2} \end{pmatrix}.$$

from which somewhat tedious computations give $\tilde{D}_{\text{ca2}}(s, q^2)$, and this is $\mathcal{O}(\epsilon^2)$ -close to $D_{\text{ca2}}(s, q^2)$ for $s \in B_\epsilon(0)$.

We claim that $\beta_1 > 0$ if $d > 1$. Set $-\mu_1 = |\mu|e^{i\theta}$ and $-\mu_2 = |\mu|e^{-i\theta}$, where without loss of generality $\theta \in (0, \pi/2)$. Then β_1 simplifies, which directly shows the claim:

$$\begin{aligned} \beta_1(\gamma, d) &= \frac{a_1(d-1)((-\mu_2)^{1-\gamma}-(-\mu_1)^{1-\gamma})+\mu_1\mu_2((-\mu_1)^{-\gamma}-(-\mu_2)^{-\gamma})+d((-\mu_2)^{2-\gamma}-(-\mu_1)^{2-\gamma})}{\mu_1-\mu_2} \\ &= \frac{a_1(d-1)|\mu|^{-\gamma}\sin(\theta(1-\gamma))+|\mu|^{1-\gamma}\sin(\theta\gamma)+d|\mu|^{1-\gamma}\sin(\theta(2-\gamma))}{\sin(\theta)}. \end{aligned}$$

Since $\text{tr}(A) < 0$, the prefactor of s in (2.61) is positive so that (2.61) has a solution $s(q) > 0$ if and only if $h(q^2) < 0$ for some q . We note that $\det(A) > 0$ and

$$\det(C) = \det((- \bar{A})^{1-\gamma}) = (\mu_1\mu_2)^{1-\gamma} > 0,$$

so $h(q^2) < 0$ for some real q requires

$$\beta_2 d + \beta_3 > 0, \quad (2.63)$$

where $\beta_3 < 0$ follows by straightforward calculation. As to the sign of β_2 we compute

$$\begin{aligned} \beta_2(\gamma) &= -\frac{\mu_1\mu_2}{\mu_1-\mu_2} \left(a_1 ((-\mu_2)^{-\gamma}-(-\mu_1)^{-\gamma}) + ((-\mu_2)^{1-\gamma}-(-\mu_1)^{1-\gamma}) \right) \\ &= \frac{|\mu|^{1-\gamma}}{\sin(\theta)} (a_1 \sin(\theta\gamma) - |\mu| \sin(\theta(1-\gamma))). \end{aligned}$$

Hence, $H(\gamma) := a_1 \sin(\theta\gamma) - |\mu| \sin(\theta(1-\gamma))$ has the sign of $\beta_2(\gamma)$, and $\beta_2(\gamma) = 0$ if and only if $H(\gamma) = 0$, which is equivalent to

$$\cot(\theta\gamma) = \frac{a_1}{|\mu| \sin(\theta)} + \cot(\theta). \quad (2.64)$$

The solution to (2.64) is given by γ_{cc} ; note that it depends on A only. From (2.64) we know that $\cot(\theta\gamma_{\text{cc}}) > \cot(\theta)$, so $\gamma_{\text{cc}} < 1$. Since

$$\frac{d}{d\gamma}H(\gamma) = a_1\theta \cos(\theta\gamma) + \mu\theta \cos(\theta(1-\gamma)) > 0.$$

we have $\text{sgn}(H(\gamma)) = \gamma - \gamma_{\text{cc}}$. For $\gamma < \gamma_{\text{cc}}$ the condition (2.63) implies $d < -\beta_3/\beta_2 < 0$, which violates the assumption $d > 0$. Hence, the following conditions must be satisfied

$$\gamma > \gamma_{\text{cc}} \quad \text{and} \quad d > -\beta_3/\beta_2 > 0, \quad (2.65)$$

and $\gamma \rightarrow \gamma_{\text{cc}}^+$ implies $\beta_2 \rightarrow 0^+$, which means $d \rightarrow +\infty$.

Straightforward computations give the minimum of $h(q^2)$ and the associated argument

$$h_{\min} = \frac{4d \det(AC) - (\beta_2 d + \beta_3)^2}{4d \det(C)}, \quad q_{\min}^2 = \frac{\beta_2 d + \beta_3}{2d \det(C)}.$$

If $h_{\min} < 0$, then $h(q^2) < 0$ for $q^2 \in (q_-^2, q_+^2)$, where q_{\pm}^2 are the two roots of $h(q^2) = 0$. Furthermore, $h_{\min} < 0$ gives

$$\beta_2^2 d^2 + (2\beta_2\beta_3 - 4 \det(AC)) d + \beta_3^2 > 0,$$

whose boundary points are

$$d_{\pm} = -\frac{\beta_3}{\beta_2} + \frac{2}{\beta_2^2} \left(\det(AC) \pm \sqrt{(\det(AC))^2 - \beta_2\beta_3 \det(AC)} \right).$$

Since the discriminant is positive $d_{\pm} \in \mathbb{R}$ exist, but $d < d_-$ does not satisfy (2.65). Hence, d_{γ} is the Turing bifurcation point and satisfies Item (1) for (2.61). Since this means the onset of instability is through the origin $s = 0$, the same and the following characterisation hold for the subdiffusion spectrum sufficiently close to the origin. Moreover, $\lim_{\gamma \rightarrow \gamma_{\text{cc}}} d_{\gamma} = +\infty$ and $\lim_{\gamma \rightarrow 1} d_{\gamma} = d_c$. The critical wavenumber is given by q_{γ}^2 .

Case nr: Similar to the case **cc**, the dispersion relation (2.60) can be approximated by (2.62) within $B_{\epsilon}(0)$, but here the minimum anomalous exponent is given by γ_{nr} . We note $\mu_1 \neq \mu_2$, $a_1 \neq \mu_1$ and $a_1 \neq \mu_2$ due to the Turing conditions on A , which guarantees the existence of γ_{nr} . \square

This theorem shows that the critical spectrum of system (2.4) has the ‘Turing shape’ of regular diffusion, i.e., near the origin it is real, has maxima at selected wavenumbers, and crosses the origin for increasing d . Moreover, the relation of reaction and subdiffusive motion in (2.4) stabilises the solution, i.e., the more anomalous the diffusion is, the more ‘difficult’ in terms of the diffusion ratio it is for the solution to become unstable. It is even impossible to be unstable when the diffusion motion becomes too anomalous, i.e., is below γ_A . We illustrate the stable and unstable region in §2.5.4, cf. Fig. 2.11 below.

Remark 2.5.11. *Theorem 2.5.10 is valid only near the origin and thus instabilities through the imaginary axis may be missed. However, due to Theorem 2.5.8, if γ is close to 1, this cannot happen.*

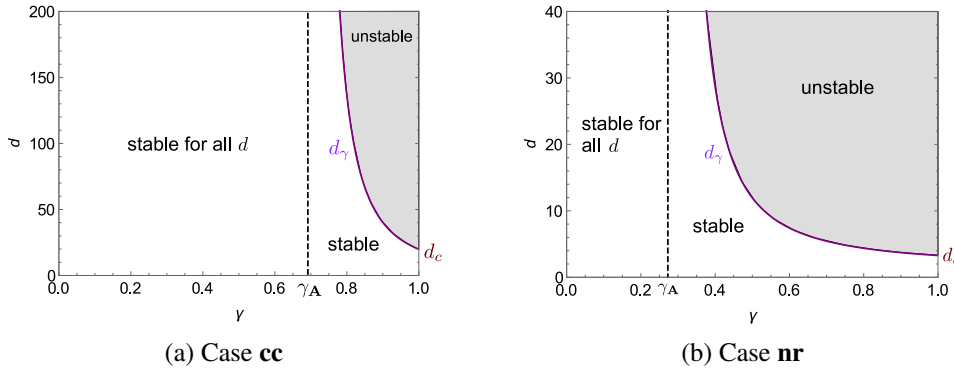


Figure 2.11: Plotted are samples of stability and instability regions of spectra for (2.4) near the origin in terms of the Turing threshold d_γ (purple solid curves), which terminates at the regular threshold d_c and lies above the minimum anomalous exponents γ_A (vertical dashed lines). (a) $\gamma_A = 0.69$, $d_c = 19.798$ and (b) $\gamma_A = 0.27$, $d_c = 3.28$.

2.5.4 Numerical computations of spectra

We illustrate Theorem 2.5.8 with numerical computations for the cases **cc** and **nr**, respectively, where A in (2.4) is given by

$$A_{\text{cc}} = \begin{pmatrix} \frac{1}{2} & -\frac{3}{16} \\ 8 & -1 \end{pmatrix} \quad \text{and} \quad A_{\text{nr}} = \begin{pmatrix} 1 & 1 \\ -\frac{17}{8} & -2 \end{pmatrix}.$$

Here A_{cc} has eigenvalues $\mu_{\pm} \approx -0.25 \pm 0.968i$, and A_{nr} has eigenvalues $\mu_1 \approx -0.854$, $\mu_2 \approx -0.146$. In Fig. 2.11 we plot the Turing instability threshold d_γ and the minimum anomalous exponent γ_A , and determine the stable and unstable region based on the results of §2.5.2.

In Fig. 2.12 we plot results with fixed diffusion coefficient d and different anomalous exponents. As predicted, the subdiffusion (pseudo-)spectrum approaches the regular one as γ increases towards 1. Remark that in case **nr** a gap within the pseudo-spectra occurs as a result of solutions to (2.60) outside Ω_{ca} .

In Fig. 2.13 we plot results with fixed anomalous exponent γ and different diffusion coefficients d for case **cc**. As predicted, the subdiffusion spectrum becomes unstable when d exceeds d_γ . Notably, the spectrum from (2.61) nicely approximates the numerical spectrum computed from (2.60). Furthermore, the subdiffusive transport stabilises the spectrum, since the maximum of the subdiffusion spectrum is less than that of the regular spectrum. The situation is similar for case **nr**, except the subdiffusion (pseudo-)spectrum in this region connects with the regular spectrum.

2.6 Subdiffusion with nonlinear creation and annihilation

Compared to the analysis of the previous sections, much less can be said about (1.7). We aim to study the (formal) linearisation of (1.7) in homogeneous steady state u_* with $r(u_*) = 0$, in

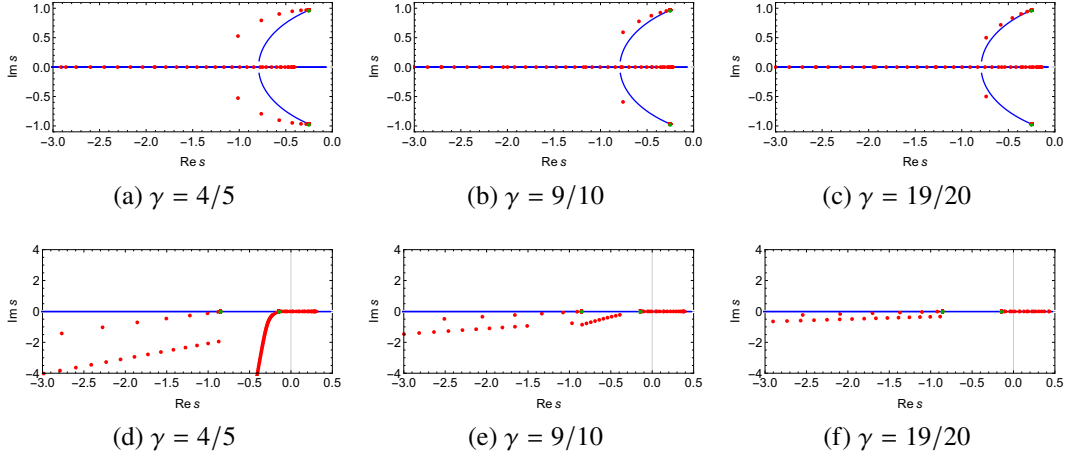


Figure 2.12: Plotted are (pseudo-)spectra of (2.4) for $A = A_{\text{cc}}, A_{\text{nr}}$ for wavenumbers $q = 0.04n, n = 0, 1, \dots, 100$: regular diffusion ($\gamma = 1$, blue solid lines) and subdiffusion ($\gamma \in (0, 1)$, red dotted lines), and the eigenvalues of A (green diamonds). Top row: $A = A_{\text{cc}}$ (case **cc**), $d = 15$; bottom row: $A = A_{\text{nr}}$ (case **nr**), $d = 20$.

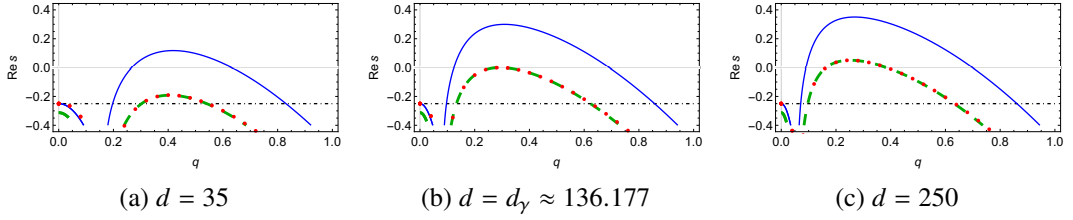


Figure 2.13: Plotted are (pseudo-)spectra of (2.4) for $A = A_{\text{cc}}$ and $\gamma = 4/5$. Subdiffusion (pseudo-)spectra (red dotted) computed from (2.58), regular diffusion spectra (blue solid), and approximate subdiffusion (pseudo-)spectra computed from (2.61) (green dashed). Horizontal dotted dashed lines are $s = \mu_1 \notin \Omega_{\text{ca}}$.

particular its stability properties. This linearisation reads (1.8), where $\sigma := r'(u_*)u_*$. Notably, for $u_* = 0$ this is (2.3) with $a = r(0)$ discussed in §2.5. In contrast, for $u_* \neq 0$ the model is rather different.

We note that like all other scalar models (1.8) reduces to regular diffusion $u_t = du_{xx} + \sigma u$ at $\gamma = 1$, to $u_t = \sigma u$ for constant $u(x, 0) = u_0 \in \mathbb{R}$, and to the subdiffusion equation (2.27) at $\sigma = 0$ (corresponding to $a = 0$ for the other models). However, for $\sigma \neq 0$ equation (1.8) has a different character and does not allow to determine the spectrum with the methods used before due to the non-explicit Laplace transform acting on the product term $\mathcal{D}_{0,t}^{1-\gamma}1 \cdot \mathcal{D}_{0,t}^{-1}u$.

Remark that for $\sigma > 0$, constant initial data remain so and grow exponentially, which implies the expected instability of the non-zero homogeneous steady state.

2.6.1 Energy estimate

In preparation of estimates, let us first consider two cases of (1.8) for which the problematic term vanishes.

For $\gamma = 0$ (1.8) reduces to the PDE

$$u_t = d(u_{t,xx} - \sigma u_{xx}) + \sigma u \Leftrightarrow (1 - d\partial_{xx})u_t = \sigma(1 - d\partial_{xx})u,$$

whose Fourier transform in x reads $\hat{u}_t = \sigma\hat{u}$, i.e., the dispersion relation is $(\lambda - \sigma)(1 + dq^2) = 0$, and $\hat{u}(t, q) = e^{\sigma t}\hat{u}(0, q)$. In particular, $\sigma < 0$ (> 0) implies exponential decay (growth) of $\|u(\cdot, t)\|_{L^2(\mathbb{R})}$.

Related to [64], we start with the following energy-type estimate of (1.8) for $\sigma < 0$.

Theorem 2.6.1. *Let $u(x, t)$ be the solution to (1.8) in $C^1([0, T]; H^2(\mathbb{R}))$ with $u(\cdot, 0) = u_0 \in H^2(\mathbb{R})$ for $t \in [0, T]$, $T > 0$. For any $\gamma \in (0, 1)$ and $\sigma < 0$, there exists a t_σ , such that*

$$\frac{d}{dt} \left(\|u(\cdot, t)\|_{L^2(\mathbb{R})}^2 + d \left\| \left(k_\gamma * (u_x)^2 \right) (\cdot, t) \right\|_{L^1(\mathbb{R})} \right) < 0$$

for $t \in [0, \min\{t_\sigma, T\}]$ with $t_\sigma = -\frac{1}{\sigma}(2 - \gamma)^{\frac{\gamma-2}{\gamma-1}}$, where $\lim_{\gamma \rightarrow 0} t_\sigma = 4$ and $\lim_{\gamma \rightarrow 1} t_\sigma = e$.

Proof. The linear operator in (1.8) is given by

$$\mathcal{L}_\gamma := d \left(\mathcal{D}_{0,t}^{1-\gamma} - \sigma \mathcal{D}_{0,t}^{-\gamma} + \sigma \mathcal{D}_{0,t}^{1-\gamma} 1 \cdot \mathcal{D}_{0,t}^{-1} \right).$$

Testing (1.8) by u and integrating in space gives

$$\int_{\mathbb{R}} u_t \cdot u dx = - \int_{\mathbb{R}} \mathcal{L}_\gamma u_x \cdot u_x dx + \int_{\mathbb{R}} \sigma u^2 dx.$$

so that

$$\frac{1}{2} \frac{d}{dt} \|u\|_{L^2}^2 = -d \int_{\mathbb{R}} u_x \frac{d}{dt} (k_\gamma * u_x) - \sigma (k_\gamma * u_x) u_x + \sigma k_\gamma(t) (1 * u_x) u_x dx + \sigma \|u\|_{L^2}^2. \quad (2.66)$$

Straightforward calculation [64, Lemma 2.2] provides the relation

$$u \frac{d}{dt} (k_\gamma * u) - \frac{1}{2} \frac{d}{dt} (k_\gamma * u^2) = \frac{1}{2} \int_0^t (-k'_\gamma(s)) (u(t) - u(t-s))^2 ds + \frac{1}{2} k_\gamma(t) (u(t))^2,$$

and applying to (2.66) gives

$$\begin{aligned} \frac{1}{2} \frac{d}{dt} (\|u\|_{L^2}^2 + d \|k_\gamma * (u_x)^2\|_{L^1}) &= \sigma \|u\|_{L^2}^2 - \frac{d}{2} k_\gamma(t) \|u_x\|_{L^2}^2 + I_1 + I_2, \\ I_1 &:= -\frac{d}{2} \int_{\mathbb{R}} \int_0^t (-k'_\gamma(s)) (u_x(x, t) - u_x(x, t-s))^2 ds dx, \\ I_2 &:= \sigma d \int_{\mathbb{R}} \int_0^t (k_\gamma(s) - k_\gamma(t)) u_x(x, t) u_x(x, t-s) ds dx. \end{aligned}$$

From $\sigma < 0$, $k_\gamma(t) > 0$ and $k'_\gamma(t) < 0$ for $t \geq 0$, it is clear that $I_1 < 0$, but the sign of I_2 is unclear. We will show that with the bound on t it holds that $I_1 + I_2 \leq 0$. For this we compute

$$\begin{aligned} I_1 + I_2 = -d \int_{\mathbb{R}} \int_0^t & \left(\left(\frac{-k'_\gamma(s)}{2} \right) \left((u_x(x, t))^2 + (u_x(x, t-s))^2 \right) \right. \\ & \left. + \left(k'_\gamma(s) - \sigma(k_\gamma(s) - k_\gamma(t)) \right) u_x(x, t) u_x(x, t-s) \right) ds dx. \end{aligned}$$

If the integrand is nonnegative, then $I_1 + I_2 \leq 0$. Denote $a := -k'_\gamma(s)/2 > 0$, $b := k'_\gamma(s) - \sigma(k_\gamma(s) - k_\gamma(t))$, $f := u_x(t)$ and $g := u_x(t-s)$, so the integrand can be written as $a(f^2 + g^2) + bfg = \frac{-b}{2} \left(\frac{-2a}{b} (f^2 + g^2) - 2fg \right) \geq 0$ if $-2a \leq b < 0$ for all $0 \leq s \leq t$. Clearly, $-2a \leq b$ is satisfied for $\sigma < 0$, and $b < 0$ is equivalent to $\sigma > \frac{k'_\gamma(s)}{k_\gamma(s) - k_\gamma(t)}$, and we analyse the function $h(s) := \frac{k'_\gamma(s)}{k_\gamma(s) - k_\gamma(t)} = \frac{(\gamma-1)s^{\gamma-2}}{s^{\gamma-1}-t^{\gamma-1}}$ in the following. We observe $\lim_{s \rightarrow 0} h(s) = \lim_{s \rightarrow t} h(s) = -\infty$. Then we calculate $\sup_{0 \leq s \leq t} h(s)$. Set the derivative $(d/ds)h(s) = 0$. The solution is $s = s_0 := (2-\gamma)^{\frac{1}{\gamma-1}} t$, where $(2-\gamma)^{\frac{1}{\gamma-1}} \in (0, 1)$ implies $0 < s_0 < t$. We then evaluate $(d^2/ds^2)h(s)$ at $s = s_0$ and we can get $(d^2/ds^2)h(s_0) < 0$ for $\gamma \in [0, 1]$. Hence $\sup_{0 \leq s \leq t} h(s) = h(s_0) = -(2-\gamma)^{\frac{\gamma-2}{\gamma-1}}/t < 0$. Therefore, if $b < 0$, then $\sigma > h(s)$ for all s implies that $\sigma > h(s_0) = -(2-\gamma)^{\frac{\gamma-2}{\gamma-1}}/t$, which leads to $t < -\frac{1}{\sigma}(2-\gamma)^{\frac{\gamma-2}{\gamma-1}} = t_\sigma$. The limit at $\gamma = 0$ is obvious, the limit at $\gamma = 1$ a straightforward application of L'Hopital's rule. \square

Theorem 2.6.1 shows that the ‘energy’ of (1.8) decays at least locally in time, however, we do not know the rate. Moreover, we observe that if σ tends to 0, i.e., to the subdiffusion equation, then the guaranteed time of decay increases unboundedly. In contrast, if $-\sigma$ increases the guaranteed interval for decay becomes shorter. This result is somewhat counterintuitive and in contrast to the global exponential decay for constant solutions. The reason is that our sufficient conditions, that the integrand in $I_1 + I_2$ is nonnegative, does not capture the relevant features. Nevertheless, we believe the approach is instructive as it illustrates the counter-oriented signs one encounters when trying to obtain estimates in more generality for this model.

2.6.2 Existence and uniqueness

In this section, we discuss the linearisation (1.8) in Fourier space, namely

$$\partial_t \hat{u} = -dq^2 \left(\mathcal{D}_{0,t}^{1-\gamma} \hat{u} - \sigma \mathcal{D}_{0,t}^{-\gamma} \hat{u} + \sigma \mathcal{D}_{0,t}^{1-\gamma} 1 \cdot \mathcal{D}_{0,t}^{-1} \hat{u} \right) + \sigma \hat{u}. \quad (2.67)$$

To our knowledge, this fractional ODE (for fixed q and $\sigma \neq 0$) has not been previously studied, so we start with existence and uniqueness considerations before discussing the qualitative behaviour of the solution. Notably, we only prove the existence and uniqueness of the mild solution to (2.67). The classical solution is still an open problem.

In preparation of global existence results, we give the following lemmas.

Lemma 2.6.2. *For fixed q , the function $\hat{u}(t, q)$ is the solution of (2.67) for $t \in [0, T]$ with initial condition $\hat{u}(0, q) = \hat{u}_0(q)$ if and only if $\hat{u}(\cdot, q) \in C([0, T]) \cap C^1((0, T])$ satisfies the following integral equation*

$$\hat{u}(t, q) = \hat{u}_0(q)e^{\sigma t} - dq^2(k_\gamma * \hat{u})(t, q) - \sigma dq^2 \int_0^t e^{\sigma(t-s)} k_\gamma(s) \int_0^s \hat{u}(\tau, q) d\tau ds, \quad t \geq 0. \quad (2.68)$$

Proof. If $\hat{u}(\cdot, q) \in C([0, T]) \cap C^1((0, T])$, then we can rewrite (2.67) in the form

$$\partial_t(\hat{u} + dq^2 \mathcal{D}_{0,t}^{-\gamma} \hat{u}) = \sigma(\hat{u} + dq^2 \mathcal{D}_{0,t}^{-\gamma} \hat{u}) - \sigma dq^2 \mathcal{D}_{0,t}^{1-\gamma} 1 \cdot \mathcal{D}_{0,t}^{-1} \hat{u}. \quad (2.69)$$

Then the second summand on the right-hand side is continuous in $(0, T]$ and integrable on $[0, T]$. Therefore, we obtain the integral equation (2.68) using the variation-of-constants with initial condition $\hat{u}(0, q) = \hat{u}_0(q)$, and using Lemma 2.3.4(2) yields the first summand on the right-hand side of (2.68).

Conversely, the second and third summand on the right-hand side of (2.68) are continuous on $[0, T]$ and continuously differentiable in $(0, T]$. Then we can differentiate both side of (2.68) with respect to t and obtain (2.67) for $t > 0$. For $t \rightarrow 0$, the convolutions in (2.68) vanish and yields $\hat{u}(0, q) = \hat{u}_0(q)$. \square

Lemma 2.6.3. *For $\sigma < 0$ and any $0 \leq t_0 \leq t$, the following estimate holds:*

$$|\sigma| \int_{t_0}^t e^{\sigma(t-s)} s^{\gamma-1} (s-t_0) ds \leq (t-t_0)^\gamma.$$

In particular, $|\sigma| \int_{t_0}^t e^{\sigma(t-s)} s^{\gamma-1} (s-t_0) ds \sim (t-t_0)^\gamma$ for $t \gg 1$.

Proof. Denote $f(t) := |\sigma| \int_{t_0}^t e^{-\sigma s} s^{\gamma-1} (s-t_0) ds$ and $g(t) := e^{-\sigma t} (t-t_0)^\gamma$. Then $f(t_0) = g(t_0) = 0$. The derivatives with respect to t are given by

$$f'(t) = |\sigma| e^{-\sigma t} t^{\gamma-1} (t-t_0), \quad g'(t) = -\sigma e^{-\sigma t} (t-t_0)^\gamma + \gamma e^{-\sigma t} (t-t_0)^{\gamma-1}.$$

The second term in $g'(t)$ is strictly positive and $t^{\gamma-1} \leq (t-t_0)^{\gamma-1}$ for $0 \leq t_0 \leq t$. Hence $f'(t) < g'(t)$ for $0 \leq t_0 \leq t$. Then we have $f(t) \leq g(t)$ for $0 \leq t_0 \leq t$ which is equivalent to the claimed estimate. Moreover, we have $\lim_{t \rightarrow \infty} f(t)/g(t) = 1$ by L'Hôpital's rule, which gives the claimed asymptotic approximation. \square

Lemma 2.6.4. *For $\sigma > 0$ and any $0 \leq t_0 \leq t$, there exists a unique $T_*(t_0) > t_0$ such that the following estimate holds*

$$|\sigma| \int_{t_0}^t e^{\sigma(t-s)} s^{\gamma-1} (s-t_0) ds \leq (t-t_0)^\gamma, \quad (2.70)$$

for $t \in [t_0, T_*(t_0)]$, where $t = T_*(t_0)$ is the solution to the above equality.

Moreover, $\inf_{0 \leq t_0 \leq T_*(t_0)} (T_*(t_0) - t_0) = T_*(0)$.

Proof. We use the notations defined in the proof of Lemma 2.6.3. We have $f(t_0) = g(t_0) = 0$ and $\lim_{t \rightarrow \infty} g(t) = 0$ for $\sigma > 0$. Moreover, $f'(t_0) = 0$ and $g'(t_0) = +\infty$. Hence $f(t) \leq g(t)$ for small t . We observe that $f'(t) > 0$ for $t > t_0$, whereas $g'(t)$ becomes negative for $t > t_0 + \gamma/\sigma$ and $\lim_{t \rightarrow \infty} g(t) = 0$. Therefore, there exists a unique point $t_* > t_0$ such that $f(t_*) = g(t_*)$ and $f(t) < g(t)$ for $t < t_*$, which is same as the claimed upper bound $T_*(t_0)$.

We suppress the effect of $e^{\sigma t}$ on $f'(t)$ and $g'(t)$, that means we consider $\check{f}'(t) := |\sigma|t^{\gamma-1}(t-t_0)$ and $\check{g}'(t) := -\sigma(t-t_0)^\gamma + \gamma(t-t_0)^{\gamma-1}$. We denote $\rho := t - t_0$, then $\check{f}'(t) = |\sigma|(\rho+t_0)^{\gamma-1}\rho$ and $\check{g}'(t) := -\sigma\rho^\gamma + \gamma\rho^{\gamma-1}$. We note that $\check{g}'(t)$ does not depend on t_0 explicitly, whereas $\check{f}'(t)$ does and decreases for increasing t_0 . Therefore, the length of the interval $t \in [t_0, T_*(t_0)]$ such that (2.70) is satisfied becomes larger for increasing t_0 . This implies the length of interval $[0, T_*(0)]$ is the smallest for all $t_0 \geq 0$. \square

In the following, we give the local existence and uniqueness theorem of the integral equation (2.68) and prove by using Banach fixed point theorem. Recall that for $\sigma = 0$ the equation turns into the subdiffusion equation for which global existence is known.

Theorem 2.6.5 (Local existence and uniqueness). *For any fixed q and initial condition $\hat{u}(0, q) = \hat{u}_0(q)$ there exists T_σ and for any $T < T_\sigma$ a unique local solution $\hat{u}(\cdot, q) \in C([0, T])$ of (2.68), where for $\sigma < 0$ we have $T_\sigma = T_\gamma := (\Gamma(\gamma+1)/(dq^2(\gamma+1)))^{1/\gamma}$, and for $\sigma > 0$ we have $T_\sigma = \min\{T_\gamma, T_*(0)\}$ from Lemma 2.6.4.*

Proof. We recall (2.68) and define a map $K : C([0, T_0]) \rightarrow C([0, T_0])$ which is given by

$$(K\hat{u})(t) = \hat{u}_0 e^{\sigma t} - dq^2(k_\gamma * \hat{u})(t) - \sigma dq^2 \int_0^t e^{\sigma(t-s)} k_\gamma(s) \int_0^s \hat{u}(\tau) d\tau ds,$$

For $\sigma < 0$, we have the estimate

$$\begin{aligned} |(K\hat{u})(t) - (K\hat{v})(t)| &\leq |dq^2(k_\gamma * (\hat{u} - \hat{v}))(t)| + \left| \sigma dq^2 \int_0^t e^{\sigma(t-s)} k_\gamma(s) \int_0^s (\hat{u} - \hat{v})(\tau) d\tau ds \right| \\ &\leq \frac{dq^2 t^\gamma}{\gamma \Gamma(\gamma)} \sup_{0 \leq s \leq t} |\hat{u}(s) - \hat{v}(s)| + \sup_{0 \leq \tau \leq t} |\hat{u}(\tau) - \hat{v}(\tau)| \frac{dq^2}{\Gamma(\gamma)} |\sigma| \int_0^t e^{\sigma(t-s)} s^\gamma ds \end{aligned} \quad (2.71)$$

$$\leq \frac{dq^2(\gamma+1)t^\gamma}{\Gamma(\gamma+1)} \sup_{0 \leq s \leq t} |\hat{u}(s) - \hat{v}(s)|, \quad (2.72)$$

where Lemma 2.6.3 gives the estimate for the second summand in (2.71). Hence we have

$$\|K\hat{u} - K\hat{v}\|_{C([0, T_0])} \leq \frac{dq^2(\gamma+1)}{\Gamma(\gamma+1)} T_0^\gamma \|\hat{u} - \hat{v}\|_{C([0, T_0])}$$

We choose T_0 such that $dq^2(\gamma+1)T_0^\gamma/\Gamma(\gamma+1) < 1$, i.e., $T_0 < T_\gamma$, so K is a contraction and, being linear, it is then a self-map of any ball. Existence of a unique solution now follows from the contraction principle.

For $\sigma > 0$ Lemma 2.6.4 provides $T_*(0)$ such that the above estimates of K hold for $T_0 < \min\{T_\gamma, T_*(0)\}$ and the claim follows as before. \square

We note that for fixed γ and $\sigma < 0$, the upper bound of the existence $T_\sigma \rightarrow \infty$ for $|q| \rightarrow 0$ and does not depend on σ . However, $T_\sigma \rightarrow 0$ for $|q| \rightarrow \infty$. Therefore, we need the extendibility of existence and uniqueness interval, and we have the following result.

Theorem 2.6.6 (Global existence and uniqueness). *For fixed q and initial condition $\hat{u}(0, q) = \hat{u}_0(q)$ there exists a unique solution $\hat{u}(\cdot, q) \in C([0, \infty))$ of (2.68).*

Proof. For $\sigma = 0$ it is clear from the subdiffusion equation. Otherwise, the previous theorem gives the existence of a unique solution in $C([0, T_0])$ for $0 < T_0 < T_\sigma$. We want to extend the interval to $t \in [T_0, T_1]$, $T_1 > T_0$ using that the integral equation (2.68) allows for the following separation

$$\begin{aligned}\hat{u}(t) &= \hat{u}_0 e^{\sigma t} - dq^2 (k_\gamma * \hat{u})(t) - \sigma dq^2 \int_0^t e^{\sigma(t-s)} k_\gamma(s) \int_0^s \hat{u}(\tau) d\tau ds \\ &= \hat{u}_0 e^{\sigma t} - dq^2 \int_0^{T_0} k_\gamma(t-s) \hat{u}(s) ds - \sigma dq^2 \int_0^{T_0} e^{\sigma(t-s)} k_\gamma(s) \int_0^s \hat{u}(\tau) d\tau ds \quad (2.73)\end{aligned}$$

$$- \sigma dq^2 \int_{T_0}^t e^{\sigma(t-s)} k_\gamma(s) \int_0^{T_0} \hat{u}(\tau) d\tau ds \quad (2.74)$$

$$- dq^2 \int_{T_0}^t k_\gamma(t-s) \hat{u}(s) ds - \sigma dq^2 \int_{T_0}^t e^{\sigma(t-s)} k_\gamma(s) \int_{T_0}^s \hat{u}(\tau) d\tau ds. \quad (2.75)$$

We denote the right-hand side except (2.75) by $\phi_0(t; T_0)$ and note this is defined uniquely in terms of the local solution from Theorem 2.6.5 (the idea is from [27, Eq. 3.2.24 & 3.2.25]). Then we define a map $K_0 : C([T_0, T_1]) \rightarrow C([T_0, T_1])$, whose fixed points are the solutions of (2.68) by

$$(K_0 \hat{u})(t) = \phi_0(t; T_0) - dq^2 \int_{T_0}^t k_\gamma(t-s) \hat{u}(s) ds - \sigma dq^2 \int_{T_0}^t e^{\sigma(t-s)} k_\gamma(s) \int_{T_0}^s \hat{u}(\tau) d\tau ds. \quad (2.76)$$

For $\sigma < 0$ we estimate analogous to (2.72) that

$$\begin{aligned}|(K_0 \hat{u})(t) - (K_0 \hat{v})(t)| &\leq \frac{dq^2}{\gamma \Gamma(\gamma)} (t^\gamma - T_0^\gamma) \sup_{T_0 \leq s \leq t} |\hat{u}(s) - \hat{v}(s)| \\ &\quad + \sup_{T_0 \leq \tau \leq t} |\hat{u}(\tau) - \hat{v}(\tau)| \left| \frac{\sigma dq^2}{\Gamma(\gamma)} \right| \int_{T_0}^t e^{\sigma(t-s)} s^{\gamma-1} (s - T_0) ds \\ &\leq \frac{dq^2(\gamma+1)}{\Gamma(\gamma+1)} (t - T_0)^\gamma \sup_{T_0 \leq s \leq t} |\hat{u}(s) - \hat{v}(s)|,\end{aligned}$$

where we have used Lemma 2.6.3 again and, $t^\gamma - T_0^\gamma \leq (t - T_0)^\gamma$ for $t \geq T_0 > 0$. Therefore,

$$\|K_0 \hat{u} - K_0 \hat{v}\|_{C([T_0, T_1])} \leq \frac{dq^2(\gamma+1)}{\Gamma(\gamma+1)} (T_1 - T_0)^\gamma \|\hat{u} - \hat{v}\|_{C([T_0, T_1])}.$$

We choose T_1 such that $dq^2(\gamma+1)(T_1 - T_0)^\gamma / \Gamma(\gamma+1) < 1$, i.e., $T_1 - T_0 < T_\gamma$, the map K_0 is a contraction, which implies existence of a unique solution as before. Without loss of generality, we can choose a fixed constant $\alpha \in (0, 1)$ so that $T_0 = \alpha T_\gamma < T_\gamma$. Then we choose $T_1 - T_0 = \alpha T_\gamma < T_\gamma$ and thus $T_1 = 2\alpha T_\gamma$. Iterating the above procedure gives the upper interval bounds $T_n = \alpha(n+1)T_\gamma$. Since $\lim_{n \rightarrow \infty} T_n = \infty$ we have global existence and uniqueness.

For $\sigma > 0$, by Lemma 2.6.4, $T_*(0) \leq T_*(T_0) - T_0$ and the above estimates of K_0 are valid for $T_1 \leq T_*(T_0)$, and choosing T_1 so that in addition $T_1 - T_0 < T_\gamma$ renders K_0 a contraction. Thus we can choose $T_1 - T_0 < \min\{T_\gamma, T_*(0)\}$ and such a choice is $T_1 := 2\beta T_\sigma$ where fixed $\beta \in (0, 1)$ and $T_\sigma := \min\{T_\gamma, T_*(0)\}$. Upon iterating this procedure global existence follows as before. \square

2.6.3 Dynamics of Fourier modes

In this section, we give the locally decaying properties of solution to (2.67).

Theorem 2.6.7. *Let $\hat{u}(\cdot, q) \in C^1((0, T))$, $T > 0$ be the solution to (2.67) with initial condition $\hat{u}(0, q) = \hat{u}_0(q)$. For any fixed q and $\sigma < 0$, there exists $t_\epsilon > 0$ such that $|\hat{u}(t, q)| < |\hat{u}_0(q)|e^{\sigma t}$ for $t \in (0, t_\epsilon)$.*

Proof. For any fixed q , let us suppress the dependence of \hat{u} on q for readability. Set $v(t) = (\hat{u}_t - \sigma \hat{u})(t)$, so $v \in C((0, T))$. Then we can rewrite (2.67) in the form of

$$v(t) = -dq^2 \left(\int_0^t (k_\gamma(t-s) - k_\gamma(t)) v(s) ds + k_\gamma(t) \hat{u}(t) \right). \quad (2.77)$$

On the other hand, we can solve $\hat{u}(t)$ by variation-of-constants, namely

$$\hat{u}(t) = \hat{u}(0)e^{\sigma t} + \int_0^t e^{\sigma(t-s)} v(s) ds.$$

Substitution into (2.77) gives

$$\begin{aligned} v(t) &= F_1(t) + F_2(t), \\ F_1(t) &:= -dq^2 \int_0^t (k_\gamma(t-s) - k_\gamma(t) + k_\gamma(t)e^{\sigma(t-s)}) v(s) ds, \\ F_2(t) &:= -dq^2 k_\gamma(t) \hat{u}(0) e^{\sigma t}. \end{aligned}$$

Without loss of generality, let $\hat{u}(0) > 0$. Hence $F_2(t) < 0$ for all $t > 0$. Moreover, $k_\gamma(t-s) - k_\gamma(t) + k_\gamma(t)e^{\sigma(t-s)} > 0$ for all $0 \leq s \leq t < \infty$. We discuss the sign of $v(t)$ for $t \in (0, t_\epsilon)$, $t_\epsilon > 0$ as follows:

- (1) Assume $v(t) > 0$ for all $t \in (0, t_\epsilon)$. Then $F_1(t) < 0$ which leads to $v(t) < 0$. It is a contradiction.
- (2) Assume $v(t) = 0$ for all $t \in (0, t_\epsilon)$. Then $F_1(t) = 0$ which leads to $v(t) < 0$. It is also a contradiction.

Hence the only possibility is $v(t) < 0$ for $t \in (0, t_\epsilon)$ and Grönwall's inequality gives the claimed result. \square

Theorem 2.6.7 shows that each Fourier mode decays exponentially at the onset of evolution at least with the rate σ . This also implies $\|u(\cdot, t)\|_{L^2}$ decays exponentially. However, the decaying rate for $t > t_\epsilon$ is unclear.

We note that $v(t)$ either changes to positive, or stays negative and tends to zero for $t \rightarrow \infty$. We can see it from the relation $v(t) - F_1(t) = F_2(t)$. If $v(t)$ stays negative, and does not tend to zero or does not have limit, then the left-hand side does not tend to zero or does not have limit either, which contradict the exponential decay on the right-hand side. The explicitly decaying rate is unclear, but both of these two cases imply that the decay of $\hat{u}(t, q)$ becomes slower for increasing t . It is consistent with the numerical computation in §2.6.5 where the Fourier mode decays slower than $|\hat{u}_0(q)|e^{\sigma t}$ for large t , cf. Fig. 2.14e.

2.6.4 Linear analysis

As mentioned, the Fourier-Laplace transform of (1.8) does not give a dispersion relation which explicitly depends on the spectrum. In this section, we introduce an alternatively method to study the linear behaviour of the solution. To simplify the notations, we denote $U(x, t)$ as the solution to (1.7). Set $V = e^{\int_0^t r(U(x, s))ds}$ and $W = U e^{-\int_0^t r(U(x, s))ds}$, which gives $U = VW$. Then (1.7) can be transformed into the following system

$$\begin{cases} W_t = d \left(\mathcal{D}_{0,t}^\alpha W_{xx} + \frac{2V_x}{V} \mathcal{D}_{0,t}^\alpha W_x + \frac{V_{xx}}{V} \mathcal{D}_{0,t}^\alpha W \right) \\ V_t = r(VW)V \end{cases} \quad (2.78)$$

where $\alpha := 1 - \gamma$. The homogeneous steady state is given by $(W_*, V_*) = (u_*, 1)$ with $u_* \neq 0$. Moreover, $u \geq 0$ leads to $V > 0$ and $W \geq 0$. We consider the perturbation such that $(W, V) = (u_* + \epsilon w, 1 + \epsilon v)$, then the linearisation of (2.78) in $(u_*, 1)$ is given by

$$\begin{cases} w_t = d \left(\mathcal{D}_{0,t}^\alpha w_{xx} + v_{xx} \mathcal{D}_{0,t}^\alpha u_* \right) \\ v_t = r'(u_*)w + r'(u_*)u_*v \end{cases} \quad (2.79)$$

Notably, $U = WV = u_* + \epsilon(w + u_*v) + O(\epsilon^2)$ implies that the perturbation u , i.e., the solution of (1.8), can be expressed by $u = w + u_*v + O(\epsilon)$. We remark that since $V(x, t) = e^{\int_0^t r(U(x, s))ds}$, the initial condition $V(x, 0) = 1$. This leads to $1 = V(x, 0) = 1 + \epsilon v(x, 0)$ and thus $v(x, 0) = 0$, which implies that the initial condition for perturbation $v(x, t)$ is restricted to 0.

We aim to construct two systems such that (2.79) is uniformly bounded by these two systems which are so-called lower and upper bound systems. The solutions of these two systems should be easily handled.

In the rest of this section, we construct the following two systems

$$\text{Lower bound: } \begin{cases} \underline{w}_t = d \mathcal{D}_{0,t}^\alpha \underline{w}_{xx} \\ \underline{v}_t = r'(u_*)\underline{w} + r'(u_*)u_*\underline{v} \end{cases} \quad (2.80)$$

$$\text{Upper bound: } \begin{cases} \bar{w}_t = d \mathcal{D}_{0,t}^\alpha \bar{w}_{xx} + Mt^{-\eta} \\ \bar{v}_t = r'(u_*)\bar{w} + r'(u_*)u_*\bar{v} \end{cases}, \quad \eta > 0, |M| > 0. \quad (2.81)$$

and analyse their solutions. We still have an open problem, however, that is to prove (2.79) is uniformly bounded by the above systems.

Lower bound We first analyse the lower bound system (2.80). The Green's function of the first equation in (2.80) is given by (2.31), which can be represented in terms of the Wright function (cf. (A.3)) as follows

$$\underline{w} = \Phi(x, t) = \frac{1}{2\sqrt{d}} t^{-\mu} \mathcal{W}\left(-\mu, 1 - \mu; -\frac{|x|}{\sqrt{d}} t^{-\mu}\right),$$

where $\mu := (1 - \alpha)/2 \in (0, 1/2)$. Then the substitution into the second equation in (2.80) and the variation-of-constants give

$$\underline{y}(x, t) = r'(u_*) e^{\sigma t} \int_0^t e^{-\sigma s} \Phi(x, s) ds,$$

here the initial condition $\underline{y}(x, 0) = 0$ as mentioned. Hence the perturbation \underline{u} is given to the leading order by

$$\underline{u} = \underline{w} + u_* \underline{y} = \Phi(x, t) + \sigma e^{\sigma t} \int_0^t e^{-\sigma s} \Phi(x, s) ds.$$

Lemma 2.6.8. *If $\sigma < 0$, then $\underline{u} \sim \frac{\mu}{2\sigma\sqrt{d}\Gamma(1-\mu)} t^{-\mu-1}$ as $t \rightarrow \infty$.*

Proof. First, we assume that $\lim_{t \rightarrow \infty} e^{-\sigma t} \underline{u} = \infty$ and introduce an exponent $\beta > 0$. Then we compute the following limit using L'Hôpital's rule,

$$\begin{aligned} \lim_{t \rightarrow \infty} \frac{\underline{u}}{t^{-\beta}} &= \lim_{t \rightarrow \infty} \frac{e^{-\sigma t} \underline{u}}{e^{-\sigma t} t^{-\beta}} = \lim_{t \rightarrow \infty} \frac{-\sigma e^{-\sigma t} \underline{u} + e^{-\sigma t} \partial_t \underline{u}}{-\sigma e^{-\sigma t} t^{-\beta} - \beta e^{-\sigma t} t^{-\beta-1}} = \lim_{t \rightarrow \infty} \frac{\partial_t \Phi}{-\sigma t^{-\beta} - \beta t^{-\beta-1}} \\ &= \lim_{t \rightarrow \infty} \frac{\frac{-\mu}{2\sqrt{d}} t^{-\mu-1} \mathcal{W}_1 + \frac{|x|\mu}{2d} t^{-2\mu-1} \mathcal{W}_2}{-\sigma t^{-\beta} - \beta t^{-\beta-1}} = \lim_{t \rightarrow \infty} \frac{\frac{-\mu}{2\sqrt{d}} \mathcal{W}_1 + \frac{|x|\mu}{2d} t^{-\mu} \mathcal{W}_2}{-\sigma - (\mu+1)t^{-1}} \\ &= \frac{\mu}{2\sigma\sqrt{d}\Gamma(1-\mu)}, \end{aligned}$$

here we choose $\beta = \mu + 1$, and denote $\mathcal{W}_j := \mathcal{W}\left(-\mu, 1 - j\mu; -\frac{|x|t^{-\mu}}{\sqrt{d}}\right)$, $j \in \mathbb{N}$, and see Appendix A.3 for the derivative $\partial_t \Phi$. The above limit is consistent with the assumption and implies the claimed result.

Next, we assume that $\lim_{t \rightarrow \infty} e^{-\sigma t} \underline{u} < \infty$, thus \underline{u} is decreasing to zero exponentially. Using L'Hôpital's rule twice and properties of the derivatives of Φ (cf. Appendix A.3), we obtain the following limit

$$\begin{aligned} \lim_{t \rightarrow \infty} \frac{\underline{u}}{t^{-\beta}} &= \lim_{t \rightarrow \infty} \frac{\partial_t \underline{u}}{-\beta t^{-\beta-1}} = \lim_{t \rightarrow \infty} \frac{e^{-\sigma t} \partial_t \underline{u}}{-\beta e^{-\sigma t} t^{-\beta-1}} \\ &= \lim_{t \rightarrow \infty} \frac{-\sigma e^{-\sigma t} \partial_t \underline{u} + e^{-\sigma t} \partial_t^2 \underline{u}}{\beta \sigma e^{-\sigma t} t^{-\beta-1} + \beta(\beta+1)e^{-\sigma t} t^{-\beta-2}} = \lim_{t \rightarrow \infty} \frac{\partial_t^2 \Phi}{\beta \sigma t^{-\beta-1} + \beta(\beta+1)t^{-\beta-2}} \\ &= \lim_{t \rightarrow \infty} \frac{\frac{\mu(\mu+1)}{2\sqrt{d}} t^{-\mu-2} \mathcal{W}_1 + \frac{|x|(-3\mu^2-\mu)}{2d} t^{-2\mu-2} \mathcal{W}_2 + \frac{|x|^2\mu^2}{2d^{3/2}} t^{-3\mu-2} \mathcal{W}_3}{\beta \sigma t^{-\beta-1} + \beta(\beta+1)t^{-\beta-2}} \\ &= \lim_{t \rightarrow \infty} \frac{\frac{\mu(\mu+1)}{2\sqrt{d}} \mathcal{W}_1 + \frac{|x|(-3\mu^2-\mu)}{2d} t^{-\mu} \mathcal{W}_2 + \frac{|x|^2\mu^2}{2d^{3/2}} t^{-2\mu} \mathcal{W}_3}{(\mu+1)\sigma + (\mu+1)(\mu+2)t^{-1}} \\ &= \frac{\mu}{2\sigma\sqrt{d}\Gamma(1-\mu)}, \end{aligned}$$

here we choose $\beta = \mu + 1$. This result implies that \underline{u} is algebraically decaying and thus $\lim_{t \rightarrow \infty} e^{-\sigma t} \underline{u} = \infty$, which contradicts the assumption. \square

We claim that \underline{u} grows exponentially in t for $\sigma > 0$. The derivative $\frac{d}{dt} \int_0^t e^{-\sigma s} \Phi(x, s) ds = e^{-\sigma t} \Phi(x, t) > 0$ due to the positivity of Φ , cf. §2.3.2. Hence $\int_0^t e^{-\sigma s} \Phi(x, s) ds$ is increasing in t and it leads to the claimed result.

Upper bound We then analyse the upper bound system (2.81) with the initial condition $\bar{w}(x, 0) = \delta(x)$ where $\delta(x)$ is the Dirac delta distribution. Assume the solution has the form $\bar{w}(x, t) = \Phi(x, t) + c(t)$. The substitution gives

$$\Phi_t + c' = d\mathcal{D}_{0,t}^\alpha \Phi_{xx} + Mt^{-\eta} \Rightarrow c(t) = c(0) + \frac{M}{1-\eta} t^{1-\eta}.$$

Since $\delta(x) = \bar{w}(x, 0) = \Phi(x, 0) + c(0) = \delta(x) + c(0)$, it leads to $c(0) = 0$. Hence

$$\bar{w} = \Phi(x, t) + At^{1-\eta},$$

here $A := \frac{M}{1-\eta}$. The solution to the second equation in (2.81) is given by

$$\bar{v}(x, t) = r'(u_*) e^{\sigma t} \int_0^t e^{-\sigma s} \bar{w}(x, s) ds,$$

with initial condition $\bar{v}(x, 0) \equiv 0$. Hence

$$\begin{aligned} \bar{u} &= \bar{w} + u_* \bar{v} \\ &= \Phi(x, t) + At^{1-\eta} + \sigma e^{\sigma t} \int_0^t e^{-\sigma s} \Phi(x, s) ds + A\sigma e^{\sigma t} \int_0^t e^{-\sigma s} s^{1-\eta} ds, \quad \eta \in (0, 1). \end{aligned}$$

Lemma 2.6.9. *If $\sigma < 0$ and $\eta \in (0, 1)$, then $\bar{u} \sim -\frac{M}{\sigma} t^{-\eta}$ as $t \rightarrow \infty$.*

Proof. First, we assume $\lim_{t \rightarrow \infty} e^{-\sigma t} \bar{u} = \infty$ and introduce the exponent $\beta > 0$, then we compute the following limit using L'Hôpital's rule,

$$\begin{aligned} \lim_{t \rightarrow \infty} \frac{\bar{u}}{t^{-\beta}} &= \lim_{t \rightarrow \infty} \frac{e^{-\sigma t} \bar{u}}{e^{-\sigma t} t^{-\beta}} = \lim_{t \rightarrow \infty} \frac{-\sigma e^{-\sigma t} \bar{u} + e^{-\sigma t} \partial_t \bar{u}}{-\sigma e^{-\sigma t} t^{-\beta} - \beta e^{-\sigma t} t^{-\beta-1}} = \lim_{t \rightarrow \infty} \frac{\partial_t \Phi + Mt^{-\eta}}{-\sigma t^{-\beta} - \beta t^{-\beta-1}} \\ &= \lim_{t \rightarrow \infty} \frac{\frac{-\mu}{2\sqrt{d}} t^{-\mu-1} \mathcal{W}_1 + \frac{|x|\mu}{2d} t^{-2\mu-1} \mathcal{W}_2 + Mt^{-\eta}}{-\sigma t^{-\beta} - \beta t^{-\beta-1}} \\ &= \lim_{t \rightarrow \infty} \frac{\frac{-\mu}{2\sqrt{d}} t^{-\mu-1+\eta} \mathcal{W}_1 + \frac{|x|\mu}{2d} t^{-2\mu-1+\eta} \mathcal{W}_2 + M}{-\sigma - \eta t^{-1}} \\ &= -\frac{M}{\sigma}, \end{aligned}$$

here we choose $\beta = \eta$, and note that $-j\mu - 1 + \eta < 0$, $j = 1, 2$ for $\eta \in (0, 1)$. The above limit implies the claimed result.

Next, we assume $\lim_{t \rightarrow \infty} e^{-\sigma t} \bar{u} < \infty$, so \bar{u} decreases to zero exponentially. Using L'Hôpital's rule twice and properties of the derivatives of Φ (cf. Appendix A.3), we then obtain the following limit

$$\begin{aligned} \lim_{t \rightarrow \infty} \frac{\bar{u}}{t^{-\beta}} &= \lim_{t \rightarrow \infty} \frac{\partial_t \bar{u}}{-\beta t^{-\beta-1}} = \lim_{t \rightarrow \infty} \frac{e^{-\sigma t} \partial_t \bar{u}}{-\beta e^{-\sigma t} t^{-\beta-1}} \\ &= \lim_{t \rightarrow \infty} \frac{-\sigma e^{-\sigma t} \partial_t \bar{u} + e^{-\sigma t} \partial_t^2 \bar{u}}{\beta \sigma e^{-\sigma t} t^{-\beta-1} + \beta(\beta+1)e^{-\sigma t} t^{-\beta-2}} = \lim_{t \rightarrow \infty} \frac{\partial_t^2 \Phi - M\eta t^{-\eta-1}}{\beta \sigma t^{-\beta-1} + \beta(\beta+1)t^{-\beta-2}} \\ &= \lim_{t \rightarrow \infty} \frac{\frac{\mu(\mu+1)}{2\sqrt{d}} t^{-\mu-2} \mathcal{W}_1 + \frac{|x|(-3\mu^2-\mu)}{2d} t^{-2\mu-2} \mathcal{W}_2 + \frac{|x|^2 \mu^2}{2d^{3/2}} t^{-3\mu-2} \mathcal{W}_3 - M\eta t^{-\eta-1}}{\beta \sigma t^{-\beta-1} + \beta(\beta+1)t^{-\beta-2}} \\ &= \lim_{t \rightarrow \infty} \frac{\frac{\mu(\mu+1)}{2\sqrt{d}} t^{-\mu-1+\eta} \mathcal{W}_1 + \frac{|x|(-3\mu^2-\mu)}{2d} t^{-2\mu-1+\eta} \mathcal{W}_2 + \frac{|x|^2 \mu^2}{2d^{3/2}} t^{-3\mu-1+\eta} \mathcal{W}_3 - M\eta}{\eta \sigma + \eta(\eta+1)t^{-1}} \\ &= -\frac{M}{\sigma}, \end{aligned}$$

here we choose $\beta = \eta$ and $-3\mu - 1 + \eta < 0$ for $\eta \in (0, 1)$. Then we obtain $\bar{u} \sim -\frac{M}{\sigma} t^{-\eta}$ as $t \rightarrow \infty$. This implies that $\lim_{t \rightarrow \infty} e^{-\sigma t} \bar{u} = \infty$ which contradicts the assumption. \square

We claim that \bar{u} grows exponentially for $\sigma > 0, t > 0$. Since $\frac{d}{dt} \int_0^t e^{-\sigma s} \Phi(x, s) ds = e^{-\sigma t} \Phi > 0$ and $\frac{d}{dt} \int_0^t e^{-\sigma s} s^{1-\eta} ds = e^{-\sigma t} t^{1-\eta} > 0$, it implies that $\int_0^t e^{-\sigma s} \Phi(x, s) ds$ and $\int_0^t e^{-\sigma s} s^{1-\eta} ds$ increase in time. Hence \bar{u} is exponential growth for $\sigma > 0$.

2.6.5 Numerical solution

In this section, we show the numerical computation of the solution to (2.67). We introduce the Grünwald-Letnikov definition

$$\mathfrak{D}_{0,t}^\alpha f(t) = \lim_{h \rightarrow 0} h^{-\alpha} \sum_{n=0}^m (-1)^n \binom{\alpha}{n} f(t - nh),$$

where $t = mh$ and $\binom{\alpha}{n} = \frac{\Gamma(\alpha+1)}{\Gamma(n+1)\Gamma(\alpha-n+1)}$. This definition represents integral for $\alpha < 0$ and derivative for $\alpha > 0$. The Grünwald-Letnikov integral is equivalent to fractional integral (2.23) [49, Eq. 2.40]; the Grünwald-Letnikov derivative is equivalent to Riemann-Liouville derivative (2.25) for $f \in AC([0, T])$, $T > 0$ [49, Eq. 2.134].

We transform (2.67) into difference scheme as follows. We take the points t_0, t_1, \dots, t_m such that $0 = t_0 < t_1 < \dots < t_n < \dots < t_m = t$ and $t_n - t_{n-1} = h$. Then we can rewrite (2.67) as a difference equation in the following form

$$\begin{aligned} \frac{u(t_m) - u(t_m - h)}{h} &= -dq^2 \left(h^{-(1-\gamma)} \sum_{n=0}^m (-1)^n \binom{1-\gamma}{n} u(t_m - nh) \right. \\ &\quad \left. - \sigma h^\gamma \sum_{n=0}^m (-1)^n \binom{-\gamma}{n} u(t_m - nh) + \sigma \frac{t_m^{\gamma-1}}{\Gamma(\gamma)} h \sum_{n=0}^m u(t_m - nh) \right) + \sigma u(t_m). \end{aligned}$$

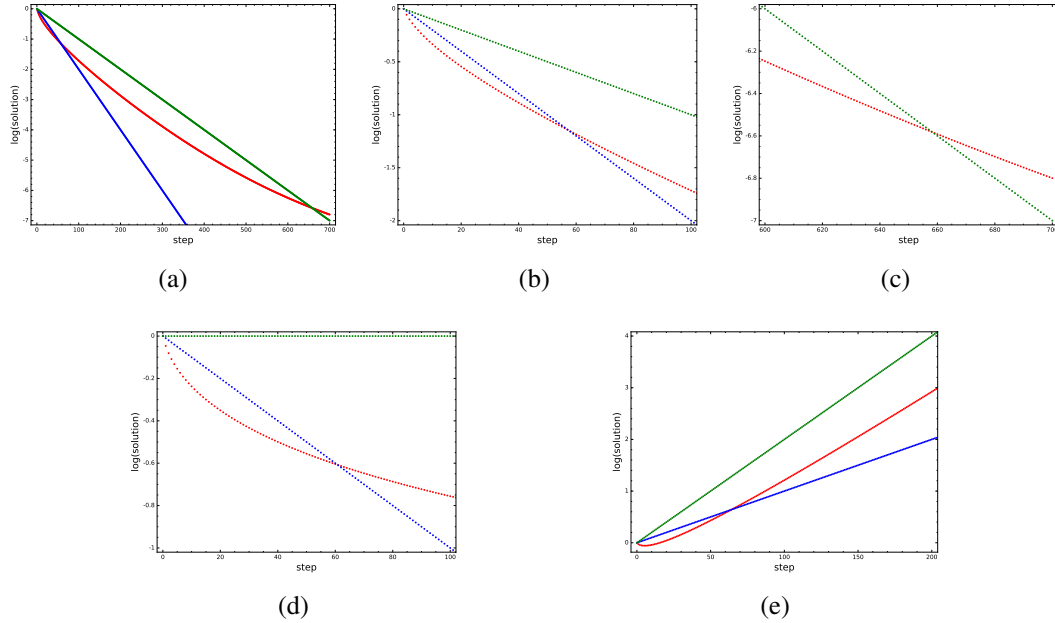


Figure 2.14: Comparison of the logarithm of solutions. Red dotted lines: solutions to (2.67); green: $\hat{u}(0) \exp(\sigma t)$; blue: $\hat{u}(0) \exp((\sigma - dq^2)t)$. Setting $q = 1$, $d = 1$, $h = 0.01$, $\gamma = 0.5$, $\hat{u}(0) = 1$. (a) $\sigma = -1$. (b) The magnification of (a) shows $\hat{u}(t)$ becomes larger than $\hat{u}(0) \exp((\sigma - dq^2)t)$ after a certain time. (c) The magnification of (a) shows $\hat{u}(t)$ becomes larger than $\hat{u}(0) \exp(\sigma t)$. (d) $\sigma = 0$. (e) $\sigma = 2$.

Rewriting the above equation gives the following iteration formulae

$$u(t_m) = A_m u(t_{m-1}) + \sum_{n=2}^m B_{m,n} u(t_{m-n}), \quad m = 2, 3, \dots,$$

where

$$A_m = \frac{h^{-1} - dq^2 \left(-(1-\gamma)h^{-(1-\gamma)} - \gamma\sigma h^\gamma + \sigma \frac{(mh)^{\gamma-1}}{\Gamma(\gamma)} h \right)}{h^{-1} + dq^2 \left(h^{-(1-\gamma)} - \sigma h^\gamma + \sigma \frac{(mh)^{\gamma-1}}{\Gamma(\gamma)} h \right) - \sigma}, \quad m = 1, 2, \dots,$$

$$B_{m,n} = \frac{-dq^2 \left(h^{-(1-\gamma)} C_n(1-\gamma) - \sigma h^\gamma C_n(-\gamma) + \sigma \frac{(mh)^{\gamma-1}}{\Gamma(\gamma)} h \right)}{h^{-1} + dq^2 \left(h^{-(1-\gamma)} - \sigma h^\gamma + \sigma \frac{(mh)^{\gamma-1}}{\Gamma(\gamma)} h \right) - \sigma}, \quad m = 2, 3, \dots,$$

$$C_n(1-\gamma) = (-1)^n \binom{1-\gamma}{n}, \quad C_n(-\gamma) = (-1)^n \binom{-\gamma}{n}.$$

We solve the above solution numerically and show the logarithm of solutions in Fig. 2.14.

For $\sigma < 0$, the solution is decaying in time, cf. Fig. 2.14a. We note that $\hat{u}(t)$ decays faster than $\hat{u}(0) \exp((\sigma - dq^2)t)$ which is the Fourier mode to the linear reaction diffusion equation for short time. However, $\hat{u}(t)$ decays slower than $\hat{u}(0) \exp((\sigma - dq^2)t)$ after a certain time, cf. Fig. 2.14b, and even slower than the exponential function $\hat{u}(0) \exp(\sigma t)$ for increasing t , cf. Fig. 2.14c.

For $\sigma = 0$, the equation (1.8) becomes subdiffusion equation, and the numerical result shows that the Fourier mode to (1.8) decays exponentially for short time then decays slower for large time, cf. Fig. 2.14d, which is consistent with (2.29).

For $\sigma > 0$, the Fourier mode is decaying at the onset, then exponentially growing in time, cf. Fig. 2.14e. Moreover, it is even faster than $\hat{u}(0) \exp((\sigma - dq^2)t)$ for large time, and the growing rate is similar to that of $\hat{u}(0) \exp(\sigma t)$.

Chapter 3

Reaction-diffusion-advection systems

3.1 Introduction

In this chapter, we study the generic form of the planar reaction-diffusion-advection systems (1.9). Our main results with more details may be summarised as follows. Here the parameters are $\mu = (\alpha, \beta, \tilde{\kappa})$ where $\alpha = \lambda_M \check{\alpha}$ for certain $\lambda_M \neq 0$ and $\tilde{\kappa} = \kappa - \mathbf{k}_c$ is the deviation of the stripes' nonlinear wavenumber from \mathbf{k}_c , i.e., the stripes' spatial period is $2\pi/\kappa$. Lastly, \tilde{l} is the deviation of the domain's spatial extent from a symmetric domain along the stripe. Throughout we consider $|\mu| \ll 1$, and consider stripes $U_s(x; \mu)$ that are constant in y with amplitude parameter $A = \|\widehat{U_s}(\mathbf{k}_c; \mu)\|$ the norm of the first Fourier mode.

Existence of stripes The existence of striped solutions $U_s(x; \mu)$ to (1.9) with small amplitude A near the onset of the Turing instability is equivalent to solving an algebraic equation

$$\alpha + \rho_\beta \beta^2 + \rho_{\tilde{\kappa}} \tilde{\kappa}^2 + \rho_{nl} A^2 = 0,$$

where $\rho_\beta, \rho_{\tilde{\kappa}}$ are determined by the linearisation in $u = 0$, and ρ_{nl} involves the nonlinear terms. We have $\rho_\beta > 0$, $\rho_{\tilde{\kappa}} < 0$ so that the bifurcation loci form a hyperbolic paraboloid, and in the supercritical case $\rho_{nl} < 0$ the corresponding amplitudes A follow a family of supercritical pitchfork bifurcations, cf. Fig. 3.1 (dashed curves).

Zigzag instability We determine the leading order curvature of the spectrum for modes parallel to the stripes as

$$\mathbf{k}_c \rho_{\tilde{\kappa}} \tilde{\kappa} + \rho_{\check{\alpha}} \alpha + \rho_{\beta\beta} \beta^2,$$

which means zigzag instability for a positive value. For $\rho_{\check{\alpha}} = 0$ the leading order zigzag boundary is independent of α as in the isotropic case of Swift-Hohenberg equation mentioned in §1.4. It turns out that $\rho_{\check{\alpha}} = a + b$, where $a = 0$ if $M = \text{Id}$ and $b = 0$ if $Q = 0$, which highlights the impact of non-trivial M and the quadratic term. The sign of $\rho_{\beta\beta}$ determines whether β has a stabilising or destabilising effect, and we determine this for ‘small’ Q . It turns out that if the first

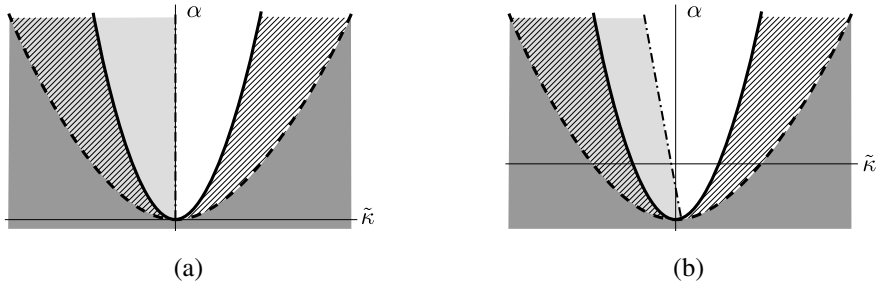


Figure 3.1: We plot sketches of the leading order existence and stability boundaries near the Turing bifurcation point at the origin in (a). Stripes exist in the complement of the dark grey regions. Hatched region: Eckhaus unstable. Light grey region: zigzag unstable. (a) $\beta = 0, M = \text{Id}, Q = 0$, (b) sample for $\beta \neq 0, M \neq \text{Id}, Q \neq 0$. Note in (b) the existence and Eckhaus boundaries are shifted downwards, the zigzag boundary is tilted and the attachment point to the existence shifted.

component is the inhibitor, $a_1 < 0$, then $\rho_{\beta\beta} < 0$. However, the different combinations of signs allow to move and tilt the zigzag boundary, cf. Fig. 3.5 (dotted dashed curves).

Eckhaus instability To leading order the curvature of the spectrum for modes orthogonal to the stripe has the sign of

$$-(\tilde{\alpha} + 3\rho_{\tilde{\kappa}}\tilde{\kappa}^2),$$

where $\tilde{\alpha} = \alpha + \rho_{\beta}\beta^2$ is the deviation from the bifurcation loci. Hence, in terms of $\tilde{\alpha}$ the leading order curvature is independent of the advection β , and just according to the well-known Eckhaus boundary as a function of $\tilde{\kappa}$, cf. Fig. 3.1 (solid curves). Thus, in contrast to the zigzag instability, relative to the bifurcation loci there is no leading order impact of the advection on this large wavelength stability. Nevertheless, for fixed unfolding parameter α the interval of stable $\tilde{\kappa}$ is larger, i.e., stripes are more resilient to stretching/compressing compared to the isotropic case.

As mentioned in §1.4, we study the stability on lattices, in particular on (quasi-)square and (quasi-)hexagonal lattices. We assume the scaling relation

$$(A, \alpha, \beta, \tilde{\kappa}, \tilde{\ell}) = (\varepsilon A', \varepsilon^2 \alpha', \varepsilon \beta', \varepsilon \tilde{\kappa}', \varepsilon \tilde{\ell}'), \quad (3.1)$$

with a scaling parameter $\varepsilon > 0$, as this greatly simplifies the discussion. This scaling is homogeneous for μ with respect to the relevant terms in the expansion of stripes.

As is well known from the isotropic case, the quadratic terms enter at lower order into stability on the hexagonal lattice and thus should be small in order to discuss changes of stability. A convenient, though not necessary, implementation of this is the following uniform smallness hypothesis.

Hypothesis 3.1.1. $Q[\cdot, \cdot] = \varepsilon Q'[\cdot, \cdot]$.

Notably, in the amplitude/modulation equation approach this assumption is required a priori, while in our approach it enters only a posteriori in order to obtain non-trivial stability boundaries.

It turns out that certain quasi-hexagonal modes are more unstable than others, and therefore the resulting stability boundaries are briefly illustrated next. In order to build the foundation for this case, in the body of this chapter we begin by discussing quasi-square modes in §3.5.3 and exact hexagonal modes in §3.5.4.

Quasi-hexagonal stability boundaries. We consider periodic boundary conditions on the rectangular domains $\mathbf{x} \in \Omega_{qh} := [0, 4\pi/\kappa] \times [0, 4\pi/(\sqrt{3}\ell)]$, $\kappa := \mathbf{k}_c + \tilde{\kappa}$, $\ell := \mathbf{k}_c + \tilde{\ell}$, $\tilde{\ell} \neq \tilde{\kappa}$. We prove that the ratio $\tilde{\kappa}/\tilde{\ell} = -3$ yields the most unstable modes near onset – it is the scale ratio on which the hexagonal modes of the homogeneous steady state are critical. For generic quadratic term, in the isotropic case $\beta = 0$ the stripes are unstable near the onset of Turing instability (Fig. 3.2a & 3.3a). In the anisotropic case, $\beta \neq 0$, any advection strength stabilises the stripes with wavenumbers close to the Turing critical wavenumber (Fig. 3.3b), but this ‘small’ stability region is not connected to the stable region of larger amplitude stripes. However, the size of the small stability region increases with advection strength and eventually connects to that of larger amplitude stripes (Fig. 3.2c & 3.3d). Notably, the thresholds are of the form $\beta_{ep} = c_{ep}|\tilde{\kappa}|$, $\beta_{tp} = c_{tp}|q|$ with explicit constants $c_{ep}, c_{tp} > 0$, cf. Fig. 3.2d and 3.3f, respectively. This ‘opening’ of the stability region shows how under increasing advection strength the isotropic 2D stability region transitions to be like the 1D region augmented by the zigzag boundary.

The quasi-hexagonal instability compares with the Eckhaus instability as follows. Recall that the Eckhaus instability is a large-wavelength instability orthogonal to the stripe and the dominant instability mechanism for wavetrains in 1D; we disregard the leading order zigzag instability region $\{\tilde{\kappa} < 0\}$. In the presence of a generic quadratic term, the quasi-hexagonal instability is dominant near onset in the isotropic case (Fig. 3.3a) while the Eckhaus instability is dominant near onset in the anisotropic case (Fig. 3.3b to 3.3e). In particular, the Eckhaus instability is completely dominant for relatively strong advection $\beta > \beta_{ex} = c_{ex}|q|$ for an explicit constant $c_{ex} > 0$ (Fig. 3.3e).

In our analysis, we consider the leading order bifurcation and stability boundaries of stripes with the scaling relation (3.1). This leads to the reflection symmetric bifurcation and stability boundaries, cf. Fig. 3.3. Relaxing the scaling relation and including the higher order terms will generically break such symmetry as shown for the zigzag stability boundary in Fig. 3.1b. Indeed, we observe asymmetry of the stability diagrams in the numerical computations of Klausmeier model in §3.6.2.

This chapter is organised as follows: In §3.2 we discuss linear stability of the homogeneous state near the Turing instability as a preparation for the analysis of stripes. The existence of stripes is studied in §3.3, and in §3.4 we study the large-wavelength in/stabilities, i.e., zigzag and Eckhaus in/stabilities. The in/stabilities against lattice modes are discussed in §3.5. In §3.6, we

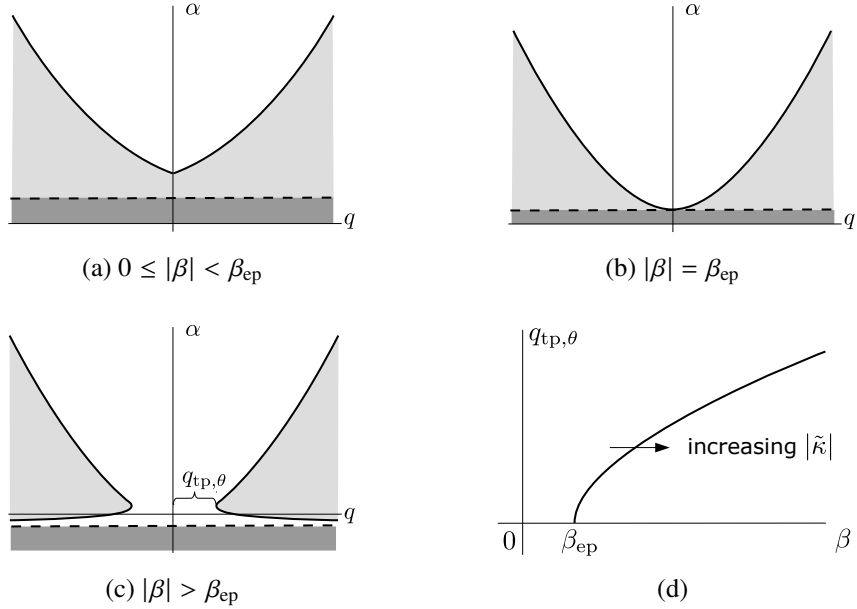


Figure 3.2: In (a)–(c) we plot sketches of the quasi-hexagonal stability regions in the (q, α) -plane for fixed $\tilde{\kappa} \neq 0$ and $\theta \in (0, 1]$, the quadratic term $q = q(Q) = O(\varepsilon)$ measures the effect of the quadratic nonlinearity. Stripes exist in the complement of the dark grey regions; light grey: quasi-hex-unstable; white: quasi-hex-stable. Stripe bifurcation (3.6) (dashed), quasi-hexagonal boundaries (3.50) (solid). In (d) we sketch the half width of the stable window shown in (c), cf. (3.57). The curve intersects with β -axis at β_{ep} linearly increasing with $|\tilde{\kappa}|$. The stripes are quasi-hex-stable below the curve for any α . It shows that the stable window ‘opens’ later for larger $|\tilde{\kappa}|$ and ‘opens’ wider for larger $|\beta|$.

illustrate these results by a concrete example of the form (1.9) and in §3.6.2, we study the large wavelength instabilities numerically for the extended Klausmeier model that was used in [59].

3.2 Turing instability

The linearisation of (1.9) in $u_{\text{hom}} = 0$ is

$$\mathcal{L} := D\Delta + L + \check{\alpha}M + \beta B\partial_x,$$

whose spectrum is most easily studied via the Fourier transform

$$\hat{\mathcal{L}}(k, \ell) = -(k^2 + \ell^2)D + L + \check{\alpha}M + ik\beta B,$$

with Fourier-wavenumbers k in x -direction and ℓ in y -direction. It is well known, e.g., [54], that in the common function spaces such as $L^2(\mathbb{R}^2)$ the spectrum $\Sigma(\mathcal{L})$ of \mathcal{L} equals that of $\hat{\mathcal{L}}$ and is the set of roots of the (linear) dispersion relation

$$d(\lambda, k, \ell) = \det(\hat{\mathcal{L}}(k, \ell) - \lambda \text{Id}). \quad (3.2)$$

Let $S_{\mathbf{k}_c} \subset \mathbb{R}^2$ be the circle of radius \mathbf{k}_c .

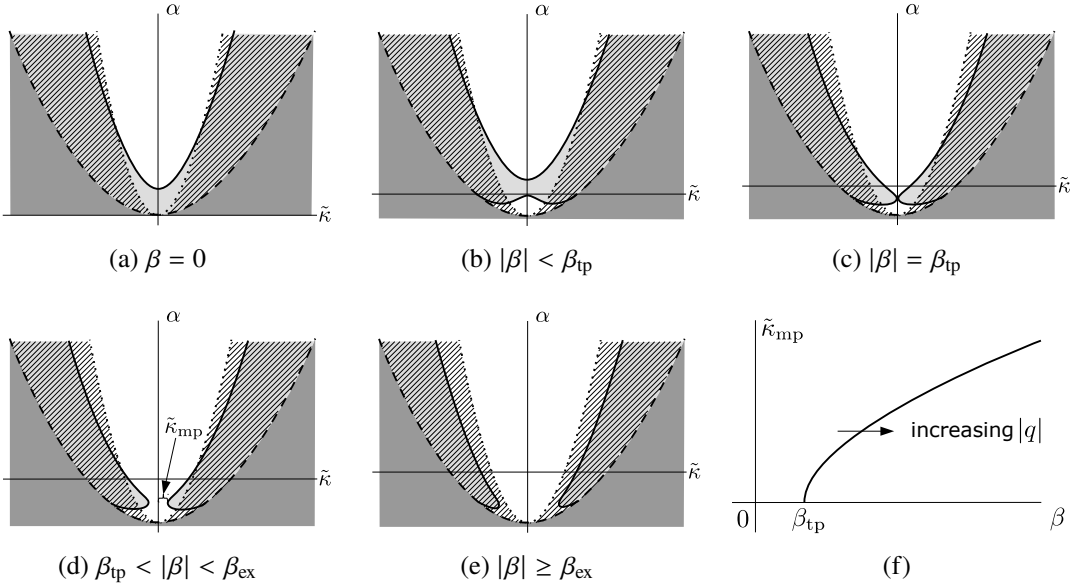


Figure 3.3: In (a)–(e) we plot sketches of the quasi-hexagonal stability regions in the $(\tilde{\kappa}, \alpha)$ -plane for fixed quadratic coefficient $q \neq 0$, $q = q(Q) = O(\varepsilon)$ and fixed $\theta \in (0, 1]$. Stripes exist in the complement of the dark grey regions. Light grey: quasi-hex-unstable; hatched regions: Eckhaus-unstable; zigzag-unstable stripes occurs for $\tilde{\kappa} < 0$. Stripe bifurcation (3.6) (dashed), Eckhaus boundaries (3.30) (dotted), quasi-hexagonal boundaries (3.50) (solid). In (f) we sketch the half width of the stable window shown in (d) and (e), cf. (3.60). The curve intersects with β -axis at β_{tp} linearly increasing with $|q|$. The stripes are quasi-hex-stable below the curve for any α . It shows that the stable window ‘opens’ later for larger $|q|$ and ‘opens’ wider for larger $|\beta|$.

Definition 3.2.1. We say that $\check{\alpha} = \beta = 0$ is a (non-degenerate) *Turing instability point* for u_{hom} in (1.9) with wavelength \mathbf{k}_c if

- (1) L has strictly stable spectrum $\Sigma(L) \subset \{\lambda \in \mathbb{C} : \text{Re}(\lambda) < 0\}$,
- (2) The spectrum of \mathcal{L} is critical for wavevectors (k, ℓ) of length $\mathbf{k}_c > 0$:

$$d(\lambda, k, \ell) = 0 \text{ & } \text{Re}(\lambda) \geq 0 \quad \Leftrightarrow \quad \lambda = 0, (k, \ell) \in S_{\mathbf{k}_c}$$

which in particular means $\Sigma(\mathcal{L}) \cap \{z \in \mathbb{C} : \text{Re}(z) \geq 0\} = \{0\}$,

- (3) $\partial_\lambda d \neq 0$ at $\lambda = 0$ and $(k_c, \ell_c) \in S_{\mathbf{k}_c}$. We denote the unique continuation of these solutions to (3.2) by $\lambda_c(k, \ell; \check{\alpha}, \beta)$, i.e., (k, ℓ) in a neighbourhood of $S_{\mathbf{k}_c}$.

Writing $L = \begin{pmatrix} a_1 & a_2 \\ a_3 & a_4 \end{pmatrix}$, condition (1) implies negative trace of L , $a_1 + a_4 < 0$, and positive determinant $a_1 a_4 > a_2 a_3$, and (3) implies the well known condition $d_1 a_4 + d_2 a_1 > 0$, which together imply $a_2 a_3 < a_1 a_4 < 0$, e.g., [41].

As a first step to understand the impact of advection, the next lemma shows that, for this two-component case, the unfolding by β is only to quadratic order.

Lemma 3.2.2. *For the critical eigenvalues near a Turing instability of (1.9) as in Definition 3.2.1 it holds for any $(k_c, \ell_c) \in S_{\mathbf{k}_c}$ that*

$$\lambda_c(k_c, \ell_c; \beta) = ik_c(\lambda_\beta + c)\beta + k_c^2\lambda_{\beta\beta}\beta^2 + O(|k_c\beta|^3),$$

where $\lambda_\beta = \frac{a_4 - \mathbf{k}_c^2 d_2}{a_1 + a_4 - \mathbf{k}_c^2(d_1 + d_2)}$, $\lambda_{\beta\beta} = \frac{(a_1 - \mathbf{k}_c^2 d_1)(a_4 - \mathbf{k}_c^2 d_2)}{(a_1 + a_4 - \mathbf{k}_c^2(d_1 + d_2))^3} > 0$. In particular, the real part grows fastest for 1D-modes with $\ell_c = 0$ and remains zero for transverse modes with $k_c = 0$.

Proof. This follows immediately from the next lemma upon setting $\delta = k_c\beta$, $b_1 = -(k_c^2 + \ell_c^2)d_1 + a_1$, $b_2 = a_2$, $b_3 = a_3$, $b_4 = -(k_c^2 + \ell_c^2)d_2 + a_4$ and shifting by $ik_c\beta c$. The last statement of the lemma is simply a consequence of the fact that the largest value real part of λ_c is attained at the largest value of k_c^2 , which occurs at $\ell_c = 0$ since $k_c^2 + \ell_c^2 = \mathbf{k}_c^2$. \square

Remark 3.2.3. *The lemma in fact proves the plots in Figure 2 of [59] near onset. It is well known that for a two-component system $\mathbf{k}_c^2 = \frac{d_1 a_4 + d_2 a_1}{2 d_1 d_2}$ and $a_2 a_3 = (a_1 - \mathbf{k}_c^2 d_1)(a_4 - \mathbf{k}_c^2 d_2)$.*

Lemma 3.2.4. *For a matrix $\begin{pmatrix} b_1 + i\delta & b_2 \\ b_3 & b_4 \end{pmatrix}$ with $b_1 \neq 0$ and simple zero eigenvalue, the expansion of that eigenvalue reads*

$$\lambda(\delta) = i\lambda_{|}\delta + \lambda_{||}\delta^2 + O(|\delta|^3),$$

where $\lambda_{|} = \frac{b_4}{b_1 + b_4}$, $\lambda_{||} = \frac{b_1 b_4}{(b_1 + b_4)^3}$.

Proof. Straightforward implicit differentiation, expansion of characteristic polynomial and use of assumptions, which in particular imply $(b_1 + b_4)b_1 \neq 0$. \square

Note that $b_2 = 0$ or $b_3 = 0$ is not possible due to the assumption $b_1 \neq 0$ and $b_1 b_4 = b_2 b_3$.

Remark 3.2.5. *For the matrix $\begin{pmatrix} b_1 & b_2 \\ b_3 & b_4 \end{pmatrix}$ in Lemma 3.2.4, i.e., $\delta = 0$, we can choose the kernel eigenvector E_0 and the adjoint kernel eigenvector E_0^* with $\langle E_0, E_0 \rangle = 1$ and $\langle E_0, E_0^* \rangle = 1$ as*

$$E_0 = (b_2, -b_1)^T / c_0, \quad E_0^* = (b_3, -b_1)^T / c_0^*,$$

with $c_0 := \sqrt{b_2^2 + b_1^2}$, $c_0^* := (b_2 b_3 + b_1^2)/c_0$. Here $c_0^* \neq 0$ since $b_1^2 + b_2 b_3 = b_1^2 + b_1 b_4 = b_1(b_1 + b_4) \neq 0$.

In contrast to β , the change of real parts of the critical eigenvalue through $\check{\alpha}$, with matrix $M = (m_{ij})_{1 \leq i,j \leq 2}$, is linear with coefficient

$$\begin{aligned} \lambda_M &:= -\left. \frac{\partial \check{\alpha} d}{\partial \lambda d} \right|_{\check{\alpha}=0, \lambda=0} \\ &= \frac{m_{11}(a_4 - \mathbf{k}_c^2 d_2) - m_{12}a_3 - m_{21}a_2 + m_{22}(a_1 - \mathbf{k}_c^2 d_1)}{a_1 + a_4 - \mathbf{k}_c^2(d_1 + d_2)} \neq 0, \end{aligned} \tag{3.3}$$

where we assume $\lambda_M \neq 0$ throughout this chapter. Notably, $\lambda_M = 1$ if $M = \text{Id}$ in which case $\check{\alpha}$ just rigidly moves the real part of the spectrum.

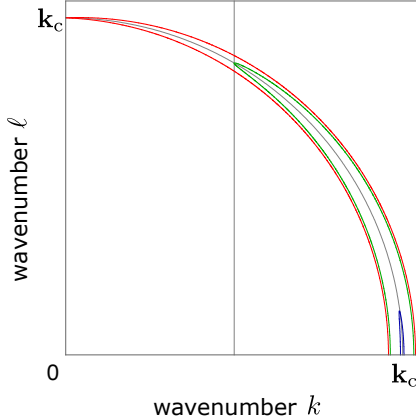


Figure 3.4: Based on the example (3.61) below, we illustrate the locations of the critical spectrum of homogeneous state, i.e., $\text{Re}(\lambda(k, \ell; \alpha, \beta)) = 0$, on the (k, ℓ) -plane for ‘small’ fixed $\beta = 0.2$, and $\text{Re}(\lambda) > 0$ inside each horn-shaped region. The unfolding parameter $\alpha = 12.24\check{\alpha}$. Grey curve: wavevectors $(k_c, \ell_c) \in S_{\mathbf{k}_c}$ with radius $\mathbf{k}_c = 1$; grey vertical line: $k = 1/2$; blue: $\check{\alpha} = -3.6 \times 10^{-4}$ ($\alpha \approx -0.00441$); green: $\check{\alpha} = -9.15 \times 10^{-5}$ ($\alpha \approx -0.00112$); red: $\check{\alpha} = \alpha = 0$. These contours are reflection symmetric with respect to the axes.

In the following we therefore change parameters and use the effective impact on the real part given by

$$\alpha := \lambda_M \check{\alpha}$$

as the new parameter so that

$$\begin{aligned} \lambda_c(k_c, \ell_c; \alpha, \beta) = & \alpha + i(k_c(\lambda_\beta + c) + a_M \lambda_M \beta \alpha) \beta + k_c^2 \lambda_{\beta\beta} \beta^2 \\ & + O(a_M \alpha^2 + |k_c \beta|^3), \end{aligned} \quad (3.4)$$

with $\lambda_M \beta := k_c \frac{m_{22} - \lambda_M - (2\lambda_M - m_{11} - m_{22})\lambda_\beta}{\lambda_M(a_1 + a_4 - \mathbf{k}_c^2(d_1 + d_2))}$, and we emphasise the special case $M = \text{Id}$ through the factor a_M , where $a_M = 0$ if $M = \text{Id}$ and $a_M = 1$ otherwise.

We illustrate the region of $\text{Re}(\lambda) \geq 0$ in the wavevector space (k, ℓ) in Fig. 3.4 based on the example (3.61) below. For ‘small’ fixed $\beta = 0.2$, the Fourier modes with (the leading order) wavevectors $(\pm \mathbf{k}_c, 0)$ first become unstable for $\alpha > -k_c^2 \lambda_{\beta\beta} \beta^2 \approx -0.00448$, where $\alpha = 12.24\check{\alpha}$, thus the stripes with the wavelength $2\pi/\mathbf{k}_c$ may bifurcate from the homogeneous steady state. Then the modes with (the leading order) wavevectors $(\pm \mathbf{k}_c/2, \pm \sqrt{3}\mathbf{k}_c/2)$ touch zero at $\alpha = -k_c^2 \lambda_{\beta\beta} \beta^2/4 \approx -0.00112$ so that the hexagons may bifurcate. Lastly, the modes with wavevectors $(0, \pm \mathbf{k}_c)$ touch zero plane for $\alpha = 0$ and thus squares may bifurcate.

Here we highlight an a priori consequence for the $L^2(\mathbb{R}^2)$ -stability of striped solutions U_s with wavenumber $\kappa = \mathbf{k}_c + \tilde{\kappa}$ that are oriented orthogonal to the x -direction, i.e., $\partial_y U_s \equiv 0$. We assume (and prove in the next section) the existence of a curve of such striped solutions $U_s(x; \tau)$ parametrised by $\tau \in [0, \tau_0]$ for some $\tau_0 > 0$, with $U_s(x; 0) = 0$, and corresponding parameter curve $\mu(\tau) = (\alpha, \beta, \tilde{\kappa})(\tau)$ with $\beta(0) \neq 0$, $|\mu(0)| \ll 1$, and velocity parameter $c(\tau)$.

Corollary 3.2.6. *For $0 < \tau \ll 1$ and $\beta(0) = 0$ the spectral stability in $L^2(\mathbb{R}^2)$ of U_s is entirely determined by large-wavelength modes, i.e., if U_s is zigzag and Eckhaus stable then it is spectrally stable in $L^2(\mathbb{R}^2)$.*

In particular, a family with constant $\tilde{\kappa} = 0$, i.e., stripes with wavenumber \mathbf{k}_c , bifurcates stably, if it is zigzag-stable at onset.

Proof. Since $\beta(0) \neq 0$, by Lemma 3.2.2, see also the Squire-theorem [59, Theorem 2], the spectrum of $U_s(x; 0) = u_{\text{hom}}$ with parameters $\mu(0), c(0)$ is critical only for $\tilde{\kappa}, \ell \approx 0$. More precisely, for all sufficiently small $\epsilon > 0$ there is $\delta > 0$ such that $\text{Re}(\lambda_c(\mathbf{k}_c + \tilde{\kappa}, \ell; \alpha(0), \beta(0))) < -\delta$ for all $\tilde{\kappa}, \ell$ with $|\tilde{\kappa}|, |\ell| > \epsilon$. It suffices to show that the same holds for the spectrum of the linearisation \mathcal{L}_{st} of (1.9) in U_s for any sufficiently small τ .

Via Floquet-Bloch decomposition, the spectrum of \mathcal{L}_{st} can be encoded in a complex analytic dispersion relation $d_{\text{st}}(\lambda, \gamma, \ell)$, $\gamma \in [0, 2\pi]$, e.g., [10, 40, 50], and §3.4. Since $\mathcal{L}_{\text{st}}(0) = \mathcal{L}$ roots of d_{st} converge locally uniformly in \mathbb{C} to roots of d for $k = 2\pi m + \gamma$ with suitable $m \in \mathbb{Z}$. Hence, any spectrum that is bounded away from $i\mathbb{R}$ for u_{hom} will be bounded away from $i\mathbb{R}$ for all sufficiently small τ . \square

Remark 3.2.7. *We highlight that the homogeneous steady state which is unstable against large-wavelength modes $e^{i(\kappa x + \ell y)}$, $\ell \approx 0$ evolves into zigzag-unstable stripes with wavelength $2\pi/\kappa$, since the spectrum of \mathcal{L}_{st} inherits the instability from the unstable spectrum of \mathcal{L} due to the continuation. However, the stable homogeneous state does not necessarily evolve into zigzag-stable stripes, since the spectrum of \mathcal{L}_{st} does not need to converge to that of \mathcal{L} in C^1 -norm by approaching the bifurcation.*

The above statements are verified by the concrete example (3.61). Fig. 3.4 shows that the spectrum $\text{Re}(\lambda_c(\mathbf{k}_c + \tilde{\kappa}, \ell)) > 0$ for $\tilde{\kappa} < 0$, $\ell \approx 0$ and $\text{Re}(\lambda_c(\mathbf{k}_c + \tilde{\kappa}, \ell)) < 0$ for $\tilde{\kappa} > 0$ and all ℓ . However, these produce the zigzag-unstable stripes for both $\tilde{\kappa} < 0$ and ‘small’ positive $\tilde{\kappa}$, cf. Fig. 3.13b. Notably, we use different values of β in Fig. 3.4 and 3.13b, however, the qualitative shape of the zigzag stability boundary near onset would not change by varying non-zero β , cf. (3.29).

3.3 Bifurcation of stripes

Stripes are travelling waves solutions of (1.9) that are constant in y and periodic in x for any t . In order to determine the bifurcation of stripes it thus suffices to consider the 1D case $\mathbf{x} = x \in [0, 2\pi/\kappa]$ with periodic boundary conditions and wavenumber κ . The definition of a Turing instability point implies that \mathcal{L} restricted to 1D possesses a kernel at $\alpha = \beta = 0$ on spaces of $2\pi/\mathbf{k}_c$ -periodic functions and upon unfolding also for nearby periods. Let us therefore rescale space and consider periodic boundary conditions on $[0, 2\pi]$. This modifies the linear part (1.9) to

$$\mathcal{L}_\mu := \kappa^2 D \partial_x^2 + L + \check{\alpha} M + \beta \kappa B \partial_x$$

with the off-critical parameter $\tilde{\kappa}$ in $\kappa = \mathbf{k}_c + \tilde{\kappa}$ that allows to detect stripes with nearby wavenumber. We recall the parameter vector $\mu = (\alpha, \beta, \tilde{\kappa})$. By Lemma 3.2.2, (3.4), and straightforward generalisation to include $\tilde{\kappa}$, the continuation of the zero eigenvalue of \mathcal{L}_μ has an expansion

$$\begin{aligned}\lambda_\mu &= \alpha + \rho_\beta \beta^2 + \rho_{\tilde{\kappa}} \tilde{\kappa}^2 + i(\gamma_\beta + \gamma_{\tilde{\kappa}\beta} \tilde{\kappa} + a_M \lambda_{M\beta} \alpha) \beta \\ &\quad + a_M \lambda_{M\tilde{\kappa}} \alpha \tilde{\kappa} + O(a_M \alpha^2 + |\tilde{\kappa}|^3 + |\beta|^3),\end{aligned}\tag{3.5}$$

where again $a_M = 0$ if $M = \text{Id}$ and $a_M = 1$ otherwise. The coefficients are

$$\rho_\beta = \mathbf{k}_c^2 \lambda_{\beta\beta} > 0, \quad \gamma_\beta = \mathbf{k}_c (\lambda_\beta + c),$$

as in Lemma 3.2.2 and with $\gamma_{\tilde{\kappa}\beta} = \lambda_{\tilde{\kappa}\beta} + c$, the dispersion relation $d(\lambda, k; \mu) = 0$ as well as $\partial_k \lambda_c(\mathbf{k}_c; 0) = 0$ yields

$$\begin{aligned}\lambda_{\tilde{\kappa}\beta} &= i \frac{\partial_{k,\lambda} d \cdot \partial_\beta \lambda + \partial_k^2 d}{\partial_\lambda d} \Big|_{k=\mathbf{k}_c, \mu=0, \lambda=0} \in \mathbb{R}, \\ \lambda_{M\tilde{\kappa}} &= - \frac{\lambda_M \partial_{k,\lambda} d + \partial_k^2 d}{\lambda_M \partial_\lambda d} \Big|_{k=\mathbf{k}_c, \mu=0, \lambda=0} \in \mathbb{R}, \\ \rho_{\tilde{\kappa}} &= - \frac{\partial_k^2 d}{2 \partial_\lambda d} \Big|_{k=\mathbf{k}_c, \lambda=0} < 0\end{aligned}$$

with the last sign due to $d_1 a_4 + d_2 a_1 > 0$, $a_1 + a_4 < 0$ and

$$\rho_{\tilde{\kappa}} = - \frac{d_1 a_4 + d_2 a_1 - 6 d_1 d_2 \mathbf{k}_c^2}{a_1 + a_4 - (d_1 + d_2) \mathbf{k}_c^2} = \frac{2(d_1 a_4 + d_2 a_1)}{a_1 + a_4 - (d_1 + d_2) \mathbf{k}_c^2}.$$

Vanishing real part $\text{Re}(\lambda_\mu) = 0$ thus occurs to leading order on a hyperbolic paraboloid

$$\alpha = \mathcal{B}(\tilde{\kappa}, \beta) := -(\rho_{\tilde{\kappa}} \tilde{\kappa}^2 + \rho_\beta \beta^2)\tag{3.6}$$

in μ -space. Since the eigenvalue is stable (unstable) for $\alpha < \mathcal{B}(\tilde{\kappa}, \beta)$ ($\alpha > \mathcal{B}(\tilde{\kappa}, \beta)$), this constitutes the bifurcation surface at leading order.

The next theorem specifies the bifurcation and expansion of the stripe solutions near $\mu = 0$, where our main point is the effect of β and its interaction with $\alpha, \tilde{\kappa}$. Rather than expanding with abstract coefficients, we provide explicit formulae evaluated at $\mu = 0$ in terms of the following quantities.

$$\begin{aligned}Q_0 &:= -2L^{-1} Q[\overline{E_0}, E_0], \quad Q_2 := -2(-4\mathbf{k}_c^2 D + L)^{-1} Q[E_0, E_0], \\ q_0 &:= \langle Q[E_0, Q_0], E_0^* \rangle, \quad q_2 := \langle Q[\overline{E_0}, Q_2], E_0^* \rangle, \\ k_0 &:= \langle K[E_0, E_0, \overline{E_0}], E_0^* \rangle, \quad \rho_{\text{nl}} := 3k_0 + 2q_0 + q_2, \\ w_{A\check{\alpha}} &:= (-\mathbf{k}_c^2 D + L)^{-1} (\langle M E_0, E_0^* \rangle - M) E_0, \\ w_{A\beta} &:= \mathbf{k}_c (-\mathbf{k}_c^2 D + L)^{-1} (\langle B E_0, E_0^* \rangle - B) E_0, \\ w_{A\tilde{\kappa}} &:= 2\mathbf{k}_c (-\mathbf{k}_c^2 D + L)^{-1} D E_0, \\ w_{A\beta\beta} &:= 2\mathbf{k}_c (-\mathbf{k}_c^2 D + L)^{-1} (B w_{A\beta} - \langle B w_{A\beta}, E_0^* \rangle) E_0, \\ e_\mu(x) &:= (E_0 + \check{\alpha} w_{A\check{\alpha}} + i\beta w_{A\beta} + \tilde{\kappa} w_{A\tilde{\kappa}} + \beta^2 w_{A\beta\beta}) e^{ix}.\end{aligned}\tag{3.7}$$

Here $-\mathbf{k}_c^2 D + L$ has a one-dimensional generalised kernel spanned by E_0 , and thus has an inverse from its range to the kernel of the projection $\langle \cdot, E_0^* \rangle E_0$. We note that the evaluation at $\mu = 0$ in the following theorem gives the velocity parameter $c = -\lambda_\beta$ and at this value of c we have $\langle BE_0, E_0^* \rangle = 0$.

Theorem 3.3.1 (Stripe existence). *Up to spatial translation, non-trivial stripe solutions to (1.9) with parameters μ , and sufficiently small $|\mu|, A$ with $\|U_s(\cdot; \mu)\|_{L^2} = O(A)$ on $[0, 2\pi/\kappa]$, are in 1-to-1 correspondence with solutions $A > 0$ to*

$$\operatorname{Re}(\tilde{\lambda}(\mu)) + \rho_{\text{nl}} A^2 + O(A^3) = 0, \quad (3.8)$$

where $\tilde{\lambda}(\mu) = r(\mu)\lambda_\mu$, cf. (3.5), and r is smooth with $r(0) = 1$. Stripes have velocity βc with

$$c = -\lambda_\beta - \frac{\lambda_{M\beta}}{\mathbf{k}_c} a_M \alpha - \frac{\lambda_{\tilde{\kappa}\beta} - \lambda_\beta}{\mathbf{k}_c} \tilde{\kappa} + O(a_M |\alpha \tilde{\kappa}| + \tilde{\kappa}^2 + |A|^3) \quad (3.9)$$

and, in this comoving frame, are of the form

$$U_s(x; \mu) = A(e_\mu(x) + \overline{e_\mu(x)}) + \frac{A^2}{2} Q_2 \left(e^{2ix} + e^{-2ix} \right) + A^2 Q_0 + \mathcal{R}, \quad (3.10)$$

with the smooth remainder $\mathcal{R} = O(|A|(A^2 + a_M \alpha^2 + \tilde{\kappa}^2 + |\beta \tilde{\kappa}| + |\beta|^3))$ near $\mu = 0$. Moreover, the coefficients in the expansion of $\tilde{\lambda}$ analogous to (3.5) satisfy

$$\begin{aligned} \lambda_M &= \langle ME_0, E_0^* \rangle, & \lambda_{M\beta} &= \langle Mw_{A\beta} + \mathbf{k}_c B w_{A\tilde{\kappa}}, E_0^* \rangle / \lambda_M, \\ \lambda_{M\tilde{\kappa}} &= \langle Mw_{A\tilde{\kappa}} - 2\mathbf{k}_c D w_{A\tilde{\kappa}}, E_0^* \rangle / \lambda_M, \\ \rho_\beta &= -\mathbf{k}_c \langle B w_{A\beta}, E_0^* \rangle, & \rho_{\tilde{\kappa}} &= -2\mathbf{k}_c \langle D w_{A\tilde{\kappa}}, E_0^* \rangle, \\ \gamma_\beta &= \mathbf{k}_c \langle BE_0, E_0^* \rangle, & \gamma_{\tilde{\kappa}\beta} &= \mathbf{k}_c \langle B w_{A\tilde{\kappa}} - 2D w_{A\beta}, E_0^* \rangle + \langle BE_0, E_0^* \rangle. \end{aligned} \quad (3.11)$$

We defer the proof to Appendix D. In case $M = \text{Id}$ clearly α uniformly shifts spectra so that α does not impact higher orders in λ_μ as can be seen from the fact that $\lambda_M = 1$ and $w_{A\tilde{\kappa}} = \lambda_{M\beta} = \lambda_{M\tilde{\kappa}} = 0$ in this case.

In its simplest case, the theorem reflects the well-known fact that, up to translation symmetry, for $\rho_{\text{nl}} \neq 0$ the bifurcation is a generic pitchfork. Specifically, with respect to α the bifurcation is supercritical if $\rho_{\text{nl}} < 0$, which we shall assume in the following stability study.

Our main interest lies in the role of β and Q . As noted in the discussion of the eigenvalues above, β shifts the bifurcation points by order β^2 . From (3.8) we readily solve for the stripe amplitude as

$$A = \left(1 + O \left(\sqrt{\operatorname{Re}(\tilde{\lambda}(\mu))} \right) \right) \sqrt{-\frac{\operatorname{Re}(\tilde{\lambda}(\mu))}{\rho_{\text{nl}}}}. \quad (3.12)$$

Remark 3.3.2. *The sign of $c = c(\mu)$ is the direction of stripe motion relative to β , and is determined by λ_β as $\operatorname{sgn}(c) = -\operatorname{sgn}(\lambda_\beta)$. In terms of a_1, a_4 we have*

$$\operatorname{sgn}(c) = -\operatorname{sgn}(a_1)$$

so the motion is with β if the first component is an inhibitor and against β otherwise.

Proof. Recall the notation of Lemma 3.2.2 and Lemma 3.2.4, which gives $\lambda_\beta = \frac{b_4}{b_1+b_4}$, and we have $b_1 b_4 = b_2 b_3 < 0$ and $b_1 + b_4 < 0$. For case (1) we note $a_1 < 0$ implies $b_1 < 0$, which implies $b_4 > 0$ and thus the claim. For case(2) similarly from $a_4 < 0$, we have $b_4 < 0$ which leads to $b_1 > 0$. Hence $\lambda_\beta = \frac{b_1+b_4-b_1}{b_1+b_4} = 1 - \frac{b_1}{b_1+b_4} > 1$ implies $c < -1$. \square

Notably, the bifurcation loci, where $A = 0$, occur on a surface in μ -space that includes $\mu = 0$ since the signs of ρ_β and $\rho_{\tilde{\kappa}}$ are opposite. The leading order part $\alpha + \rho_\beta \beta^2 + \rho_{\tilde{\kappa}} \tilde{\kappa}^2$ of $\text{Re}(\tilde{\lambda}(\mu))$ coincides with that of $\text{Re}(\lambda_\mu)$, cf. (3.5), and is homogeneous with respect to the scalings

$$(A, \alpha, \beta, \tilde{\kappa}) = (\varepsilon A', \varepsilon^2 \alpha', \varepsilon \beta', \varepsilon \tilde{\kappa}'), \quad (3.13)$$

with a scaling parameter $\varepsilon > 0$ and consider primed quantities A' and $\mu' = (\alpha', \beta', \tilde{\kappa}')$ bounded with respect to ε . This scaling is homogeneous for μ with respect to the relevant first three terms in (3.5) and the scaling $A = \varepsilon A'$ is natural due to the relation between the parameters and the amplitude of the striped solutions. In terms of primed quantities, the bifurcation loci, where $A' = 0$, occur at $\mu' = (\alpha', \beta', \tilde{\kappa}') = 0$ only. Notably, the impact of $M \neq \text{Id}$ is now at higher order and highlights that leading order results with the scalings (3.13) will have additional symmetry.

In these scaled parameters with $A', \mu' = O(1)$ the order analysis of remainders in (3.10) drastically simplifies to $\mathcal{R} = O(\varepsilon^3)$.

Corollary 3.3.3. *Up to spatial translation, non-trivial stripe solutions to (1.9) with parameters $\mu = \varepsilon \mu'$, and sufficiently small $|\mu|$, $A = \varepsilon A'$ with $\|U_s(\cdot; \mu)\|_{L^2} = O(\varepsilon)$ on $[0, 2\pi/\kappa]$, are in 1-to-1 correspondence with solutions $A > 0$ to*

$$\varepsilon^2 \left(\alpha' + \rho_\beta \beta'^2 + \rho_{\tilde{\kappa}} \tilde{\kappa}'^2 + \rho_{\text{nl}} A'^2 + O(\varepsilon) \right) = 0. \quad (3.14)$$

Stripes have velocity βc with

$$c = -\lambda_\beta + O(\varepsilon) \quad (3.15)$$

and, in this comoving frame, are up to translation of the form

$$U_s(x; \mu) = \varepsilon A'(e_\mu(x) + \overline{e_\mu(x)}) + \varepsilon^2 A'^2 \left(\frac{1}{2} Q_2 \left(e^{2ix} + e^{-2ix} \right) + Q_0 \right) + O(\varepsilon^3). \quad (3.16)$$

Proof. Using (3.5) the bifurcation equation (3.8) expands as

$$\alpha + \rho_\beta \beta^2 + \rho_{\tilde{\kappa}} \tilde{\kappa}^2 + \rho_{\text{nl}} A^2 + O(|A|^3 + |\mu|(|\alpha| + \beta^2 + \tilde{\kappa}^2)) = 0. \quad (3.17)$$

Then substituting the homogeneous scalings (3.13) into the above equation yields the claimed result. \square

In terms of scaled parameters, the amplitude formula (3.12) simplifies to

$$A' = \sqrt{-\frac{\alpha' + \rho_\beta \beta'^2 + \rho_{\tilde{\kappa}} \tilde{\kappa}'^2}{\rho_{\text{nl}}}} + O(\varepsilon).$$

3.4 Large wavelength stability

Linearising (D.1) in a striped solution gives the operator and eigenvalue problem for a perturbation U ,

$$\mathcal{L}_\mu U + 2Q[U_s, U] + 3K[U_s, U_s, U] = \lambda U, \quad (3.18)$$

e.g. in the function space setting noted in Appendix D. It is convenient to write the stripes in real terms,

$$\begin{aligned} U_s(x; \mu) = & 2A(E_0 + \tilde{\kappa}w_{A\tilde{\kappa}} + \check{\alpha}w_{A\check{\alpha}} + \beta^2 w_{A\beta\beta}) \cos(x) - 2A\beta w_{A\beta} \sin(x) \\ & + A^2 Q_2 \cos(2x) + A^2 Q_0 + \mathcal{R}. \end{aligned}$$

As we now view stripes $U_s(x)$ in two space dimensions $\mathbf{x} = (x, y) \in \mathbb{R}^2$ we may Fourier-transform (3.18) with respect to y thus replacing ∂_y^2 by $-\ell^2$. In x we perform a Floquet-Bloch-transform, i.e., in $\mathcal{L}_\mu = \mathcal{L}_\mu(\partial_x)$ replace ∂_x by $\partial_x + i\gamma$ and impose periodic boundary conditions on $[0, 2\pi]$, e.g., [50]. From (3.18) this gives the operator

$$\mathcal{T} := \kappa^2 D((\partial_x + i\gamma)^2 - \ell^2) + L + \check{\alpha}M + \beta\kappa B(\partial_x + i\gamma) + 2Q[U_s, \cdot] + 3K[U_s, U_s, \cdot],$$

which, as usual, arises for the perturbation in the form

$$U(\mathbf{x}) = e^{i(\gamma x + \ell y)} V(x; \gamma),$$

where $V(x; \gamma)$ has periodicity of $U_s(x)$ in x and we write $V_0(x) := V(x; 0) \in \mathbb{R}^2$.

Here we are interesting in the stability of stripes against large wavelength perturbations, i.e., $\gamma, \ell \approx 0$. Let us consider the eigenvalue problem $\mathcal{T}V = \lambda V$ with respect to a parameter $p \in \{\ell, \gamma\}$ and denote evaluations at $p = 0$ by subindex zero. The curve of eigenvalues attached to the translation mode at the origin thus has $\lambda|_0 = 0$, which is a simple zero eigenvalue with eigenvector V_0 . The kernel of \mathcal{T}_0 is therefore spanned by

$$\begin{aligned} \partial_x U_s = & -2A(E_0 + \tilde{\kappa}w_{A\tilde{\kappa}} + \check{\alpha}w_{A\check{\alpha}} + \beta^2 w_{A\beta\beta}) \sin(x) - 2A\beta w_{A\beta} \cos(x) \\ & - 2A^2 Q_2 \sin(2x) + O(\mathcal{R}). \end{aligned}$$

Differentiating $\mathcal{T}V = \lambda V$ with respect to p and evaluating at $p = 0$ gives

$$\mathcal{T}_0(\partial_p V)_0 = (\partial_p \lambda)_0 V_0 - (\partial_p \mathcal{T})_0 V_0. \quad (3.19)$$

By Fredholm alternative, this is solvable in $(\partial_p V)_0$ if and only if the right-hand side is orthogonal to the kernel of adjoint operator of \mathcal{T}_0 and thus

$$(\partial_p \lambda)_0 = \langle (\partial_p \mathcal{T})_0 V_0, V_0^* \rangle \quad (3.20)$$

with the normalisation $\langle V_0, V_0^* \rangle = 1$ and V_0^* in the kernel of the adjoint operator

$$\mathcal{T}_0^* := \kappa^2 D\partial_x^2 + L^T + \check{\alpha}M^T - \beta\kappa B\partial_x + (2Q[U_s, \cdot] + 3K[U_s, U_s, \cdot])^T.$$

In case $p = \ell$ we have $(\partial_\ell \mathcal{T})_0 = 0$ and it follows that $(\partial_\ell \lambda)_0 = 0$. In case $p = \gamma$,

$$(\partial_\gamma \mathcal{T})_0 = 2i\kappa^2 D\partial_x + i\beta\kappa B, \quad (3.21)$$

and it follows that

$$(\partial_\gamma \lambda)_0 = i\kappa \langle (2\kappa D\partial_x + \beta B)V_0, V_0^* \rangle \in i\mathbb{R}, \quad (3.22)$$

which measures the correction of the phase velocity c to the group velocity, cf. [10] and Remark E.2.1 in Appendix E.2. It is well known to vanish for stationary wavetrains $c = 0$ due to reflection symmetry in x of $V_0 = \partial_x U_s$ and V_0^* ; here this occurs for $\beta = 0$ so that $(\partial_\gamma \lambda)_0 = O(|\beta|)$ as we shall confirm in Appendix E.2.

Differentiating again and evaluating at $p = 0$ gives

$$\mathcal{T}_0(\partial_p^2 V)_0 = (\partial_p^2 \lambda)_0 V_0 - (\partial_p^2 \mathcal{T})_0 V_0 + 2(\partial_p \lambda)_0 (\partial_p V)_0 - 2(\partial_p \mathcal{T})_0 (\partial_p V)_0.$$

Proceeding as above, in case $p = \ell$ we have

$$(\partial_\ell^2 \lambda)_0 = \langle (\partial_\ell^2 \mathcal{T})_0 V_0, V_0^* \rangle = -2\kappa^2 \langle DV_0, V_0^* \rangle, \quad (3.23)$$

and in case $p = \gamma$ we have

$$(\partial_\gamma^2 \lambda)_0 = \langle (\partial_\gamma^2 \mathcal{T})_0 V_0 - 2(\partial_\gamma \lambda)_0 (\partial_\gamma V)_0 + 2(\partial_\gamma \mathcal{T})_0 (\partial_\gamma V)_0, V_0^* \rangle. \quad (3.24)$$

These quantities give the curvatures of spectrum at the origin in ℓ and γ directions, respectively. Other directional derivatives are not relevant since $(\partial_\ell V)_0 \in \ker \mathcal{T}_0$ and thus $(\partial_{\ell\gamma} \lambda)_0 = 0$. Hence, the signs of (3.23), (3.24) determine the sideband stability or instability of stripes, which is commonly referred to as Eckhaus un/stable for the x -direction, i.e. with respect to γ and $\ell = 0$, and as zigzag un/stable for the y -direction, i.e., with respect to ℓ and $\gamma = 0$.

Zigzag instability It is well-known that stripes become unstable against large wavelength perturbations parallel to the stripes if the stripes are stretched, while stripes are not as sensitive to compression. The canonical example is the Swift-Hohenberg equation which has not advection or quadratic terms. The main point of the next theorem is to exhibit the effect of advection through β and also the role of quadratic terms in the system.

Theorem 3.4.1 (Zigzag instability). *For μ such that the stripe solution (3.10) with the amplitude $A(\mu) > 0$ exists in (1.9), the curve of spectrum of \mathcal{T} for $\gamma = 0$ and $|\ell| \ll 1$ attached to the origin is given by*

$$\lambda_{zz}(\ell) = \left(\mathbf{k}_c \rho_{\tilde{\kappa}} \tilde{\kappa} + \rho_{\check{\alpha}} \alpha + \rho_{\beta\beta} \beta^2 + \mathcal{R}_{zz} \right) \ell^2, \quad (3.25)$$

with $\rho_{\tilde{\kappa}}$ as in §3.3, and

$$\begin{aligned} \rho_{\check{\alpha}} &:= -a_M \mathbf{k}_c^2 (\langle DE_0, w_{A\check{\alpha}}^* \rangle + \langle Dw_{A\check{\alpha}}, E_0^* \rangle) / \lambda_M - q_{22} / \rho_{nl}, \\ \rho_{\beta\beta} &:= -\mathbf{k}_c^2 (\langle DE_0, w_{A\beta\beta}^* \rangle + \langle Dw_{A\beta\beta}, E_0^* \rangle - \langle Dw_{A\beta}, w_{A\beta}^* \rangle) - q_{22} \rho_{\beta} / \rho_{nl}, \\ q_{22} &:= -\mathbf{k}_c^2 \langle DQ_2, Q_2^* \rangle, \quad \mathcal{R}_{zz} = O(a_M \alpha^2 + \tilde{\kappa}^2 + a_M |\alpha| \beta^2 + \ell^2), \end{aligned} \quad (3.26)$$

where $a_M = 0$ if $M = \text{Id}$, $a_M = 1$ otherwise.

The proof is presented in Appendix E.1. The theorem in particular shows that λ_{zz} depends to quadratic order on the advection parameter β . In particular, for $\rho_\alpha \neq 0$, the theorem gives the zigzag stability boundary to leading order as

$$\alpha = \mathcal{Z}(\tilde{\kappa}, \beta) = -(\mathbf{k}_c \rho_{\tilde{\kappa}} \tilde{\kappa} + \rho_{\beta\beta} \beta^2) / \rho_\alpha. \quad (3.27)$$

Recall that $A = 0$ holds for a surface in μ -space that includes $\mu = 0$. The natural scalings discussed after (3.12) give the following reduced spectrum.

Corollary 3.4.2. *Assume the conditions in Theorem 3.4.1 and the scalings (3.13), then the curve of spectrum of \mathcal{T} for $\gamma = 0$ and $|\ell| \ll 1$ attached to the origin is given by*

$$\lambda_{zz}(\ell) = \varepsilon (\mathbf{k}_c \rho_{\tilde{\kappa}} \tilde{\kappa}' + O(|\varepsilon|)) \ell^2.$$

Here the zigzag stability boundary is given by $\tilde{\kappa} = 0$ to leading order, independent of the advection, cf. Fig. 3.5a & 3.5b (green lines).

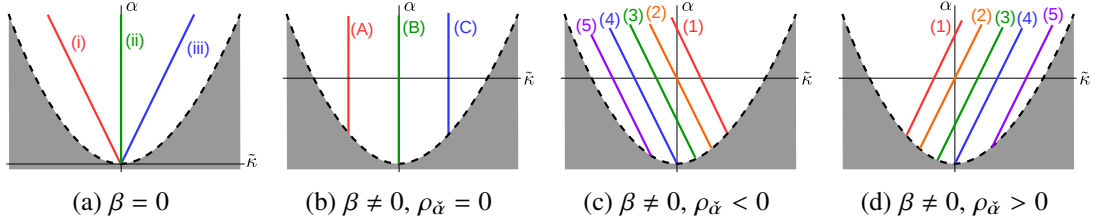


Figure 3.5: Sketches of the different leading order zigzag boundaries in the $(\tilde{\kappa}, \alpha)$ -plane. Stripes exist in the white regions. Dashed curves: bifurcation curves; coloured solid lines: zigzag boundaries. The zigzag unstable region lies to the left of each zigzag boundary. In (a): (i) $\rho_\alpha < 0$, (ii) $\rho_\alpha = 0$, zigzag boundary is $\tilde{\kappa} = 0$, (iii) $\rho_\alpha > 0$. In (b): (A) $\rho_{\beta\beta} < 0$, (B) $\rho_{\beta\beta} = 0$, zigzag boundary is $\tilde{\kappa} = 0$, (C) $\rho_{\beta\beta} > 0$. In (c) and (d): (1) $\mathcal{Z}(0, \beta) > 0$ ($\rho_{\beta\beta}/\rho_\alpha < 0$), (2) $\mathcal{Z}(0, \beta) = 0$ ($\rho_{\beta\beta} = 0$), (3) $\mathcal{B}(0, \beta) < \mathcal{Z}(0, \beta) < 0$ ($0 < \rho_{\beta\beta}/\rho_\alpha < \rho_\beta$), (4) $\mathcal{Z}(0, \beta) = \mathcal{B}(0, \beta)$ ($\rho_{\beta\beta}/\rho_\alpha = \rho_\beta$), (5) $\mathcal{Z}(0, \beta) < \mathcal{B}(0, \beta)$ ($\rho_{\beta\beta}/\rho_\alpha > \rho_\beta$).

Relaxing these scalings assumptions yields a variety of zigzag stability boundaries depending on the signs of ρ_α and $\rho_{\beta\beta}$, cf. Fig. 3.5. Non-zero ρ_α creates a sloping zigzag boundary and non-zero $\rho_{\beta\beta}$ shifts the zigzag boundary horizontally. As mentioned in Fig. 3.1b, the attachment point of the zigzag boundary to the bifurcation loci can be moved and rotated relative to $\tilde{\kappa} = 0$. The bifurcation curve at $\tilde{\kappa} = 0$ lies at

$$\alpha = \mathcal{B}(0, \beta) = -\rho_\beta \beta^2,$$

and the zigzag boundary at $\tilde{\kappa} = 0$ lies at

$$\alpha = \mathcal{Z}(0, \beta) = -\frac{\rho_{\beta\beta}}{\rho_\alpha} \beta^2$$

for $\rho_\alpha \neq 0$. Hence we can compare $\mathcal{B}(0, \beta)$ and $\mathcal{Z}(0, \beta)$ and obtain the more accurate positions of the zigzag boundaries near the bifurcation curve and close to $\tilde{\kappa} = 0$, cf. Fig. 3.5.

Notably, the term q_{22} related to the quadratic form Q appears in both ρ_α and $\rho_{\beta\beta}$. In particular, vanishing quadratic form $Q = 0$ gives $q_{22} = 0$.

Remark 3.4.3. For $Q = 0$ we have $q_{22} = 0$, and from Remark 3.2.5, as well as (3.7) and (3.9) a tedious computation gives

$$\rho_{\beta\beta} = \frac{\mathbf{k}_c^4 b_3^2 d_1}{b_1^2 (b_1 + b_4)^4} b_4 (5b_1 + b_4).$$

Recall $b_1 b_4 = b_2 b_3 < 0$, $b_1 + b_4 < 0$ and $a_1 < 0$ implies $b_1 < 0$. Hence, for all sufficiently small coefficients in Q , we have $\rho_{\beta\beta} < 0$ for either $a_1 < 0$, or $a_1 > 0$ and $a_1 > \mathbf{k}_c^2 d_1 - (a_4 - \mathbf{k}_c^2 d_2)/5$, $\rho_{\beta\beta} > 0$ otherwise.

From Theorem 3.3.1 we know that the bifurcation curve for $\tilde{\kappa} = 0$ in the (β, α) -plane is to leading order given by $\alpha = -\rho_\beta \beta^2$. In order to study the stability at the onset of bifurcation, let us consider $\tilde{\alpha} := \alpha + \rho_\beta \beta^2$ so the bifurcations occur at $\tilde{\alpha} = 0$ in the $(\beta, \tilde{\alpha})$ -plane. It follows that

$$\begin{aligned} \lambda_{zz}(\ell) &= \left(\mathbf{k}_c \rho_{\tilde{\kappa}} \tilde{\kappa} + \rho_{\tilde{\alpha}} (\tilde{\alpha} - \rho_\beta \beta^2) + \rho_{\beta\beta} \beta^2 + \mathcal{R}_{zz} \right) \ell^2 \\ &= \left(\mathbf{k}_c \rho_{\tilde{\kappa}} \tilde{\kappa} + \rho_{\tilde{\alpha}} \tilde{\alpha} + (\rho_{\beta\beta} - \rho_{\tilde{\alpha}} \rho_\beta) \beta^2 + \mathcal{R}_{zz} \right) \ell^2, \end{aligned} \quad (3.28)$$

and thus the zigzag boundary for $\rho_{\tilde{\alpha}} \neq 0$ is given by

$$\tilde{\alpha} = -(\mathbf{k}_c \rho_{\tilde{\kappa}} \tilde{\kappa} + (\rho_{\beta\beta} - \rho_{\tilde{\alpha}} \rho_\beta) \beta^2) / \rho_{\tilde{\alpha}}. \quad (3.29)$$

This dependence on β shows that the advection influences the form of the zigzag stability boundary near the bifurcation.

Eckhaus instability It is well known that a supercritical Turing bifurcation for $\beta = \tilde{\kappa} = 0$ implies stable Eckhaus sideband, and we next determine the expansion including $\beta, \tilde{\kappa}$. Recall the Eckhaus instability arises from perturbations that vary only in x -direction, i.e., $p = \gamma$ and $\ell = 0$.

Theorem 3.4.4 (Eckhaus instability). *For μ such that the stripe solution (3.10) with amplitude $A(\mu) > 0$ exists in (1.9), the curve of spectrum of \mathcal{T} for $\ell = 0$ and $|\gamma| \ll 1$ attached to the origin is given by*

$$\lambda_{eh} = i \mathbf{k}_c \left((\lambda_{\tilde{\kappa}} \beta - \lambda_\beta) \beta + O(A^2) \right) \gamma - \mathbf{k}_c^2 \frac{\rho_{\tilde{\kappa}}}{\rho_{nl}} A^{-2} \left(\alpha + \rho_\beta \beta^2 + 3\rho_{\tilde{\kappa}} \tilde{\kappa}^2 + \mathcal{R}_{eh} \right) \gamma^2,$$

with $\mathcal{R}_{eh} := O(\mu^2 + A^2 |\mu| + A^4 + |\gamma|)$.

See Appendix E.2 for the proof and revisit Fig. 3.1 for the (un)stable regions. Here we have simplified the estimate of \mathcal{R}_{eh} – more details can be found in the proof.

Hence, the Eckhaus stability boundary is given to leading order by

$$\alpha = \mathcal{E}(\tilde{\kappa}, \beta) = -3\rho_{\tilde{\kappa}} \tilde{\kappa}^2 - \rho_\beta \beta^2. \quad (3.30)$$

We note that for $\tilde{\kappa} = 0$ this is $\mathcal{E}(0, \beta) = -\rho_\beta \beta^2 = \mathcal{B}(0, \beta)$. Moreover, since $\rho_{\tilde{\kappa}} < 0$, we have $\mathcal{E}(\tilde{\kappa}, \beta) \geq \mathcal{B}(\tilde{\kappa}, \beta)$ so that, as usual, the Eckhaus boundary touches the bifurcation curve at $\tilde{\kappa} = 0$

and lies in the existence region of stripes. Therefore, for $\tilde{\kappa} = 0$ the bifurcating stripes are Eckhaus stable and unstable otherwise.

Analogous to the zigzag stability, we consider $\tilde{\alpha} := \alpha + \rho_\beta \beta^2$ so that

$$\text{Re}(\lambda_{\text{eh}}) = -\mathbf{k}_c^2 \frac{\rho_{\tilde{\kappa}}}{\rho_{\text{nl}}} A^{-2} \left(\tilde{\alpha} + 3\rho_{\tilde{\kappa}} \tilde{\kappa}^2 + \mathcal{R}_{\text{eh}} \right) \gamma^2, \quad (3.31)$$

and the Eckhaus boundary becomes

$$\tilde{\alpha} = -3\rho_{\tilde{\kappa}} \tilde{\kappa}^2, \quad (3.32)$$

which is independent on β to leading order – in contrast to the zigzag boundary. Hence, the leading order effect of advection through β is just a translation of the Eckhaus boundary downwards ($\rho_\beta > 0$) with order β^2 . In other words, for any fixed α in the existence region, the width of Eckhaus stable region increases with $|\beta|$. The advection can well influence the Eckhaus stability at higher order, cf. (E.10), but an analysis of this is beyond the scope of this thesis.

3.5 Stability of stripes on lattices

In this section we analyse the stability of stripes on rectangular domains with periodic boundary conditions that are nearly square or nearly ‘hexagonal’ in the sense that Fourier modes with wave vectors on a nearly hexagonal lattice are permitted. Indeed, in the Fourier picture these domains have wavevectors on a lattice, and the stability can be studied by centre manifold reduction. While this reduction also allows to study other solutions and nonlinear interactions, here we consider the stability of stripes only.

3.5.1 Centre manifold reduction

In preparation of the concrete cases, we first consider somewhat abstractly centre manifold reductions for (1.9). Let us denote

$$L(\mu) := \mathcal{L}_\mu - \mathcal{L}_0 = \check{\alpha} M + \beta (\mathbf{k}_c + \tilde{\kappa}) B \partial_x + (2\mathbf{k}_c \tilde{\kappa} + \tilde{\kappa}^2) D \Delta.$$

Theorem 3.5.1 (Centre manifold reduction). *Consider (1.9) posed on the interval $\Omega_1 = [0, 2\pi]$ or on a square $\Omega_2 = [0, 2\pi]^2$ or a rectangle $\Omega_3 = [0, 4\pi] \times [0, 4\pi/\sqrt{3}]$ on the space $X = (\mathbb{L}^2(\Omega_j))^2$ with periodic boundary conditions and assume a Turing instability occurs at $\mu = 0$. The generalised kernel N of the associated realisation of \mathcal{L}_0 and its co-kernel Y have dimension $2j$ on Ω_j , $j = 1, 2, 3$. In all cases, a $2j$ -dimensional centre manifold exists for $|\mu| \ll 1$, which is the graph of $\Psi \in C^2(N \times \Lambda, Y)$ with $\Psi(0, 0) = 0$, $\partial_u \Psi(0, 0) = 0$, and the reduced ODE for $u_c(t) \in N$ is of the form*

$$\dot{u}_c = f(u_c; \mu) := PL(\mu)(u_c + \Psi(u_c, \mu)) + PF(u_c + \Psi(u_c, \mu)),$$

where $P : X \rightarrow N$ is the projection with kernel Y . In particular,

$$\partial_u f(u_c; \mu) = P(L(\mu) + \partial_u F(u_c + \Psi(u_c; \mu)))(\text{Id} + \partial_u \Psi(u_c; \mu)) + O(|u_c|^3).$$

Proof. It suffices to show the claimed dimension of the kernel depending on j ; the result then follows from standard centre manifold theory, e.g., [20], by the definition of Turing instability. For Ω_1 this was already discussed in the previous section. From Lemma 3.2.2 the critical eigenmodes of \mathcal{L}_0 are explicitly known, in particular their wavevectors satisfy $(k_j, \ell_j) \in S^1$. Hence, on Ω_2 these are the four choices $\mathbf{k}_1^{\text{sq}} := (1, 0)$, $\mathbf{k}_2^{\text{sq}} := (0, 1)$ and their negatives, and on Ω_3 the six choices $\mathbf{k}_1 := (1, 0)$, $\mathbf{k}_2 := (-1/2, \sqrt{3}/2)$, $\mathbf{k}_3 := -(1/2, \sqrt{3}/2)$ and their negatives. \square

Remark 3.5.2. As to nonlinear terms of f we note that $Pv = 0$ if v consists of Fourier modes whose wavevectors are not in S^1 , which leads to the following resonance condition. Since wavevectors are added in products, any nonlinear term must stem from products of terms for which the sum of wavevectors from S^1 lies again in S^1 . Such resonant interactions require at least three terms, and on Ω_2 are possible only among wavevectors in the same spatial direction. In contrast, Ω_3 allows for the so-called resonance triads (or three-wave interactions) $\mathbf{k}_1 + \mathbf{k}_2 + \mathbf{k}_3 = 0$.

Next, we expand the linearisation on the centre manifold somewhat abstractly in order to be conveniently used for different settings later.

Let us denote $\Psi_{j\ell} := \partial_u^j \partial_\mu^\ell \Psi(0; 0)/(j! \ell!)$ so that $\Psi_{00} = \Psi_{10} = 0$ in general and due to the zero equilibrium for all parameters also $\Psi_{0j} = 0$ for all $j \geq 0$.

Corollary 3.5.3. Assume the conditions and notations of Theorem 3.5.1 and the scaling (3.13) so that $u_c = \varepsilon A' u_1 \in N$, $\mu = \varepsilon \mu_1 + \varepsilon^2 \mu_2$ and $u_1, \mu_1, \mu_2 = O(1)$ with respect to ε . We have $\Psi(u_c; \mu) = \varepsilon^2 u_2 + O(\varepsilon^3)$ with $u_2 := A'^2 \Psi_{20}[u_1, u_1] + A' \Psi_{11}[\mu_1, u_1]$, and it holds that

$$\begin{aligned} \partial_u f(u_c; \mu) &= 2\varepsilon A' PQ[u_1, \cdot] \\ &\quad + \varepsilon^2 P \left(L(\mu_2) + (L(\mu_1) + 2A' Q[u_1, \cdot])(2A' \Psi_{20}[u_1, \cdot] + \Psi_{11}[\mu_1, \cdot]) \right. \\ &\quad \left. + 2Q[u_2, \cdot] + 3A'^2 K[u_1, u_1, \cdot] \right) + O(\varepsilon^3). \end{aligned} \quad (3.33)$$

Proof. Substituting u_c , μ as assumed gives $L(\mu) = \varepsilon L(\mu_1) + \varepsilon^2 L(\mu_2)$ and Taylor expanding $\Psi(u_c; \mu) = \varepsilon^2 u_2 + O(\varepsilon^3)$ as well as

$$\begin{aligned} \partial_u \Psi(u_c, \mu) &= \varepsilon (2A' \Psi_{20}[u_1, \cdot] + \Psi_{11}[\mu_1, \cdot]) + O(\varepsilon^2), \\ \partial_u F(u_c + \Psi(u_c, \mu)) &= 2\varepsilon A' Q[u_1, \cdot] + 2\varepsilon^2 Q[u_2, \cdot] + 3\varepsilon^2 A'^2 K[u_1, u_1, \cdot] + O(\varepsilon^3). \end{aligned}$$

Combining these, $\partial_u f$ from Theorem 3.5.1 and using that $\langle BE_0, E_0^* \rangle|_{\mu=0} = 0$ and $\langle DE_0, E_0^* \rangle = 0$, which removes $PL(\mu_1)$, we obtain the claimed form. \square

3.5.2 Stability in one space-dimension

We first note that due to lack of triads, cf. Remark 3.5.2 a number of terms in (3.33) vanish: $U = U_0 e^{ix}$ with any $U_0 \in \mathbb{C}^2$ gives $PQ[U, \cdot] = 0$ on N . Analogously, $Q[u_1, \cdot]$, $Q[u_1, \Psi_{11}[\mu_1, \cdot]]$, $L(\mu_1) \Psi_{20}[u_1, \cdot]$, $Q[\Psi_{11}[\mu_1, u_1], \cdot]$ vanish so that (3.33) simplifies to

$$\begin{aligned} \partial_u f(u_c; \mu) &= \varepsilon^2 P \left(L(\mu_2) + L(\mu_1) \Psi_{11}[\mu_1, \cdot] + 2A'^2 Q[\Psi_{20}[u_1, u_1], \cdot] \right. \\ &\quad \left. + 4A'^2 Q[u_1, \Psi_{20}[u_1, \cdot]] + 3A'^2 K[u_1, u_1, \cdot] \right) + O(\varepsilon^3). \end{aligned} \quad (3.34)$$

Next we infer the matrix form of the linearisation from the existence result. It is convenient to also span the centre eigenspace by \sin and \cos , i.e., $u_c = u_0 \cos + u_1 \sin$ for $u_0, u_1 \in \mathbb{R}$; the projection in these coordinates is given by $P := \text{Id} - P_h = \langle \cdot, E_0^* \cos \rangle \cos + \langle \cdot, E_0^* \sin \rangle \sin$ and, up to translation in x , stripes are given by

$$\begin{aligned} U_s(x; \mu) &= 2\epsilon A'E_0 \cos(x) \\ &+ 2\epsilon^2 A' \left(\tilde{\kappa}' w_{A\tilde{\kappa}} \cos(x) - \beta' w_{AB} \sin(x) + A'(Q_2 \cos(2x) + Q_0) \right) + O(\epsilon^3). \end{aligned}$$

Theorem 3.5.4. *Assume the conditions and notations of Theorem 3.5.1 for the domain $\Omega = [0, 2\pi]$ with periodic boundary conditions and velocity parameter $c = c(\mu)$ as in (3.9). Stripes U_s are in 1-to-1 correspondence with equilibria $u_c \in N$, $f(u_c, \mu) = 0$, μ solving (3.8) and, up to translation in x , $U_s = u_c + \Psi(u_c; \mu)$ for $u_c = 2AE_0 \cos(x)$. The linearisation in stripes satisfies $\partial_u f(u_c; \mu)E_0 \sin = 0$ as well as $\partial_u f(u_c; \mu)E_0 \cos = 2A^2 \rho_{nl} + O(\epsilon^3)$ with (3.13), and, up to this order, has the matrix forms*

$$A^2 \begin{pmatrix} 2\rho_{nl} & 0 \\ 0 & 0 \end{pmatrix}, \quad A^2 \begin{pmatrix} \rho_{nl} & \rho_{nl} \\ \rho_{nl} & \rho_{nl} \end{pmatrix},$$

in the coordinates \cos, \sin and e_0, \overline{e}_0 , respectively.

Proof. Centre manifold equilibria $f(u_c; \mu) = 0$ correspond to equilibria near bifurcation and, due to Theorem 3.3.1, these are stripes so that $u_c = 2A \cos$. By translation symmetry $P\partial_x U_s$ lies in the kernel of $\partial_u f(2A \cos; \mu)$ and in particular each expansion order with respect to A of the linearisation has the corresponding order of $P\partial_x U_s$ as its kernel. In fact, due to the translation symmetry of (1.9), the ODE in Theorem 3.5.1 is independent of the translation direction, cf. [20]. Hence, the matrix is diagonal in (\cos, \sin) -coordinates and it remains to determine the second eigenvalue. In this reduced equation, the bifurcation of stripes is a generic pitchfork with λ_μ the normal form unfolding parameter, and it is well known that the eigenvalue of the bifurcating branch is to leading order $-2\lambda_\mu = 2\rho_{nl}A^2$ [20]. \square

Remark 3.5.5. *The proof for the matrix form in Theorem 3.5.4 does not rely on the detailed expansion of the linearisation (3.34), but can of course be derived from it. This is somewhat tedious since Ψ_{20}, Ψ_{11} enter in general, and we do this for the hexagonal lattice in Appendix E.3.*

Remark 3.5.6. *Here we highlight an a priori consequence for the upcoming stability on lattices: Under the scalings (3.13), the stripes are Eckhaus- and (neutrally) zigzag-stable for $\tilde{\kappa} = 0$, cf. §3.4. As mentioned in [70, Corollary 2.6], such stripes are spectrally stable in $L^2(\mathbb{R}^2)$ near onset of Turing instability for $\beta \neq 0$ and thus are stable against each Fourier mode. Hence, in the stability analysis on lattices, for $\beta \neq 0$ the stripes must be stable against lattice perturbations near the Turing bifurcation at $\tilde{\kappa} = 0$, which is indeed the case, cf. Fig. 3.6b, 3.8d, 3.11a.*

3.5.3 Stability against (quasi-)square perturbations

We start with the simplest case, the stability against (quasi-)square perturbations. Although it turns out that these are not the dominant instability mechanisms among planar modes, it is instructive and adds to completeness of the analyses of lattice modes.

We consider the problem (1.9) with periodic boundary conditions on the (quasi-)square domain

$$\Omega_{\text{sq}} := [0, 2\pi/\kappa] \times [0, 2\pi/\ell], \quad \kappa := \mathbf{k}_c + \tilde{\kappa}, \quad \ell := \mathbf{k}_c + \tilde{\ell},$$

with the scaling $\tilde{\ell} = \varepsilon \tilde{\ell}'$ in accordance with (3.13), so that $\tilde{\ell} = O(\varepsilon)$. In particular, the quasi-square domain reduces to the square domain when $\kappa = \ell$. Rescaling the spatial variables with $\tilde{x} = x/\kappa$ and $\tilde{y} = y/\ell$, so that the scaled domain is given by $\Omega_2 = [0, 2\pi]^2$ with dual lattice wavevectors $\mathbf{k}_j^{\text{sq}} = (k_j, \ell_j) \in \mathbb{R}^2$, where

$$\mathbf{k}_1^{\text{sq}} = (1, 0), \quad \mathbf{k}_2^{\text{sq}} = (0, 1),$$

and for convenience $\mathbf{k}_{-j}^{\text{sq}} = -\mathbf{k}_j^{\text{sq}}$, $j = 1, 2$. As noted in Theorem 3.5.1 this leads to a four dimensional centre manifold for

$$u_c(x) = U_{\text{sq}}(x) = \sum_{j=-2, j \neq 0}^2 u_j e_j,$$

where $u_j = \overline{u_{-j}} \in \mathbb{C}$ and $e_j := e^{i\mathbf{k}_j^{\text{sq}} \cdot \mathbf{x}} E_0$ are the four linearly independent kernel eigenvectors that appear for Ω_2 ; we also denote $e_j^* := e^{i\mathbf{k}_j^{\text{sq}} \cdot \mathbf{x}} E_0^*$.

Theorem 3.5.7. *Assume the conditions and notations of Theorem 3.5.1 for the domain Ω_2 with periodic boundary conditions and the scaling (3.13). Let the velocity parameter $c = c(\mu)$ be as in (3.9). The subspace $\{u_j = 0, j = \pm 2\}$ is invariant for the reduced ODE and contains the stripes as equilibria. The linearisation in stripes in the index ordering $(1, -1, 2, -2)$ has a block diagonal matrix of the form $L_{\text{sq}} = \text{diag}(L_1, L_2^{\text{sq}}) + O(\varepsilon^3)$ with 2×2 -subblocks*

$$L_1 = A^2 \begin{pmatrix} \rho_{\text{nl}} & \rho_{\text{nl}} \\ \rho_{\text{nl}} & \rho_{\text{nl}} \end{pmatrix}, \quad L_2^{\text{sq}} = \varepsilon^2 \begin{pmatrix} \lambda'_{\tilde{\ell}} + A'^2 \xi & 0 \\ 0 & \lambda'_{\tilde{\ell}} + A'^2 \xi \end{pmatrix},$$

where $\lambda'_{\tilde{\ell}} := \alpha' + \rho_{\tilde{\kappa}} \tilde{\ell}'^2 + O(\varepsilon)$ is real and

$$\xi := 6k_0 + 2q_0 + 8q_{11}, \quad q_{11} := \langle Q[E_0, Q_{11}], E_0^* \rangle, \quad Q_{11} := -(-2\mathbf{k}_c^2 D + L)^{-1} Q[E_0, E_0].$$

See Appendix E.3 for the proof.

The eigenvalues of the matrix L_1 are 0 and $2\rho_{\text{nl}}A^2 < 0$, as in Theorem 3.5.4, which reflects that the stripes are stable against perturbations in the x -direction on this domain.

Concerning the subblock L_2^{sq} , we first note the general form of eigenvalues.

Lemma 3.5.8. *Under the assumptions of Theorem 3.5.7, the double eigenvalue of the matrix L_2^{sq} is real and given by*

$$\lambda = \varepsilon^2 \left(A'^2 (3k_0 - q_2 + 8q_{11}) - \rho_\beta \beta'^2 + \rho_{\tilde{\kappa}} (\tilde{\ell}'^2 - \tilde{\kappa}'^2) \right) + O(\varepsilon^3),$$

where $A' = \sqrt{-(\alpha' + \rho_\beta \beta'^2 + \rho_{\tilde{\kappa}} \tilde{\kappa}'^2)/\rho_{\text{nl}}} + O(\varepsilon)$.

Proof. The two eigenvalues are the same diagonal term which, by (3.8), read

$$\varepsilon^2 (\lambda'_{\tilde{\ell}} + A'^2 \xi) = \varepsilon^2 (-A'^2 \rho_{\text{nl}} - \rho_\beta \beta'^2 - \rho_{\tilde{\kappa}} \tilde{\kappa}'^2 + \rho_{\tilde{\kappa}} \tilde{\ell}'^2 + A'^2 \xi) + O(\varepsilon^3),$$

and (3.8) gives A' as claimed; that $\lambda'_{\tilde{\ell}}$ is real was already stated in Theorem 3.5.7. \square

We note that the signs of q_2, q_{11} depend on Q . For the sake of simplicity and comparison with (quasi-)hexagonal stabilities discussed below, we consider Hypothesis 3.1.1. This immediately gives the following rectangular stability result.

Corollary 3.5.9 ((Quasi-)square lattice stabilities). *Under the assumptions of Theorem 3.5.7 and Hypothesis 3.1.1 the double eigenvalue of matrix L_2^{sq} is given by*

$$\lambda_{\text{sq}} = \varepsilon^2 \left(-\alpha' - 2\rho_\beta \beta'^2 + \rho_{\tilde{\kappa}} (\tilde{\ell}'^2 - 2\tilde{\kappa}'^2) \right) + o(\varepsilon^2). \quad (3.35)$$

The stability boundary $\lambda_{\text{sq}} = 0$ in terms of unscaled parameters is given by

$$\alpha = Q(\tilde{\kappa}, \beta; \tilde{\ell}) := -2\rho_\beta \beta^2 + \rho_{\tilde{\kappa}} (\tilde{\ell}^2 - 2\tilde{\kappa}^2). \quad (3.36)$$

For any $\tilde{\kappa}$ and fixed β , if $|\tilde{\ell}| \geq |\tilde{\kappa}|$, then $Q(\tilde{\kappa}, \beta; \tilde{\ell}) \leq \mathcal{B}(\tilde{\kappa}, \beta)$ and thus the stripes are stable against the square perturbation and the quasi-square perturbations with $|\tilde{\ell}| > |\tilde{\kappa}|$. The curvature of Q with respect to $\tilde{\kappa}$ is larger than that of \mathcal{B} for $|\tilde{\ell}| < |\tilde{\kappa}|$, which causes unstable stripes against quasi-square perturbations. The most unstable quasi-square perturbation occurs at $\tilde{\ell} = 0$, cf. Fig. 3.6. However, note that the Eckhaus boundary is dominant since $\alpha = \mathcal{E}(\tilde{\kappa}, \beta) \geq Q(\tilde{\kappa}, \beta; 0)$.

3.5.4 Stability against hexagonal perturbations

Concerning the six-dimensional lattice modes, we first study the exact hexagonal perturbation as a basis for the more unstable quasi-hexagonal perturbations. On the one hand, it is natural and relatively easier to consider the hexagonal case as, e.g. in the amplitude equations approach. On the other hand, the stability proof is neat and can be extended to the quasi-hexagonal case.

We consider the system (1.9) with periodic boundary condition on the rectangular domains

$$\Omega_{\text{hex}} = [0, 4\pi/\kappa] \times [0, 4\pi/(\sqrt{3}\kappa)], \quad \kappa = \mathbf{k}_c + \tilde{\kappa},$$

and isotropically rescale to $\Omega_3 = [0, 4\pi] \times [0, 4\pi/\sqrt{3}]$ with dual lattice wavevectors $\mathbf{k}_j = (k_j, \ell_j) \in \mathbb{R}^2$, where $\mathbf{k}_{-j} = -\mathbf{k}_j$, $j = 1, 2, 3$, cf. Remark 3.5.2,

$$\mathbf{k}_1 = (1, 0), \quad \mathbf{k}_2 = (-1/2, \sqrt{3}/2), \quad \mathbf{k}_3 = -(1/2, \sqrt{3}/2).$$

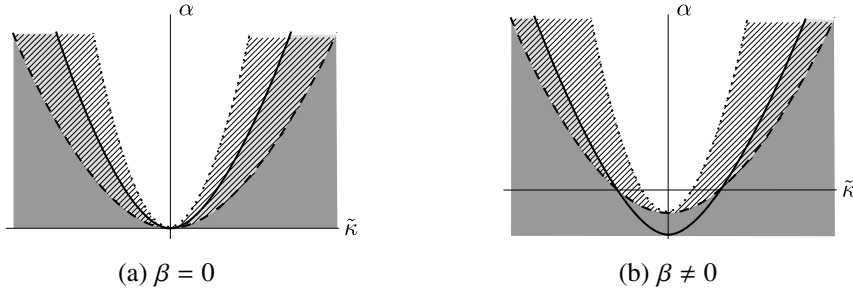


Figure 3.6: Sketches of the stability regions in the $(\tilde{\kappa}, \alpha)$ -plane for $\tilde{\ell} = 0$. Stripes exist in the complements of the dark grey regions. Light grey: quasi-square-unstable; hatched region: Eckhaus-unstable; white: stable; dashed curve: bifurcation curve $\alpha = \mathcal{B}(\tilde{\kappa}, \beta)$; dotted curve: Eckhaus boundary $\alpha = \mathcal{E}(\tilde{\kappa}, \beta)$; black solid curves: quasi-square stability boundary $\alpha = Q(\tilde{\kappa}, \beta; 0)$.

As noted in Theorem 3.5.1 this leads to a six dimensional centre manifold for

$$u_c(x) = U_{\text{hex}}(x) = \sum_{j=-3, j \neq 0}^3 u_j e_j,$$

where $u_j = \overline{u_{-j}} \in \mathbb{C}$ and $e_j := e^{i\mathbf{k}_j \cdot \mathbf{x}} E_0$ are the six linearly independent kernel eigenvectors that appear for Ω_3 ; we also denote $e_j^* := e^{i\mathbf{k}_j \cdot \mathbf{x}} E_0^*$. For convenience, here we use the same notation for the wavevectors and (adjoint) eigenvectors as in §3.5.3.

Theorem 3.5.10. Assume the conditions and notations of Theorem 3.5.1 for the domain Ω_3 with periodic boundary conditions, and the parameter scaling (3.13) for μ . Let the velocity parameter $c = c(\mu)$ be as in (3.9). The subspace $\{u_j = 0, j = \pm 2, \pm 3\}$ is invariant for the reduced ODE and contains the stripes as equilibria. The linearisation in stripes in the index ordering $(1, -1, 2, -3, 3, -2)$ has a block diagonal matrix of the form $L_{\text{hex}} = \text{diag}(L_1, L_2^{\text{hex}}, L_2^{\text{hex}}) + O(\varepsilon^3)$ with 2×2 -subblocks

$$L_1 = A^2 \begin{pmatrix} \rho_{\text{nl}} & \rho_{\text{nl}} \\ \rho_{\text{nl}} & \rho_{\text{nl}} \end{pmatrix}, \quad L_2^{\text{hex}} = \varepsilon^2 \begin{pmatrix} \lambda'_{\mu,2} + A'^2 \eta & 2A' \frac{q}{\varepsilon} + A' p(\mu_1) \\ 2A' \frac{q}{\varepsilon} + A' p(\mu_1) & \lambda'_{\mu,2} + A'^2 \eta \end{pmatrix},$$

where $\lambda'_{\mu,2} := \alpha' + \frac{1}{4}\rho_\beta\beta'^2 + \rho_{\tilde{\kappa}}\tilde{\kappa}'^2 + O(\varepsilon)$ and

$$\begin{aligned} q &:= \langle Q[E_0, E_0], E_0^* \rangle, \quad \eta := 6k_0 + 2q_0 + 8q_1, \quad q_1 := \langle Q[E_0, Q_1], E_0^* \rangle, \\ Q_1 &:= (-\mathbf{k}_c^2 D + L)^{-1}(\langle Q[E_0, E_0], E_0^* \rangle E_0 - Q[E_0, E_0]), \\ p(\mu_1) &:= \langle Q[\mathbf{i}\beta' w_{A\beta} + 4\tilde{\kappa}' w_{A\tilde{\kappa}}, E_0], E_0^* \rangle + \langle (-4\tilde{\kappa}' \mathbf{k}_c D - \mathbf{i}\beta' \mathbf{k}_c B) Q_1, E_0^* \rangle. \end{aligned}$$

See Appendix E.4 for the proof.

Since L_1 concerns perturbations in the x -direction, i.e., orthogonal to stripe, from Theorem 3.5.4 we know that L_1 has the eigenvalues 0 and $2\rho_{\text{pl}}A^2 < 0$.

Concerning the subblock L_2^{hex} , we first note the general form of eigenvalues.

Lemma 3.5.11. *Under the assumptions of Theorem 3.5.10, the eigenvalues of the matrix L_2^{hex} are*

$$\lambda_{\pm} = \varepsilon^2 \left(A'^2 (3k_0 - q_2 + 8q_1) - \frac{3}{4} \rho_{\beta} \beta'^2 \pm A' \left| \frac{2q}{\varepsilon} + A' p(\mu_1) \right| \right) + O(\varepsilon^3),$$

where $A' = \sqrt{-(\alpha' + \rho_{\beta} \beta'^2 + \rho_{\tilde{\kappa}} \tilde{\kappa}'^2)/\rho_{\text{nl}}} + O(\varepsilon)$.

Proof. The matrix L_2^{hex} is of the form $\begin{pmatrix} a & b \\ \bar{b} & a \end{pmatrix}$ with $a \in \mathbb{R}$, $b \in \mathbb{C}$, and such a matrix possesses the two real eigenvalues $\lambda_{\pm} = a \pm |b|$. For λ_{\pm} , b is as in the matrix unchanged, and for a we have

$$a = \varepsilon^2 (\lambda'_{\mu,2} + A'^2 \eta) = \varepsilon^2 \left(-A'^2 \rho_{\text{nl}} - \frac{3}{4} \rho_{\beta} \beta'^2 + A'^2 \eta \right) + O(\varepsilon^3)$$

and using (3.8) gives the claimed form. \square

The lemma shows that for small ε and $q = O(1)$ with respect to ε we have $\lambda_+ > 0$, and the stripe thus unstable. In order to study destabilisation of stripes near onset, and thus the competition of quadratic term and advection, we therefore assume $q = \varepsilon q'$ with $q' = O(1)$. This is most easily realised by Hypothesis 3.1.1, which assumes the entire quadratic term has a prefactor ε , though we note that $q = \varepsilon q'$ can be realised by a scaling assumption on certain parts of Q only.

In this case we can rewrite the entries in L_2^{hex} related to Q as follows

$$q = \varepsilon q', \quad q_1 = \varepsilon^2 q'_1, \quad \eta = 6k_0 + \varepsilon^2 (2q'_0 + 8q'_1), \quad Q_1 = \varepsilon Q'_1, \quad p(\mu_1) = \varepsilon p'(\mu_1),$$

with bounded primed quantities. Moreover, we recall

$$\rho_{\text{nl}} = 3k_0 + \varepsilon^2 (2q'_0 + q'_2) < 0$$

with sign due to the assumed supercriticality of the stripe bifurcating so that also $k_0 < 0$. This gives the following hexagonal in/stability result.

Theorem 3.5.12 (Hexagonal lattice stability). *Under the assumptions of Theorem 3.5.10 and Hypothesis 3.1.1 the eigenvalues of the matrix L_2^{hex} are given by*

$$\lambda_{\text{hex}}^{\pm} = \varepsilon^2 \left(3k_0 \tilde{A}'^2 - \frac{3}{4} \rho_{\beta} \beta'^2 \pm 2\tilde{A}' |q'| + O(\varepsilon) \right), \quad (3.37)$$

where $\tilde{A}' := \sqrt{-(\alpha' + \rho_{\beta} \beta'^2 + \rho_{\tilde{\kappa}} \tilde{\kappa}'^2)/(3k_0)}$. In particular, $\lambda_{\text{hex}}^{\pm} \in \mathbb{R}$.

Proof. Using Lemma 3.5.11 the claim directly follows from Hypothesis 3.1.1 and the resulting factors of ε as noted above. The term \tilde{A}' stems from the leading order of A' , i.e., $A' = \tilde{A}' + O(\varepsilon)$. \square

In particular, under these assumptions, q' is the only relevant quantity that relates to Q . In case $Q = o(\varepsilon)$ we have $q' = 0$ so that $\lambda_{\text{hex}}^\pm < 0$, i.e., stripes are always stable on the hexagonal lattice, since $k_0 < 0$ and $\rho_\beta > 0$.

In Theorem 3.5.12 the eigenvalue λ_{hex}^- is stable for all μ and q such that the striped solution (3.10) exists. The sign of λ_{hex}^+ , however, depends on both μ and q . A critical eigenvalue $\lambda_{\text{hex}}^+ = 0$ to leading order requires $3k_0\tilde{A}'^2 - \frac{3}{4}\rho_\beta\beta'^2 < 0$ or equivalently

$$\alpha > -\frac{7}{4}\rho_\beta\beta^2 - \rho_{\tilde{\kappa}}\tilde{\kappa}^2$$

in terms of unscaled parameters. Since $-\frac{7}{4}\rho_\beta\beta^2 - \rho_{\tilde{\kappa}}\tilde{\kappa}^2 < \mathcal{B}(\tilde{\kappa}, \beta)$ the above condition is automatically fulfilled for μ such that the stripes exist.

Solving $\lambda_{\text{hex}}^+ = 0$ yields the hex-stability boundaries to leading order. In terms of the unscaled parameters this reads

$$\{\alpha = \mathcal{H}_\pm(\tilde{\kappa}, \beta, q) : \alpha \geq \mathcal{B}(\tilde{\kappa}, \beta), \delta_{\mathcal{H}} \geq 0\}, \quad (3.38)$$

where

$$\mathcal{H}_\pm(\tilde{\kappa}, \beta, q) := -\frac{7}{4}\rho_\beta\beta^2 - \rho_{\tilde{\kappa}}\tilde{\kappa}^2 - \frac{1}{3k_0} \left(2q^2 \pm \sqrt{\delta_{\mathcal{H}}} \right), \quad (3.39)$$

$$\delta_{\mathcal{H}} := 4q^4 + 9k_0q^2\rho_\beta\beta^2. \quad (3.40)$$

We remark that since $\alpha \in \mathbb{R}$, the condition $\delta_{\mathcal{H}} \geq 0$ appears. The stripes are hex-unstable for $\delta_{\mathcal{H}} > 0$ and $\alpha \in (\mathcal{H}_-, \mathcal{H}_+)$, and hex-stable otherwise.

For the sake of simplicity of the notations, we formulate the hex-stability boundaries in terms of the unscaled parameters in §3.5.4 and §3.5.4.

Stripes with critical wavenumber

We first consider the stripes with the Turing critical wavenumber, i.e., $\tilde{\kappa} = 0$.

Case $\beta = 0, \tilde{\kappa} = 0$ (Fig. 3.7a) The hex-stability boundary reduces to a parabola

$$\alpha = \mathcal{H}_+(0, 0, q) = -\frac{4}{3k_0}q^2. \quad (3.41)$$

This coincides with the well-known result that the stripes are hex-unstable near the onset of Turing bifurcation except for $q = 0$ [19]. The other curve $\alpha = \mathcal{H}_-(0, 0, q) = 0$ overlaps the bifurcation curve $\alpha = \mathcal{B}(0, 0) = 0$.

Case $\beta \neq 0, \tilde{\kappa} = 0$ (Fig. 3.7b) The hex-stability boundaries are given by

$$\alpha = \mathcal{H}_\pm(0, \beta, q) := -\frac{7}{4}\rho_\beta\beta^2 - \frac{1}{3k_0} \left(2q^2 \pm \sqrt{4q^4 + 9k_0q^2\rho_\beta\beta^2} \right). \quad (3.42)$$

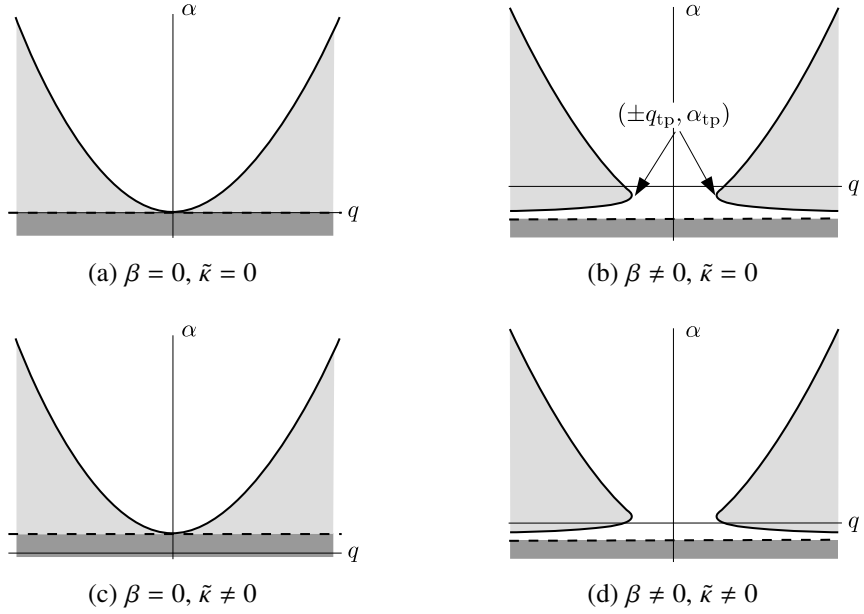


Figure 3.7: Sketches of the hexagonal stability regions of stripes in the (q, α) -plane. Stripes exist in the complement of the dark grey regions. White: hex-stable; grey: hex-unstable. Dashed line: bifurcation line $\alpha = \mathcal{B}(0, \beta)$; solid curves: hex-stability boundaries (a) $\alpha = \mathcal{H}_+(0, 0, q)$, cf. (3.41) (b) $\alpha = \mathcal{H}_{\pm}(0, \beta, q)$, cf. (3.42) (c) $\alpha = \mathcal{H}_+(\tilde{\kappa}, 0, q)$, cf. (3.45) (d) $\alpha = \mathcal{H}_{\pm}(\tilde{\kappa}, \beta, q)$, cf. (3.39).

There exist two turning points $(\pm q_{tp}, \alpha_{tp})$ given by

$$q_{tp} = \frac{3}{2}|\beta|\sqrt{-k_0\rho\beta}, \quad \alpha_{tp} = -\frac{1}{4}\rho\beta\beta^2. \quad (3.43)$$

The boundaries below the turning points are given by \mathcal{H}_- which decreases to zero for increasing $|q|$. Hence there exists a hex-stable region near the bifurcation. In particular, for $|q| < q_{tp}$, the stripes are hex-stable for all α . These indicate that the advection stabilises the stripes: for $\beta \neq 0$ stripes bifurcate stably in accordance with Remark 3.5.6, and advection ‘opens’ a stable window for small quadratic effects. Nevertheless, the hex-unstable region becomes larger for larger $|q|$, which highlights the destabilising effect of the quadratic term.

Remark 3.5.13. *For fixed $|q| > q_{tp}$, the stable stripes lose the stability when α increases to α_* where $\alpha_* < \alpha_{tp}$. In fact, at $\alpha = \alpha_{tp}$ the homogeneous steady state becomes unstable against hexagonal modes, cf. (3.5), also see Fig. 3.4 (green curve). Hence, the stable stripes lose stability ‘before’ the bifurcation of hexagons.*

Stripes with off-critical wavenumber

Now we turn to hex-stability of stripes with off-critical wavenumber $\kappa = \mathbf{k}_c + \tilde{\kappa}$, $\tilde{\kappa} \neq 0$. We also compare the hex-instability with Eckhaus instability in $(\tilde{\kappa}, \alpha)$ -plane. Recall that the stripes are zigzag unstable (stable) for $\tilde{\kappa} < 0$ ($\tilde{\kappa} > 0$).

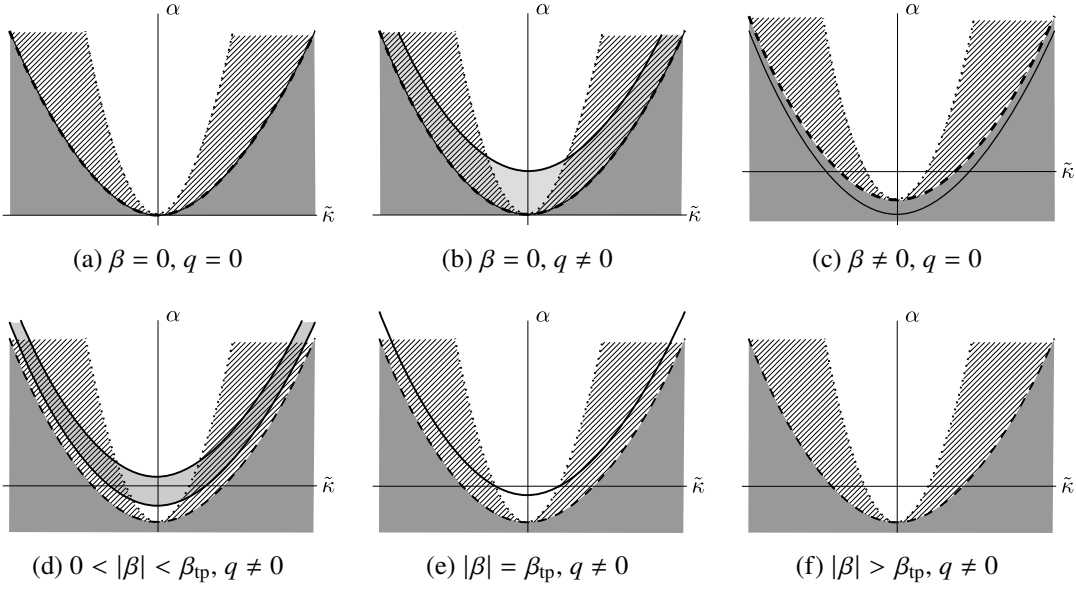


Figure 3.8: Sketches of the stability regions in the $(\tilde{\kappa}, \alpha)$ -plane. Stripes exist in the complement of the dark grey regions; light grey: hex-unstable; hatched regions: Eckhaus-unstable; white: hex-stable. Bifurcation $\alpha = \mathcal{B}(\tilde{\kappa}, \beta)$ (dashed); Eckhaus boundary $\alpha = \mathcal{E}(\tilde{\kappa}, \beta)$ (dotted); hex-stability boundaries (solid) in (a) $\alpha = \mathcal{H}_{\pm}(\tilde{\kappa}, 0, 0) = \mathcal{B}(\tilde{\kappa}, 0)$, cf. (3.44) (b) $\alpha = \mathcal{H}_+(\tilde{\kappa}, 0, q) > \mathcal{B}(\tilde{\kappa}, 0)$ and $\alpha = \mathcal{H}_-(\tilde{\kappa}, 0, q) = \mathcal{B}(\tilde{\kappa}, 0)$, cf. (3.45) (c) $\alpha = \mathcal{H}_{\pm}(\tilde{\kappa}, \beta, 0) < \mathcal{B}(\tilde{\kappa}, \beta)$, cf. (3.46) (d) $\alpha = \mathcal{H}_{\pm}(\tilde{\kappa}, \beta, q) > \mathcal{B}(\tilde{\kappa}, \beta)$, cf. (3.39) (e) $\alpha = \mathcal{H}_{\pm}(\tilde{\kappa}, \beta_{tp}, q)$, (f) do not exist.

In the (q, α) -plane, for any fixed β , the stability boundaries are shifted upwards compared with $\tilde{\kappa} = 0$, cf. Fig. 3.7c & 3.7d.

In the $(\tilde{\kappa}, \alpha)$ -plane the situation is more involved and can be compared with the Eckhaus instability. In Fig. 3.8 we plot all cases in terms of β and q , and derive these next.

Case $\beta = 0, q = 0$ (Fig. 3.8a) The hex-stability boundary is given by

$$\alpha = \mathcal{H}_{\pm}(\tilde{\kappa}, 0, 0) = -\rho_{\tilde{\kappa}}\tilde{\kappa}^2, \quad (3.44)$$

which coincides with the bifurcation curve since $\mathcal{H}_{\pm}(\tilde{\kappa}, 0, 0) = \mathcal{B}(\tilde{\kappa}, 0)$. Hence the stripes are hex-stable, and the dominant instability mechanism is the Eckhaus boundary.

Case $\beta = 0, q \neq 0$ (Fig. 3.8b) The hex-stability boundaries are given by

$$\begin{aligned} \alpha &= \mathcal{H}_+(\tilde{\kappa}, 0, q) = -\frac{4}{3k_0}q^2 - \rho_{\tilde{\kappa}}\tilde{\kappa}^2, \\ \alpha &= \mathcal{H}_-(\tilde{\kappa}, 0, q) = -\rho_{\tilde{\kappa}}\tilde{\kappa}^2, \end{aligned} \quad (3.45)$$

where $\mathcal{H}_-(\tilde{\kappa}, 0, q) = \mathcal{B}(\tilde{\kappa}, 0)$. Hence the stripes are hex-unstable near the bifurcation, which is thus the dominant mechanism near onset. In addition, the curvature of each of the hex-stability boundaries is smaller than that of Eckhaus boundary since $\partial_{\tilde{\kappa}}^2 \mathcal{H}_{\pm} < \partial_{\tilde{\kappa}}^2 \mathcal{E}$.

Case $\beta \neq 0, q = 0$ (Fig. 3.8c) The hex-stability boundary is given by

$$\alpha = \mathcal{H}_{\pm}(\tilde{\kappa}, \beta, 0) = -\frac{7}{4}\rho_{\beta}\beta^2 - \rho_{\tilde{\kappa}}\tilde{\kappa}^2. \quad (3.46)$$

Since $\mathcal{H}_{\pm}(\tilde{\kappa}, \beta, 0) < \mathcal{B}(\tilde{\kappa}, \beta)$, the bifurcating stripes are always hex-stable, and the Eckhaus instability is dominant, again in accordance with Remark 3.5.6.

Case $\beta \neq 0, q \neq 0$ (bottom row of Fig. 3.8) The hex-stability boundaries are given by (3.39), and roots of the discriminant $\delta_{\mathcal{H}} = 0$ from (3.40), lie at

$$\beta = \beta_{\text{tp}} := \frac{2|q|}{3\sqrt{-k_0\rho_{\beta}}}. \quad (3.47)$$

We summarise the stability results in terms of β for fixed $q \neq 0$ as follows.

- (1) $|\beta| < \beta_{\text{tp}}$ (Fig. 3.8d): hex-stability boundaries satisfy $\mathcal{H}_{\pm}(\tilde{\kappa}, \beta, q) > \mathcal{B}(\tilde{\kappa}, \beta)$ so that stripes are hex-stable near onset, but there is a hex-unstable ‘band’ which intersects the α -axis on the interval $[\mathcal{H}_-(0, \beta, q), \mathcal{H}_+(0, \beta, q)]$.
- (2) $|\beta| = \beta_{\text{tp}}$ (Fig. 3.8e): The hex-stability boundaries collapse along

$$\alpha = \mathcal{H}_{\pm}(\tilde{\kappa}, \beta_{\text{tp}}, q) = \frac{q^2}{9k_0} - \rho_{\tilde{\kappa}}\tilde{\kappa}^2,$$

which intersects α -axis at $\alpha_{\text{tp}} = -\rho_{\beta}\beta_{\text{tp}}^2/4 = q^2/(9k_0)$, cf. (3.43). Notably, this degenerate case does not occur for quasi-hexagonal lattices discussed below.

- (3) $|\beta| > \beta_{\text{tp}}$ (Fig. 3.8f): \mathcal{H}_{\pm} are complex, so there is no hex-stability boundary in the real parameter space and the stripes are hex-stable.

In addition, we recall the threshold q_{tp} , cf. (3.43), and highlight the relation $\text{sgn}(|\beta| - \beta_{\text{tp}}) = -\text{sgn}(|q| - q_{\text{tp}})$. Therefore, by increasing $|q|$ for fixed $\beta \neq 0$ the hexagonal boundaries change as from Fig. 3.8f to 3.8d.

Remark 3.5.14. Recall that the zigzag stability boundary is $\tilde{\kappa} = 0$, which we suppressed to ease the exposition. Hence, compared to the hex-stability, for $\beta = q = 0$ the large wavelength instabilities are dominant near onset, whereas for $\beta \neq 0$ the large wavelength instabilities are always dominant sufficiently close to onset as predicted in Remark 3.5.6, cf. bottom row of Fig. 3.8. We thus infer stabilisation by the advection and destabilisation by the quadratic term with respect to hexagonal modes.

We consider the width of the unstable band for fixed q in Fig. 3.8d by setting $\tilde{\alpha} := \alpha + \rho_{\beta}\beta^2 + \rho_{\tilde{\kappa}}\tilde{\kappa}^2$ so that stripe bifurcations occur at $\tilde{\alpha} = 0$. Then the hex-stability boundaries in the $(\beta, \tilde{\alpha})$ -plane are

$$\tilde{\alpha} = \tilde{\mathcal{H}}_{\pm}(\beta) := -\frac{3}{4}\rho_{\beta}\beta^2 - \frac{1}{3k_0} \left(2q^2 \pm \sqrt{4q^4 + 9k_0q^2\rho_{\beta}\beta^2} \right), \quad (3.48)$$

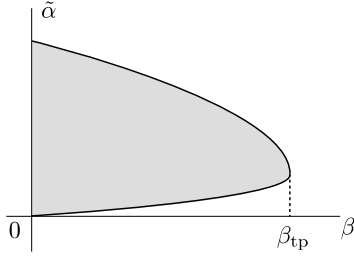


Figure 3.9: Sketch of the hex-unstable region in the $(\beta, \tilde{\alpha})$ -plane for fixed $q \neq 0$. Solid curve: hex-boundary $\tilde{\alpha} = \tilde{\mathcal{H}}_\pm(\beta)$, cf. (3.48); grey: hex-unstable; white: hex-stable.

see Fig. 3.9. In particular, $\tilde{\mathcal{H}}_-(0) = 0$, $\tilde{\mathcal{H}}_+(0) = -4q^2/(3k_0)$ and $\tilde{\mathcal{H}}_\pm(\beta_{tp}) = -q^2/(3k_0)$ so the width of hex-unstable band is smaller for larger $|\beta|$, showing the stabilisation of the advection. Note that the width of the unstable band is independent of $\tilde{\kappa}$, which will be different for the quasi-hexagonal lattice modes considered next.

3.5.5 Stability against quasi-hexagonal perturbations

We consider the stability of stripes against *quasi-hexagonal perturbation*, which are nearly hexagonal perturbations that still possess triads $\mathbf{k}_1 + \mathbf{k}_2 + \mathbf{k}_3 = 0$.

We consider (1.9) with periodic boundary conditions on the rectangular domain

$$\Omega_{qh} := [0, 4\pi/\kappa] \times [0, 4\pi/(\sqrt{3}\ell)], \quad \kappa := \mathbf{k}_c + \tilde{\kappa}, \quad \ell := \mathbf{k}_c + \tilde{\ell}, \quad \tilde{\ell} \neq \tilde{\kappa},$$

with the scaling $\tilde{\ell} = \varepsilon \tilde{\ell}'$ so that $\tilde{\ell} = O(\varepsilon)$ analogous to $\tilde{\kappa}$. Rescaling the spatial variables with $\tilde{x} = x/\kappa$ and $\tilde{y} = y/\ell$, the rectangular domain becomes $\Omega_3 = [0, 4\pi] \times [0, 4\pi/\sqrt{3}]$ with dual lattice wavevectors $\mathbf{k}_j = (k_j, \ell_j) \in \mathbb{R}^2$, and the perturbation on the six dimensional kernel is given by $U_{\text{hex}}(x)$, cf. §3.5.4. Analogous to Theorem 3.5.10, we have the following.

Theorem 3.5.15. *Consider (1.9) with periodic boundary conditions on rectangular domain Ω_{qh} . Assume the conditions and notations of Theorem 3.5.1 for the domain Ω_3 with periodic boundary conditions and the parameter scaling (3.13) for μ . Let the velocity parameter $c = c(\mu)$ be as in (3.9). The subspace $\{u_j = 0, j = \pm 2, \pm 3\}$ is invariant for the reduced ODE and contains the stripes as equilibria. The linearisation in stripes in the index ordering $(1, -1, 2, -3, 3, -2)$ has a block diagonal matrix of the form $L_{qh} = \text{diag}(L_1, L_2^{qh}, L_2^{qh}) + O(\varepsilon^3)$ with 2×2 -subblocks*

$$L_1 = A^2 \begin{pmatrix} \rho_{nl} & \rho_{nl} \\ \rho_{nl} & \rho_{nl} \end{pmatrix}, \quad L_2^{qh} = \varepsilon^2 \begin{pmatrix} \lambda'_{\mu, \tilde{\ell}} + A'^2 \eta & 2A' \frac{q}{\varepsilon} + A' p(\mu_1, \tilde{\ell}') \\ 2A' \frac{q}{\varepsilon} + A' p(\mu_1, \tilde{\ell}') & \lambda'_{\mu, \tilde{\ell}} + A'^2 \eta \end{pmatrix}$$

where η is as in Theorem 3.5.10 and

$$\begin{aligned} \lambda'_{\mu, \tilde{\ell}} &:= \alpha' + \frac{1}{4} \rho_{\beta} \beta'^2 + \frac{\rho_{\tilde{\kappa}}}{16} (\tilde{\kappa}' + 3\tilde{\ell}')^2 + O(\varepsilon), \\ p(\mu_1, \tilde{\ell}') &:= \langle Q[i\beta' w_{A\beta} + (\frac{5}{2}\tilde{\kappa}' + \frac{3}{2}\tilde{\ell}') w_{A\tilde{\kappa}}, E_0] - (i\beta' \mathbf{k}_c B + (\tilde{\kappa}' + 3\tilde{\ell}') \mathbf{k}_c D) Q_1, E_0^* \rangle. \end{aligned}$$

Proof. The rescaled linear operator of (1.9) is given by

$$\mathcal{L}_\mu^{\text{qh}} := \kappa^2 D \partial_x^2 + \ell^2 D \partial_y^2 + L + \check{\alpha} M + \beta \kappa B \partial_x.$$

Analogous to the proof of Theorem 3.5.10, the linearisation in stripes gives the same matrix L_1 since the rescaling in y -direction does not influence the one-dimensional stability. The matrix L_2^{qh} , however, is different from L_2^{hex} . The eigenvalue $\lambda'_{\mu, \tilde{\ell}}$ is that of the linearisation in the trivial equilibrium whose expansion can be determined analogous to Lemma 3.2.2. The term $p(\mu_1)$ is replaced by $p(\mu_1, \tilde{\ell}')$ by straightforward calculation, which is analogous to the proof in Appendix E.4. \square

Concerning the subblock L_2^{qh} , we first note the general form of eigenvalues.

Lemma 3.5.16. *Under the assumptions of Theorem 3.5.15, the eigenvalues of the matrix L_2^{qh} are*

$$\lambda_\pm = \varepsilon^2 \left(A'^2 (3k_0 - q_2 + 8q_1) - \frac{3}{4} \rho_\beta \beta'^2 + \omega' \pm A' \left| \frac{2q}{\varepsilon} + A' p(\mu_1, \tilde{\ell}') \right| \right) + O(\varepsilon^3),$$

where $A' = \sqrt{-(\alpha' + \rho_\beta \beta'^2 + \rho_{\tilde{\kappa}} \tilde{\kappa}'^2)/\rho_{\text{nl}}} + O(\varepsilon)$ and $\omega' := (9\tilde{\ell}' + 15\tilde{\kappa}')(\tilde{\ell}' - \tilde{\kappa}')\rho_{\tilde{\kappa}}/16$. The most unstable quasi-hexagonal perturbation with respect to $\tilde{\ell}$ occurs at $\tilde{\ell} = -\tilde{\kappa}/3$ for which $\omega = -\rho_{\tilde{\kappa}} \tilde{\kappa}^2 \geq 0$, and $\tilde{\ell} = 0$ gives $\omega = 0$ and $\lambda_\pm = \lambda_{\text{hex}}^\pm$.

Proof. The eigenvalues are derived as in Lemma 3.5.11. As a function of $\tilde{\ell}$, the parabola $\omega = \omega(\tilde{\ell})$ has positive maximum $\max_{\tilde{\ell} \in \mathbb{R}} \omega = -\rho_{\tilde{\kappa}} \tilde{\kappa}^2$ at $\tilde{\ell} = -\tilde{\kappa}/3$. \square

Remark 3.5.17. *We note a relation of the most unstable quasi-hexagonal modes at $\tilde{\ell} = -\tilde{\kappa}/3$ to the critical circle of spectrum $S_{\mathbf{k}_c}$ at the onset of the Turing instability. Indeed, it follows from $(\frac{1}{2}(\mathbf{k}_c + \tilde{\kappa}))^2 + (\frac{\sqrt{3}}{2}(\mathbf{k}_c + \tilde{\ell}))^2 = \mathbf{k}_c^2$ that $\tilde{\ell} = -\frac{1}{3}\tilde{\kappa} - \frac{2}{9\mathbf{k}_c}\tilde{\kappa}^2 + O(\tilde{\kappa}^3)$. Therefore, the locations of the most unstable oblique wavevectors are to leading order on the critical circle $S_{\mathbf{k}_c}$.*

In the remainder of this section, we focus on the quasi-hexagonal perturbation that are more unstable than the hexagonal ones, i.e. in case $\omega > 0$, and parametrise $\omega \in (0, -\rho_{\tilde{\kappa}} \tilde{\kappa}^2]$ by $\theta \in (0, 1]$ via

$$\omega = -\theta \rho_{\tilde{\kappa}} \tilde{\kappa}^2,$$

so $\theta = 1$ is the most unstable quasi-hexagonal perturbation and the limit $\theta = 0$ yields the hexagonal one. The previous lemma shows that as for hexagonal perturbations, a smallness assumption on q is required, and as in Theorem 3.5.12 this changes A' in Lemma 3.5.16 to where $\tilde{A}' := \sqrt{-(\alpha' + \rho_\beta \beta'^2 + \rho_{\tilde{\kappa}} \tilde{\kappa}'^2)/(3k_0)}$. However, unlike the hexagonal stability, for $Q = o(\varepsilon)$ the stripes are not necessarily stable against quasi-hexagonal perturbations. The previous lemma then directly gives

Theorem 3.5.18. *Under the assumptions of Theorem 3.5.15 and $\theta \in (0, 1]$ the quasi-hexagonal stability boundary, i.e., zero real part of the eigenvalues of the matrix L_2^{qh} is to leading order given as follows.*

If $Q = g(\varepsilon)Q'$, $g(\varepsilon) = o(\varepsilon)$ this stability boundary reads

$$\alpha = \mathcal{M}_{\text{qh}}(\tilde{\kappa}, \beta; \theta) := -\frac{7}{4}\rho_\beta\beta^2 - (\theta + 1)\rho_{\tilde{\kappa}}\tilde{\kappa}^2. \quad (3.49)$$

Under Hypothesis 3.1.1 this stability boundary is given by the two curves

$$\{\alpha = \mathcal{M}_{\text{qh}}^\pm(\tilde{\kappa}, \beta, q; \theta) : \alpha \geq \mathcal{M}_{\text{qh}}(\tilde{\kappa}, \beta; \theta), \delta_M \geq 0\}, \quad (3.50)$$

$$\{\alpha = \mathcal{M}_{\text{qh}}^\pm(\tilde{\kappa}, \beta, q; \theta) : \alpha \leq \mathcal{M}_{\text{qh}}(\tilde{\kappa}, \beta; \theta), \delta_M \geq 0\}, \quad (3.51)$$

corresponding to the two eigenvalues λ_σ with possibly different $\sigma = \pm$, where

$$\begin{aligned} \mathcal{M}_{\text{qh}}^\pm(\tilde{\kappa}, \beta, q; \theta) &:= -\frac{7}{4}\rho_\beta\beta^2 - (\theta + 1)\rho_{\tilde{\kappa}}\tilde{\kappa}^2 - \frac{1}{3k_0}(2q^2 \pm \sqrt{\delta_M}), \\ \delta_M &:= 4q^4 + 9k_0\rho_\beta\beta^2q^2 + 12k_0\theta\rho_{\tilde{\kappa}}\tilde{\kappa}^2q^2. \end{aligned} \quad (3.52)$$

Isotropic case $\beta = 0$

For $Q = O(\varepsilon)$, the quasi-hex-stability boundary is given to leading order by the following two parts, see Fig. 3.2a.

$$\alpha = \mathcal{M}_{\text{qh}}^+(\tilde{\kappa}, 0, q; \theta) = -(\theta + 1)\rho_{\tilde{\kappa}}\tilde{\kappa}^2 - \frac{2}{3k_0}\left(q^2 + \sqrt{q^4 + 3k_0\theta\rho_{\tilde{\kappa}}\tilde{\kappa}^2q^2}\right), \quad (3.53)$$

$$\alpha = \mathcal{M}_{\text{qh}}^-(\tilde{\kappa}, 0, q; \theta) = -(\theta + 1)\rho_{\tilde{\kappa}}\tilde{\kappa}^2 - \frac{2}{3k_0}\left(q^2 - \sqrt{q^4 + 3k_0\theta\rho_{\tilde{\kappa}}\tilde{\kappa}^2q^2}\right). \quad (3.54)$$

In the (q, α) -plane, the boundary $\alpha = \mathcal{M}_{\text{qh}}^+(\tilde{\kappa}, 0, q; \theta)$ intersects the α -axis at $\mathcal{M}_{\text{qh}}^+(\tilde{\kappa}, 0, 0; \theta)$, where $\mathcal{M}_{\text{qh}}^+(\tilde{\kappa}, 0, 0; \theta) = -(\theta + 1)\rho_{\tilde{\kappa}}\tilde{\kappa}^2$. Since $\theta > 0$, we have $\mathcal{M}_{\text{qh}}^+(\tilde{\kappa}, 0, q; \theta) > \mathcal{B}(\tilde{\kappa}, 0)$. Thus the stripes are quasi-hex-unstable near onset. Note that for $Q = o(\varepsilon)$, the stability boundary (3.49) is independent of q .

In the $(\tilde{\kappa}, \alpha)$ -plane, the following cases for the quasi-hex-stability boundary occur.

Case $\beta = 0, q = 0$ (Fig. 3.10a) The quasi-hex-stability boundaries are independent of q . Hence for both $Q = O(\varepsilon)$ and $Q = o(\varepsilon)$, the quasi-hex-stability boundaries read

$$\alpha = \mathcal{M}_{\text{qh}}^\pm(\tilde{\kappa}, 0, 0; \theta) = -(\theta + 1)\rho_{\tilde{\kappa}}\tilde{\kappa}^2 = \mathcal{M}_{\text{qh}}(\tilde{\kappa}, 0; \theta). \quad (3.55)$$

Note that since $\theta \in (0, 1]$, we have $\mathcal{B}(\tilde{\kappa}, 0) \leq \mathcal{M}_{\text{qh}}^\pm(\tilde{\kappa}, 0, 0; \theta) = \mathcal{M}_{\text{qh}}(\tilde{\kappa}, 0; \theta) \leq \mathcal{E}(\tilde{\kappa}, 0)$.

Case $\beta = 0, q \neq 0$ (Fig. 3.10b) For $Q = O(\varepsilon)$, the quasi-hex-stability boundary is on the one hand given by (3.50) as (3.53) at $\beta = 0$, which intersects the vertical axis at $\mathcal{M}_{\text{qh}}^+(0, 0, q; \theta) = -4q^2/(3k_0)$. The ordinate of intersections of Eckhaus boundary and quasi-hex-stability boundary is given by $\alpha_{\text{sec}} := -\frac{8q^2}{k_0(2-\theta)^2} = O(\varepsilon^2)$. Hence, the quasi-hexagonal instability is the dominant instability mechanism near onset. On the other hand, (3.51) gives as (3.54) at $\beta = 0$ a quasi-hex-stability boundary which passes through the origin with curvature larger than that of Eckhaus boundary.

For $Q = o(\varepsilon)$, the quasi-hex-stability boundary is given by $\alpha = \mathcal{M}_{\text{qh}}(\tilde{\kappa}, 0; \theta)$, and we have the relation $\mathcal{M}_{\text{qh}}^-(\tilde{\kappa}, 0, q; \theta) \leq \mathcal{M}_{\text{qh}}(\tilde{\kappa}, 0; \theta) < \mathcal{M}_{\text{qh}}^+(\tilde{\kappa}, 0, q; \theta)$.

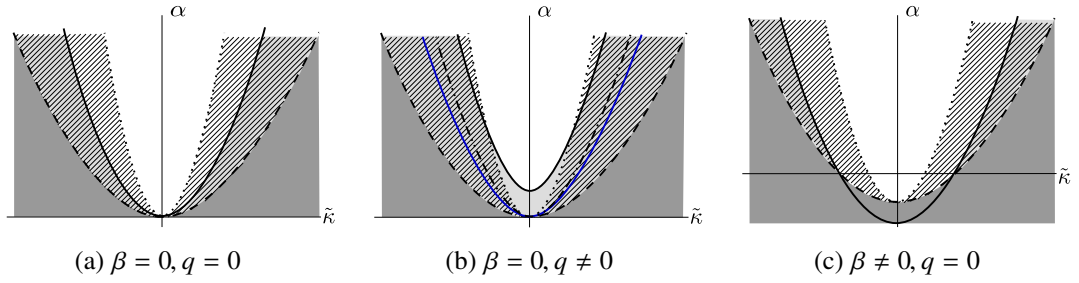


Figure 3.10: Sketches of the stability regions in the $(\tilde{\kappa}, \alpha)$ -plane for $\theta \in (0, 1]$. Stripes exist in the complements of the dark grey regions. Light grey: quasi-hex-unstable; hatched region: Eckhaus-unstable; white: stable; dashed curve: bifurcation curve $\alpha = \mathcal{B}(\tilde{\kappa}, 0)$; dotted curve: Eckhaus boundary $\alpha = \mathcal{E}(\tilde{\kappa}, 0)$. (a) Quasi-hex-boundary (3.55) (black solid). (b) Quasi-hex-boundary for $Q = O(\varepsilon)$ (3.53) (black solid), (3.54) (blue solid) and for $Q = o(\varepsilon)$ (3.49) (dotted dashed). (c) Quasi-hex-boundary (3.58) (black solid).

Anisotropic case $\beta \neq 0$

We first consider the quasi-hex-stability in the (q, α) -plane. Since $Q = o(\varepsilon)$ the quasi-hex-stability boundary is independent of q we omit this case.

For $Q = O(\varepsilon)$, roots of $\delta_M = 0$ from (3.52) occur as a function of q precisely when $9\rho_\beta\beta^2 + 12\theta\rho_{\tilde{\kappa}}\tilde{\kappa}^2 \leq 0$ so that the threshold in terms of β lies at

$$\beta = \beta_{ep} := 2|\tilde{\kappa}| \sqrt{-\theta\rho_{\tilde{\kappa}}/(3\rho_\beta)}. \quad (3.56)$$

Notably, $\beta_{ep} = 0$ for the hexagonal modes, i.e., $\theta = 0$, which is consistent with Fig. 3.7.

We summarise the quasi-hex-stability boundaries in the (q, α) -plane as follows.

- (1) $|\beta| < \beta_{ep}$ (Fig. 3.2a): $\alpha = M_{qH}^+(\tilde{\kappa}, \beta, q; \theta)$ has minimum at $q = 0$ where $M_{qH}^+(\tilde{\kappa}, \beta, 0; \theta) > \mathcal{B}(\tilde{\kappa}, \beta)$. Thus the stripes are unstable near the bifurcation.
- (2) $|\beta| = \beta_{ep}$ (Fig. 3.2b): $\alpha = M_{qH}^+(\tilde{\kappa}, \beta_{ep}, q; \theta)$ is a parabola in q which touches the bifurcation line at $q = 0$ since $M_{qH}^+(\tilde{\kappa}, \beta_{ep}, 0; \theta) = \mathcal{B}(\tilde{\kappa}, \beta_{ep})$.
- (3) $|\beta| > \beta_{ep}$ (Fig. 3.2c): $\alpha = M_{qH}^\pm(\tilde{\kappa}, \beta, q; \theta)$ ‘opened up’: the stripes are unstable for $\alpha \in (M_{qH}^-, M_{qH}^+)$ and stable elsewhere; in particular the stripes are stable near onset and there are two turning points given by $(\pm q_{tp, \theta}, \alpha_{tp, \theta})$ where

$$q_{tp, \theta} := \frac{1}{2} \sqrt{-12k_0\theta\rho_{\tilde{\kappa}}\tilde{\kappa}^2 - 9k_0\rho_\beta\beta^2}, \quad \alpha_{tp, \theta} := -\frac{1}{4}\rho_\beta\beta^2 + (\theta - 1)\rho_{\tilde{\kappa}}\tilde{\kappa}^2. \quad (3.57)$$

In particular, the stripes are stable for $|q| < q_{tp, \theta}$ and all α , cf. Fig. 3.2d. Such stable window ‘opens’ later for larger $|\tilde{\kappa}|$ and ‘opens’ larger for larger $|\beta|$.

Next, we discuss the quasi-hex-stability boundary in the $(\tilde{\kappa}, \alpha)$ -plane.

Case $\beta \neq 0, q = 0$ (Fig. 3.10c) The quasi-hex-stability boundary is independent of q . Hence for both $Q = O(\varepsilon)$ and $Q = o(\varepsilon)$, the quasi-hex-stability boundary is given by

$$\alpha = \mathcal{M}_{\text{qh}}^\pm(\tilde{\kappa}, \beta, 0; \theta) = -\frac{7}{4}\rho_\beta\beta^2 - (\theta + 1)\rho_{\tilde{\kappa}}\tilde{\kappa}^2 = \mathcal{M}_{\text{qh}}(\tilde{\kappa}, \beta; \theta), \quad (3.58)$$

which is a parabola in $\tilde{\kappa}$ and is shifted downwards by increasing $|\beta|$. Its curvature is smaller than that of Eckhaus boundary since $\partial_{\tilde{\kappa}}^2 \mathcal{M}_{\text{qh}}^\pm < \partial_{\tilde{\kappa}}^2 \mathcal{E}$, and thus the Eckhaus instability is dominant.

Case $\beta \neq 0, q \neq 0$ (Fig. 3.11) For $Q = o(\varepsilon)$, the quasi-hex-stability boundary is given by $\alpha = \mathcal{M}_{\text{qh}}(\tilde{\kappa}, \beta; \theta)$, cf. (3.49), which is a parabola in $\tilde{\kappa}$.

For $Q = O(\varepsilon)$, we recall that the quasi-hex-stability boundaries are given by (3.50) and (3.51), respectively. The boundaries (3.50) have been shown in Fig. 3.3b–3.3e. For the completeness of the stability diagrams, however, we replot them in Fig. 3.11. Solving $\mathcal{E}(\tilde{\kappa}, \beta) = \mathcal{M}_{\text{qh}}^\pm(\tilde{\kappa}, \beta, q; \theta)$ we find the critical value β_{ex} such that \mathcal{E} and $\mathcal{M}_{\text{qh}}^\pm$ have only two intersection points for $\beta = \beta_{\text{ex}}$, where

$$\beta_{\text{ex}} = \frac{2}{3}|q|\sqrt{\frac{2}{k_0(\theta - 2)\rho_\beta}} \quad (3.59)$$

and $\beta_{\text{ex}} > \beta_{\text{tp}}$ where β_{tp} is given by (3.47). This gives the following subcases:

- (1) $|\beta| < \beta_{\text{tp}}$ (Fig. 3.11a): The quasi-hex-stability boundary is given by (3.50) and composed of two curves. The lower curve touches the bifurcation curve at the endpoints $(\pm\tilde{\kappa}_{\text{ep}}, \alpha_{\text{ep}})$ where

$$\tilde{\kappa}_{\text{ep}} = |\beta|\sqrt{-\frac{3\rho_\beta}{4\theta\rho_{\tilde{\kappa}}}} > 0, \quad \alpha_{\text{ep}} := \left(\frac{3}{4\theta} - 1\right)\rho_\beta\beta^2.$$

In particular, the stripes are quasi-hex-stable near onset for $|\tilde{\kappa}| < \tilde{\kappa}_{\text{ep}}$ only, and these endpoints diverge $\theta \rightarrow 0$, thus limiting to the hexagonal case, cf. Fig. 3.8d. In addition, the stability boundaries intersect the vertical axis at $\mathcal{M}_{\text{qh}}^\pm(0, \beta, q; \theta) = \mathcal{H}_\pm(0, \beta, q)$. Moreover, the ordinate of intersections of quasi-hex-stability and Eckhaus boundary is given by

$$\begin{aligned} \alpha_{\text{sec}, \beta}^\pm &= -\frac{1}{4k_0(2-\theta)^2} \left(16q^2 + k_0\rho_\beta\beta^2(4\theta^2 - 25\theta + 34) \right. \\ &\quad \left. \pm 4\sqrt{16q^4 + 18k_0(2-\theta)q^2\rho_\beta\beta^2} \right) = O(\varepsilon^2). \end{aligned}$$

Compared to the isotropic case (cf. Fig. 3.10b), non-zero β creates a stable region near the bifurcation and moves the upper boundary downwards, thus the advection stabilises the stripes.

- (2) $|\beta| = \beta_{\text{tp}}$ (Fig. 3.11b): The quasi-hex-stability boundaries intersect with the vertical axis at a single point $\mathcal{M}_{\text{qh}}^\pm(0, \beta_{\text{tp}}, q; \theta) = \mathcal{H}_\pm(0, \beta_{\text{tp}}, q) = -\frac{1}{4}\rho_\beta\beta_{\text{tp}}^2 = q^2/(9k_0)$.

- (3) $\beta_{\text{tp}} < |\beta| < \beta_{\text{ex}}$ (Fig. 3.11c): The quasi-hex-stability boundary ‘opened up’ and consists of two curves whose turning points are given by $(\pm\tilde{\kappa}_{\text{mp}}, \alpha_{\text{mp}})$, where

$$\tilde{\kappa}_{\text{mp}} := \sqrt{-\frac{3\rho_\beta\beta^2}{4\theta\rho_{\tilde{\kappa}}} - \frac{q^2}{3k_0\theta\rho_{\tilde{\kappa}}}} > 0, \quad \alpha_{\text{mp}} := \frac{4q^2(1-\theta) + 3k_0(3-4\theta)\rho_\beta\beta^2}{12k_0\theta}. \quad (3.60)$$

The stripes are quasi-hex-stable for $|\tilde{\kappa}| < \tilde{\kappa}_{\text{mp}}$ and all α , cf. Fig. 3.3f. Such stable window ‘opens’ later for larger $|q|$ and ‘opens’ larger for larger $|\beta|$. The turning points diverge as $\theta \rightarrow 0$ and so do the endpoints $(\pm\tilde{\kappa}_{\text{ep}}, \alpha_{\text{ep}})$, thus limiting to the hexagonal case, cf. Fig. 3.8f. In contrast to the hexagonal case, here we have two regions where the stripes are quasi-hex-unstable but Eckhaus stable.

- (4) $|\beta| \geq \beta_{\text{ex}}$ (Fig. 3.11d): The quasi-hex-stability boundaries touch the Eckhaus boundary for $|\beta| = \beta_{\text{ex}}$ and lie inside the Eckhaus unstable region.

Notably, in each case the Eckhaus instability is dominant near the bifurcation as predicted in Remark 3.5.6. We recall the threshold q_{tp} , cf. (3.43) and have $\text{sgn}(|\beta| - \beta_{\text{tp}}) = -\text{sgn}(|q| - q_{\text{tp}})$, also $\text{sgn}(|\beta| - \beta_{\text{ex}}) = -\text{sgn}(|q| - q_{\text{ex}})$, where

$$q_{\text{ex}} := \frac{3}{2}|\beta|\sqrt{k_0(2-\theta)\rho_\beta/2},$$

and $q_{\text{ex}} < q_{\text{tp}}$. Therefore, by increasing $|q|$ for fixed $\beta \neq 0$ the quasi-hex-stability boundaries change as from Fig. 3.11d to 3.11a.

3.6 Examples

3.6.1 Exact example: zigzag-unstable stripes

For illustration of the expansions we consider the concrete system

$$\begin{aligned} u_t &= \Delta u + 3u - v + \check{\alpha}u + 4\check{\alpha}v + \beta u_x + \epsilon u^2 + \frac{1}{4}\epsilon v^2 - uv^2 \\ v_t &= \frac{7}{2}\Delta v + 14u - \frac{7}{2}v - \frac{1}{5}\check{\alpha}u + \check{\alpha}v + \epsilon u^2 + \frac{1}{4}\epsilon v^2 + uv^2 \end{aligned} \quad (3.61)$$

where $U := (u, v)^T$, $D = \text{diag}(1, 7/2)$,

$$L = \begin{pmatrix} 3 & -1 \\ 14 & -\frac{7}{2} \end{pmatrix}, \quad M = \begin{pmatrix} 1 & 4 \\ -\frac{1}{5} & 1 \end{pmatrix}, \quad Q[U, U] = \epsilon \begin{pmatrix} u^2 + \frac{1}{4}v^2 \\ u^2 + \frac{1}{4}v^2 \end{pmatrix}, \quad K[U, U, U] = \begin{pmatrix} -uv^2 \\ uv^2 \end{pmatrix}.$$

The generic form of Q is given by $Q[U_1, U_2] = (Q_{||}[U_1, U_2], Q_{|||[U_1, U_2])^T}$ with

$$Q_{||}[U_1, U_2] = Q_{|||[U_1, U_2] = \epsilon U_1^T \begin{pmatrix} 1 & 0 \\ 0 & \frac{1}{4} \end{pmatrix} U_2,$$

where $U_j := (u_j, v_j)^T$, $j = 1, 2, 3$.

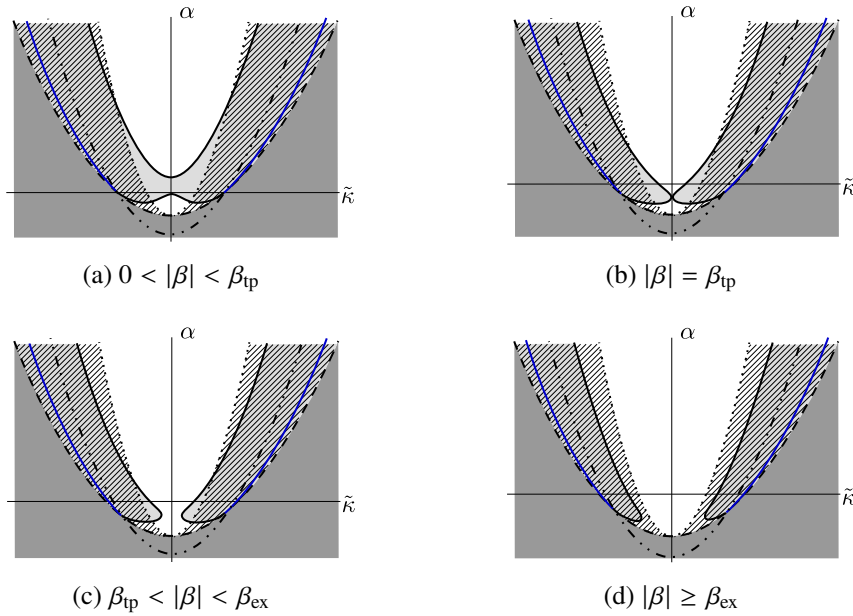


Figure 3.11: Sketches of the stability boundaries and Eckhaus boundary \mathcal{E} for $\beta \neq 0$, $q \neq 0$ and $\theta \in (0, 1]$. Stripes exist in the complement of the dark grey regions; light grey: quasi-hex-unstable; hatched region: Eckhaus-unstable; white: stable. Dashed curve: bifurcation curve $\alpha = \mathcal{B}(\tilde{\kappa}, \beta)$; dotted curve: $\alpha = \mathcal{E}(\tilde{\kappa}, \beta)$; quasi-hex-boundary for $Q = O(\varepsilon)$ (3.50) (black solid), (3.51) (blue solid), quasi-hex-boundary for $Q = o(\varepsilon)$ (3.49) (dashed-dotted). Zigzag instability occurs for $\tilde{\kappa} < 0$.

In this system, the Turing conditions are fulfilled and the critical wavevectors $(k, \ell) \in S_{\mathbf{k}_c}$ with $\mathbf{k}_c = 1$. We have

$$\hat{\mathcal{L}}_0 := -\mathbf{k}_c^2 D + L = \begin{pmatrix} 2 & -1 \\ 14 & -7 \end{pmatrix}.$$

From Remark 3.2.5 the rescaled kernel eigenvector of $\hat{\mathcal{L}}_0$ and its adjoint kernel eigenvector are given by

$$E_0 = -\frac{1}{\sqrt{5}}(1, 2)^T, \quad E_0^* = \frac{1}{\sqrt{5}}(-7, 1)^T.$$

We examine the coefficients in (3.7), (3.11) and (3.26) so that they are non-zero. The bifurcation curves, zigzag and Eckhaus boundaries are given by, cf. Fig. 3.13,

$$\text{bifurcation curve: } \alpha = -0.112\beta^2 + 2.8\tilde{\kappa}^2, \quad (3.62)$$

$$\text{Eckhaus boundary: } \alpha = -0.112\beta^2 + 8.4\tilde{\kappa}^2, \quad (3.63)$$

$$\text{zigzag boundary: } \alpha = -0.046\beta^2 - 3.118\tilde{\kappa}, \quad (3.64)$$

where $\alpha = 12.24\check{\alpha}$. The striped solutions exist for $\alpha > -0.112\beta^2 + 2.8\tilde{\kappa}^2$. We remark that the scaling (3.13) gives the zigzag boundary $\tilde{\kappa} = 0$ to leading order. In Fig. 3.12 we choose $\epsilon = 0.5$

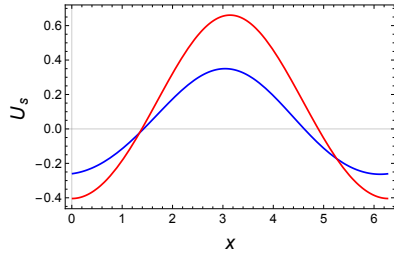


Figure 3.12: The leading order of the rescaled striped solution U_s (u -component blue, v -component red) in $x \in [0, 2\pi]$ to the system (1.9) for $\alpha = 0.2$, $\beta = 0.7$, $\tilde{\kappa} = 0.1$ and $\epsilon = 0.5$.

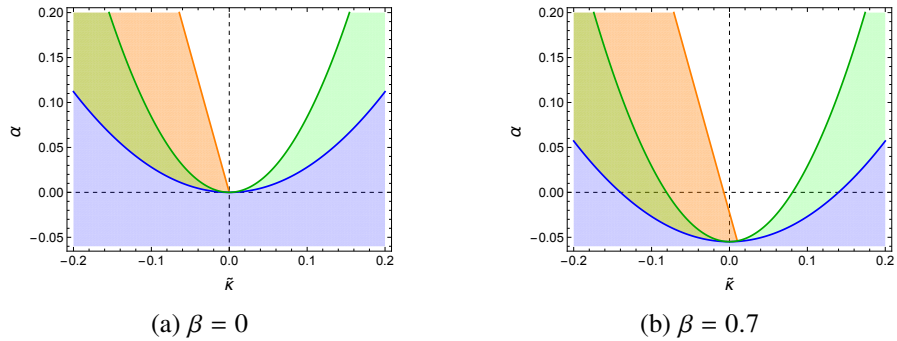


Figure 3.13: Numerical computations of the leading order Eckhaus and zigzag (in)stability regions of the stripes for (3.61) in the $(\tilde{\kappa}, \alpha)$ -plane for $\epsilon = 0.5$. Stripes exist in the complement of the blue regions. Blue lines: bifurcation curves (3.62); green regions: Eckhaus unstable; green lines: Eckhaus boundaries (3.63); orange regions: zigzag unstable; orange lines: zigzag boundaries (3.64); white regions: stable stripes. (a) $\beta = 0$. (b) $\beta = 0.7$. In (a) the zigzag boundary is attached to the origin, whereas in (b) the origin is stable, but advection shifts attachment point of the zigzag boundary to the right; $M \neq \text{Id}$ destabilises the stripes near $\tilde{\kappa} = 0$.

and plot the leading order form of a stripe based on (3.10) for $\alpha = 0.2$, $\beta = 0.7$ and $\tilde{\kappa} = 0.1$, which gives the velocity parameter $c = -1.4$.

The advection term shifts the bifurcation curve and the Eckhaus boundary downwards since the coefficient of β^2 are both negative in (3.62) and (3.63), cf. Fig. 3.13. Thus the advection stabilises the large wavelength perturbations in the x -direction.

The negative coefficient of $\tilde{\kappa}$ in (3.64) adds a negative value to the slope of the zigzag boundary, cf. Fig. 3.13, where we choose $\epsilon = 0.5$. The negative coefficient of β^2 shifts the zigzag boundary to the left. Hence the advection stabilises the large wavelength perturbations in the y -direction for any $\alpha > 0$. Since the coefficient of β^2 in (3.64) is larger than that of (3.62), however, there exists a zigzag unstable region near the bifurcation curve and for $\tilde{\kappa} > 0$, cf. Fig. 3.5c. We plot the resulting curves in Fig. 3.13b. In particular, the width of this unstable region is of order β^2 . Hence the advection destabilises the large wavelength perturbations in the y -direction at the onset of Turing bifurcation. This can also be seen from the positive coefficient of β^2 in (3.28).

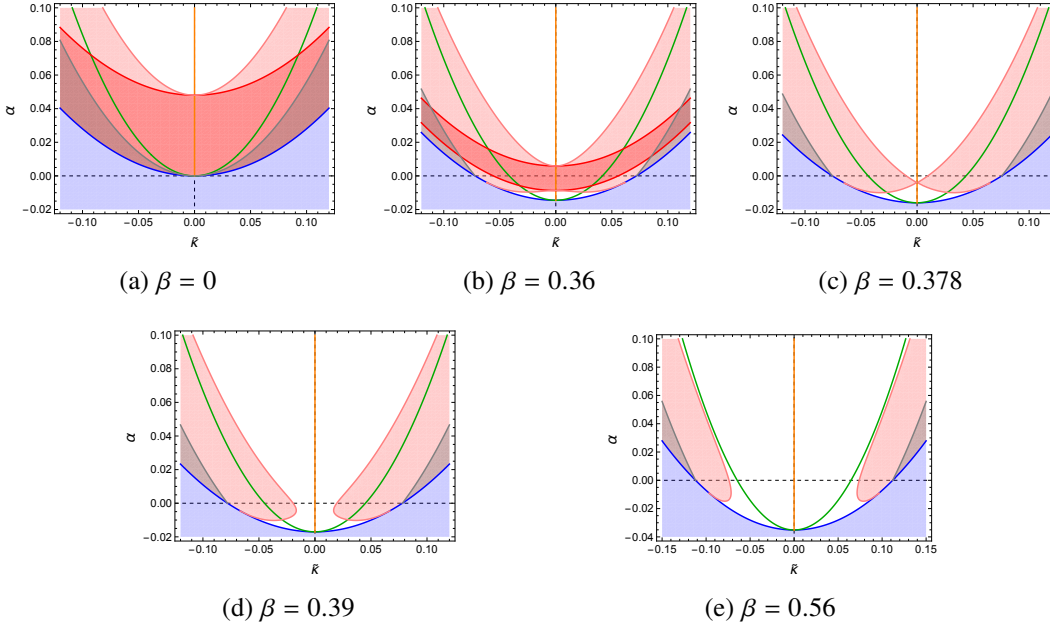


Figure 3.14: Numerical computations based on the analytic leading order formulae of the leading order of instability regions and boundaries of the stripes for (3.61) in the $(\tilde{\kappa}, \alpha)$ -plane for $\epsilon = 0.4$. Stripes exist in the complement of the blue regions. Bifurcation (3.62) (blue); Eckhaus boundaries (3.63) (green, unstable below); zigzag boundaries (unstable to the left) $\tilde{\kappa} = 0$ (orange); grey regions: most quasi-square-unstable ($\tilde{\ell}' = 0$); red regions: hex-unstable; pink regions: most quasi-hex-unstable ($\tilde{\ell}' = -\tilde{\kappa}/3$); otherwise stable. Here $q = -0.215$. (b) $\beta \in (0, \beta_{tp})$. (c) $\beta = \beta_{tp}$ (d) $\beta \in (\beta_{tp}, \beta_{ex})$. (e) $\beta > \beta_{ex}$.

Fig. 3.14 illustrates the stabilities of stripes against the lattice modes. We consider the most unstable quasi-square mode (i.e., $\tilde{\ell}' = 0$, cf. (3.35)), hexagonal mode and the most unstable quasi-hexagonal mode (i.e., $\tilde{\ell}' = -\tilde{\kappa}'/3$, cf. Lemma 3.5.16). The quadratic coefficient q is linearly dependent on the coefficient ϵ so that $q = -0.537\epsilon$. We choose $\epsilon = 0.4$, which leads to $q = -0.215$. The critical value $\beta_{tp} \approx 0.378$ (cf. (3.47)) is such that the quasi-hex-stable window is ‘open’ and the hex-unstable band vanishes for $\beta > \beta_{tp}$. The critical value $\beta_{ex} \approx 0.535$ (cf. (3.59) with $\theta = 1$ most unstable) is such that the quasi-hex-unstable regions are completely covered by the Eckhaus-unstable regions for $\beta > \beta_{ex}$. The quasi-hexagonal mode is more unstable than the quasi-square and hexagonal modes.

In Fig. 3.15 the stability of stripes against quasi-/hexagonal perturbations are depicted. For convenience, and with some abuse of notation we use the coefficient ϵ as the horizontal axis rather than the quadratic coefficient q . The opening threshold $\beta_{ep} \approx 0.577$ (cf. (3.56) with $\theta = 1$ most unstable) is such that the quasi-hex-stable window is ‘open’ for $\beta > \beta_{ep}$. In particular, the hex-stable window is ‘open’ for $\beta > 0$. The quasi-hexagonal mode is more unstable than the hexagonal one.

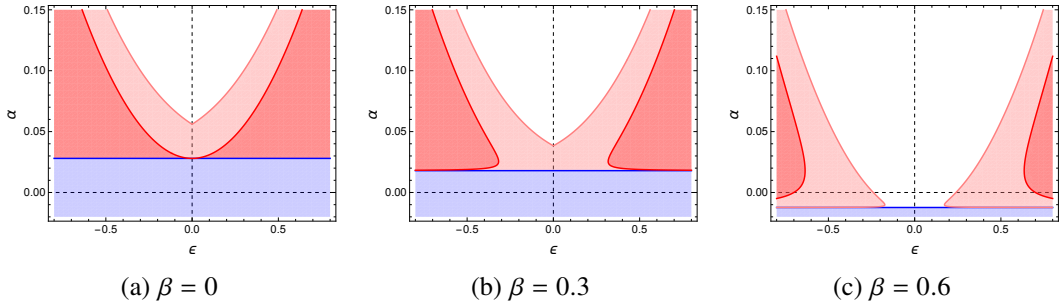


Figure 3.15: Numerical computations based on the analytic leading order formulae of the leading order of hex- and quasi-hex-instability regions and boundaries of the stripes for (3.61) in the (ϵ, α) -plane. Colors as in Fig. 3.14. The off-critical parameter $\tilde{\kappa} = 0.1$. (b) $\beta \in (0, \beta_{ep})$. (c) $\beta > \beta_{ep}$.

3.6.2 Numerical example: extended Klausmeier model

The extended Klausmeier in two-dimensional space [28, 59] is a two-component model for studying vegetation patterns on the earth's surface in drylands. In scaled form it is given by:

$$\begin{aligned} u_t &= d\Delta u + \beta u_x + a - u - uv^2, \\ v_t &= \Delta v - mv + uv^2. \end{aligned} \tag{3.65}$$

The isotropic spread of (surface) water u is modelled by $d\Delta u$, downhill flow by βu_x , precipitation by a and evaporation by $-u$. The uptake of water by vegetation $\pm uv^2$ is quadratic in the vegetation to model enhanced water infiltration at locations with vegetation. Vegetation dispersal is modelled by Δv and mortality by $-mv$. We fix the parameters to customary values $d = 500$ and $m = 0.45$ and investigate how (small) advection impacts the patterns by ‘brute force’ computing them and their stability against large-wavelength instabilities with pde2path [63]. For this we choose $\beta = 0$ or 50 or 100, which are relatively small values [59]. The parameter a is chosen so that the system is near Turing(-Hopf) instability.

A spatially homogeneous steady state is given by $(u, v) = (a, 0)$ and for $a \geq 2m$ there are two more:

$$u_{\pm}(a) = \frac{2m^2}{a \pm \sqrt{a^2 - 4m^2}}, \quad v_{\pm}(a) = \frac{a \pm \sqrt{a^2 - 4m^2}}{2m}.$$

From these two, only (u_+, v_+) is stable against spatially homogeneous perturbations, and becomes Turing(-Hopf) unstable when a drops below a critical value.

In Fig. 3.16 the large-wavelength stability of stripes near onset is depicted. Contrary to the previous example, for increasing advection β the zigzag boundary shifts to the left of the Turing(-Hopf) instability, so in this case the stripes with critical wavenumber that emerge are zigzag-stable.

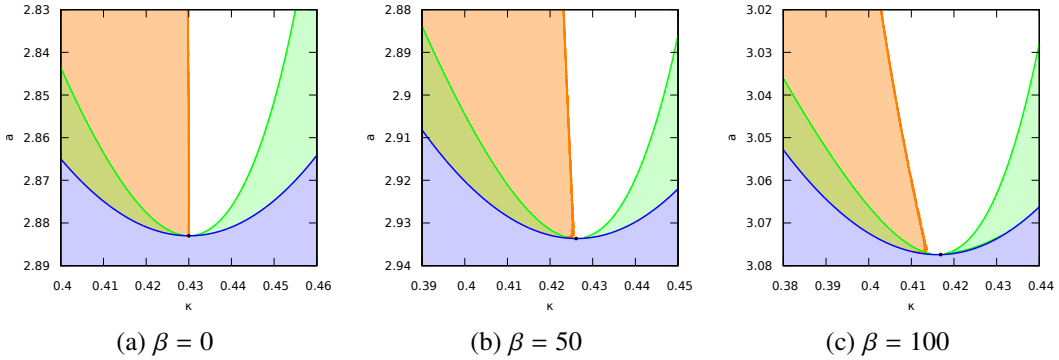


Figure 3.16: Eckhaus and zigzag (in)stability regions of the stripes for (3.65) in the (κ, a) -plane, by numerically checking the spectrum on an equidistant grid with spacing between neighbouring grid points of $a = 0.0001$ and $\kappa = 0.0001$. Stripes exist in the complement of the blue region; green regions: Eckhaus unstable; orange regions: zigzag unstable. (a) $\beta = 0$. (b) $\beta = 50$. (c) $\beta = 100$. In (a) the zigzag boundary is attached to the Turing instability locus and visually vertical, whereas in (b) and particularly (c) the zigzag boundary has shifted and tilted to the left.

3.6.3 Further analysis of extended Klausmeier model

We analyse the bifurcation and various stability boundaries of (3.65) for relatively small advection, e.g. $\beta < 1$. The results are based on the analytic leading order formulae in this thesis.

We first transform (3.65) into the framework of (1.9). Since (u_+, v_+) is a function of a , we consider $u = u_+ + \tilde{u}$, $v = v_+ + \tilde{v}$ such that the equilibrium is shifted to $(\tilde{u}, \tilde{v}) = (0, 0)$. Removing the ‘tilde’ yields

$$\begin{aligned} u_t &= d\Delta u - (1 + v_+^2)u - 2mv + \beta u_x - 2v_+uv - u_+v^2 - uv^2, \\ v_t &= \Delta v + v_+^2u + mv + 2v_+uv + u_+v^2 + uv^2, \end{aligned} \quad (3.66)$$

where the linear matrix, quadratic and cubic forms are given by

$$\tilde{L} = \begin{pmatrix} -1 - v_+^2 & -2m \\ v_+^2 & m \end{pmatrix}, \quad Q[U, U] = \begin{pmatrix} -2v_+uv - u_+v^2 \\ 2v_+uv + u_+v^2 \end{pmatrix}, \quad K[U, U, U] = \begin{pmatrix} -uv^2 \\ uv^2 \end{pmatrix},$$

with $U := (u, v)^T$. In particular, the generic form of Q is given by

$$Q[U_1, U_2] = (Q_{||}[U_1, U_2], Q_{|||[U_1, U_2])^T}$$

with

$$-Q_{||}[U_1, U_2] = Q_{|||[U_1, U_2] = U_1^T \begin{pmatrix} 0 & v_+ \\ v_+ & u_+ \end{pmatrix} U_2,$$

where $U_j = (u_j, v_j)^T$, $j = 1, 2$. Since the Turing bifurcation occurs at $a = a_T \approx 2.883$ [59], expanding \tilde{L} near $a = a_T$ yields

$$\tilde{L} = \tilde{L}(a) = \tilde{L}(a_T) + \partial_a \tilde{L}(a_T)(a - a_T) + O((a - a_T)^2).$$

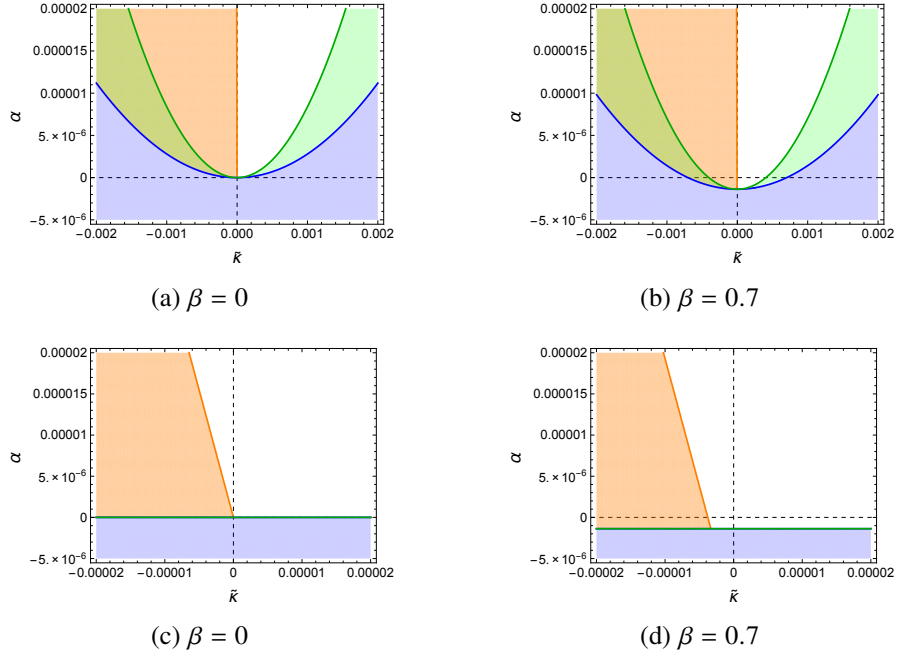


Figure 3.17: Numerical computations based on the analytic leading order formulae of the leading order of Eckhaus and zigzag (in)stability regions and boundaries of the stripes for (3.65) in the $(\tilde{\kappa}, \alpha)$ -plane. Stripes exist in the complement of the blue regions. Blue lines: bifurcation curves (3.67); green regions: Eckhaus unstable; green lines: Eckhaus boundaries (3.68); orange regions: zigzag unstable; orange lines: zigzag boundaries (3.69); white regions: stable stripes. (a) $\beta = 0$. (b) $\beta = 0.7$. (c) and (d) are the magnifications of (a) and (b) near the origin, respectively. In (a) the zigzag boundary is attached to the origin, whereas in (b) the advection shifts attachment point of the zigzag boundary to the left so that stripes are zigzag-stable near onset.

In terms of the notations in (1.9), we denote $L := \tilde{L}(a_T)$, $M := \partial_a \tilde{L}(a_T)$ and $\check{\alpha} := a - a_T$. The higher order term $\mathcal{O}(\check{\alpha}^2)$ is not relevant to the analysis in this thesis, so we omit it. Therefore, we transform (3.65) into the framework of (1.9), and the analysis of (1.9) for ‘sufficiently small’ $\check{\alpha}, \beta$ can be applied to (3.65). We list the leading order of the existence, zigzag and Eckhaus boundaries of the extended Klausmeier model (3.65) for small μ as follows ($\alpha \approx -0.137\check{\alpha}$).

$$\text{bifurcation curve: } \alpha \approx -2.81 \times 10^{-6} \beta^2 + 8.39 \tilde{\kappa}^2, \quad (3.67)$$

$$\text{Eckhaus boundary: } \alpha \approx -2.81 \times 10^{-6} \beta^2 + 2.80 \tilde{\kappa}^2, \quad (3.68)$$

$$\text{zigzag boundary: } \alpha \approx -2.38 \times 10^{-5} \beta^2 - 3.09 \tilde{\kappa}. \quad (3.69)$$

The advection shifts the bifurcation curve and the Eckhaus boundary downwards, and shifts the zigzag boundary to the left, cf. Fig. 3.17. Notably, the zigzag boundary has a negative slope and it is true for $\beta = 0$ as well, cf. Fig. 3.17 (lower row). This can also be seen from Fig. 3.16a that the zigzag boundary is not precisely vertical.

Chapter 4

Outlook

In this chapter, we outline possible future research topics.

4.1 Further analysis of reaction-subdiffusion equations

There are many problems are still open in the reaction-subdiffusion equations discussed in this thesis. So we would like to extend the results in Chapter 2 as follows.

Theorem 2.4.5 shows that the Fourier modes algebraically decay and exponentially grow for stable and unstable (pseudo-)spectrum, respectively. This verifies that the equilibrium of (2.36) does not have exponential dichotomy which is a characteristic of an equilibrium that extends the idea of hyperbolicity to non-autonomous systems (without fractional derivative). The expansions $\hat{u}(q, t)$ in Theorem 2.4.5, however, can be phrased as the decomposition into spaces with different growth and decay, which are analogous to the eigenspaces in linear systems. This may provide a direction of extending the idea of exponential dichotomy to fractional differential equations.

In both Theorem 2.4.5 & 2.5.4 the decay and growth of Fourier modes is obtained only for rational anomalous exponent γ . This limitation comes from the computation of the inverse Laplace transform. Relaxing this limitation, i.e., for irrational γ , will lead to the following problem: for any fixed wavenumber, there are infinitely many solutions to the dispersion relation and these solutions form certain curves, thus one cannot choose a branch cut which does not pass through any singularities, and any auxiliary contours also pass through the singularities. Therefore, the ILT for irrational γ may be a future work.

Theorem 2.4.5 & 2.5.4 give the decay and growth of Fourier modes only. The dynamics of the solutions in physical space is an open problem. The difficulty is that the coefficients C_{exp} , C_{alg} , C_{bp} are dependent on the wavenumber implicitly, thus their ILT are complicated. A possible solution is to prove that these coefficients behave like $-q^2$ which happens for the heat equations, or are uniformly bounded by the initial condition $\hat{u}(q, 0)$. Then the L^2 -norm of the solution to the reaction-subdiffusion equations can be estimated by Plancherel's theorem, cf. Theorem A.1.1.

In §2.6 we study the nonlinear reaction-subdiffusion equation (1.7) and its linearisation (1.8). However, the stability of solutions to (1.8) is still an open problem. The possible directions could be: extending the energy estimate (Theorem 2.6.1) and decaying estimate (Theorem 2.6.7) such that the estimates are available for all $t > 0$; proving the existence and uniqueness of the classical solution to (2.67); analysing the stability of the solution to (1.8) using comparison principle.

The dynamics of the reaction-subdiffusion equations is an open problem. Since they are not dynamical systems on the phase space of the natural initial condition $u(x, 0)$, one needs to find suitable function spaces with appropriate initial conditions in which the reaction-subdiffusion equations are dynamical systems.

4.2 Turing-type systems coupled to ODE

In Chapter 2 we consider the Turing instability in reaction-diffusion systems in a subdiffusive medium. In particular, in (2.2) the spectrum is close to zero for large wavenumber, which differs from that of RD systems, and such spectrum is caused by the ‘slow’ diffusive process. It would be natural to ask what happens to the spectrum if one of the components has zero diffusion, e.g. as a toy model: the SH equation coupled to an ODE. Indeed, the spectrum of such system has aforementioned property. In this case, the stability of a homogeneous state against high-frequency perturbations may differ from that of the Turing-type systems which possesses parabolicity.

Since the spectrum is close to zero for large wavenumber, the selection of the wavenumber may be different and this leads to the next analyses – the bifurcations of different types of patterns and their stabilities. Due to the continuation of the spectrum, the bifurcating patterns may be unstable against high-frequency wavenumber. Therefore, in one-dimensional space, the sideband modes might not be the dominant instability mechanism. Moreover, one can add the advection term into such systems, e.g., the Klausmeier model [28] – one component has diffusion and another one does not but has advection. However, our expected model would be more complicated than the Klausmeier model, since our model is composed of a RD system and an ODE which is at least a three-component system.

4.3 Bifurcation and stability of oblique stripes

In Chapter 3 we only consider the existence and stability of the primary bifurcating stripes, i.e., the stripes orthogonal to the direction of the advection. However, the stripes which are at an oblique angle to the advection may also bifurcate thereafter. Such oblique striped solutions have been studied via the amplitude equations with weak anisotropy in the context of Bénard convection [6]. The oblique stripes have also been considered as a result of a growing domain in the context of isotropic SH equation [17]. However, we are not aware of any further analysis of oblique stripes in planar RD systems with weak anisotropy.

It would be natural to extend the methodology used in this thesis to the study of oblique stripes. The existence of the oblique stripes may be studied by using Lyapunov-Schmidt reduction which can provide a rigorous parameter expansion. A foreseeable difficulty would be that, however, it is not sufficient to only consider the stripes in one-dimensional space as we did in this thesis since the oblique stripes are periodic in both directions. One may resolve this problem by changing coordinates so that the oblique effect can be transferred from the stripes to the advection. As a result, however, the advection would depend on both spatial variables. Therefore, it is uncertain about which approach is easier to be handled up to now.

Analogous to the analyses in this thesis, the study of the stability of oblique stripes against the large-wavelength and lattice modes would naturally be the next step. Unlike the orthogonal stripes, in the presence of the advection, the oblique stripes and hexagons can bifurcate synchronously near the onset in certain domains, e.g. $\Omega_3 = [0, 4\pi] \times [0, 4\pi/\sqrt{3}]$. So the question would be that which pattern would bifurcate stably therein. Moreover, the stability of orthogonal stripes against aforementioned oblique stripes may also be worth to analyse.

4.4 Subcritically bifurcating stripes

In Chapter 3 the stripes bifurcate supercritically from the homogeneous state if $\rho_{nl} < 0$. Notably, the stripes bifurcate subcritically if $\rho_{nl} > 0$. It has been shown that the subcritically bifurcating stripes are unstable near the onset, e.g. in the context of vegetation patterns [74]. However, if $\rho_{nl} = 0$, then one has to consider the higher order terms in the bifurcation equation, cf. (3.8). Analogous to the analyses in this thesis, the stability of this type of bifurcating stripes (not pitchfork) against various perturbations may be a future topic.

Appendix A

Prerequisites

A.1 Fourier transform

We recall the definition of the Fourier transform and its inversion, and briefly introduce their properties. We refer to [12] for more details.

The Fourier transform is an integral transform for $f(x)$ where the variable $x \in \mathbb{R}^n$, $x = (x_1, \dots, x_n)$ represents the n -dimensional space in this thesis. The Fourier transform of the integrable function $f(x)$, denoted by $\hat{f}(q)$ or $(\mathcal{F}f)(q)$, is defined by

$$\hat{f}(q) = \mathcal{F}[f(x)](q) = \int_{\mathbb{R}^n} f(x) e^{-iqx} dx, \quad q \in \mathbb{R}^n, \quad (\text{A.1})$$

and the inverse Fourier transform is defined by

$$f(x) = \mathcal{F}^{-1}[\hat{f}(q)](x) = \frac{1}{(2\pi)^n} \int_{\mathbb{R}^n} \hat{f}(q) e^{iqx} dq, \quad x \in \mathbb{R}^n.$$

The following theorem shows that the Fourier transform is an isometry with respect to the L^2 -norm.

Theorem A.1.1 (Plancherel's theorem). *Assume $f \in L^1(\mathbb{R}^n) \cap L^2(\mathbb{R}^n)$, then $f, \hat{f} \in L^2(\mathbb{R}^n)$ and*

$$\|f\|_{L^2(\mathbb{R}^n)} = \|\hat{f}\|_{L^2(\mathbb{R}^n)}.$$

Next, we list some properties of the Fourier transform which are used in this thesis.

- Linearity: $\mathcal{F}[af(x) + bg(x)](q) = a\hat{f}(q) + b\hat{g}(q)$.
- Gradient: $\mathcal{F}[\nabla f(x)](q) = -iq\hat{f}(q)$, $\nabla := (\partial_{x_1}, \dots, \partial_{x_n})$.
- Laplacian: $\mathcal{F}[\Delta f(x)](q) = -|q|^2 \hat{f}(q)$, where $\Delta := \partial_{x_1}^2 + \dots + \partial_{x_n}^2$.
- Convolution: $\mathcal{F}[(f * g)(x)](q) = \hat{f}(q) \cdot \hat{g}(q)$, where $(f * g)(x) := \int_{\mathbb{R}^n} f(y)g(x-y) dy$.

A.2 Laplace transform

We recall the definition of the Laplace transform and its inversion, and briefly introduce their applications to the fractional integral and derivative for the preparation. We refer to [27, 35, 61] for more details.

The Laplace transform is an integral transform for $f(t)$ where the variable t usually takes positive real values, e.g. t represents time in this thesis. The Laplace transform of the integrable function $f(t)$, denoted by $\tilde{f}(s)$ or $(\mathcal{L}f)(s)$, is defined by

$$\tilde{f}(s) = (\mathcal{L}f)(s) = \mathcal{L}[f(t)](s) = \int_0^\infty f(t)e^{-st}dt. \quad (\text{A.2})$$

The following theorem gives the sufficient condition for the existence of the Laplace transform.

Theorem A.2.1 (Existence of Laplace transform). *If $f(t)$ is sectionally continuous in every finite interval $0 \leq t \leq N$ and of exponential order $c \in \mathbb{R}$, i.e., $|f(t)| \leq Ae^{ct}$ with $A > 0$, for $t > N$, then its Laplace transform $(\mathcal{L}f)(s)$ exists for all $s > c$.*

Next, we list some properties of the Laplace transform which are used in this thesis.

- Linearity: $\mathcal{L}[af(t) + bg(t)](s) = a\tilde{f}(s) + b\tilde{g}(s)$.
- Exponential function: $\mathcal{L}[e^{at}](s) = \frac{1}{s-a}$.
- Shift: $\mathcal{L}[e^{at}f(t)](s) = \tilde{f}(s-a)$.
- Differentiation: $\mathcal{L}[f'(t)](s) = s\tilde{f}(s) - f(0)$, where $' := d/dt$.
- Integration: $\mathcal{L}[\int_0^t f(\tau)d\tau](s) = \tilde{f}(s)/s$.
- Convolution: $\mathcal{L}[(f * g)(t)](s) = \tilde{f}(s) \cdot \tilde{g}(s)$, where $(f * g)(t) := \int_0^t f(\tau)g(t-\tau)d\tau$.

If the Laplace transform of a function $f(t)$ is $\tilde{f}(s)$, i.e., $(\mathcal{L}f)(s) = \tilde{f}(s)$, then $f(t)$ is called an inverse Laplace transform (ILT) of $\tilde{f}(s)$ and denoted by $f(t) = (\mathcal{L}^{-1}\tilde{f})(t)$ and given for $t > 0$ by the formula

$$f(t) = (\mathcal{L}^{-1}\tilde{f})(t) = \frac{1}{2\pi i} \int_{c-i\infty}^{c+i\infty} \tilde{f}(s)e^{st}ds.$$

It is known as Bromwich's integral formula.

A.3 Wright function

The Wright function is defined by the series [27, Section 1.11]

$$\mathcal{W}(a, b; z) := \sum_{n=0}^{\infty} \frac{1}{\Gamma(an+b)} \frac{z^n}{n!}, \quad a, b, z \in \mathbb{C}. \quad (\text{A.3})$$

If $a > -1$, this series is absolutely convergent for all $z \in \mathbb{C}$ and it is an entire function of z . Hence, this series is uniformly convergent within $|z| < R$, where R is any positive constant. The derivatives with respect to z is given by

$$\frac{d^n}{dz^n} \mathcal{W}(a, b; z) = \mathcal{W}(a, a + nb; z), \quad n \in \mathbb{N}.$$

Concerning the Green's function (2.31), we have, with $\mu := \gamma/2 \in (0, 1/2)$,

$$\Phi(x, t) = \frac{1}{\sqrt{4dt^\gamma}} \sum_{n=0}^{\infty} \frac{(-1)^n}{n! \Gamma(1 - \frac{\gamma}{2} - \frac{\gamma}{2}n)} \left(\frac{|x|}{\sqrt{dt^\gamma}} \right)^n = \frac{t^{-\mu}}{2\sqrt{d}} \mathcal{W}\left(-\mu, 1 - \mu; -\frac{|x|}{\sqrt{d}} t^{-\mu}\right),$$

and $\Phi(x, t) > 0$ for any $t > 0, x \in \mathbb{R}$ [32, Eq. 4.26-a]. Since the Wright function in $\Phi(x, t)$ is uniformly convergent for $t > (|x|/(R\sqrt{d}))^{1/\mu}$, we can interchange the limit and sum for compact set of x , yields

$$\begin{aligned} \lim_{t \rightarrow \infty} \frac{\Phi(x, t)}{t^{-\mu}} &= \lim_{t \rightarrow \infty} \frac{1}{2\sqrt{d}} \mathcal{W}\left(-\mu, 1 - \mu; -\frac{|x|}{\sqrt{d}} t^{-\mu}\right) \\ &= \frac{1}{2\sqrt{d}} \left(\frac{1}{\Gamma(1 - \mu)} + \sum_{n=1}^{\infty} \lim_{t \rightarrow \infty} \frac{(-1)^n}{n! \Gamma(1 - \frac{\gamma}{2} - \frac{\gamma}{2}n)} \left(\frac{|x|}{\sqrt{dt^\gamma}} \right)^n \right) = \frac{1}{2\sqrt{d}\Gamma(1 - \mu)}, \end{aligned}$$

so the Green's function $\Phi(x, t) \sim (2\sqrt{d}\Gamma(1 - \mu)t^\mu)^{-1}$ is algebraically decaying locally uniformly in x for $t \rightarrow \infty$.

Concerning the derivatives of Φ with respect to t , we have

$$\begin{aligned} \partial_t \Phi &= \frac{-\mu}{2\sqrt{d}} t^{-\mu-1} \mathcal{W}\left(-\mu, 1 - \mu; -\frac{|x|}{\sqrt{d}} t^{-\mu}\right) + \frac{|x|\mu}{2d} t^{-2\mu-1} \mathcal{W}\left(-\mu, 1 - 2\mu; -\frac{|x|}{\sqrt{d}} t^{-\mu}\right), \\ \partial_t^2 \Phi &= \frac{\mu(\mu+1)}{2\sqrt{d}} t^{-\mu-2} \mathcal{W}\left(-\mu, 1 - \mu; -\frac{|x|}{\sqrt{d}} t^{-\mu}\right) \\ &\quad + \frac{|x|(-3\mu^2 - \mu)}{2d} t^{-2\mu-2} \mathcal{W}\left(-\mu, 1 - 2\mu; -\frac{|x|}{\sqrt{d}} t^{-\mu}\right) \\ &\quad + \frac{|x|^2 \mu^2}{2d^{3/2}} t^{-3\mu-2} \mathcal{W}\left(-\mu, 1 - 3\mu; -\frac{|x|}{\sqrt{d}} t^{-\mu}\right). \end{aligned}$$

The limit of Wright functions for $t \rightarrow \infty$ are obtained as follows

$$\lim_{t \rightarrow \infty} \mathcal{W}\left(-\mu, 1 - j\mu; -\frac{|x|}{\sqrt{d}} t^{-\mu}\right) = \frac{1}{\Gamma(1 - j\mu)}, \quad j \in \mathbb{N}.$$

Moreover, $\Phi(x, t)$ has the following asymptotic representation for $|x|/(\sqrt{dt^\mu}) \rightarrow \infty$ [32, Eq. 4.27],

$$\begin{aligned} \Phi(x, t) &\sim \frac{t^{-\mu}}{2\sqrt{d}} A_0 Y^{\mu-1/2} \exp(-Y), \\ A_0 &= (\sqrt{2\pi}(1 - \mu)^\mu \mu^{2\mu-1})^{-1}, \quad Y = (1 - \mu)(\mu^\mu |x| t^{-\mu} / \sqrt{d})^{1/(1-\mu)}. \end{aligned}$$

Therefore, $\Phi(x, t)$ is algebraically decaying in t for $|x| \gg \sqrt{dt^\mu}$ with power $-\mu/(2-2\mu) \in (-\mu, 0)$.

Appendix B

Inverse Laplace transform

B.1 Inverse Laplace transform with zero branch point

This proof relies on calculating the ILT with zero branch point, but where no roots of the dispersion relation are on the branch point at the origin.

For any fixed q , the Fourier-Laplace solution $\mathcal{L}\hat{u} = (\mathcal{L}\hat{u}_1, \mathcal{L}\hat{u}_2)$ of (2.35) can be written as

$$\mathcal{L}\hat{u}_1(q, s) = \frac{(s + s^{\ell/m} dq^2 - a_4)\hat{u}_1(q, 0) + a_2\hat{u}_2(q, 0)}{(s + s^{\ell/m} q^2 - a_1)(s + s^{\ell/m} dq^2 - a_4) - a_2 a_3} =: \Psi(s), \quad (\text{B.1})$$

cf. [22]. It suffices to discuss $\mathcal{L}\hat{u}_1(q, s)$ and we suppress the subscript for convenience.

The denominator of (B.1) is the subdiffusion dispersion relation (2.37), where $\ell/m = \delta = 1 - \gamma$, $\ell < m$, and $\ell, m \in \mathbb{N}$ without loss coprime. Here $z \mapsto \Psi(z^m)$ is rational with denominator of degree $2m$ thus giving $2m$ poles $z_j \neq 0, j = 1, \dots, 2m$.

First, we assume that all poles are simple, so there are $\alpha_j \in \mathbb{C}$, such that

$$\Psi(s) = \sum_{j=1}^{2m} \Psi_j(s), \quad \Psi_j(s) := \frac{\alpha_j}{s^{1/m} - z_j}, \quad j = 1, 2, \dots, 2m.$$

The formula of the ILT gives

$$\hat{u}(q, t) = \sum_{j=1}^{2m} U_j(q, t), \quad U_j(t) := \frac{1}{2\pi i} \int_{c-i\infty}^{c+i\infty} \Psi_j(s) e^{st} ds, \quad j = 1, 2, \dots, 2m,$$

where $c > 0$ is chosen to the right of the finitely many singularities. For the ILT of Ψ_j , we take a modified Bromwich contour with branch cut $\mathfrak{B}_0^{\theta_1}$, cf. Fig. B.1, so that

$$\begin{aligned} U_j(t) &= \frac{1}{2\pi i} \int_{c-i\infty}^{c+i\infty} \Psi_j(s) e^{st} ds = \frac{1}{2\pi i} \lim_{T \rightarrow \infty} \int_{IA} \Psi_j(s) e^{st} ds \\ &= \frac{1}{2\pi i} \left(\lim_{R \rightarrow \infty} \oint_{\Gamma} - \lim_{R \rightarrow \infty} \int_{ABCD} - \lim_{R \rightarrow \infty} \int_{DE+FG} - \lim_{\epsilon \rightarrow 0} \int_{EF} - \lim_{R \rightarrow \infty} \int_{GHI} \right) \Psi_j(s) e^{st} ds. \end{aligned}$$

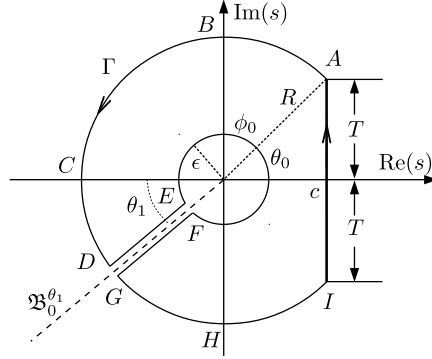


Figure B.1: Notation and geometry of the integration contours.

We split the integration along the closed contour Γ as follows.

Along EF : With $s = \epsilon e^{i\theta}$, $ds = i\epsilon e^{i\theta} d\theta$, $\lim_{\epsilon \rightarrow 0} \Psi_j(\epsilon e^{i\theta}) = -\alpha_j/z_j$ independent of θ , we have

$$\frac{1}{2\pi i} \lim_{\epsilon \rightarrow 0} \int_{EF} \Psi_j(s) e^{st} ds = \frac{1}{2\pi i} \lim_{\epsilon \rightarrow 0} \int_{\pi+\theta_1}^{-\pi+\theta_1} \Psi_j(\epsilon e^{i\theta}) e^{\epsilon e^{i\theta} t} \cdot i\epsilon e^{i\theta} d\theta = 0.$$

Along $ABCD$ and GHI : We claim $|\Psi_j(Re^{i\theta})| \leq M/R^{1/m}$ with M independent of R . Substituting $s = Re^{i\theta}$ into $\Psi_j(s)$ yields (cf. [61, p. 212])

$$|\Psi_j(Re^{i\theta})| = \left| \frac{\alpha_j}{(Re^{i\theta})^{1/m} - z_j} \right| = |\alpha_j| \left| \frac{1}{R^{1/m} e^{i\theta/m}} \right| \left| \frac{1}{1 - z_j (Re^{i\theta})^{-1/m}} \right|.$$

For sufficiently large R we have

$$\left| 1 - z_j (Re^{i\theta})^{-1/m} \right| \geq 1 - \left| z_j (Re^{i\theta})^{-1/m} \right| = 1 - |z_j| R^{-1/m} \geq 1/2,$$

so $|z_j| R^{-1/m} \leq 1/2$, which means $R \geq (2|z_j|)^m$ and

$$|\Psi(Re^{i\theta})| \leq 2|\alpha_j|/R^{1/m} \leq M/R^{1/m}.$$

It follows that $\lim_{R \rightarrow \infty} \int_{ABCD} \Psi_j(s) e^{st} ds = 0$ and $\lim_{R \rightarrow \infty} \int_{GHI} \Psi_j(s) e^{st} ds = 0$, cf. [61, Theorem 7-1].

Along DE and FG : $s = r e^{i(\pi+\theta_1)} = -r e^{i\theta_1}$, $s^{1/m} = r^{1/m} e^{i(\pi+\theta_1)/m}$, $ds = -e^{i\theta_1} dr$, yields

$$\frac{1}{2\pi i} \lim_{\substack{R \rightarrow \infty \\ \epsilon \rightarrow 0}} \int_{DE} \Psi_j(s) e^{st} ds = \frac{e^{i\theta_1}}{2\pi i} \lim_{\substack{R \rightarrow \infty \\ \epsilon \rightarrow 0}} \int_{\epsilon}^R \Psi_j(r e^{i(\pi+\theta_1)}) e^{-r e^{i\theta_1} t} dr =: I_{DE}.$$

Analogously, $s = r e^{i(-\pi+\theta_1)} = -r e^{i\theta_1}$, $s^{1/m} = r^{1/m} e^{i(-\pi+\theta_1)/m}$, $ds = -e^{i\theta_1} dr$, yields

$$\frac{1}{2\pi i} \lim_{\substack{R \rightarrow \infty \\ \epsilon \rightarrow 0}} \int_{FG} \Psi_j(s) e^{st} ds = -\frac{e^{i\theta_1}}{2\pi i} \lim_{\substack{R \rightarrow \infty \\ \epsilon \rightarrow 0}} \int_{\epsilon}^R \Psi_j(r e^{i(-\pi+\theta_1)}) e^{-r e^{i\theta_1} t} dr =: I_{FG}.$$

Combining I_{DE} with I_{FG} gives

$$I_{DE} + I_{FG} = \frac{e^{i\theta_1}}{2\pi i} \lim_{\substack{R \rightarrow \infty \\ \epsilon \rightarrow 0}} \int_{\epsilon}^R f_j(r) e^{-re^{i\theta_1}t} dr,$$

where $f_j(r) := \Psi_j(re^{i(\pi+\theta_1)}) - \Psi_j(re^{i(-\pi+\theta_1)})$ and $\lim_{\epsilon \rightarrow 0} f_j(\epsilon) = \lim_{R \rightarrow \infty} f_j(R) = 0$. Recall $\theta_1 = \theta_1(q)$. Since there is no pole on $\mathfrak{B}_0^{\theta_1}$ for any fixed q , $f_j(r)$ is bounded, i.e., $|f_j(r)| \leq G_{j,\gamma}$ for $r \in [0, \infty)$, where $G_{j,\gamma} > 0$ is a constant for fixed γ . Hence,

$$|I_{DE} + I_{FG}| \leq \frac{1}{2\pi} \lim_{\substack{R \rightarrow \infty \\ \epsilon \rightarrow 0}} \int_{\epsilon}^R G_{j,\gamma} e^{-rt \cos(\theta_1)} dr = \frac{G_{j,\gamma}}{2\pi t \cos(\theta_1)} = O(t^{-1}).$$

We refine this estimate as follows. For any $r_0 > 0$, we have $\int_{r_0}^{\infty} f_j(r) e^{-re^{i\theta_1}t} dr \leq C t^{-1} e^{-r_0 t \cos \theta_1}$ for a constant C . Taylor expansion in $r = 0$ gives

$$f_j(r) = Ar^{1/m} + O(r^{2/m}), \quad A := -\frac{\alpha_j}{z_j^2} e^{i\theta_1/m} 2i \sin(\pi/m).$$

Therefore,

$$\int_0^{r_0} f_j(r) e^{-re^{i\theta_1}t} dr = \int_0^{r_0} Ar^{1/m} e^{-re^{i\theta_1}t} dr + O\left(\int_0^{r_0} r^{2/m} e^{-re^{i\theta_1}t} dr\right). \quad (\text{B.2})$$

For any α, β with $\alpha > 0, \operatorname{Re}(\beta) > 0$ we have, as $t \rightarrow \infty$, that

$$\begin{aligned} \int_0^{r_0} r^\alpha e^{-\beta rt} dr &= (\beta t)^{-1-\alpha} \int_0^{\beta r_0 t} w^\alpha e^{-w} dw \\ &= (\beta t)^{-1-\alpha} \left(\int_0^\infty w^\alpha e^{-w} dw - \int_{\beta r_0 t}^\infty w^\alpha e^{-w} dw \right) \\ &= (\beta t)^{-1-\alpha} \Gamma(1+\alpha) + O(t^{-1} e^{-\beta r_0 t}). \end{aligned}$$

Application to the right-hand side of (B.2) and combination with the previous gives

$$I_{DE} + I_{FG} = -\frac{\alpha_j \sin(\pi/m)}{z_j^2 \pi} \Gamma(1+1/m) t^{-1-1/m} + O(t^{-1-2/m}). \quad (\text{B.3})$$

Along Γ : If $z_j^m \notin \Omega_0$, i.e., there is no pole inside Γ for any ϵ, R , then Cauchy's integral theorem gives

$$\frac{1}{2\pi i} \lim_{\substack{R \rightarrow \infty \\ \epsilon \rightarrow 0}} \oint_{\Gamma} \Psi_j(s) e^{st} ds = 0.$$

If $z_j^m \in \Omega_0$, the residue theorem gives,

$$\begin{aligned} \frac{1}{2\pi i} \lim_{\substack{R \rightarrow \infty \\ \epsilon \rightarrow 0}} \oint_{\Gamma} \Psi_j(s) e^{st} ds &= \frac{1}{2\pi i} \lim_{\substack{R \rightarrow \infty \\ \epsilon \rightarrow 0}} \oint_{\Gamma} \frac{\alpha_j}{s^{1/m} - z_j} e^{st} ds = \operatorname{Res}_{s=z_j^m} \left(\frac{\alpha_j}{s^{1/m} - z_j} e^{st} \right) \\ &= \lim_{s \rightarrow z_j^m} \frac{\alpha_j}{s^{1/m} - z_j} e^{st} (s - z_j^m) = \alpha_j m z_j^{m-1} e^{tz_j^m}. \end{aligned}$$

Now, we determine the coefficients α_j . Denote $P(s)$ and $Q(s)$ the numerator and denominator of $\Psi(s)$, respectively, i.e.,

$$\Psi(s) = \frac{P(s)}{Q(s)} = \sum_{j=1}^{2m} \frac{\alpha_j}{s^{1/m} - z_j},$$

and $Q(s)$ is the dispersion relation. Fix j , multiply both sides by $s^{1/m} - z_j$ and let $s \rightarrow z_j^m$. Then all the terms vanish except j -th term, which yields

$$\lim_{s \rightarrow z_j^m} \frac{P(s)}{Q(s)} (s^{1/m} - z_j) = \alpha_j.$$

By L'Hôpital's rule $\lim_{s \rightarrow z_j^m} \frac{s^{1/m} - z_j}{Q(s)} = \lim_{s \rightarrow z_j^m} \frac{1}{Q'(s)ms^{1-1/m}}$ where $' := d/ds$, so together

$$\lim_{s \rightarrow z_j^m} \frac{P(s)}{Q(s)} (s^{1/m} - z_j) = \lim_{s \rightarrow z_j^m} \frac{P(s)}{Q'(s)ms^{1-1/m}} \Rightarrow \alpha_j = \frac{P(z_j^m)}{Q'(z_j^m)mz_j^{m-1}}.$$

All in all we infer the solution in Fourier space can be written as

$$\begin{aligned} \hat{u}(q, t) &= \sum_{\substack{z_j^m \in \Omega_0 \\ z_j^m \neq 0}} \frac{P(z_j^m)}{Q'(z_j^m)} e^{z_j^m t} - \frac{e^{i\theta_1}}{2\pi i} \sum_{j=1}^{2m} \int_0^\infty f_j(r) e^{-r e^{i\theta_1} t} dr \\ &= C_{\text{exp}} e^{s_* t} + C_{\text{alg}} t^{-1-1/m} + O(t^{-1-2/m}). \end{aligned} \quad (\text{B.4})$$

Here $s_* = \operatorname{argmax}\{\operatorname{Re}(z_j^m) : z_j^m \in \Omega_0, P(z_j^m) \neq 0\}$ for the largest exponential rate, $C_{\text{exp}} = (P/Q')(s_*) \neq 0$ for almost all initial conditions since both coefficients of $P(s)$ with respect to the initial conditions are nonzero (neither vanishes at roots of Q). Moreover, for the algebraic rate we have

$$C_{\text{alg}} := -\frac{\sin(\pi/m)}{\pi} \Gamma(1+1/m) \sum_{j=1}^{2m} \frac{\alpha_j}{z_j^2} = -\frac{\sin(\pi/m)}{\pi} \Gamma(1+1/m) \sum_{j=1}^{2m} \frac{P(z_j^m)}{Q'(z_j^m)mz_j^{m+1}}.$$

Second, we consider the case which poles are not all simple. $\Psi(s)$ can be written as

$$\Psi(s) = \sum_j \sum_{k=1}^{k_j} \Psi_{jk}, \quad \Psi_{jk} := \frac{\alpha_{jk}}{(s^{1/m} - z_j)^k},$$

where k_j denotes the multiplicity of z_j and $\sum_j k_j = 2m$. Similarly, we compute ILT for each Ψ_{jk} . The integral along each arc tends to 0 as $\epsilon \rightarrow 0$ and $R \rightarrow \infty$. Along DE and FG :

$$I_{DE} + I_{FG} = \frac{e^{i\theta_1}}{2\pi i} \lim_{\epsilon \rightarrow 0} \int_\epsilon^R f_{jk}(r) e^{-r e^{i\theta_1} t} dr,$$

where $f_{jk} = \Psi_{jk}(r e^{i(\pi+\theta_1)}) - \Psi_{jk}(r e^{i(-\pi+\theta_1)})$. Similarly, we obtain

$$I_{DE} + I_{FG} = -\frac{\alpha_{jk} k (-z_j)^{k-1}}{z_j^{2k}} \frac{\sin \pi/m}{\pi} \Gamma(1+1/m) t^{-1-1/m} + O(t^{-1-2/m}).$$

Along Γ , if $z_j \notin \Omega_0$, then the integral along Γ vanishes. If $z_j \in \Omega_0$, then

$$\begin{aligned} \frac{1}{2\pi i} \lim_{\epsilon \rightarrow 0} \oint_{\Gamma} \Psi_{jk}(s) e^{st} ds &= \frac{1}{2\pi i} \lim_{\epsilon \rightarrow 0} \oint_{\Gamma} \frac{\alpha_{jk}}{(s^{1/m} - z_j)^k} e^{st} ds = \operatorname{Res}_{s=z_j^m} \left(\frac{\alpha_{jk}}{(s^{1/m} - z_j)^k} e^{st} \right) \\ &= \lim_{s \rightarrow z_j^m} \frac{1}{(k-1)!} \left(\frac{d}{ds} \right)^{k-1} \left(\frac{\alpha_{jk}(s - z_j^m)^k}{(s^{1/m} - z_j)^k} e^{st} \right) \\ &= \lim_{s \rightarrow z_j^m} \frac{\alpha_{jk}}{(k-1)!} \left(\frac{d}{ds} \right)^{k-1} \left(\left(\sum_{n=0}^{m-1} s^{\frac{m-n-1}{m}} z_j^n \right)^k e^{st} \right) \\ &= \lim_{s \rightarrow z_j^m} \alpha_{jk} e^{st} \sum_{p=0}^{k-1} \frac{t^{k-1-p}}{p!(k-1-p)!} \left(\frac{d}{ds} \right)^p \left(\sum_{n=0}^{m-1} s^{\frac{m-n-1}{m}} z_j^n \right)^k. \end{aligned}$$

Now we determine the coefficient α_{jk} . Define $g_{jk}(z) = (z - z_j)^{k-1} \Psi(z^m)$ where $z = s^{1/m}$, so α_{jk} is the coefficient of $(z - z_j)^{-1}$ in Laurent expansion of $g_{jk}(z)$ evaluated at $z = z_j$. Hence α_{jk} is the residue of $g_{jk}(z)$ at $z = z_j$ and, z_j is the pole of $g_{jk}(z)$ with multiplicity $k_j - k + 1$. Therefore we have

$$\begin{aligned} \alpha_{jk} &= \operatorname{Res}_{z=z_j} g_{jk}(z) = \operatorname{Res}_{z=z_j} \frac{(z - z_j)^{k_j} \Psi(z^m)}{(z - z_j)^{k_j - k + 1}} \\ &= \frac{1}{(k_j - k)!} \lim_{z \rightarrow z_j} \left(\frac{d}{dz} \right)^{k_j - k} \left((z - z_j)^{k_j} \Psi(z^m) \right) \end{aligned} \quad (\text{B.5})$$

Note that this formula generalises the case of simple pole, i.e., $\alpha_{jk} = \alpha_j$ for $k_j = k = 1$. In particular, by assumption on the multiplicity, $\alpha_{jk_j} \neq 0$.

Finally, we obtain the solution in Fourier space as the following

$$\begin{aligned} \hat{u}(q, t) &= \sum_{z_j^m \in \Omega_0} \sum_{k=1}^{k_j} \lim_{s \rightarrow z_j^m} \alpha_{jk} e^{st} \sum_{p=0}^{k-1} \frac{t^{k-1-p}}{p!(k-1-p)!} \left(\frac{d}{ds} \right)^p \left(\sum_{n=0}^{m-1} s^{\frac{m-n-1}{m}} z_j^n \right)^k \\ &\quad - \sum_j \sum_{k=1}^{k_j} \frac{e^{i\theta_1}}{2\pi i} \int_0^\infty f_{jk}(r) e^{-r e^{i\theta_1} t} dr \\ &= C_{\text{exp}}^{\text{multi}} t^{k_j - 1} e^{s_* t} + C_{\text{alg}}^{\text{multi}} t^{-1 - 1/m} + O(t^{-1 - 2/m} + t^{k_j - 2} e^{\operatorname{Re}(s_*) t}). \end{aligned} \quad (\text{B.6})$$

Here $s_* = \operatorname{argmax}\{\operatorname{Re}(z_j^m) : z_j^m \in \Omega_0, C_{\text{exp}}^{\text{multi}} \neq 0\}$ for the largest exponential rate. The coefficients are given by

$$\begin{aligned} C_{\text{exp}}^{\text{multi}} &:= \frac{\alpha_{jk_j}}{(k_j - 1)!} (m z_j^{m-1})^{k_j} \neq 0, \\ C_{\text{alg}}^{\text{multi}} &:= -\frac{\sin(\pi/m)}{\pi} \Gamma(1 + 1/m) \sum_j \sum_{k=1}^{k_j} \alpha_{jk} k (-z_j)^{-k-1}. \end{aligned}$$

If $C_{\text{alg}}^{\text{multi}} \neq 0$, then \hat{u} decays algebraically for $\operatorname{Re}(s_*) < 0$. If $C_{\text{exp}}^{\text{multi}} \neq 0$ and $\operatorname{Re}(s_*) > 0$, then \hat{u} grows exponentially.

B.2 Inverse Laplace transform with nonzero branch points

In the following, we omit some parts that are very similar to parts of the proof of Theorem 2.4.5, see Appendix B.1.

We consider the ILT of $\mathcal{L}\hat{w}_j$, $j = 1, 2$ for fixed q , and only discuss $\mathcal{L}\hat{w}_1(q, s)$; we suppress the subscript for convenience. If all roots (except $s = \mu_1, \mu_2$) are simple for $D_{\text{ca}}(z_1, z_2, q^2)$, then the solution $\mathcal{L}\hat{w}$ can be written as

$$\begin{aligned} \Psi(s) &:= \frac{\left(s - \mu_2 + d_4 q^2 (s - \mu_2)^{\frac{n}{m}}\right) \hat{w}_1(q, 0) - d_2 q^2 (s - \mu_2)^{\frac{n}{m}} \hat{w}_2(q, 0)}{\left(s - \mu_1 + d_1 q^2 (s - \mu_1)^{\frac{n}{m}}\right) \left(s - \mu_2 + d_4 q^2 (s - \mu_2)^{\frac{n}{m}}\right) - (s - \mu_1)^{\frac{n}{m}} (s - \mu_2)^{\frac{n}{m}} d_2 d_3 q^4} \\ &= \sum_{j=1}^{m-n} \left(\frac{\alpha_j}{(s - \mu_1)^{\frac{1}{m}} - \xi_j} + \frac{\beta_j}{(s - \mu_2)^{\frac{1}{m}} - \eta_j} \right) + \sum_{k=1}^n \left(\frac{\varphi_k}{(s - \mu_1)^{\frac{k}{m}}} + \frac{\psi_k}{(s - \mu_2)^{\frac{k}{m}}} \right) \\ &= \sum_{j=1}^{m-n} (\Psi_{1j}(q, s) + \Psi_{2j}(q, s)) + \sum_{k=1}^n (\Psi_{3k}(q, s) + \Psi_{4k}(q, s)), \end{aligned}$$

where $\Psi_{1j}(s) := \frac{\alpha_j}{(s - \mu_1)^{1/m} - \xi_j}$, etc. The ILT gives

$$\begin{aligned} \hat{w}(q, t) &= \frac{1}{2\pi i} \int_{c-i\infty}^{c+i\infty} \Psi(s) e^{st} ds \\ &= \frac{1}{2\pi i} \sum_{j=1}^{m-n} \int_{c-i\infty}^{c+i\infty} (\Psi_{1j}(s) + \Psi_{2j}(s)) e^{st} ds + \frac{1}{2\pi i} \sum_{k=1}^n \int_{c-i\infty}^{c+i\infty} (\Psi_{3k}(s) + \Psi_{4k}(s)) e^{st} ds \\ &= \sum_{j=1}^{m-n} (I_{1j} + I_{2j}) + \sum_{k=1}^n (I_{3k} + I_{4k}) = I_1 + I_2 + I_3 + I_4, \end{aligned}$$

where $I_{1j} := \frac{1}{2\pi i} \int_{c-i\infty}^{c+i\infty} \Psi_{1j}(s) e^{st} ds$, $I_1 := \sum_{j=1}^{m-n} I_{1j}$, etc.

We have $|\Psi_{1j}| < M/R^{1/m}$ for $R > 0$ and suitable constant $M > 0$ since multiplication with $R^{1/m}$, gives denominator $|(\mathrm{e}^{i\theta} - R^{-1}\mu_1)^{1/m} - \xi_j R^{-1/m}|$, which is continuous in R and nonzero at $R = \infty$.

Case cc: We first calculate I_{1j} and choose the branch cut $\mathfrak{B}_{\mu_1}^{-\theta_1}$. The corresponding principal branch is $\Omega_1 := \{s \in \mathbb{C} \setminus \{\mu_1\} : \arg(s - \mu_1) \in (-\pi - \theta_1, \pi - \theta_1), \theta_1 \in (0, \pi/2)\}$, cf. Fig. B.2a. The integral I_{1j} can be written in the form of

$$\begin{aligned} I_{1j} &= \frac{1}{2\pi i} \lim_{R \rightarrow \infty} \int_{IA} \Psi_{1j}(s) e^{st} ds \\ &= \frac{1}{2\pi i} \left(\lim_{\substack{R \rightarrow \infty \\ \epsilon \rightarrow 0}} \oint_{\Gamma} - \lim_{\substack{R \rightarrow \infty \\ \epsilon \rightarrow 0}} \int_{ABC} - \lim_{\substack{R \rightarrow \infty \\ \epsilon \rightarrow 0}} \int_{CD+EF} - \lim_{\epsilon \rightarrow 0} \int_{DE} - \lim_{R \rightarrow \infty} \int_{FGHI} \right) \Psi_{1j}(s) e^{st} ds, \end{aligned}$$

Since $|\Psi_{1j}(s)| < M/R^{1/m}$, the integrals along ABC , $FGHI$ vanish. Similar to the proof of Theorem 2.4.5, the integral along DE vanishes as well.

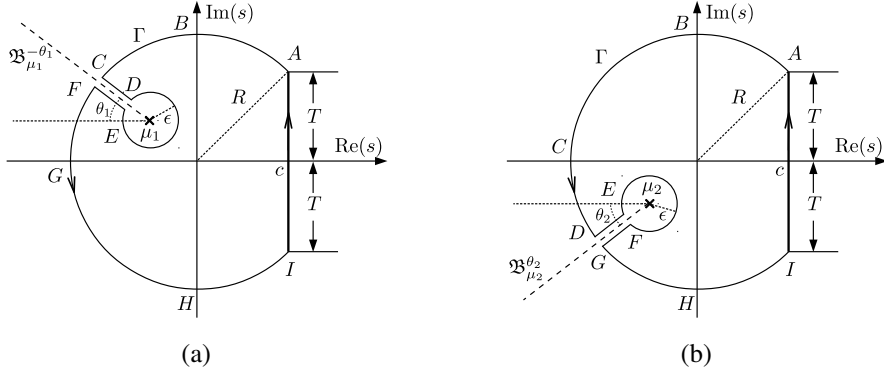


Figure B.2: Notation and geometry of the integration contours for case **cc**.

Along CD : $s - \mu_1 = re^{i(\pi - \theta_1)} = -re^{-i\theta_1}$, $ds = -e^{-i\theta_1}dr$; along EF : $s - \mu_1 = re^{i(-\pi - \theta_1)} = -re^{-i\theta_1}$, $ds = -e^{-i\theta_1}dr$. Then we have

$$I_{CD} := \frac{1}{2\pi i} \lim_{\epsilon \rightarrow 0} \int_{CD} \Psi_{1j}(s) e^{st} ds = \frac{1}{2\pi i} \int_0^\infty \Psi_{1j} \left(\mu_1 + r e^{i(\pi - \theta_1)} \right) e^{(\mu_1 - r e^{-i\theta_1})t - i\theta_1} dr,$$

$$I_{EF} := \frac{1}{2\pi i} \lim_{\epsilon \rightarrow 0} \int_{EF} \Psi_{1j}(s) e^{st} ds = -\frac{1}{2\pi i} \int_0^\infty \Psi_{1j} \left(\mu_1 + r e^{i(-\pi - \theta_1)} \right) e^{(\mu_1 - r e^{-i\theta_1})t - i\theta_1} dr.$$

Now $f_{1j}(r) := \Psi_{1j}(\mu_1 + re^{i(\pi-\theta_1)}) - \Psi_{1j}(\mu_1 + re^{i(-\pi-\theta_1)})$ satisfies $f_{1j}(0) = 0$ and $f_{1j}(\infty) = 0$, and is uniformly bounded by some $C > 0$ since there are no poles on $\mathfrak{B}_{\mu_1}^{-\theta_1}$ for any fixed q , where we recall $\theta_1 = \theta_1(q)$. Similar to the calculation in Appendix B.1 we have

$$I_{CD} + I_{EF} = -\frac{\alpha_j \sin(\pi/m)}{\xi_j^2} \frac{\pi}{\Gamma(1+1/m)} t^{-1-1/m} e^{\mu_1 t} + O(t^{-1-2/m} e^{\operatorname{Re}(\mu_1)t}).$$

Along Γ : If $\mu_1 + \xi_j^m \notin \Omega_1$, then $\lim_{R \rightarrow \infty, \epsilon \rightarrow 0} \oint_{\Gamma} \Psi_{1j}(s) e^{st} ds = 0$. If $\mu_1 + \xi_j^m \in \Omega_1$, then residue theorem gives,

$$\begin{aligned} I_\Gamma &:= \frac{1}{2\pi i} \lim_{\epsilon \rightarrow 0} \oint_{\Gamma} \Psi_{1j}(s) e^{st} ds = \frac{1}{2\pi i} \lim_{\epsilon \rightarrow 0} \oint_{\Gamma} \frac{\alpha_j}{(s - \mu_1)^{1/m} - \xi_j} e^{st} ds \\ &= \operatorname{Res}_{s=\mu_1+\xi_j^m} \left(\frac{\alpha_j}{(s - \mu_1)^{1/m} - \xi_j} e^{st} \right) = \lim_{s \rightarrow \mu_1+\xi_j^m} \frac{\alpha_j ((s - \mu_1) - \xi_j^m)}{(s - \mu_1)^{1/m} - \xi_j} e^{st} \\ &= \alpha_j m \xi_j^{m-1} e^{(\mu_1 + \xi_j^m)t} = \frac{P(\mu_1 + \xi_j^m)}{Q'(\mu_1 + \xi_j^m)} e^{(\mu_1 + \xi_j^m)t} \end{aligned}$$

where $P(s)$ and $Q(s)$ are numerator and denominator of $\Psi(s)$, respectively, i.e., $\Psi(s) = (P/Q)(s)$, $' := d/ds$, and $\alpha_j := \frac{P(\mu_1 + \xi_j^m)}{Q'(\mu_1 + \xi_j^m)m\xi_j^{m-1}}$. Combining the above results we obtain

$$\begin{aligned} I_1 &= \sum_{\mu_1 + \xi_j^m \in \Omega_1} \frac{P(\mu_1 + \xi_j^m)}{Q'(\mu_1 + \xi_j^m)} e^{(\mu_1 + \xi_j^m)t} + C_{\text{alg},1} t^{-1-1/m} e^{\mu_1 t} + O(t^{-1-2/m} e^{\operatorname{Re}(\mu_1)t}) \\ &= C_{\exp,1} e^{s_1 t} + C_{\text{alg},1} t^{-1-1/m} e^{\mu_1 t} + O(t^{-1-2/m} e^{\operatorname{Re}(\mu_1)t}) + o(e^{\operatorname{Re}(s_1)t}), \end{aligned}$$

$s_1 = \operatorname{argmax}\{\operatorname{Re}(\mu_1 + \xi_j^m) : \mu_1 + \xi_j^m \in \Omega_1, C_{\exp,1} \neq 0\}, C_{\exp,1}, C_{\text{alg},1} \in \mathbb{C}$ and

$$C_{\text{alg},1} := -\frac{\sin(\pi/m)}{\pi} \Gamma(1+1/m) \sum_{j=1}^{m-n} \frac{P(\mu_1 + \xi_j^m)}{Q'(\mu_1 + \xi_j^m) m \xi_j^{m+1}}.$$

Similarly, we can obtain

$$\begin{aligned} I_2 &= \sum_{\mu_2 + \eta_j^m \in \Omega_2} \frac{P(\mu_2 + \eta_j^m)}{Q'(\mu_2 + \eta_j^m)} e^{(\mu_2 + \eta_j^m)t} + C_{\text{alg},2} t^{-1-1/m} e^{\mu_2 t} + O(t^{-1-2/m} e^{\operatorname{Re}(\mu_2)t}) \\ &= C_{\exp,2} e^{s_2 t} + C_{\text{alg},2} t^{-1-1/m} e^{\mu_2 t} + O(t^{-1-2/m} e^{\operatorname{Re}(\mu_2)t}) + o(e^{\operatorname{Re}(s_2)t}), \end{aligned}$$

$s_2 = \operatorname{argmax}\{\operatorname{Re}(\mu_2 + \eta_j^m) : \mu_2 + \eta_j^m \in \Omega_2, C_{\exp,2} \neq 0\}$, the branch cut is $\mathfrak{B}_{\mu_2}^{\theta_1}$ and the corresponding principal branch is $\Omega_2 := \{s \in \mathbb{C} \setminus \{\mu_2\} : \arg(s - \mu_2) \in (-\pi + \theta_2, \pi + \theta_2), \theta_2 \in (0, \pi/2)\}$, cf. Fig. B.2b.

The calculation of I_{3k} is similar to that of I_{1j} except the integral along Γ vanishes as there is no poles inside Ω_{ca} , and the integral along CD and EF gives

$$\begin{aligned} I_{CD} + I_{EF} &= \frac{1}{2\pi i} \int_0^\infty \left(\frac{\varphi_k}{r^{k/m} e^{i(\pi-\theta_1)k/m}} - \frac{\varphi_k}{r^{k/m} e^{i(-\pi-\theta_1)k/m}} \right) e^{(\mu_1 - r e^{-i\theta_1})t} e^{-i\theta_1} dr \\ &= \frac{1}{2\pi i} \varphi_k e^{\mu_1 t - i\theta_1} \left(e^{i(\theta_1 - \pi)k/m} - e^{i(\theta_1 + \pi)k/m} \right) \int_0^\infty r^{-k/m} e^{-r e^{-i\theta_1} t} dr \\ &= \frac{1}{2\pi i} \varphi_k \Gamma(1 - k/m) e^{2i(k/m-1)} \left(e^{-i\pi k/m} - e^{i\pi k/m} \right) e^{\mu_1 t} t^{k/m-1}. \end{aligned}$$

Hence we have (with I_4 form a similar computation),

$$I_3 = \frac{1}{\pi} e^{\mu_1 t} \sum_{k=1}^n \varphi_k \Gamma(1 - k/m) e^{2i(k/m-1)} \sin(\pi k/m) t^{k/m-1}, \quad (\text{B.7})$$

$$I_4 = \frac{1}{\pi} e^{\mu_2 t} \sum_{k=1}^n \psi_k \Gamma(1 - k/m) e^{-2i(k/m-1)} \sin(\pi k/m) t^{k/m-1}, \quad (\text{B.8})$$

where the coefficients φ_k, ψ_k are given by

$$\begin{aligned} \varphi_k &= \frac{1}{(n-k)!} \lim_{z \rightarrow 0} \left(\frac{d}{dz} \right)^{n-k} (z^n \Psi(z^m + \mu_1)), \\ \psi_k &= \frac{1}{(n-k)!} \lim_{z \rightarrow 0} \left(\frac{d}{dz} \right)^{n-k} (z^n \Psi(z^m + \mu_2)). \end{aligned}$$

In particular, $\varphi_n \neq 0$ and $\psi_n = 0$ since $P(s)$ and $Q(s)$ have common factor $(s - \mu_2)^{n/m}$. Note that I_3 and I_4 do not depend on θ_1 .

All in all, since $\operatorname{Re}(\mu_1) = \operatorname{Re}(\mu_2)$, the solution in Fourier space can be written as

$$\hat{w}(q, t) = C_{\exp} e^{\lambda t} + e^{\mu_1 t} \sum_{k=1}^n C_{\text{bp},k} t^{k/m-1} + O(t^{-1-1/m} e^{\operatorname{Re}(\mu_1)t}) + o(e^{\operatorname{Re}(\lambda)t}), \quad (\text{B.9})$$

$\lambda := \operatorname{argmax}\{\operatorname{Re}(s), s = s_j \in \Omega_1 \cap \Omega_2, j = 1, 2\}$. If $\operatorname{Re}(\lambda) \geq \operatorname{Re}(\mu_1)$, then the first summand is the leading order and, \hat{w} grows exponentially for $\operatorname{Re}(\lambda) > 0$ and decays exponentially for $\operatorname{Re}(\lambda) < 0$. If $\operatorname{Re}(\lambda) < \operatorname{Re}(\mu_1)$, then the second summand is the leading order and \hat{w} decays as $t^{n/m-1} e^{\mu_1 t}$ and

$$C_{bp,n} = \frac{1}{\pi} \Gamma(1 - n/m) \sin(\pi n/m) \varphi_n e^{2i(n/m-1)} \neq 0.$$

Note that if $\{s : s \in \Omega_{ca}^{cc}, D_{ca}(s, q^2) = 0, q \in \mathbb{R}\} = \emptyset$, then the decay fully depends on the second summand in (B.9).

We conclude the proof of case **cc** by considering multiple roots.

Remark B.2.1. *In case **cc**, if the poles are multiple besides μ_1, μ_2 , then $\Psi(s)$ has the form*

$$\begin{aligned} \Psi(s) &= \sum_j \sum_{l=1}^{l_j} \frac{\alpha_{jl}}{((s - \mu_1)^{1/m} - \xi_j)^l} + \sum_p \sum_{\ell=1}^{\ell_p} \frac{\beta_{p\ell}}{((s - \mu_2)^{1/m} - \eta_p)^\ell} \\ &\quad + \sum_{k=1}^n \left(\frac{\varphi_k}{(s - \mu_1)^{\frac{k}{m}}} + \frac{\psi_k}{(s - \mu_2)^{\frac{k}{m}}} \right) \\ &=: \sum_j \sum_{l=1}^{l_j} \Psi_{jl}(s) + \sum_p \sum_{\ell=1}^{\ell_p} \Psi_{p\ell}(s) + \sum_{k=1}^n (\Psi_{3k}(s) + \Psi_{4k}(s)), \end{aligned}$$

where $\sum_j l_j = \sum_p \ell_p = m - n$. For the integral along Γ we obtain

$$\begin{aligned} \frac{1}{2\pi i} \lim_{\substack{R \rightarrow \infty \\ \epsilon \rightarrow 0}} \oint_{\Gamma} \Psi_{jl}(s) e^{st} ds &= \lim_{s \rightarrow \mu_1 + \xi_j^m} \alpha_{jl} e^{st} \sum_{h=0}^{l-1} \frac{t^{l-1-h}}{h!(l-1-h)!} \left(\frac{d}{ds} \right)^h \left(\sum_{n=0}^{m-1} (s - \mu_1)^{\frac{m-n-1}{n}} \xi_j^n \right)^l \\ \frac{1}{2\pi i} \lim_{\substack{R \rightarrow \infty \\ \epsilon \rightarrow 0}} \oint_{\Gamma} \Psi_{p\ell}(s) e^{st} ds &= \lim_{s \rightarrow \mu_2 + \eta_p^m} \beta_{p\ell} e^{st} \sum_{h=0}^{\ell-1} \frac{t^{\ell-1-h}}{h!(\ell-1-h)!} \left(\frac{d}{ds} \right)^h \left(\sum_{n=0}^{m-1} (s - \mu_2)^{\frac{m-n-1}{n}} \eta_p^n \right)^\ell \end{aligned}$$

where

$$\begin{aligned} \alpha_{jl} &= \frac{1}{(l_j - l)!} \lim_{z \rightarrow \xi_j} \left(\frac{d}{dz} \right)^{l_j - l} \left((z - \xi_j)^{l_j} \Psi(z^m + \mu_1) \right) \\ \beta_{p\ell} &= \frac{1}{(\ell_p - \ell)!} \lim_{z \rightarrow \eta_p} \left(\frac{d}{dz} \right)^{\ell_p - \ell} \left((z - \eta_p)^{\ell_p} \Psi(z^m + \mu_2) \right). \end{aligned}$$

The integrals along branch cuts are given by (B.7) and (B.8) (leading order). The integrals along other paths vanish. Hence, if $\operatorname{Re}(\lambda) \geq \operatorname{Re}(\mu_1)$, then \hat{w} behaves exponentially as $t^{\rho-1} e^{\lambda t}$, where $\rho = \max\{\rho_j : j = 1, 2\}$ and ρ_j is the multiplicity of $z_j = (\lambda - \mu_j)^{1/m}$ if it is the root of polynomial $D_{ca}(z_1, z_2, q^2) = 0$. If $\operatorname{Re}(\lambda) < \operatorname{Re}(\mu_1)$, then \hat{w} decays as $t^{n/m-1} e^{\mu_1 t}$.

Remark B.2.2. *In case **nr**, the calculation is completely analogous to the case **cc**, so we omit the details of the proof.*

Appendix C

Some proofs

C.1 Proof of Lemma 2.4.18

We recall (2.44), i.e., $D_{ss}(s, q^2) = 0$. Rescaling $q = \kappa/\varepsilon$ and $s = x/\varepsilon^r$, where $0 < \varepsilon \ll 1$ and $r > 0$, substitution into (2.44) and balancing the powers of ε gives $r = 2/(1 - \delta)$. The dispersion relation becomes

$$\left(x + x_0^\delta \kappa^2 - \varepsilon^{2/(1-\delta)} a_1 \right) \left(x + x_0^\delta d\kappa^2 - \varepsilon^{2/(1-\delta)} a_4 \right) - \varepsilon^{\frac{4}{1-\delta}} a_2 a_3 = 0. \quad (\text{C.1})$$

and we seek solutions of the form

$$x = x_0 + \varepsilon^\alpha x_1 + O(\varepsilon^\beta), \quad \beta > \alpha > 0. \quad (\text{C.2})$$

Substitution into (C.1) yields the expansion $(x_0 + \varepsilon^\alpha x_1 + O(\varepsilon^\beta))^\delta = x_0^\delta + \delta x_0^{\delta-1} (\varepsilon^\alpha x_1 + O(\varepsilon^\beta)) + O(\varepsilon^{2\alpha})$ for $x_0 \neq 0$ so that ordering powers of ε gives

$$\begin{aligned} & (x_0 + x_0^\delta \kappa^2)(x_0 + x_0^\delta d\kappa^2) \\ & + \varepsilon^\alpha \left((x_0 + x_0^\delta \kappa^2)(x_1 + \delta x_0^{\delta-1} x_1 d\kappa^2) + (x_0 + x_0^\delta d\kappa^2)(x_1 + \delta x_0^{\delta-1} x_1 \kappa^2) \right) \\ & - \varepsilon^{\frac{2}{1-\delta}} \left(a_1(x_0 + x_0^\delta d\kappa^2) + a_4(x_0 + x_0^\delta \kappa^2) \right) \\ & + \varepsilon^{2\alpha} \left(x_1 + \delta x_0^{\delta-1} x_1 \kappa^2 \right) \left(x_1 + \delta x_0^{\delta-1} x_1 d\kappa^2 \right) \\ & - \varepsilon^{\alpha+\frac{2}{1-\delta}} \left(a_1(x_1 + \delta x_0^{\delta-1} x_1 d\kappa^2) + a_4(x_1 + \delta x_0^{\delta-1} x_1 \kappa^2) \right) \\ & + \varepsilon^{\frac{4}{1-\delta}} (a_1 a_4 - a_2 a_3) \\ & + O(\varepsilon^\beta)(2x_0 + x_0^\delta \kappa^2 + x_0^\delta d\kappa^2) + O(\varepsilon^{\alpha+\beta} + \varepsilon^{3\alpha}) = 0. \end{aligned}$$

Let us compare coefficients by orders of ε :

$O(1)$: $(x_0 + x_0^\delta \kappa^2)(x_0 + x_0^\delta d\kappa^2) = 0$, solutions are $x_{01} = (-\kappa^2)^{1/(1-\delta)}$ or $x_{02} = (-d\kappa^2)^{1/(1-\delta)}$.

$O(\varepsilon^\alpha)$: For $x_{01} = (-\kappa^2)^{1/(1-\delta)}$, balancing the coefficients of order $O(\varepsilon^{2/(1-\delta)})$ and $O(\varepsilon^\alpha)$ yields $\alpha = 2/(1 - \delta)$, and substituting x_{01} into the term of order $O(\varepsilon^\alpha)$ gives $x_{11} = a_1/(1 - \delta)$.

Combining the scaling $s = x/\varepsilon^r$ with the expansion (C.2) gives the approximation

$$s_{\infty 1} = (-q^2)^{1/(1-\delta)} + \frac{a_1}{1-\delta} + O(q^{\alpha-\beta}),$$

Since $\arg((-q^2)^{1/(1-\delta)}) = \pi/(1-\delta)$, the real part $\operatorname{Re}((-q^2)^{1/(1-\delta)}) < 0$ if $\pi/(1-\delta) \in (\pi/2, \pi+\theta_1)$, i.e., $\delta \in (0, \theta_1/(\pi+\theta_1))$. Hence, for any $\delta \in (0, \theta_1/(\pi+\theta_1))$, there exists $Q_1 > 0$ such that for $q > Q_1$ we have

$$\operatorname{Re}(s_{\infty 1}) = \operatorname{Re}\left(\left(-q^2\right)^{\frac{1}{1-\delta}} + \frac{a_1}{1-\delta} + O(q^{\alpha-\beta})\right) < \operatorname{Re}\left(\left(-Q_1^2\right)^{\frac{1}{1-\delta}} + \frac{a_1}{1-\delta} + 1\right) < 0. \quad (\text{C.3})$$

Similarly, for $x_{02} = (-d\kappa^2)^{1/(1-\delta)}$, the solution is given by

$$s_{\infty 2} = \left(-dq^2\right)^{\frac{1}{1-\delta}} + \frac{a_4}{1-\delta} + O(q^{\alpha-\beta}).$$

For any $\delta \in (0, \theta_1/(\pi+\theta_1))$, there exists $Q_2 > 0$ such that for $q > Q_2$ we have

$$\operatorname{Re}(s_{\infty 2}) = \operatorname{Re}\left(\left(-dq^2\right)^{\frac{1}{1-\delta}} + \frac{a_4}{1-\delta} + O(q^{\alpha-\beta})\right) < \operatorname{Re}\left(\left(-dQ_2^2\right)^{\frac{1}{1-\delta}} + \frac{a_4}{1-\delta} + 1\right) < 0. \quad (\text{C.4})$$

With $Q = \max\{Q_1, Q_2\}$ (C.3) and (C.4) both hold if $q > Q$. Finally, $\delta \in (0, \theta_1/(\pi+\theta_1))$ is the necessary condition for $s_{\infty 1}$ and $s_{\infty 2}$ to lie in Ω_0 , cf. Lemma 2.4.24.

In the case $x_0 = 0$, however, we transform the problem via $s^\delta = z \Rightarrow s = z^{1/\delta}$, and (2.44) reads

$$D_{ss}(z^{1/\delta}, q^2) = \left(z^{1/\delta} + zq^2 - a_1\right) \left(z^{1/\delta} + zdq^2 - a_4\right) - a_2a_3 = 0.$$

Rescaling $q = \kappa/\varepsilon$, $z = y/\varepsilon^\mu$, balancing the power of ε gives $\mu = 2\delta/(1-\delta)$, which leads to

$$\left(y^{1/\delta} + y\kappa^2 - \varepsilon^{2/(1-\delta)}a_1\right) \left(y^{1/\delta} + yd\kappa^2 - \varepsilon^{2/(1-\delta)}a_4\right) - \varepsilon^{4/(1-\delta)}a_2a_3 = 0 \quad (\text{C.5})$$

and we seek solutions of the form

$$y = y_0 + \varepsilon^\alpha y_1 + o(\varepsilon^\alpha). \quad (\text{C.6})$$

Substituting into (C.5), and using that the first derivative of $y^{\frac{1}{\delta}}$ exists for $y = 0$, we have

$(y_0 + \varepsilon^\alpha y_1 + o(\varepsilon^\alpha))^{1/\delta} = y_0^{1/\delta} + \frac{1}{\delta} y_0^{1/\delta-1} (\varepsilon^\alpha y_1 + o(\varepsilon^\alpha)) + o(\varepsilon^\alpha)$, which yields

$$\begin{aligned} & \left(y_0^{\frac{1}{\delta}} + y_0 \kappa^2 \right) \left(y_0^{\frac{1}{\delta}} + y_0 d \kappa^2 \right) \\ & + \varepsilon^\alpha \left(\left(y_0^{\frac{1}{\delta}} + y_0 \kappa^2 \right) \left(\frac{1}{\delta} y_0^{\frac{1}{\delta}-1} y_1 + y_1 d \kappa^2 \right) + \left(y_0^{\frac{1}{\delta}} + y_0 d \kappa^2 \right) \left(\frac{1}{\delta} y_0^{\frac{1}{\delta}-1} y_1 + y_1 \kappa^2 \right) \right) \\ & - \varepsilon^{\frac{2}{1-\delta}} \left(a_1 \left(y_0^{\frac{1}{\delta}} + y_0 d \kappa^2 \right) + a_4 \left(y_0^{\frac{1}{\delta}} + y_0 \kappa^2 \right) \right) \\ & + \varepsilon^{2\alpha} \left(\frac{1}{\delta} y_0^{\frac{1}{\delta}-1} y_1 + y_1 \kappa^2 \right) \left(\frac{1}{\delta} y_0^{\frac{1}{\delta}-1} y_1 + y_1 d \kappa^2 \right) \\ & - \varepsilon^{\alpha+\frac{2}{1-\delta}} \left(a_1 \left(\frac{1}{\delta} y_0^{\frac{1}{\delta}-1} y_1 + y_1 d \kappa^2 \right) + a_4 \left(\frac{1}{\delta} y_0^{\frac{1}{\delta}-1} y_1 + y_1 \kappa^2 \right) \right) \\ & + \varepsilon^{\frac{4}{1-\delta}} (a_1 a_4 - a_2 a_3) \\ & + o(\varepsilon^\alpha) \left(2 y_0^{\frac{1}{\delta}} + y_0 \kappa^2 + y_0 d \kappa^2 \right) + o(\varepsilon^{2\alpha}) + o(\varepsilon^{\alpha+\frac{2}{1-\delta}}) = 0. \end{aligned}$$

In the present case of $x_0 = 0$ we have $y_0 = 0$, so the coefficients of order $O(1)$, $O(\varepsilon^\alpha)$ and $O(\varepsilon^{2/(1-\delta)})$ vanish.

$O(\varepsilon^{2\alpha})$: Balancing the coefficients of order $\varepsilon^{2\alpha}$, $\varepsilon^{\alpha+2/(1-\delta)}$ and $\varepsilon^{4/(1-\delta)}$ yields $\alpha = 2/(1-\delta)$, and combining the coefficients gives

$$d \kappa^4 y_1^2 - (a_1 d \kappa^2 + a_4 \kappa^2) y_1 + a_1 a_4 - a_2 a_3 = 0,$$

which has some roots $y_{1\pm}$. Combining $s = z^{1/\delta}$, $z = y/\varepsilon^\mu$ and (C.6) gives the solution

$$s_{0\pm} = z^{1/\delta} = (y/\varepsilon^\mu)^{1/\delta} = \varepsilon^{2/\delta} y_{1\pm}^{1/\delta} + o(\varepsilon^{2/\delta}).$$

Hence, $\lim_{\varepsilon \rightarrow 0} s_{0\pm} = 0$, which implies that $\lim_{|q| \rightarrow \infty} s_{0\pm}(q) = 0$.

This completes proof of Lemma 2.4.18.

C.2 Proof of Proposition 2.4.22

We prove Proposition 2.4.22 by the following series of lemmas. In summary, Lemma C.2.1 and Lemma C.2.2 give the stability threshold d_δ^∞ ; Lemma C.2.1, Lemma C.2.3 and Lemma C.2.5 give the existence threshold \tilde{d}_δ^∞ .

We recall $\zeta := 4d(a_1 a_4 - a_2 a_3) - (a_1 d + a_4)^2$, $b := a_1 d + a_4$, $y_{1\pm} = (b \pm i\sqrt{\zeta})/(2d) =: \rho e^{\pm i\theta}$.

Note $P_{\min} > 0$ implies $\zeta > 0$.

We make a case distinction in terms of the sign of b .

Case $b > 0$, i.e., $d > -\frac{a_4}{a_1}$.

Lemma C.2.1. *For any $\delta \in (0, \frac{\pi}{2(\pi+\theta_1)})$, there exists a $Q > 0$ such that for any $|q| > Q$ we have $s_{0+}(q) \in \Omega_0^-$ if $\tilde{d}_{\delta+}^\infty < d < d_\delta^\infty$, whereas $s_{0\pm}(q) \notin \Omega_0$ if $-\frac{a_4}{a_1} < d < \tilde{d}_{\delta+}^\infty$, with $\tilde{d}_{\delta+}^\infty$ the larger root of (2.53).*

Proof. $\operatorname{Re}(y_{1+}^{1/\delta}) < 0$ if $\arg(y_{1+}^{1/\delta}) = \frac{\theta}{\delta} \in (\frac{\pi}{2}, \pi + \theta_1)$. We remark that we do not discuss $y_{1-}^{1/\delta}$ here, since $y_{1+}^{1/\delta}$ and $y_{1-}^{1/\delta}$ are complex conjugate, $\arg(y_{1-}^{1/\delta}) = -\arg(y_{1+}^{1/\delta}) \in (-\pi - \theta_1, -\pi/2)$, which means if $y_{1-}^{1/\delta} \in \Omega_0$ then $y_{1+}^{1/\delta} \in \Omega_0$, but not vice versa, and if $y_{1+}^{1/\delta} \notin \Omega_0$, then $y_{1-}^{1/\delta} \notin \Omega_0$.

We consider $(\frac{\pi\delta}{2}, (\pi + \theta_1)\delta) \subset (0, \frac{\pi}{2})$, i.e., $\delta < \frac{\pi}{2(\pi + \theta_1)}$. The condition $\frac{\theta}{\delta} \in (\frac{\pi}{2}, \pi + \theta_1)$ leads to $\arctan(\sqrt{\zeta}/b) \in (\pi\delta/2, (\pi + \theta_1)\delta)$ which yields

$$b^2 \tan^2(\pi\delta/2) < \zeta < b^2 \tan^2((\pi + \theta_1)\delta).$$

Using $c := \cos^2(\pi\delta/2)$, $\tilde{c} := \cos^2((\pi + \theta_1)\delta)$, these two inequalities can be written as

$$H(d) := a_1^2 d^2 + (4c(a_2 a_3 - a_1 a_4) + 2a_1 a_4)d + a_4^2 < 0, \quad (\text{C.7})$$

$$\tilde{H}(d) := a_1^2 d^2 + (4\tilde{c}(a_2 a_3 - a_1 a_4) + 2a_1 a_4)d + a_4^2 > 0. \quad (\text{C.8})$$

With d_- from the proof of Lemma 2.4.21, the solutions of (C.7) are $d \in (d_-, d_\delta^\infty)$ and the solutions of (C.8) are $d > \tilde{d}_{\delta+}^\infty$; here we omit $d < \tilde{d}_{\delta-}^\infty$ as in the proof of Lemma 2.4.21. Using $\tilde{d}_{\delta+}^\infty > -\frac{a_4}{a_1}$, combining these solutions gives $\tilde{d}_{\delta+}^\infty < d < d_\delta^\infty$.

Whereas, $y_{1+} \notin \Sigma_0$ if $\theta \notin (\pi\delta/2, (\pi + \theta_1)\delta)$ so we infer $\theta > (\pi + \theta_1)\delta$. Since $\arg(y_{1+}) = \arctan(\sqrt{\zeta}/b)$, we have $\arctan(\sqrt{\zeta}/b) > (\pi + \theta_1)\delta$, which implies $\tilde{d}_{\delta-}^\infty < d < \tilde{d}_{\delta+}^\infty \Rightarrow -\frac{a_4}{a_1} < d < \tilde{d}_{\delta+}^\infty$. \square

Lemma C.2.2. *For any $\delta \in [\frac{\pi}{2(\pi + \theta_1)}, 1)$, there exists a $Q > 0$ such that for any $|q| > Q$ we have $s_{0+}(q) \in \Omega_0^-$ if $-\frac{a_4}{a_1} < d < d_\delta^\infty$.*

Proof. Since $b > 0$, we have $\theta = \arctan(\sqrt{\zeta}/b) < \pi/2$. In combination with the assumption $\theta \in (\pi\delta/2, (\pi + \theta_1)\delta)$, we get $\theta \in (\pi\delta/2, \pi/2) \Rightarrow \arctan(\sqrt{\zeta}/b) \in (\pi\delta/2, \pi/2)$ which yields

$$\zeta^2 > b^2 \tan^2(\pi\delta/2).$$

Hence

$$H(d) = a_1^2 d^2 + (2a_1 a_4 + 4c(a_2 a_3 - a_1 a_4))d + a_4^2 < 0,$$

The solution is $d_- < d < d_\delta^\infty$. Note $d_- < -\frac{a_4}{a_1}$, thus we have $-\frac{a_4}{a_1} < d < d_\delta^\infty$. \square

Case $b < 0$, i.e., $d < -\frac{a_4}{a_1}$

Lemma C.2.3. *In each of the following, for any δ in the given interval there exists a $Q > 0$ such that for any $|q| > Q$ the given statement holds.*

(1) For $[\frac{\pi}{\pi + \theta_1}, 1)$ we have $s_{0+}(q) \in \Omega_0^-$ if $d < -\frac{a_4}{a_1}$;

(2) For $(0, \frac{\pi}{2(\pi + \theta_1)})$ we have $s_{0\pm}(q) \notin \Omega_0$ if $d < -\frac{a_4}{a_1}$;

(3) For $(\frac{\pi}{2(\pi + \theta_1)}, \frac{\pi}{\pi + \theta_1})$ we have $s_{0\pm}(q) \notin \Omega_0$ if $d < \tilde{d}_{\delta-}^\infty$, and $s_{0+}(q) \in \Omega_0^-$ if $\tilde{d}_{\delta-}^\infty < d < -\frac{a_4}{a_1}$, where $\tilde{d}_{\delta-}^\infty$ is the smaller root of (2.53).

Proof. Since $b < 0$, if $y_{1-} \in \Sigma_0$, then $y_{1+} \in \Sigma_0$, but not vice versa, and if $y_{1+} \notin \Sigma_0$, then $y_{1-} \notin \Sigma_0$. Hence we only consider y_{1+} . It is straightforward that $\arg(y_{1+}) \in (\frac{\pi}{2}, \pi)$, so $\arg(y_{1+}^{1/\delta}) \in (\frac{\pi}{2\delta}, \frac{\pi}{\delta})$.

First, $y_{1+}^{1/\delta} \in \Omega_0$ if $(\frac{\pi}{2\delta}, \frac{\pi}{\delta}) \subseteq (-\pi + \theta_1, \pi + \theta_1) \Rightarrow \delta \geq \frac{\pi}{\pi + \theta_1}$. From $\delta \in [\frac{\pi}{\pi + \theta_1}, 1)$ we have $\arg(y_{1+}^{1/\delta}) \in (\frac{\pi}{2\delta}, \frac{\pi}{\delta}) \subset (\frac{\pi}{2}, \pi + \theta_1)$, which means $\operatorname{Re}(y_{1+}^{1/\delta}) < 0$ if $\delta \in [\frac{\pi}{\pi + \theta_1}, 1)$.

Second, $y_{1+}^{1/\delta} \notin \Omega_0$ if $\frac{\pi}{\delta} \leq -\pi + \theta_1$ or $\frac{\pi}{2\delta} \geq \pi + \theta_1$, so we have $\delta \leq \frac{\pi}{2(\pi + \theta_1)}$, which means $y_{1+}^{1/\delta} \notin \Omega_0$ if $\delta \in (0, \frac{\pi}{2(\pi + \theta_1)})$.

Next, we consider the case $\delta \in (\frac{\pi}{2(\pi + \theta_1)}, \frac{\pi}{\pi + \theta_1})$: $y_{1+} \notin \Sigma_0$ if $\arg(y_{1+}) \notin ((-\pi + \theta_1)\delta, (\pi + \theta_1)\delta)$. Since $b < 0$, $\operatorname{Re}(y_{1+}) < 0$ we infer $\arg(y_{1+}) \in ((\pi + \theta_1)\delta, \pi)$. From the assumption $\delta \in (\frac{\pi}{2(\pi + \theta_1)}, \frac{\pi}{\pi + \theta_1})$ we have $(\pi + \theta_1)\delta \in (\frac{\pi}{2}, \pi)$, so $\arg(y_{1+}) \in (\frac{\pi}{2}, \pi)$. Now $\arg(y_{1+}) = \arctan(\sqrt{\zeta}/b) + \pi > (\pi + \theta_1)\delta \Rightarrow \sqrt{\zeta}/b > \tan((\pi + \theta_1)\delta - \pi) = \tan((\pi + \theta_1)\delta) \Rightarrow \zeta < b^2 \tan^2((\pi + \theta_1)\delta)$. The solution is $d < \tilde{d}_{\delta-}^\infty$ or $d > \tilde{d}_{\delta+}^\infty$ (omit, because $\tilde{d}_{\delta+}^\infty > -\frac{a_4}{a_1}$). That means $y_{1+} \notin \Sigma_0$ if $d < \tilde{d}_{\delta-}^\infty$. Whereas $y_{1+} \in \Sigma$ if $\arg(y_{1+}) \in (\frac{\pi}{2}, (\pi + \theta_1)\delta) \Rightarrow \zeta > b^2 \tan^2((\pi + \theta_1)\delta)$, the solutions of the latter are $\tilde{d}_{\delta-}^\infty < d < \tilde{d}_{\delta+}^\infty \Rightarrow \tilde{d}_{\delta-}^\infty < d < -\frac{a_4}{a_1}$. \square

Remark C.2.4. When $\delta = \frac{\pi}{\pi + \theta_1}$, $\tilde{c} = \cos^2(\pi) = 1$, which leads to $\tilde{H}(d) = F(d)$. Therefore the solutions to $\tilde{H}(d) = 0$ and $F(d) = 0$ are equivalent, i.e., $\tilde{d}_{\delta-}^\infty = d_{fr-}$. Hence, the first statement in Lemma C.2.3 implies Case 1b of Section 2.4.4.

Case $b = 0$, i.e., $d = -\frac{a_4}{a_1}$, we have the following lemma.

Lemma C.2.5. For any $\delta \in (\frac{\pi}{2(\pi + \theta_1)}, 1)$, there exists a $Q > 0$ such that for any $|q| > Q$ we have $s_{0+}(q) \in \Omega_0^-$ if $d = -\frac{a_4}{a_1}$, and for any $\delta \in (0, \frac{\pi}{2(\pi + \theta_1)})$, $s_{0\pm}(q) \notin \Omega_0$ if $d = -\frac{a_4}{a_1}$.

Proof. Assume that $d = -\frac{a_4}{a_1}$, i.e., $b = 0$, then $\operatorname{Re}(y_{1\pm}) = 0$ and $\arg(y_{1\pm}) = \pm\pi/2$ so that again it suffices to consider y_{1+} . $y_{1+}^{1/\delta} \in \Omega_0$ if $\frac{\pi}{2\delta} \in (-\pi + \theta_1, \pi + \theta_1) \Rightarrow \delta > \frac{\pi}{2(\pi + \theta_1)}$, i.e., $\delta \in (\frac{\pi}{2(\pi + \theta_1)}, 1)$, which leads to $\arg(y_{1+}^{1/\delta}) = \frac{\pi}{2\delta} \in (\frac{\pi}{2}, \pi + \theta_1)$ and implies $\operatorname{Re}(y_{1+}^{1/\delta}) < 0$.

When $\delta \in (0, \frac{\pi}{2(\pi + \theta_1)})$, $\max((\pi + \theta_1)\delta) = \pi/2$. Hence the argument of Σ_0 is less than $\pi/2$, whereas $\arg(y_{1+}) = \pi/2$, so $y_{1+}^{1/\delta} \notin \Omega_0$. \square

Appendix D

Existence of stripes

Writing the nonlinear part as $F(u) := Q[u, u] + K[u, u, u]$ we seek wave trains as steady states, i.e. solutions to

$$\Phi(u, \mu) := \mathcal{L}_\mu u + F(u) = 0 \quad (\text{D.1})$$

with $\Phi : (\mathcal{H}_{\text{per}}^2)^2 \times \Lambda \rightarrow (\mathcal{L}^2)^2$ on the Sobolev- and Lebesgue-spaces $(\mathcal{H}_{\text{per}}^2)^2$ to $(\mathcal{L}^2)^2$ with normalised inner product $\langle u, v \rangle_{\mathcal{L}^2} = \frac{1}{2\pi} \int_0^{2\pi} u\bar{v} dx$. It is well-known that the realisation $\mathcal{L}_\mu : (\mathcal{H}_{\text{per}}^2)^2 \rightarrow (\mathcal{L}^2)^2$ is a bounded Fredholm operator with index zero. Therefore, all solutions to (D.1) which bifurcate from $\mu = 0$ can be fully determined by Lyapunov-Schmidt reduction.

By assumption, \mathcal{L}_0 has a two-dimensional kernel spanned by $e_0(x) = E_0 e^{ix}$ and its complex conjugate, where E_0 is the eigenvector in the kernel of $\hat{\mathcal{L}}_0 = -\mathbf{k}_c^2 D + L$. Let \mathcal{L}_0^* be the adjoint operator of \mathcal{L}_0 equipped with inner product $\langle \cdot, \cdot \rangle_{\mathcal{L}^2}$, and thus \mathcal{L}_0^* has a kernel spanned by $e_0^*(x) = E_0^* e^{ix}$ and its complex conjugate. Having in mind the scaled inner products, we choose the normalisation $\langle e_0, e_0^* \rangle = 1$ and $\langle e_0, e_0 \rangle = 1$, i.e., $\langle E_0, E_0^* \rangle = 1$ and $\langle E_0, E_0 \rangle = 1$ (cf. Remark 3.2.5).

By Fredholm properties there exists closed subspaces $X \subset (\mathcal{H}_{\text{per}}^2)^2$ and $Y \subset (\mathcal{L}^2)^2$ such that

$$(\mathcal{H}_{\text{per}}^2)^2 = \ker \mathcal{L}_0 \oplus X, \quad (\mathcal{L}^2)^2 = Y \oplus \text{range } \mathcal{L}_0.$$

Hence for each $u \in (\mathcal{H}_{\text{per}}^2)^2$, there exists unique $v \in \ker \mathcal{L}_0$ and $w \in X$ such that $u = v + w$. With the projection $P_h : (\mathcal{L}^2)^2 \rightarrow \text{range } \mathcal{L}_0$, equation (D.1) is equivalent to the system

$$P_h \Phi(v + w, \mu) = 0, \quad (\text{D.2})$$

$$(\text{Id} - P_h) \Phi(v + w, \mu) = 0. \quad (\text{D.3})$$

Differentiating (D.2) with respect to w at $(0, 0)$ gives $P_h \partial_w \Phi(0, 0) = P_h \mathcal{L}_0 = \mathcal{L}_0|_X : X \rightarrow \text{range } \mathcal{L}_0$ as a boundedly invertible operator. Hence, for given v (D.2) can be solved by the implicit function theorem in terms of a smooth function $W : \ker \mathcal{L}_0 \times \Lambda \rightarrow Y$ with $W(0, 0) = 0$, $\partial_v W(0, 0) = 0$ as

$$w = W(v, \mu), \quad (\text{D.4})$$

satisfying $P_h\Phi(v + W(v, \mu), \mu) = 0$. Substituting (D.4) into (D.3) yields the bifurcation equation

$$\phi(v, \mu) := (\text{Id} - P_h)\Phi(v + W(v, \mu), \mu) = 0,$$

with $\phi : \ker \mathcal{L}_0 \times \Lambda \rightarrow Y$. Since $\text{range } \mathcal{L}_0 \cap \ker \mathcal{L}_0 = \{0\}$ and we are in Hilbert spaces, we can choose

$$X = \text{range } \mathcal{L}_0 \cap (\mathbf{H}_{\text{per}}^2)^2, \quad Y = \ker \mathcal{L}_0^* = (\text{range } \mathcal{L}_0)^\perp,$$

where the adjoint \mathcal{L}_0^* has a kernel spanned by $e_0^*(x) = E_0^* e^{ix}$ and its complex conjugate. Hence, it is natural to write the projection as $P_h = \text{Id} - P$ with

$$Pu = \langle u, e_0^* \rangle e_0 + \langle u, \overline{e_0^*} \rangle \overline{e_0},$$

which equally is a projection for the splitting $u = v + w$, when constrained to $(\mathbf{H}_{\text{per}}^2)^2$. With some abuse, we use the same notation for inner products in L^2 and \mathbb{C}^2 as it is clear from the context what is meant. Note that $\langle P\Phi, e_0^* \rangle = \langle \Phi, e_0^* \rangle$ since $\langle P_h\Phi, e_0^* \rangle = 0$ for solutions.

Writing $v = Ae_0 + \overline{Ae_0}$ the bifurcation equation can be cast as

$$g(A, \overline{A}, \mu) := \langle \phi(Ae_0 + \overline{Ae_0}, \mu), e_0^* \rangle = 0 \quad (\text{D.5})$$

with $g : \mathbb{C} \times \mathbb{C} \times \Lambda \rightarrow \mathbb{R}$ which we next expand in order to expand solutions. Using (D.1) and $P\mathcal{L}_0 = 0$ gives

$$g(A, \overline{A}, \mu) = \langle (\mathcal{L}_\mu - \mathcal{L}_0)v, e_0^* \rangle + \langle (\mathcal{L}_\mu - \mathcal{L}_0)W, e_0^* \rangle + \langle F(v + W), e_0^* \rangle \quad (\text{D.6})$$

Let us first consider the last term that includes F . While E_0, E_0^* are real, we show the complex conjugate to highlight the origin of terms. It is a priori clear from the construction that $W = O(|v||\mu|) = O(|A||\mu|)$, cf. (D.10) for the details a posteriori. For $u = Ae_0 + \overline{Ae_0} + W$ we then readily compute

$$\langle K[u, u, u], e_0^* \rangle = 3A|A|^2k_0 + O(|A|^3(|\mu| + A^2)), \quad (\text{D.7})$$

where $k_0 = \langle K[E_0, E_0, \overline{E_0}], E_0^* \rangle$, and we used that orthogonality of Fourier modes removes even powers of v , i.e., even powers of A .

The more involved $\langle Q[u, u], e_0^* \rangle$ analogously gives

$$2A\langle Q[e_0, W], e_0^* \rangle + 2A\langle Q[\overline{e_0}, W], e_0^* \rangle + O(A^2(|\mu|^2 + A^2)), \quad (\text{D.8})$$

which requires expanding $W = W(A, \overline{A}, \mu)$ through (D.2), i.e., the fixed point equation $P_h\mathcal{L}_\mu W = G(W, A, \overline{A}, \mu)$ with

$$G(W, A, \overline{A}, \mu) := -P_h F(v + W) - P_h(\mathcal{L}_\mu - \mathcal{L}_0)v, \quad (\text{D.9})$$

where $v = Ae_0 + \overline{Ae_0}$ and

$$\mathcal{L}_\mu - \mathcal{L}_0 = (2\mathbf{k}_c\tilde{\kappa} + \tilde{\kappa}^2)D\partial_x^2 + \check{\alpha}M + \beta(\mathbf{k}_c + \tilde{\kappa})B\partial_x.$$

Using $\partial_v G(0) = \partial_W G(0)$ this expansion gives $\partial_A W(0) = \partial_{\bar{A}} W(0) = 0$ and, cf. (3.7),

$$\begin{aligned}\partial_{AA} W(0) &= -2(-4\mathbf{k}_c^2 D + A)^{-1} Q[E_0, E_0] = Q_2, \\ \partial_{A\bar{A}} W(0) &= -2A^{-1} Q[\bar{E}_0, E_0] = Q_0, \\ \mathcal{L}_0 \partial_{A\check{\alpha}} W(0) &= -P_h M e_0, \\ \mathcal{L}_0 \partial_{A\beta} W(0) &= -\mathbf{k}_c P_h B \partial_x e_0 = -i\mathbf{k}_c P_h B e_0, \\ \mathcal{L}_0 \partial_{A\tilde{\kappa}} W(0) &= -2\mathbf{k}_c P_h D \partial_x^2 e_0 = 2\mathbf{k}_c P_h D e_0, \\ \mathcal{L}_0 \partial_{A\beta\beta} W(0) &= -2\mathbf{k}_c P_h B \partial_x \partial_{A\beta} W(0),\end{aligned}$$

so that, looking at the Fourier modes,

$$\partial_{A\beta} W(0) = i w_{A\beta} e^{ix}, \quad \partial_{A\tilde{\kappa}} W(0) = w_{A\tilde{\kappa}} e^{ix}, \quad \partial_{A\check{\alpha}} W(0) = w_{A\check{\alpha}} e^{ix}, \quad \partial_{A\beta\beta} W(0) = w_{A\beta\beta} e^{ix}.$$

Furthermore $w_{A\beta}$, $w_{A\tilde{\kappa}}$ and $w_{A\check{\alpha}}$ satisfy, cf. (3.7),

$$\begin{aligned}(-\mathbf{k}_c^2 D + A) w_{A\check{\alpha}} &= (\langle M E_0, E_0^* \rangle - M) E_0, \\ (-\mathbf{k}_c^2 D + A) w_{A\beta} &= \mathbf{k}_c (\langle B E_0, E_0^* \rangle - B) E_0, \\ (-\mathbf{k}_c^2 D + A) w_{A\tilde{\kappa}} &= 2\mathbf{k}_c D E_0, \\ (-\mathbf{k}_c^2 D + A) w_{A\beta\beta} &= 2\mathbf{k}_c (B w_{A\beta} - \langle B w_{A\beta}, E_0^* \rangle) E_0,\end{aligned}$$

where we used $\langle D E_0, E_0^* \rangle = 0$, which follows from a direct computation with the conditions in Remark 3.2.3. Note that for $M = \text{Id}$ we have $w_{A\check{\alpha}} = 0$ and in fact W is independent of $\check{\alpha}$.

Assembling terms, we obtain

$$\begin{aligned}W(A, \bar{A}, \mu) &= i\beta w_{A\beta} (A e^{ix} - \bar{A} e^{-ix}) + (\tilde{\kappa} w_{A\tilde{\kappa}} + \check{\alpha} w_{A\check{\alpha}} + \beta^2 w_{A\beta\beta}) (A e^{ix} + \bar{A} e^{-ix}) \\ &\quad + \frac{1}{2} Q_2 \left(A^2 e^{2ix} + \bar{A}^2 e^{-2ix} \right) + A \bar{A} Q_0 + \mathcal{R},\end{aligned}\tag{D.10}$$

where $\mathcal{R} = O(|A|(A^2 + \tilde{\kappa}^2 + |\beta\tilde{\kappa}| + |\beta|^3 + a_M \check{\alpha}^2))$; recall $a_M = 0$ if $M = \text{Id}$ and $a_M = 1$ otherwise. Notably, the terms of order $|A\beta\tilde{\kappa}|$ are not relevant to the large-wavelength stability of stripes, so we put them in the remainder. By translation symmetry we can shift x to $x + a$, which gives A replaced by $A e^{ia}$ so that without loss of generality A is real. This gives (3.10).

The bifurcation equation (D.5) gives (3.8) through its real part divided by A . The velocity equation (3.9) stems from rearranging the imaginary part divided by βA . The latter is natural since imaginary terms arise from odd powers of ∂_x , which come with odd power of β . In order to separate resolved parts, that will be leading order for later purposes, and remainder terms in (3.8), (3.9), we substitute (D.10) into (D.6), where the third summand is (D.7) plus (D.8). In (D.8) only Fourier modes e^{irx} of W with $r = 0$ or $r = 2$ are nonzero. The case $r = 0$ stems only from products that have $A^j \bar{A}^j$, $j \geq 2$ as the order in A since $j = 0, 1$ are resolved terms; the case $r = 2$ has $A^{j+2} \bar{A}^j$, $j \geq 1$. Hence, terms in (D.8) that stem from \mathcal{R} are order A^4 ; from (D.7) this is order A^5 . The second summand of (D.6) is nonzero for linear terms in A only, which contribute

to higher order terms in $\tilde{\lambda}(\mu)$ as discussed below. Hence, the relevant remainder term from (D.6) is order A^4 .

The remainder term in (3.8) and (3.9) has this order divided by A , i.e., $O(A^3)$. This is also the order of the contribution of \mathcal{R} to the remainder term in (3.9); here we note that real parts turn imaginary in (D.6) only through application of $\beta \mathbf{k}_c B \partial_x$ thus gaining a power of β .

The part of (D.5) that is resolved in (3.8), (3.9) arises upon substituting the resolved terms of (D.10) into (D.8), and further into (D.6); here (D.7) directly enters. Noting cancellation due to the Fourier modes and dividing out the trivial solution $A = 0$ we obtain

$$\partial_A g(0; \mu) + \rho_{\text{nl}} A^2, \quad (\text{D.11})$$

and its complex conjugate. On the one hand, for $F = 0$ the bifurcation equation is linear in A and determines when \mathcal{L}_μ has a kernel, which means there is a smooth function $r(\mu)$ such that

$$\partial_A g(0; \mu) = \tilde{\lambda}(\mu) = r(\mu) \lambda_\mu,$$

with λ_μ the critical eigenvalue from (3.5) and $r(0) \neq 0$. Expanding r we thus have

$$\tilde{\lambda}(\mu) = r(0) \lambda_\mu + \mathcal{R}_3, \quad O(\mathcal{R}_3) = O(|\mu| |\lambda_\mu|)$$

and we can determine the expansion of $\tilde{\lambda}$ from

$$\begin{aligned} \partial_A g(0; \mu) &= \langle (\mathcal{L}_\mu - \mathcal{L}_0)(\text{Id} + \partial_\mu \partial_v W \mu + O(|\mu|^2)) e_0, e_0^* \rangle \\ &= \langle (\mathcal{L}_\mu - \mathcal{L}_0) e_0, e_0^* \rangle + \langle (\mathcal{L}_\mu - \mathcal{L}_0) \partial_\mu \partial_v W \mu + O(|\mu|^2) e_0, e_0^* \rangle. \end{aligned}$$

In particular, $\partial_\alpha \tilde{\lambda}(0) = \langle M E_0, E_0^* \rangle$ which equals λ_M by a direct computation so that $r(0) = 1$. Moreover, the real part of (D.11) gives (3.8) and solving the imaginary part divided by β for c gives (3.9) when including the remainder terms discussed before. In particular, $r(0) = 1$ yields (3.11) by comparing the other coefficients, and $\langle B E_0, E_0^* \rangle|_{\mu=0} = 0$.

Appendix E

Stability of stripes

E.1 Spectrum for zigzag instability

From (3.23) the critical spectrum is given by

$$\lambda_{zz} = -\kappa^2 \langle DV_0, V_0^* \rangle \ell^2 + O(\ell^4).$$

We may choose $V_0 = \partial_x U_s = O(|A|)$. Expanding $\mathcal{T}_0^* V_0^* = 0$ analogous to the computation of U_s gives

$$\begin{aligned} V_0 &= -2A \left((E_0 + \tilde{\kappa}w_{A\tilde{\kappa}} + \check{\alpha}w_{A\check{\alpha}} + \beta^2 w_{A\beta\beta}) \sin(x) + \beta w_{A\beta} \cos(x) \right. \\ &\quad \left. + A Q_2 \sin(2x) + O(\mathcal{R}/|A|) \right), \\ V_0^* &= -A^* \left((E_0^* + \tilde{\kappa}w_{A\tilde{\kappa}}^* + \check{\alpha}w_{A\check{\alpha}}^* + \beta^2 w_{A\beta\beta}^*) \sin(x) - \beta w_{A\beta}^* \cos(x) \right. \\ &\quad \left. + A Q_2^* \sin(2x) + O(\mathcal{R}/|A|) \right), \end{aligned}$$

where

$$\begin{aligned} w_{A\tilde{\kappa}}^* &= 2\mathbf{k}_c(-\mathbf{k}_c^2 D + A^T)^{-1} D E_0^*, \\ w_{A\beta}^* &= \mathbf{k}_c(-\mathbf{k}_c^2 D + A^T)^{-1} (\langle BE_0^*, E_0 \rangle - B) E_0^*, \\ w_{A\check{\alpha}}^* &= (-\mathbf{k}_c^2 D + A^T)^{-1} (\langle M^T E_0^*, E_0 \rangle - M^T) E_0^*, \\ w_{A\beta\beta}^* &= 2\mathbf{k}_c(-\mathbf{k}_c^2 D + A^T)^{-1} (B w_{A\beta}^* - \langle B w_{A\beta}^*, E_0 \rangle E_0^*), \\ Q_2^* &= -2(-4\mathbf{k}_c^2 D + A^T)^{-1} Q [E_0, \cdot]^T E_0^*. \end{aligned}$$

The normalised coefficient A^* is such that $\langle V_0, V_0^* \rangle = 1$, which implies $A^* = O(|A|^{-1})$ and $AA^* = 1$ in the limit $\mu \rightarrow 0$ since $\langle V_0, V_0^* \rangle|_{\mu=0} = AA^*|_{\mu=0} \langle E_0, E_0^* \rangle = 1$. By straightforward

calculation and using $\langle DE_0, E_0^* \rangle = 0$, we have

$$\begin{aligned} \frac{1}{AA^*} \langle DV_0, V_0^* \rangle &= \tilde{\kappa} (\langle DE_0, w_{A\tilde{\kappa}}^* \rangle + \langle Dw_{A\tilde{\kappa}}, E_0^* \rangle) \\ &\quad + \beta^2 (\langle DE_0, w_{A\beta\beta}^* \rangle + \langle Dw_{A\beta\beta}, E_0^* \rangle - \langle Dw_{A\beta}, w_{A\beta}^* \rangle) \\ &\quad + \check{\alpha} (\langle DE_0, w_{A\check{\alpha}}^* \rangle + \langle Dw_{A\check{\alpha}}, E_0^* \rangle) \\ &\quad + A^2 \langle DQ_2, Q_2^* \rangle + O(\mathcal{R}/|A|) \\ &= -\frac{\rho_{\tilde{\kappa}}}{\mathbf{k}_c} \tilde{\kappa} + \tilde{\rho}_{\beta\beta} \beta^2 + \tilde{\rho}_{\check{\alpha}} a_M \alpha + \tilde{q}_{22} A^2 + O(\mathcal{R}/|A|), \end{aligned} \quad (\text{E.1})$$

where $\langle Dw_{A\tilde{\kappa}}, E_0^* \rangle = \langle DE_0, w_{A\tilde{\kappa}}^* \rangle = -\rho_{\tilde{\kappa}}/(2\mathbf{k}_c)$. Upon substitution into λ_{zz} , expansion of κ and using the leading order of (3.8) yields the claimed result.

E.2 Spectrum for Eckhaus instability

The critical spectrum is given by

$$\lambda_{\text{eh}} = (\partial_\gamma \lambda)_0 \gamma + \frac{1}{2} (\partial_\gamma^2 \lambda)_0 \gamma^2 + O(|\gamma|^3).$$

We first compute $(\partial_\gamma \lambda)_0$, i.e., the terms in (3.22) and (3.24). Differentiating

$$\mathcal{L}_\mu U_s + Q[U_s, U_s] + K[U_s, U_s, U_s] = 0$$

with respect to $\tilde{\kappa}$ and rearranging terms yields

$$\mathcal{T}_0 \partial_{\tilde{\kappa}} U_s = -2(2\kappa D\partial_x + \beta B + \beta\kappa\partial_{\tilde{\kappa}} B)V_0. \quad (\text{E.2})$$

Hence, we can solve for $\partial_{\tilde{\kappa}} U_s$ if and only if

$$\langle (2\kappa D\partial_x + \beta B + \beta\kappa\partial_{\tilde{\kappa}} B)V_0, V_0^* \rangle = 0,$$

where $\partial_{\tilde{\kappa}} B = \partial_{\tilde{\kappa}} c \cdot \text{Id} = (\lambda_\beta - \lambda_{\tilde{\kappa}\beta})/\mathbf{k}_c \cdot \text{Id}$, cf. (3.9), so that from (3.22) we have

$$(\partial_\gamma \lambda)_0 = -i\kappa \langle \beta\kappa\partial_{\tilde{\kappa}} B V_0, V_0^* \rangle = -i\kappa^2 \beta \partial_{\tilde{\kappa}} c = i\kappa^2 \beta \frac{\lambda_{\tilde{\kappa}\beta} - \lambda_\beta}{\mathbf{k}_c}, \quad (\text{E.3})$$

and the leading order gives the imaginary part of the claimed spectrum.

Remark E.2.1. As in [10] $(\partial_\gamma \lambda)_0$ measures the correction of the phase velocity c to the group velocity c_g . Let $\omega(\kappa)$ denote the nonlinear dispersion relation so that

$$c = \frac{\omega(\kappa)}{\kappa}, \quad c_g = \frac{d\omega(\kappa)}{d\kappa}.$$

Differentiating c with respect to $\tilde{\kappa}$ gives

$$\partial_{\tilde{\kappa}} c = \frac{1}{\kappa} \frac{d\omega(\kappa)}{d\kappa} - \frac{\omega(\kappa)}{\kappa^2} = \frac{c_g - c}{\kappa},$$

and substituting into (E.3), yields

$$(\partial_\gamma \lambda)_0 = i\kappa \beta (c - c_g).$$

Hence, for $\beta \neq 0$, $0 \leq |\tilde{\kappa}| \ll 1$, we have $(\partial_\gamma \lambda)_0 = 0 \Leftrightarrow c = c_g$.

Next, we consider $(\partial_\gamma V)_0$. Due to (3.19), (3.21) and (E.2) we have

$$\begin{aligned}\mathcal{T}_0(\partial_\gamma V)_0 &= (\partial_\gamma \lambda)_0 V_0 - (\partial_\gamma \mathcal{T})_0 V_0 = (-i\kappa^2 \beta \partial_{\tilde{\kappa}} c - 2i\kappa^2 D \partial_x - i\kappa \beta B) V_0 \\ &= i\kappa \mathcal{T}_0 \partial_{\tilde{\kappa}} U_s = \mathcal{T}_0(i\kappa \partial_{\tilde{\kappa}} U_s),\end{aligned}$$

which implies that $(\partial_\gamma V)_0 - i\kappa \partial_{\tilde{\kappa}} U_s$ lies in the kernel of \mathcal{T}_0 , spanned by V_0 , and there is $a \in \mathbb{C}$ such that $(\partial_\gamma V)_0 = i\kappa \partial_{\tilde{\kappa}} U_s + aV_0$.

This term is not relevant for $(\partial_\gamma^2 \lambda)_0$ since we compute

$$\begin{aligned}(\partial_\gamma^2 \lambda)_0 &= \langle (\partial_\gamma^2 \mathcal{T})_0 V_0, V_0^* \rangle - 2 \langle ((\partial_\gamma \lambda)_0 - (\partial_\gamma \mathcal{T})_0)(\partial_\gamma V)_0, V_0^* \rangle \\ &= -2\kappa^2 \langle DV_0, V_0^* \rangle - 2 \langle ((\partial_\gamma \lambda)_0 - (\partial_\gamma \mathcal{T})_0)(i\kappa \partial_{\tilde{\kappa}} U_s + aV_0), V_0^* \rangle \\ &= -2\kappa^2 \langle DV_0, V_0^* \rangle - 2 \langle ((\partial_\gamma \lambda)_0 - (\partial_\gamma \mathcal{T})_0)(i\kappa \partial_{\tilde{\kappa}} U_s), V_0^* \rangle\end{aligned}$$

using (3.20) in the third equality. Upon substituting (E.3) and (3.21) we obtain

$$(\partial_\gamma^2 \lambda)_0 = -2\kappa^2 \langle 2\kappa D \partial_x \partial_{\tilde{\kappa}} U_s, V_0^* \rangle \quad (\text{E.4})$$

$$-2\kappa^2 \langle DV_0, V_0^* \rangle + 2\beta \frac{\kappa^3}{\mathbf{k}_c} (\lambda_{\tilde{\kappa}\beta} - \lambda_\beta) \langle \partial_{\tilde{\kappa}} U_s, V_0^* \rangle - 2\kappa^2 \beta \langle B \partial_{\tilde{\kappa}} U_s, V_0^* \rangle, \quad (\text{E.5})$$

and we will show that (E.4) is leading order. By (E.1) the first term in (E.5) is order $O(|a_M \alpha| + |\tilde{\kappa}| + \beta^2 + A^2)$, and we show the others are $O(A^{-2} \beta^2 (|\tilde{\kappa}| + |a_M \alpha|) + \beta^2)$.

Differentiating U_s with respect to $\tilde{\kappa}$ gives

$$\begin{aligned}\partial_{\tilde{\kappa}} U_s &= \partial_{\tilde{\kappa}} A \left(2(E_0 + \tilde{\kappa} w_{A\tilde{\kappa}} + \check{w}_{A\check{\kappa}} + \beta^2 w_{A\beta\beta}) \cos(x) - 2\beta w_{A\beta} \sin(x) \right) \\ &\quad + 2Aw_{A\tilde{\kappa}} \cos(x) + 2A\partial_{\tilde{\kappa}} A Q_2 \cos(2x) + 2A\partial_{\tilde{\kappa}} A Q_0 + \partial_{\tilde{\kappa}} \mathcal{R},\end{aligned}$$

with $\partial_{\tilde{\kappa}} \mathcal{R} = O(|A|(|\beta| + |\tilde{\kappa}|) + |\partial_{\tilde{\kappa}} A| \mathcal{R}/|A|)$ by differentiating the smooth remainder in (3.10). In the following we frequently omit remainder terms such as \mathcal{R} as the order of the remainder terms do not change and we are only interested in the resolved terms, which will be higher order in the application of the result. From Theorem 3.3.1,

$$A_{\tilde{\kappa}} := \partial_{\tilde{\kappa}} A = -\frac{2\rho_{\tilde{\kappa}} \tilde{\kappa} + \lambda_{M\tilde{\kappa}} a_M \alpha}{2\rho_{\text{nl}} A} = O(|A|^{-1} (|\tilde{\kappa}| + |a_M \alpha|)), \quad (\text{E.6})$$

which means

$$\begin{aligned}\langle \partial_{\tilde{\kappa}} U_s, V_0^* \rangle &= A_{\tilde{\kappa}} A^* \beta (\langle w_{A\beta}, E_0^* \rangle + \langle E_0, w_{A\beta}^* \rangle) + AA^* \beta \langle w_{A\tilde{\kappa}}, w_{A\beta}^* \rangle \\ \langle B \partial_{\tilde{\kappa}} U_s, V_0^* \rangle &= A_{\tilde{\kappa}} A^* \beta (\langle B w_{A\beta}, E_0^* \rangle + \langle BE_0, w_{A\beta}^* \rangle) + AA^* \beta \langle B w_{A\tilde{\kappa}}, w_{A\beta}^* \rangle,\end{aligned}$$

so that (E.5) is of order $O((1 + A^{-2} \beta^2) (|\tilde{\kappa}| + |a_M \alpha|) + \beta^2 + A^2)$.

As to (E.4), differentiating $\partial_{\tilde{\kappa}} U_s$ with respect to x gives (to leading order)

$$\begin{aligned}\partial_x \partial_{\tilde{\kappa}} U_s &= -2A_{\tilde{\kappa}} \left((E_0 + \tilde{\kappa} w_{A\tilde{\kappa}} + \check{w}_{A\check{\kappa}} + \beta^2 w_{A\beta\beta}) \sin(x) + \beta w_{A\beta} \cos(x) \right) \\ &\quad - 2Aw_{A\tilde{\kappa}} \sin(x) - 4AA_{\tilde{\kappa}} Q_2 \sin(2x),\end{aligned}$$

thus we have

$$\begin{aligned}
\langle D\partial_x \partial_{\tilde{\kappa}} U_s, V_0^* \rangle &= (A_{\tilde{\kappa}} A^* \tilde{\kappa} + AA^*) \langle Dw_{A\tilde{\kappa}}, E_0^* \rangle + A_{\tilde{\kappa}} A^* \tilde{\kappa} \langle DE_0, w_{A\tilde{\kappa}}^* \rangle \\
&\quad + A_{\tilde{\kappa}} A^* \check{\alpha} (\langle Dw_{A\check{\alpha}}, E_0^* \rangle + \langle DE_0, w_{A\check{\alpha}}^* \rangle) \\
&\quad + A_{\tilde{\kappa}} A^* \beta^2 (\langle Dw_{A\beta\beta}, E_0^* \rangle + \langle DE_0, w_{A\beta\beta}^* \rangle - \langle Dw_{A\beta}, w_{A\beta}^* \rangle) \\
&\quad + 2A^2 A_{\tilde{\kappa}} A^* \langle DQ_2, Q_2^* \rangle \\
&= (2A_{\tilde{\kappa}} A^{-1} \tilde{\kappa} + 1) \langle Dw_{A\tilde{\kappa}}, E_0^* \rangle + A_{\tilde{\kappa}} A^{-1} (\rho_{\check{\alpha}} a_M \alpha + \rho_{\beta\beta} \beta^2) \\
&\quad + 2A^2 A_{\tilde{\kappa}} A^* \langle DQ_2, Q_2^* \rangle. \tag{E.7}
\end{aligned}$$

Since $A^2 A_{\tilde{\kappa}} A^* = O(|\tilde{\kappa}| + |a_M \alpha|)$, it is a higher order term compared to $\langle Dw_{A\tilde{\kappa}}, E_0^* \rangle = O(1)$. Substituting (E.6), (3.7) and (3.8), (E.7) becomes

$$\begin{aligned}
\langle D\partial_x \partial_{\tilde{\kappa}} U_s, V_0^* \rangle &= \frac{\rho_{\tilde{\kappa}}}{2\mathbf{k}_c \rho_{nl}} A^{-2} \left(\alpha + \rho_{\beta} \beta^2 + 3\rho_{\tilde{\kappa}} \tilde{\kappa}^2 \right) \\
&\quad + O \left(A^{-2} (|a_M \alpha| + |\tilde{\kappa}|)(a_M \alpha + \beta^2) + |a_M \alpha| + |\tilde{\kappa}| \right)
\end{aligned}$$

Altogether, using $\kappa = \mathbf{k}_c + \tilde{\kappa}$ we have, omitting the refinement when $M = \text{Id}$,

$$\begin{aligned}
(\partial_y^2 \lambda)_0 &= -4\kappa^3 \langle D\partial_x (\partial_{\tilde{\kappa}} U_s), V_0^* \rangle \tag{E.8} \\
&\quad + O(A^{-2} (|\alpha| + |\tilde{\kappa}|)(|\alpha| + \beta^2) + |\alpha| + |\tilde{\kappa}| + \beta^2 + A^2)
\end{aligned}$$

$$= -2\mathbf{k}_c^2 \frac{\rho_{\tilde{\kappa}}}{\rho_{nl}} A^{-2} \left(\alpha + \rho_{\beta} \beta^2 + 3\rho_{\tilde{\kappa}} \tilde{\kappa}^2 + \mathcal{R}_{eh} \right) \tag{E.9}$$

which is as claimed and has remainder term

$$\mathcal{R}_{eh} = O \left(|\alpha \tilde{\kappa}| + \alpha^2 + |\alpha| \beta^2 + |\tilde{\kappa}| \beta^2 + |\tilde{\kappa}|^3 + A^2 (|\tilde{\kappa}| + |\alpha| + \beta^2 + A^2) \right). \tag{E.10}$$

Note that $A^2 |\tilde{\kappa}|$ is higher order compared to $\alpha + \rho_{\beta} \beta^2 + 3\rho_{\tilde{\kappa}} \tilde{\kappa}^2$ due to (3.12), and $|\alpha \tilde{\kappa}|$ is higher order since α behaves quadratically for any balanced order between $\alpha, \beta^2, \tilde{\kappa}^2$ which makes $|\alpha \tilde{\kappa}|$ cubic order.

E.3 Stability of 2D and 4D centre manifolds

We recall the simplified linearisation (3.34), namely

$$\begin{aligned}
\partial_u f(u_c; \mu) &= \varepsilon^2 P \left(L(\mu_2) + L(\mu_1) \Psi_{11}[\mu_1, \cdot] + 2A'^2 Q[\Psi_{20}[u_1, u_1], \cdot] \right. \\
&\quad \left. + 4A'^2 Q[u_1, \Psi_{20}[u_1, \cdot]] + 3A'^2 K[u_1, u_1, \cdot] \right) + O(\varepsilon^3). \tag{E.11}
\end{aligned}$$

The matrix L_1 is known a priori from Theorem 3.5.4, but for completeness, we derive it here directly. Setting $u_1 = 0$ gives the linearisation in the zero state so that the first two terms in the bracket generate the eigenvalue from (3.5), $\alpha' + \rho_{\beta} \beta'^2 + \rho_{\tilde{\kappa}} \tilde{\kappa}'^2$, which is of the form $-\rho_{nl} A'^2 + O(\varepsilon)$, cf. (3.8).

More specifically these contribute the diagonal 2-by-2 matrix $A_L := -\rho_{nl}\text{Id}$ to the linearisation at order ε^2 . As to the nonlinear terms, the simplest is $K[u_1, u_1, \cdot]$ and with $u_1 = (e^{ix} + e^{-ix})E_0$ we find the 2-by-2 matrix with entries generated by choosing $\sigma_1, \sigma_2 \in \{\pm 1\}$ as

$$\langle K[u_1, u_1, e^{\sigma_1 ix} E_0], e^{\sigma_2 ix} E_0^* \rangle = \frac{k_0}{|\Omega_1|} \int_{\Omega_1} (e^{2ix} + 2 + e^{-2ix}) e^{i(\sigma_1 - \sigma_2)x} dx.$$

This results in the matrix $A_K := k_0 \begin{pmatrix} 2 & 1 \\ 1 & 2 \end{pmatrix}$. The contributions from the quadratic term depend on Ψ_{20} , which can be computed from the general centre manifold characteristic equation [20]

$$\partial_u \Psi(u_c; \mu) f(u_c; \mu) = P_h(\mathcal{L}_\mu(u_c + \Psi(u_c; \mu)) + F(u_c + \Psi(u_c; \mu))),$$

which holds for all $u_c \in N$, $|u_c| \ll 1$. At the bifurcation point, i.e., $\dot{u}_c = f(u_c; \mu) = 0$, the above equation reduces to the fixed point equation [70, Eq. A.9]

$$P_h \mathcal{L}_\mu \Psi(u_c; \mu) = -P_h F(u_c + \Psi(u_c; \mu)) - P_h(\mathcal{L}_\mu - \mathcal{L}_0)u_c.$$

At order u_c^2 we find $P_h(\mathcal{L}_0 \Psi_{20} + 2Q) = 0$ on N in analogy to the expansion for [70, Eq. A.8], so that $\Psi_{20} = -2\mathcal{L}_0^{-1}Q$. This means

$$\begin{aligned} \Psi_{20}[u_1, u_1] &= \Psi_{20}[E_0, E_0](e^{2ix} + 2 + e^{-2ix}) = Q_0 + \frac{1}{2}Q_2(e^{2ix} + e^{-2ix}), \\ \Psi_{20}[u_1, ae_0 + b\bar{e}_0] &= \Psi_{20}[E_0, E_0](ae^{2ix} + a + b + b e^{-2ix}) \\ &= \frac{a}{2}(Q_0 + Q_2 e^{2ix}) + \frac{b}{2}(Q_0 + Q_2 e^{-2ix}). \end{aligned}$$

The first equation is in fact an immediate consequence of the formula for stripes and $f(u_c; \mu) = 0$. As to the matrix entries this generates, we compute for the first row

$$\begin{aligned} \langle Q[\Psi_{20}[u_1, u_1], e_0], e_0^* \rangle &= \langle Q[Q_0 + \frac{1}{2}Q_2 e^{2ix}, e_0], e_0^* \rangle = q_0 \\ \langle Q[\Psi_{20}[u_1, u_1], \bar{e}_0], e_0^* \rangle &= \langle Q[Q_0 + \frac{1}{2}Q_2 e^{2ix}, \bar{e}_0], e_0^* \rangle = \frac{1}{2}q_2, \end{aligned}$$

whose entries are reversed in the second row so we get $A_Q := \frac{1}{2} \begin{pmatrix} 2q_0 & q_2 \\ q_2 & 2q_0 \end{pmatrix}$. Analogously,

$$\begin{aligned} \langle Q[u_1, \Psi_{20}[u_1, e_0]], e_0^* \rangle &= \langle Q[e_0 + \bar{e}_0, \frac{1}{2}(Q_0 + Q_2 e^{2ix})], e_0^* \rangle = \frac{1}{2}(q_0 + q_2) \\ \langle Q[u_1, \Psi_{20}[u_1, \bar{e}_0]], e_0^* \rangle &= \langle Q[e_0 + \bar{e}_0, \frac{1}{2}(Q_0 + Q_2 e^{-2ix})], e_0^* \rangle = \frac{1}{2}q_0, \end{aligned}$$

whose entries are reversed in the second row so we get $B_Q := \frac{1}{2} \begin{pmatrix} q_0 + q_2 & q_0 \\ q_0 & q_0 + q_2 \end{pmatrix}$.

In sum, the matrix for the linearisation on the centre manifold is, as claimed,

$$\partial_u f(u_c; \mu) = \varepsilon^2 A'^2 (A_L + 3A_K + 2A_Q + 4B_Q) = A^2 \rho_{nl} \begin{pmatrix} 1 & 1 \\ 1 & 1 \end{pmatrix}.$$

The claimed block diagonal structure for the linearisation in stripes is a result of non-resonance between the arising wave vectors; the only relevant resonances away from the subblock L_1 are $\mathbf{k}_2^{\text{sq}} + \mathbf{k}_{-2}^{\text{sq}} = 0$. Casting L_{sq} as a matrix, its entries are

$$(L_{\text{sq}})_{j,\ell} = \langle \partial_u f(u_c; \mu) e_\ell, e_j^* \rangle, \quad j, \ell = \pm 1, \pm 2.$$

Being the linearisation in stripes, multiples of $\mathbf{k}_{\pm 1}^{\text{sq}}$ enter from $\partial_u f(u_c; \mu) e_{\pm 1}$, but (in the chosen ordering) off-diagonal entries give one additional wavevector \mathbf{k}_j^{sq} for $j \neq \pm 1$, and hence no resonance is possible. Therefore, the linearisation has block-diagonal form.

Concerning the subblock L_2^{sq} , analogous to L_1 , due to the lack of resonances, (3.33) simplifies to (E.11). Setting $u_1 = 0$ gives the linearisation in the trivial equilibrium to order ε^2 and the eigenvalues arise directly from the Fourier transform in y -direction, or by using (3.5) with $\beta = 0$, $\tilde{\kappa} = \tilde{\ell}$, i.e.,

$$\lambda_{\tilde{\ell}} = \alpha + \rho_{\tilde{\kappa}} \tilde{\ell}^2 + O(\varepsilon^3) \in \mathbb{R},$$

so that with (3.13) we have $\lambda_{\tilde{\ell}} = \varepsilon^2 \lambda'_{\tilde{\ell}}$. Concerning the simplest nonlinear term $K[u_1, u_1, \cdot]$. The stripes $u_1 = (e^{i\mathbf{k}_1^{\text{sq}} \cdot \mathbf{x}} + e^{-i\mathbf{k}_1^{\text{sq}} \cdot \mathbf{x}}) E_0$ yield

$$\langle K[u_1, u_1, e_\ell], e_j^* \rangle = \frac{k_0}{|\Omega_2|} \int_{\Omega_2} \left(e^{i2\mathbf{k}_1^{\text{sq}} \cdot \mathbf{x}} + 2 + e^{-i2\mathbf{k}_1^{\text{sq}} \cdot \mathbf{x}} \right) e^{i(\mathbf{k}_\ell^{\text{sq}} - \mathbf{k}_j^{\text{sq}}) \cdot \mathbf{x}} d\mathbf{x}$$

which, for $j, \ell \neq \pm 1$, gives a contribution on the diagonal $j = \ell$ only, namely $6k_0 \varepsilon^2 A'^2$.

It remains to consider the contributions from Q and the centre manifold Ψ_{20} , i.e. the terms from Corollary 3.5.3 at order ε^2 :

$$2PQ[\Psi_{20}[u_1, u_1], \cdot], \quad 4PQ[u_1, \Psi_{20}[u_1, \cdot]].$$

Since $\Psi_{20}[u_1, u_1] = \frac{1}{2} Q_2(e^{2i\mathbf{k}_1^{\text{sq}} x} + e^{-2i\mathbf{k}_1^{\text{sq}} x}) + Q_0$, for $\ell, j \neq \pm 1$ we find

$$2\langle Q[\Psi_{20}[u_1, u_1], e_\ell], e_j^* \rangle = 2q_0$$

for $j = \ell$ and zero otherwise due to non-resonance with $2\mathbf{k}_1^{\text{sq}}$.

As to $4PQ[u_1, \Psi_{20}[u_1, \cdot]]$ we first compute, since $\ell, j \in \{\pm 2\}$ and the only contribution comes from the identity in $P_h = \text{Id} - P$ that

$$\begin{aligned} \Psi_{20}[u_1, e_\ell] &= -\mathcal{L}_0^{-1} P_h Q[u_1, e_\ell] = -\mathcal{L}_0^{-1} (Q[u_1, e_\ell] - PQ[u_1, e_\ell]) \\ &= -\mathcal{L}_0^{-1} Q[E_0, E_0] e^{i(\mathbf{k}_1^{\text{sq}} + \mathbf{k}_\ell^{\text{sq}}) \cdot \mathbf{x}} \\ &= -(-2\mathbf{k}_c^2 D + L)^{-1} Q[E_0, E_0] e^{i(\mathbf{k}_1^{\text{sq}} + \mathbf{k}_\ell^{\text{sq}}) \cdot \mathbf{x}}. \end{aligned}$$

Substituting into $4PQ[u_1, \Psi_{20}[u_1, \cdot]]$ gives for $\ell = j$

$$4\langle Q[u_1, \Psi_{20}[u_1, e_\ell]], e_j^* \rangle = 8\langle Q[E_0, Q_{11}], E_0^* \rangle = 8q_{11},$$

and zero otherwise.

E.4 Stability of 6D centre manifold

The 1D subsystem is clearly an invariant subsystem (as are several others) and the form of the block L_1 follows from Theorem 3.5.4.

Analogous to Appendix E.3, the claimed block diagonal structure for the linearisation in stripes is a result of non-resonance between the arising wave vectors; the only relevant resonances away from the subblock L_1 are triads $\mathbf{k}_1 + \mathbf{k}_2 = \mathbf{k}_{-3}$. Casting L_{hex} as a matrix, its entries are

$$(L_{\text{hex}})_{j,\ell} = \langle \partial_u f(u_c; \mu) e_\ell, e_j^* \rangle, \quad j, \ell = \pm 1, \pm 2, \pm 3.$$

Being the linearisation in stripes, multiples of $k_{\pm 1}$ enter from $\partial_u f(u_c; \mu) e_{\pm 1}$, but (in the chosen ordering) off-diagonal entries give one additional wavevector k_j for $j \neq \pm 1$, and hence no triad is possible. Therefore, the linearisation has block-diagonal form.

The two equal subblocks L_2^{hex} are obtained by symmetry, and Corollary 3.5.3 gives the relevant terms at order ε and ε^2 . The only term at order ε is $2\varepsilon A' P Q[u_1, \cdot]$, which contributes through triads on the off-diagonal only as $2\varepsilon A' q$.

Setting $u_1 = 0$ gives the linearisation in the trivial equilibrium to order ε^2 and the eigenvalues are known a priori from Lemma 3.2.2, see also (3.17), and $\alpha, \tilde{\kappa}$ can be readily included analogous to (3.5); note that the coefficient of $\tilde{\kappa}$ stems from isotropic domain scaling. By choice of c and with k_j the first component of the wavevectors, these eigenvalues have the form

$$\lambda_{\mu,j} = \alpha + k_j^2 \rho_\beta \beta^2 + \rho_{\tilde{\kappa}} \tilde{\kappa}^2 + O(|A|^3) \in \mathbb{R},$$

which are all equal for $j \neq \pm 1$ ($k_2 = k_3 = 1/2$) and enter as entries of L_{hex} along the diagonal. Due to the scalings (3.13), we can write $\lambda_{\mu,j} = \varepsilon^2 \lambda'_{\mu,j}$.

We proceed analogous to Appendix E.3 with the simplest nonlinear term $K[u_1, u_1, \cdot]$. Stripes $u_1 = (e^{i\mathbf{k}_1 \cdot \mathbf{x}} + e^{-i\mathbf{k}_1 \cdot \mathbf{x}}) E_0$ yield

$$\langle K[u_1, u_1, e_\ell], e_j^* \rangle = \frac{k_0}{|\Omega_3|} \int_{\Omega_3} (e^{i2\mathbf{k}_1 \cdot \mathbf{x}} + 2 + e^{-i2\mathbf{k}_1 \cdot \mathbf{x}}) e^{i(\mathbf{k}_\ell - \mathbf{k}_j) \cdot \mathbf{x}} d\mathbf{x}$$

which, for $j, \ell \neq \pm 1$, gives a contribution on the diagonal $j = \ell$ only, namely $6k_0 \varepsilon^2 A'^2$.

It remains to consider the contributions from Q and the centre manifold via Ψ_{20}, Ψ_{11} , i.e. the five terms from Corollary 3.5.3 at order ε^2 :

$$\begin{aligned} & 2PQ[\Psi_{20}[u_1, u_1], \cdot], \quad 4PQ[u_1, \Psi_{20}[u_1, \cdot]], \quad 2PL(\mu_1)\Psi_{20}[u_1, \cdot], \\ & 2PQ[\Psi_{11}[\mu_1, u_1], \cdot], \quad 2PQ[u_1, \Psi_{11}[\mu_1, \cdot]]. \end{aligned}$$

Notably, the first two enter with a factor A'^2 , while the others only have a factor A' .

Since $\Psi_{20}[u_1, u_1] = \frac{1}{2} Q_2(e^{2i\mathbf{k}_1 \cdot \mathbf{x}} + e^{-2i\mathbf{k}_1 \cdot \mathbf{x}}) + Q_0$, for $\ell, j \neq \pm 1$ we find

$$2\langle Q[\Psi_{20}[u_1, u_1], e_\ell], e_j^* \rangle = 2q_0$$

for $j = \ell$ and zero otherwise due to non-resonance with $2\mathbf{k}_1$.

As to $4PQ[u_1, \Psi_{20}[u_1, \cdot]]$ we first compute, since $\ell, j \in \{\pm 2, \pm 3\}$ and the only contribution comes from a triad $\mathbf{k}_1 + \mathbf{k}_\ell = \mathbf{k}_{-j}$ that

$$\begin{aligned}\Psi_{20}[u_1, e_\ell] &= -\mathcal{L}_0^{-1} P_h Q[u_1, e_\ell] \\ &= -\mathcal{L}_0^{-1} (Q[E_0, E_0] e^{i(\mathbf{k}_1 + \mathbf{k}_\ell) \cdot \mathbf{x}} - \langle Q[E_0, E_0], E_0^* \rangle E_0 e^{i\mathbf{k}_j \cdot \mathbf{x}}) \\ &= -(-\mathbf{k}_c^2 D + L)^{-1} (Q[E_0, E_0] - \langle Q[E_0, E_0], E_0^* \rangle E_0) e^{i\mathbf{k}_j \cdot \mathbf{x}} = Q_1 e^{i\mathbf{k}_j \cdot \mathbf{x}},\end{aligned}$$

with Q_1 as in the theorem statement. Substitution into $4PQ[u_1, \Psi_{20}[u_1, \cdot]]$ gives

$$4\langle Q[u_1, \Psi_{20}[u_1, e_\ell]], e_j^* \rangle = 8\langle Q[E_0, Q_1], E_0^* \rangle = 8q_1,$$

for $\ell = j$, and zero otherwise.

As to the third term, triads $\mathbf{k}_1 + \mathbf{k}_\ell = \mathbf{k}_{-j}$ give the only non-trivial term

$$2\langle L(\mu_1)\Psi_{20}[u_1, e_\ell], e_j^* \rangle = 2\langle (-2\tilde{\kappa}'\mathbf{k}_c D + i\beta'\mathbf{k}_c k_\ell B)Q_1, E_0^* \rangle,$$

and its complex conjugate on the anti-diagonal of L_2 .

For the fourth term $2PQ[\Psi_{11}[\mu_1, u_1], \cdot]$, the characteristic equation of the centre manifold to order $u\mu$ gives $\mathcal{L}_0\Psi_{11} = -P_h\partial_\mu L(0)$, which means

$$\begin{aligned}\Psi_{11}[\mu_1, u_1] &= -\mathcal{L}_0^{-1}(i\beta'\mathbf{k}_c Bu_1 - 2\tilde{\kappa}'\mathbf{k}_c Du_1) \\ &= i\beta'w_{A\beta}(e^{ix} - e^{-ix}) + \tilde{\kappa}'w_{A\tilde{\kappa}}(e^{ix} + e^{-ix})\end{aligned}$$

note $PBu_1 = 0$ by choice of c and $PDu_1 = 0$ as remarked earlier. Therefore, only triads $\mathbf{k}_1 + \mathbf{k}_\ell = \mathbf{k}_{-j}$ give the nontrivial term

$$2\langle Q[\Psi_{11}[\mu_1, u_1], e_\ell], e_j^* \rangle = 2\langle Q[i\beta'w_{A\beta} + \tilde{\kappa}'w_{A\tilde{\kappa}}, E_0], E_0^* \rangle.$$

The final quadratic term is $2PQ[u_1, \Psi_{11}[\mu_1, \cdot]]$. Here, the triads $\mathbf{k}_1 + \mathbf{k}_\ell = \mathbf{k}_{-j}$ give the nontrivial term

$$2\langle Q[u_1, \Psi_{11}[\mu_1, e_\ell]], e_j^* \rangle = 2\langle Q[E_0, i\beta'k_\ell w_{A\beta} + \tilde{\kappa}'w_{A\tilde{\kappa}}], E_0^* \rangle.$$

Together with the previous two terms, the anti-diagonal terms generate $p(\mu_1)$ and its complex conjugated, i.e. the matrix $\begin{pmatrix} 0 & p(\mu_1) \\ \overline{p(\mu_1)} & 0 \end{pmatrix}$.

Bibliography

- [1] R. Balescu. Anomalous transport in turbulent plasmas and continuous time random walks. *Physical Review E*, 51:4807–4822, May 1995.
- [2] R. Bastiaansen, P. Carter, and A. Doelman. Stable planar vegetation stripe patterns on sloped terrain in dryland ecosystems. *Nonlinearity*, 32(8):2759–2814, July 2019.
- [3] B. P. Belousov. A periodic reaction and its mechanism. *Rad. Med., Medgiz, Moscow*, 147:145, 1958.
- [4] H. Bénard. Les tourbillons cellulaires dans une nappe liquide. *Rev. Gen. Sci. Pures Appl.*, 11:1261–1271, 1900.
- [5] J. J. R. Bennett and J. A. Sherratt. Large scale patterns in mussel beds: stripes or spots? *Journal of Mathematical Biology*, 78(3):815–835, Feb. 2019.
- [6] T. K. Callahan and E. Knobloch. Pattern formation in weakly anisotropic systems. In *Proceedings of the International Conference on Differential Equations (berlin, 1999)*, volume 1, pages 157–162, 2000.
- [7] R. A. Cangelosi, D. J. Wollkind, B. J. Kealy-Dichone, and I. Chaiya. Nonlinear stability analyses of Turing patterns for a mussel-algae model. *Journal of Mathematical Biology*, 70(6):1249–1294, 2015.
- [8] J. Carballido-Landeira, P. Taboada, and A. P. Muñozuri. Effect of electric field on Turing patterns in a microemulsion. *Soft Matter*, 8:2945–2949, 2012.
- [9] V. Deblauwe, P. Coulteron, J. Bogaert, and N. Barbier. Determinants and dynamics of banded vegetation pattern migration in arid climates. *Ecological Monographs*, 82(1):3–21, 2012.
- [10] A. Doelman, B. Sandstede, A. Scheel, and G. Schneider. *The Dynamics of Modulated Wave Trains*. Memoirs of the American Mathematical Society, 2009.
- [11] W. S. Edwards and S. Fauve. Parametrically excited quasicrystalline surface waves. *Physical Review E*, 47:R788–R791, Feb. 1993.

- [12] L. C. Evans. *Partial Differential Equations*, volume 19. American Mathematical Society, 2nd edition, 2010.
- [13] M. Faraday. XVII. On a peculiar class of acoustical figures; and on certain forms assumed by groups of particles upon vibrating elastic surfaces. *Philosophical transactions of the Royal Society of London*, (121):299–340, 1831.
- [14] S. Fedotov. Non-Markovian random walks and nonlinear reactions: Subdiffusion and propagating fronts. *Physical Review E*, 81(1):011117, 2010.
- [15] W. Feller. *An Introduction to Probability Theory and Its Applications*, volume 2. John Wiley & Sons, 2008.
- [16] V. V. Gafiychuk and B. Y. Datsko. Pattern formation in a fractional reaction–diffusion system. *Physica A: Statistical Mechanics and its Applications*, 365(2):300–306, 2006.
- [17] R. Goh and A. Scheel. Pattern-forming fronts in a Swift–Hohenberg equation with directional quenching — parallel and oblique stripes. *Journal of the London Mathematical Society*, 98(1):104–128, 2018.
- [18] A. A. Golovin, B. J. Matkowsky, and V. A. Volpert. Turing pattern formation in the Brusselator model with superdiffusion. *SIAM Journal on Applied Mathematics*, 69(1):251–272, 2008.
- [19] K. Gowda, H. Riecke, and M. Silber. Transitions between patterned states in vegetation models for semiarid ecosystems. *Physical Review E*, 89(2):022701, 2014.
- [20] M. Haragus and G. Iooss. *Local Bifurcations, Center Manifolds, and Normal Forms in Infinite-dimensional Dynamical Systems*. Springer Science & Business Media, 2010.
- [21] S. Havlin, D. Movshovitz, B. Trus, and G. H. Weiss. Probability densities for the displacement of random walks on percolation clusters. *Journal of Physics A: Mathematical and General*, 18(12):L719–L722, Aug. 1985.
- [22] B. I. Henry, T. A. M. Langlands, and S. L. Wearne. Turing pattern formation in fractional activator-inhibitor systems. *Physical Review E*, 72(2):026101, Aug. 2005.
- [23] B. I. Henry, T. A. M. Langlands, and S. L. Wearne. Anomalous diffusion with linear reaction dynamics: from continuous time random walks to fractional reaction-diffusion equations. *Physical Review E*, 74(3):031116, 2006.
- [24] B. I. Henry and S. L. Wearne. Fractional reaction–diffusion. *Physica A: Statistical Mechanics and its Applications*, 276(3):448–455, 2000.
- [25] B. I. Henry and S. L. Wearne. Existence of Turing instabilities in a two-species fractional reaction-diffusion system. *SIAM Journal on Applied Mathematics*, 62(3):870–887, 2002.

- [26] R. Hoyle. *Pattern Formation: An Introduction to Methods*. Cambridge University Press, 2006.
- [27] A. A. Kilbas, H. M. Srivastava, and J. J. Trujillo. *Theory and Applications of Fractional Differential Equations*, volume 204 of *North-Holland Mathematics Studies*. Elsevier Science, Amsterdam, 1st edition, 2006.
- [28] C. A. Klausmeier. Regular and irregular patterns in semiarid vegetation. *Science*, 284(5421):1826–1828, 1999.
- [29] T. A. M. Langlands, B. I. Henry, and S. L. Wearne. Turing pattern formation with fractional diffusion and fractional reactions. *Journal of Physics: Condensed Matter*, 19(6):065115, 2007.
- [30] T. A. M. Langlands, B. I. Henry, and S. L. Wearne. Anomalous subdiffusion with multi-species linear reaction dynamics. *Physical Review E*, 77(2):021111, 2008.
- [31] W. D. Luedtke and U. Landman. Slip diffusion and Lévy flights of an adsorbed gold nanocluster. *Physical Review Letters*, 82:3835–3838, May 1999.
- [32] F. Mainardi, Y. Luchko, and G. Pagnini. The fundamental solution of the space-time fractional diffusion equation. *arXiv preprint cond-mat/0702419*, 2007.
- [33] F. Mainardi, A. Mura, and G. Pagnini. The M -Wright function in time-fractional diffusion processes: A tutorial survey. *International Journal of Differential Equations*, 2010, 2010.
- [34] W. McLean, K. Mustapha, R. Ali, and O. Knio. Well-posedness of time-fractional advection-diffusion-reaction equations. *Fractional Calculus and Applied Analysis*, 22(4):918–944, 2019.
- [35] V. Méndez, D. Campos, and F. Bartumeus. *Stochastic Foundations in Movement Ecology: Anomalous Diffusion, Front Propagation and Random Searches*. Springer Series in Synergetics. Springer-Verlag Berlin Heidelberg, 1st edition, 2014.
- [36] J. Merkin, R. Satnoianu, and S. Scott. The development of spatial structure in an ionic chemical system induced by applied electric fields. *Dynamics and Stability of Systems*, 15(3):209–230, 2000.
- [37] E. Meron, E. Gilad, J. von Hardenberg, M. Shachak, and Y. Zarmi. Vegetation patterns along a rainfall gradient. *Chaos, Solitons & Fractals*, 19(2):367–376, 2004.
- [38] R. Metzler and J. Klafter. The random walk’s guide to anomalous diffusion: a fractional dynamics approach. *Physics Reports*, 339(1):1–77, 2000.

- [39] R. Metzler and J. Klafter. The restaurant at the end of the random walk: recent developments in the description of anomalous transport by fractional dynamics. *Journal of Physics A: Mathematical and General*, 37(31):R161–R208, 2004.
- [40] A. Mielke. A new approach to sideband-instabilities using the principle of reduced instability. *Pitman research notes in Mathematics series*, pages 206–222, 1995.
- [41] J. D. Murray. *Mathematical Biology II: Spatial Models and Biomedical Applications*, volume 18 of *Interdisciplinary Applied Mathematics*. 3rd edition, 2003.
- [42] Y. Nec and A. A. Nepomnyashchy. Linear stability of fractional reaction-diffusion systems. *Mathematical Modelling of Natural Phenomena*, 2(2):77–105, 2007.
- [43] Y. Nec and A. A. Nepomnyashchy. Turing instability in sub-diffusive reaction–diffusion systems. *Journal of Physics A: Mathematical and Theoretical*, 40(49):14687, 2007.
- [44] Y. Nec and A. A. Nepomnyashchy. Turing instability of anomalous reaction–anomalous diffusion systems. *European Journal of Applied Mathematics*, 19(3):329–349, 2008.
- [45] Y. Nec, A. A. Nepomnyashchy, and A. A. Golovin. Oscillatory instability in super-diffusive reaction – diffusion systems: Fractional amplitude and phase diffusion equations. *EPL (Europhysics Letters)*, 82(5):58003, May 2008.
- [46] Y. Nec, V. A. Volpert, and A. A. Nepomnyashchy. Front propagation problems with sub-diffusion. *Discrete and Continuous Dynamical Systems*, 27(2):827–846, 2010.
- [47] A. A. Nepomnyashchy. Mathematical modelling of subdiffusion-reaction systems. *Mathematical Modelling of Natural Phenomena*, 11(1):26–36, 2016.
- [48] B. Peña, C. Pérez-García, A. Sanz-Anchelergues, D. G. Míguez, and A. P. Muñuzuri. Transverse instabilities in chemical Turing patterns of stripes. *Physical Review E*, 68:056206, Nov. 2003.
- [49] I. Podlubny. *Fractional Differential Equations: An Introduction to Fractional Derivatives, Fractional Differential Equations, to Methods of Their Solution and Some of Their Applications*, volume 198 of *Mathematics in Science and Engineering*. Academic press, San Diego, 1st edition, 1998.
- [50] J. D. M. Rademacher, B. Sandstede, and A. Scheel. Computing absolute and essential spectra using continuation. *Physica D: Nonlinear Phenomena*, 229(2):166–183, 2007.
- [51] L. Rayleigh. Lix. on convection currents in a horizontal layer of fluid, when the higher temperature is on the under side. *The London, Edinburgh, and Dublin Philosophical Magazine and Journal of Science*, 32(192):529–546, 1916.

- [52] A. B. Rovinsky and M. Menzinger. Chemical instability induced by a differential flow. *Physical Review Letters*, 69(8):1193, 1992.
- [53] S. G. Samko, A. A. Kilbas, and O. I. Marichev. *Fractional Integrals and Derivatives: Theory and Applications*. Gordon and Breach Science Publishers, Switzerland, 1993.
- [54] B. Sandstede. Chapter 18 - stability of travelling waves. In B. Fiedler, editor, *Handbook of Dynamical Systems*, volume 2 of *Handbook of Dynamical Systems*, pages 983–1055. Elsevier Science, 2002.
- [55] H. Scher and E. W. Montroll. Anomalous transit-time dispersion in amorphous solids. *Physical Review B*, 12:2455–2477, Sept. 1975.
- [56] G. Schneider and H. Uecker. *Nonlinear PDEs: A Dynamical Systems Approach*, volume 182. American Mathematical Society, 2017.
- [57] K. Seki, M. Wojcik, and M. Tachiya. Fractional reaction-diffusion equation. *The Journal of chemical physics*, 119(4):2165–2170, 2003.
- [58] K. Seki, M. Wojcik, and M. Tachiya. Recombination kinetics in subdiffusive media. *The Journal of chemical physics*, 119(14):7525–7533, 2003.
- [59] E. Siero, A. Doelman, M. B. Eppinga, J. D. M. Rademacher, M. Rietkerk, and K. Siteur. Striped pattern selection by advective reaction-diffusion systems: Resilience of banded vegetation on slopes. *Chaos: An Interdisciplinary Journal of Nonlinear Science*, 25(3):036411, 2015.
- [60] I. M. Sokolov, M. G. W. Schmidt, and F. Sagués. Reaction-subdiffusion equations. *Physical Review E*, 73:031102, Mar. 2006.
- [61] M. R. Spiegel. *Theory and Problems of Laplace Transforms*. Schaum’s Outline. McGraw-Hill, New York, 1st edition, 1965.
- [62] A. M. Turing. The chemical basis of morphogenesis. *Philosophical Transactions of the Royal Society of London. Series B, Biological Sciences*, 237(641):37–72, 1952.
- [63] H. Uecker, D. Wetzel, and J. D. M. Rademacher. pde2path - a Matlab package for continuation and bifurcation in 2D elliptic systems. *Numerical Mathematics: Theory, Methods and Applications*, 7(1):58–106, 2014.
- [64] V. Vergara and R. Zacher. Optimal decay estimates for time-fractional and other nonlocal subdiffusion equations via energy methods. *SIAM Journal on Mathematical Analysis*, 47(1):210–239, 2015.

- [65] V. Vergara and R. Zacher. Stability, instability, and blowup for time fractional and other non-local in time semilinear subdiffusion equations. *Journal of Evolution Equations*, 17(1):599–626, 2017.
- [66] V. A. Volpert, Y. Nec, and A. A. Nepomnyashchy. Fronts in anomalous diffusion–reaction systems. *Philosophical Transactions of the Royal Society A: Mathematical, Physical and Engineering Sciences*, 371(1982):20120179, 2013.
- [67] R.-H. Wang, Q.-X. Liu, G.-Q. Sun, Z. Jin, and J. van de Koppel. Nonlinear dynamic and pattern bifurcations in a model for spatial patterns in young mussel beds. *Journal of The Royal Society Interface*, 6(37):705–718, 2009.
- [68] M. Weiss, H. Hashimoto, and T. Nilsson. Anomalous protein diffusion in living cells as seen by fluorescence correlation spectroscopy. *Biophysical Journal*, 84(6):4043 – 4052, 2003.
- [69] J. Yang and J. D. M. Rademacher. Reaction-subdiffusion systems and memory: spectra, Turing instability and decay estimates. *arXiv preprint arXiv:1910.03822*, 2019.
- [70] J. Yang, J. D. M. Rademacher, and E. Siero. The impact of advection on large-wavelength stability of stripes near planar Turing instabilities. *arXiv preprint arXiv:1912.11294*, 2019.
- [71] J. Yang, J. D. M. Rademacher, and E. Siero. The impact of advection on the stability of stripes on lattices near planar Turing instabilities. Manuscript, 2020.
- [72] S. B. Yuste, L. Acedo, and K. Lindenberg. Reaction front in an $a + b \rightarrow c$ reaction-subdiffusion process. *Physical Review E*, 69(3):036126, 2004.
- [73] A. N. Zaikin and A. M. Zhabotinsky. Concentration wave propagation in two-dimensional liquid-phase self-oscillating system. *Nature*, 225(5232):535–537, 1970.
- [74] Y. R. Zelnik, E. Meron, and G. Bel. Gradual regime shifts in fairy circles. *Proceedings of the National Academy of Sciences*, 112(40):12327–12331, 2015.

Abbreviations and symbols

CTRW	Continuous-time random walks
ILT	Inverse Laplace transform
KPP	Kolmogorov–Petrovsky–Piskunov
MSD	Mean squared displacement
PDF	Probability density function
RD	Reaction-diffusion
SH	Swift-Hohenberg
\mathbb{C}^n	n -dimensional complex space; \mathbb{C} – complex plane
\mathbb{N}	$\{0, 1, 2, \dots\}$
\mathbb{Q}	The set of rational numbers
\mathbb{R}^n	n -dimensional real Euclidean space, $\mathbb{R} = \mathbb{R}^1$
\mathbb{Z}_+	The set of positive integers
$B_r(x)$	Open ball in \mathbb{C} with centre x and radius $r > 0$, i.e., $\{y \in \mathbb{C} : x - y < r\}$
$\partial B_r(x)$	Boundary of $B_r(x)$
Ω	Usually a domain in \mathbb{C} or \mathbb{R}^n
$S_{\mathbf{k}_c}$	$S_{\mathbf{k}_c} \subset \mathbb{R}^2$ the circle of radius \mathbf{k}_c with centre $(0, 0)$
S^1	$S^1 \subset \mathbb{R}^2$ the circle of radius 1 with centre $(0, 0)$
arg	Argument of a complex value
Im	Imaginary part of a complex number
Re	Real part of a complex number
sgn	Sign function

argmax	Argument of the maximum $\operatorname{argmax} f(x) = \{x \in X : \forall y \in X, f(y) \leq f(x)\}$
Γ	Gamma function
$o(\varepsilon)$	$\lim_{\varepsilon \rightarrow \varepsilon_0} o(\varepsilon)/\varepsilon = 0$
$O(\varepsilon)$	$\lim_{\varepsilon \rightarrow \varepsilon_0} O(\varepsilon)/\varepsilon \leq M < \infty$
\mathcal{W}	Wright function
Δ	Laplace operator $\partial_{x_1}^2 + \cdots + \partial_{x_n}^2$
$\mathcal{D}_{0,t}^{-\gamma}$	Fractional integral of order $\gamma \in (0, 1)$; $(\mathcal{D}_{0,t}^{-1}f)(t) = \int_0^t f(s)ds$
$\mathcal{D}_{0,t}^{1-\gamma}$	Riemann-Liouville fractional derivative of order $\gamma \in (0, 1)$
$\mathfrak{D}_{0,t}^\alpha$	Grünwald-Letnikov fractional derivative of order $\alpha \in (0, 1)$
$\det(A)$	Determinant of the matrix A
Id	Identity operator (matrix)
\mathcal{L}	Usually a linear operator
\mathcal{L}^*	Adjoint operator of the linear operator \mathcal{L}
$\operatorname{diag}(d_1, \dots, d_n)$	$n \times n$ diagonal matrix with diagonal entries d_1, \dots, d_n
$\operatorname{tr}(A)$	Trace of the matrix A
A^T	Transpose of the matrix A
e_0, e_0^*	Kernel eigenvectors of linear operators \mathcal{L}_0 and \mathcal{L}_0^*
E_0, E_0^*	Kernel eigenvectors of matrices A and A^T
X, Y	Some Banach spaces
$\operatorname{AC}([a, b])$	Space of absolutely continuous functions from $[a, b]$ to \mathbb{C}
$C(U)$	Space of continuous functions from U to \mathbb{C}
$C^k(U)$	Space of k -times continuously differentiable functions from U to \mathbb{C}
$C^k(X, Y)$	Space of k -times continuously differentiable functions from X to Y
$L^p(\Omega)$	Space of Lebesgue measurable functions from Ω to \mathbb{C}
$H^m(\Omega)$	Sobolev space $H^m(\Omega) = \{f \in L^2(\Omega) : D^\alpha f = \frac{\partial^{ \alpha } f}{\partial x_1^{\alpha_1} \cdots \partial x_n^{\alpha_n}} \in L^2(\Omega), \forall \alpha \in \mathbb{N}^n, \alpha = \alpha_1 + \cdots + \alpha_n \leq m\}$
$H_{\operatorname{per}}^m(0, L)$	$= \{f \in H^m(\Omega) : D^\alpha f(\cdot) = D^\alpha f(\cdot + L), \forall \alpha \in \mathbb{N}^n, \text{ bounded } \Omega \subset \mathbb{R}\}$
$X(U; Y(\Omega))$	$= \{\mathbf{f} : U \rightarrow Y(\Omega) : [\mathbf{f}(t)](x) := f(x, t), f(\cdot, t) \in Y(\Omega) \text{ for any fixed } t \in U, f(x, \cdot) \in X(U) \text{ for any fixed } x \in \Omega\}$

$\mathcal{F}, \hat{\cdot}$	Fourier transform
\mathcal{L}	Laplace transform
$f * g$	Time convolution $(f * g)(t) = \int_0^t f(t-s)g(s)ds$; space convolution $(f * g)(x) = \int_{\mathbb{R}^n} f(x-y)g(y)dy$
$\langle f, g \rangle$	Inner product in $L^2(\Omega)$ or \mathbb{C}^2